

BetonKalender

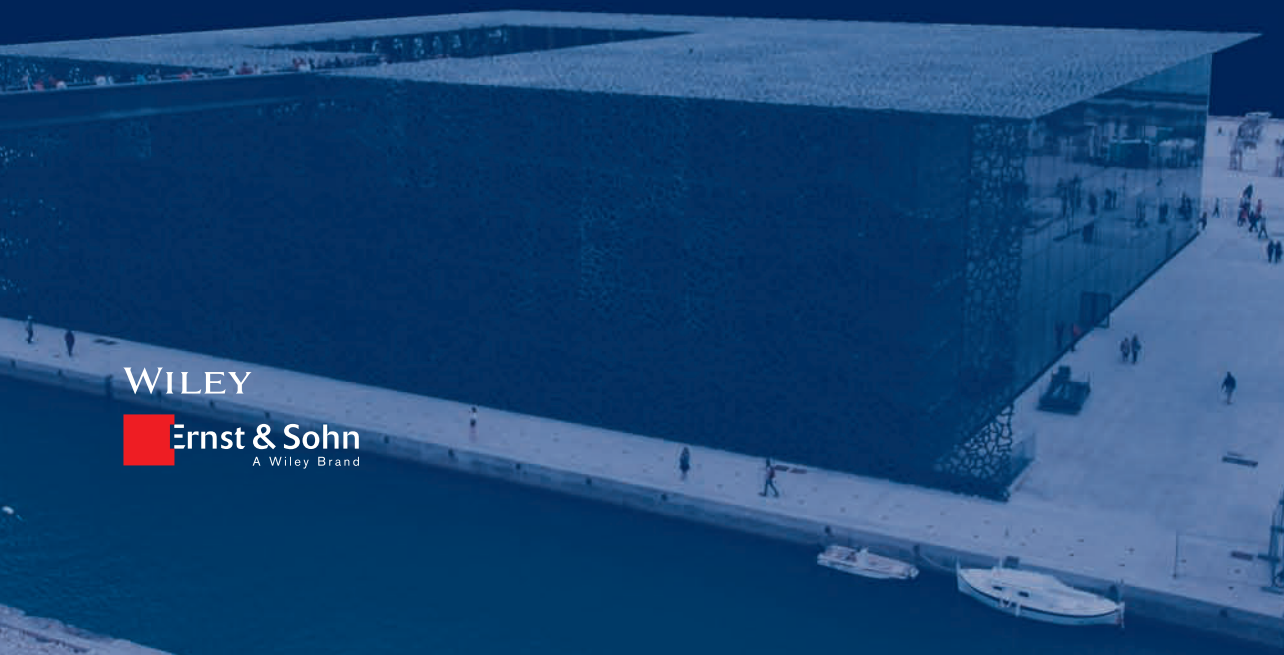
Ultra-High Performance Concrete UHPC

Fundamentals – Design – Examples

Ekkehard Fehling, Michael Schmidt, Joost Walraven,
Torsten Leutbecher, Susanne Fröhlich

WILEY

 **Ernst & Sohn**
A Wiley Brand




*Ekkehard Fehling, Michael Schmidt
Joost Walraven, Torsten Leutbecher
Susanne Fröhlich*

**Ultra-High Performance
Concrete UHPC**

Selected Chapters from the Beton-Kalender in English




**Concrete Structures
for Wind Turbines**
2013. 242 pages.
€ 49,90
ISBN: 978-3-433-03041-7
Also available as 



**Reconditioning and
Maintenance of
Concrete Structures**
2014. 210 pages.
approx. € 49,90
ISBN: 978-3-433-03043-1
Also available as 




**Design and Construction
of Nuclear Power Plants**
2013. 136 pages.
€ 49,90
ISBN: 978-3-433-03042-4
Also available as 



**Ultra-High Performance
Concrete UHPC**
Fundamentals – Design –
Examples
2014. 280 pages.
approx. € 49,90
ISBN: 978-3-433-03087-5
Also available as 



**Design of Fastenings
for Use in Concrete –
the CEN/TS 1992-4
Provisions**
2013. 158 pages.
€ 49,90
ISBN: 978-3-433-03044-8
Also available as 



**Strengthening of Concrete
Structures with Adhesively
Bonded Reinforcement**
Design and Dimensioning of
CFRP Laminates and Steel Plates
2014. 144 pages.
approx. € 49,90
ISBN: 978-3-433-03086-8
Also available as 

Order online: www.ernst-und-sohn.de

Ernst & Sohn
Verlag für Architektur und technische
Wissenschaften GmbH & Co. KG

Customer Service: Wiley-VCH
Boschstraße 12
D-69469 Weinheim

Tel. +49 (0)6201 606-400
Fax +49 (0)6201 606-184
service@wiley-vch.de

*€ Prices are valid in Germany, exclusively, and subject to alterations. Prices incl. VAT, excl. shipping. 1006146_dp

*Ekkehard Fehling, Michael Schmidt
Joost Walraven, Torsten Leutbecher
Susanne Fröhlich*

Ultra-High Performance Concrete UHPC

Fundamentals, Design, Examples

The Authors

Univ.-Prof. Dr.-Ing. Ekkehard Fehling

University of Kassel
Institute of Structural Engineering
Kurt-Wolters-Str. 3
34125 Kassel
Germany

Univ.-Prof. Dr.-Ing. habil. Michael Schmidt

University of Kassel
Institute of Structural Engineering
Mönchebergstr. 7
34125 Kassel
Germany

Prof. Dr. Ir. Dr.-Ing. h. c. Joost C. Walraven

Technical University Delft
Civil Engineering and Geosciences
Design and Construction
Structural and Building Engineering
Stevinweg 1, Building 23
2628 CN Delft
The Netherlands

Univ.-Prof. Dr.-Ing. Torsten Leutbecher

University of Siegen
Department of Civil Engineering
Chair of Structural Concrete
Paul-Bonatz-Str. 9-11
57076 Siegen
Germany

Dipl.-Ing. Susanne Fröhlich

University Kassel
Institute of Structural Engineering
Mönchebergstr. 7
34125 Kassel
Germany

The Editors of Beton-Kalender

Prof. Dipl.-Ing. Dr.-Ing. Konrad Bergmeister

Ingenieurbüro Bergmeister
Peter-Jordan-Straße 113
1190 Vienna
Austria

Dr.-Ing. Frank Fingerloos

German Society for Concrete and Construction
Technology
Kurfürstenstr. 129
10785 Berlin
Germany

Prof. Dr.-Ing. Dr. h. c. mult.

Johann-Dietrich Wörner
German Aerospace Center
Linder Höhe
51145 Cologne
Germany

The original German text is published in Beton-Kalender 2013, ISBN 978-3-433-03000-4 and titled "Ultrahochfester Beton UHPC".

All books published by **Ernst & Sohn** are carefully produced. Nevertheless, authors, editors, and publisher do not warrant the information contained in these books, including this book, to be free of errors. Readers are advised to keep in mind that statements, data, illustrations, procedural details or other items may inadvertently be inaccurate.

Library of Congress Card No.: applied for

British Library Cataloguing-in-Publication Data

A catalogue record for this book is available from the British Library.

Bibliographic information published by the Deutsche Nationalbibliothek

The Deutsche Nationalbibliothek lists this publication in the Deutsche Nationalbibliografie; detailed bibliographic data are available on the Internet at <<http://dnb.d-nb.de>>.

© 2014 Wilhelm Ernst & Sohn, Verlag für Architektur und technische Wissenschaften GmbH & Co. KG, Rotherstraße 21, 10245 Berlin, Germany

All rights reserved (including those of translation into other languages). No part of this book may be reproduced in any form – by photoprinting, microfilm, or any other means – nor transmitted or translated into a machine language without written permission from the publishers. Registered names, trademarks, etc. used in this book, even when not specifically marked as such, are not to be considered unprotected by law.

Print ISBN: 978-3-433-03087-5

ePDF ISBN: 978-3-433-60406-9

ePub ISBN: 978-3-433-60415-1

Mobi ISBN: 978-3-433-60404-5

oBook ISBN: 978-3-433-60407-6

Coverdesign: Hans Baltzer, Berlin, Germany

Typesetting: Thomson Digital, Noida, India

Printing and Binding: Betz Druck GmbH, Darmstadt, Germany

Printed in the Federal Republic of Germany

Printed on acid-free paper

Cover: Musée des Civilisations de l'Europe et de la Méditerranée, Marseille, France.

Photo: Nicolas Janberg

Contents

	Editorial	IX
1	Introduction.....	1
2	Principles for the production of UHPC.....	5
2.1	Development.....	5
2.2	Basic material concepts.....	6
2.2.1	Microstructure properties.....	6
2.2.2	Grading optimization.....	8
2.3	Raw materials.....	12
2.3.1	Cement.....	12
2.3.2	Reactive admixtures.....	12
2.3.2.1	Silica fume.....	12
2.3.2.2	Ground granulated blast furnace slag.....	13
2.3.3	Inert admixtures.....	14
2.3.4	Superplasticizers.....	14
2.3.5	Steel fibres.....	14
2.4	Mix composition.....	15
2.5	Mixing.....	15
2.6	Curing and heat treatment.....	17
2.7	Testing.....	18
2.7.1	Fresh concrete.....	18
2.7.2	Compressive and flexural tensile strengths.....	20
3	Mechanical properties of the hardened concrete	23
3.1	General.....	23
3.2	Behaviour in compression.....	23
3.2.1	UHPC without fibres.....	23
3.2.2	UHPC with steel fibres.....	24
3.2.3	Further factors affecting the compressive strength.....	27
3.2.3.1	Geometry of test specimen and test setup.....	27
3.2.3.2	Heat treatment.....	27
3.3	Behaviour in tension.....	27
3.3.1	Axial (concentric) tension loads.....	27
3.3.2	Flexural tensile strength.....	32
3.3.3	Derivation of axial tensile strength from compressive strength.....	34
3.3.4	Derivation of axial tensile strength from bending tests.....	35
3.3.5	Splitting tensile strength.....	36
3.3.6	How fibre geometry and orientation influence the behaviour of UHPC in tension.....	36
3.3.7	Converting the stress–crack width relationship into a stress–strain diagram.....	39
3.3.8	Interaction of fibres and bar reinforcement.....	41
3.4	Shrinkage.....	42
3.5	Creep.....	43

3.6	Multi-axial stresses	44
3.7	Fatigue behaviour.....	44
3.8	Dynamic actions.....	51
3.9	Fire resistance	53
3.10	UHPC with combinations of fibres ('fibre cocktails').....	53
4	Durability	59
4.1	Microstructure.....	59
4.2	Resistance to aggressive media.....	59
4.3	Classification in exposure classes	63
5	Design principles	65
5.1	Influence of fibre distribution and fibre orientation.....	65
5.2	Analyses for the ultimate limit state.....	66
5.2.1	Safety concept.....	66
5.2.2	Simplified stress–strain curve for design.....	67
5.2.2.1	Compression actions	67
5.2.2.2	Tension actions	70
5.2.3	Design for bending and normal force.....	72
5.2.4	Design for shear	75
5.2.4.1	Tests at the University of Kassel.....	75
5.2.4.2	Tests at RWTH Aachen University.....	79
5.2.4.3	Tests at Delft University of Technology	81
5.2.5	Punching shear.....	84
5.2.6	Strut-and-tie models.....	85
5.2.6.1	Load-carrying capacity of struts.....	86
5.2.6.2	Load-carrying capacity of ties.....	87
5.2.6.3	Load-carrying capacity of nodes.....	87
5.2.7	Partially loaded areas	88
5.2.8	Fatigue	88
5.3	Analyses for the serviceability limit state.....	89
5.3.1	Limiting crack widths	89
5.3.2	Minimum reinforcement	97
5.3.3	Calculating deformations	99
6	Connections.....	105
6.1	General.....	105
6.2	Dry joints	105
6.3	Glued joints.....	105
6.4	Wet joints.....	108
6.5	Grouted joints	111
6.6	Adding UHPC layers to existing components to upgrade structures ..	113
7	Projects completed	117
7.1	Bridges.....	117
7.1.1	Canada	117

7.1.1.1	Bridge for pedestrians/cyclists, Sherbrooke (1997)	117
7.1.1.2	Glenmore/Legsby footbridge, Calgary (2007)	117
7.1.2	France	118
7.1.2.1	Road bridge, Bourg-lès-Valence	118
7.1.2.2	Pont du Diable footbridge (2005)	119
7.1.2.3	Pont de la Chabotte road bridge	120
7.1.2.4	Pont Pinel road bridge (2007)	121
7.1.2.5	Strengthening the Pont sur l'Huisne, Mans	124
7.1.3	Japan	124
7.1.3.1	Sakata-Mirai footbridge (2003).....	124
7.1.3.2	GSE Bridge, Tokyo Airport (2010)	126
7.1.3.3	Tokyo Monorail, Haneda Airport line.....	128
7.1.4	South Korea	129
7.1.4.1	Seonyu 'Bridge of Peace', Seoul.....	129
7.1.4.2	KICT cable-stayed footbridge (2009)	131
7.1.4.3	Design for Jobal Bridge (KICT).....	132
7.1.5	Germany	133
7.1.5.1	Bridges over River Nieste near Kassel	133
7.1.5.2	Gärtnerplatz Bridge over River Fulda, Kassel (2007).....	134
7.1.5.3	HSLV pilot project.....	137
7.1.5.4	Bridge for pedestrians/cyclists over River Pleiße, Markkleeberg (2012).....	140
7.1.6	Austria.....	141
7.1.6.1	Wild Bridge near Völkermarkt.....	141
7.1.6.2	Bridge for pedestrians/cyclists, Lienz	143
7.1.6.3	Modular temporary bridge for high-speed rail lines.....	144
7.1.7	Switzerland	146
7.1.8	The Netherlands	147
7.2	Applications in buildings	149
7.2.1	Columns	149
7.2.2	Façades	151
7.2.3	Stairs and balconies.....	152
7.2.4	Roofs.....	155
7.3	Other applications	157
7.3.1	Runway, Haneda Airport, Tokyo, Japan	157
7.3.2	Jean Bouin Stadium, Paris	160
8	Acknowledgements	163
	References	165
	Index	183

Editorial

The *Concrete Yearbook* is a very important source of information for engineers involved in the planning, design, analysis and construction of concrete structures. It is published on a yearly basis and offers chapters devoted to various, highly topical subjects. Every chapter provides extensive, up-to-date information written by renowned experts in the areas concerned. The subjects change every year and may return in later years for an updated treatment. This publication strategy guarantees that not only is the latest knowledge presented, but that the choice of topics itself meets readers' demands for up-to-date news.

For decades, the themes chosen have been treated in such a way that, on the one hand, the reader gets background information and, on the other, becomes familiar with the practical experience, methods and rules needed to put this knowledge into practice. For practising engineers, this is an optimum combination. In order to find adequate solutions for the wide scope of everyday or special problems, engineering practice requires knowledge of the rules and recommendations as well as an understanding of the theories or assumptions behind them.

During the history of the *Concrete Yearbook*, an interesting development has taken place. In the early editions, themes of interest were chosen on an ad hoc basis. Meanwhile, however, the building industry has gone through a remarkable evolution. Whereas in the past attention focused predominantly on matters concerning structural safety and serviceability, nowadays there is an increasing awareness of our responsibility with regard to society in a broader sense. This is reflected, for example, in the wish to avoid problems related to the limited durability of structures. Expensive repairs to structures have been, and unfortunately still are, necessary because in the past our awareness of the deterioration processes affecting concrete and reinforcing steel was inadequate. Therefore, structural design should now focus on building structures with sufficient reliability and serviceability for a specified period of time, without substantial maintenance costs. Moreover, we are confronted by a legacy of older structures that must be assessed with regard to their suitability to carry safely the increased loads often applied to them today. In this respect, several aspects of structural engineering have to be considered in an interrelated way, such as risk, functionality, serviceability, deterioration processes, strengthening techniques, monitoring, dismantlement, adaptability and recycling of structures and structural materials plus the introduction of modern high-performance materials. The significance of sustainability has also been recognized. This must be added to the awareness that design should focus not just on individual structures and their service lives, but on their function in a wider context as well, i.e. harmony with their environment, acceptance by society, responsible use of resources, low energy consumption and economy. Construction processes must also become cleaner, cause less environmental impact and pollution.

The editors of the *Concrete Yearbook* have clearly recognized these and other trends and now offer a selection of coherent subjects that reside under the common "umbrella" of a broader societal development of great relevance. In order to be able to cope with the corresponding challenges, the reader can find information on progress in technology,

theoretical methods, new research findings, new ideas on design and construction, developments in production and assessment and conservation strategies. The current selection of topics and the way they are treated makes the *Concrete Yearbook* a splendid opportunity for engineers to find out about and stay abreast of developments in engineering knowledge, practical experience and concepts in the field of the design of concrete structures on an international level.

Prof. Dr. Ir. Dr.-Ing. h. c. *Joost Walraven*, TU Delft
Honorary president of the international concrete federation *fib*

1 Introduction

When *Otto Graf* managed to produce a concrete with a strength of 70 N/mm^2 in the early 1950s, the construction industry showed very little interest in this new product. And this lack of interest didn't change even as in 1966 *Kurt Walz* proved that, using special production methods, it was possible to achieve a strength of 140 N/mm^2 . Only after it was realized that adding a limited amount of silica fume plus suitable superplasticizers was a simple way of producing a concrete with high strength and at the same time good workability did the first ideas regarding potential applications begin to materialise.

Not until the late 1980s was it possible to produce concrete in strength classes up to C100/115. The discovery of the effect of silica fume, a fine, reactive material, and the development of efficient superplasticizers proved very important in this development. At the start, high-strength concrete was ascribed only a limited role, primarily because of the much higher production costs compared with conventional concretes. It turned out, however, that it is more realistic to make comparisons on the basis of an entire project. One example was Stichtse Bridge, built near the Dutch city of Amsterdam in 1997. The use of C80/90 concrete enabled the cross-sectional area of this bridge, which spans 160 m, to be reduced by 30%. The smaller cross-sectional area of the box girder resulted in a 26% saving in prestressing steel. Owing to the 60% thinner webs and bottom flange, the length of the individual segments could be increased from 3.50 to 5.00 m, which in turn led to the construction time being shortened by three months. In addition, there were the advantages of the good workability of the concrete, the low creep and shrinkage losses, the high wearing resistance and the excellent durability of the concrete. It became clear that the solution using C80/90 concrete was, on the whole, no more expensive than the alternative with conventional concrete, and at the same time resulted in a structure with a very high quality.

Increasing the strength of the concrete to values beyond about 120 N/mm^2 was regarded as unrealistic because the strength of the aggregate, as the weakest component in the mix and accounting for about 75% of the volume of the concrete, would prevent this.

Another innovation thought of as promising at that time was the development of SIFCON (Slurry Infiltrated Fibre CONcrete). The production of this material involves first introducing steel fibres into the formwork and packing these tightly. The spaces between the fibres are then filled with a cement matrix. This method results in a fibre content of 12–13%, which roughly corresponds to a 10-fold increase over the maximum fibre content of conventional fibre-reinforced concrete. The material is characterized by its very high strain at failure [1]. One disadvantage, however, is that the packing results in an inhomogeneous distribution of the fibres (predominantly 2D). When it comes to the effectiveness and hence the associated costs, this limits the potential applications. A variation on SIFCON is SIMCON (Slurry Infiltrated Mat CONcrete). This material is produced by introducing a mat of discontinuous steel fibres into the formwork and subsequently covering this with an easy-flowing cement mortar [2].

A new breakthrough came with the development of a new concept for the composition of ultra-high-strength concretes. Based on this concept, it was possible to produce concretes with compressive strengths up to 200 N/mm^2 and fibre contents up to 2.5% by vol. (175 kg/m^3). In order to produce ultra-high-strength concrete with a compressive strength in the region of $150\text{--}200 \text{ N/mm}^2$, it is important to observe the following basic rules:

- The maximum grain size should be less than that of traditional concrete mixes because large grains cause stress concentrations that lead to a decrease in strength. These days, the maximum grain size for ultra high performance concrete is usually no larger than 2 mm. However, ultra high performance concretes with a maximum grain size of 8 mm have also been developed.
- An optimum packing density for the aggregate is important. A high packing density can be achieved with the help of fine materials, which reduce the stresses on the contact surfaces and ensure that microcracks do not begin to form until a higher level of stress is reached. The microstructure is, principally, very dense, which expresses itself not only in a high strength, but also in a much higher resistance to all forms of attack that damage concrete or reinforcement (chloride, alkalis, carbonation, de-icing salts).
- The amount of cement used should be such that the water is fully bound. The remaining non-hydrated cement particles then act as fillers.
- Fine steel fibres should be added to the concrete in order to guarantee a ductile behaviour.

The Danish researcher *Hans Hendrik Bache* was the first to recognize and apply these principles. He developed a material with a high fibre content which was also reinforced with a high amount of reinforcing steel. The material was called CRC (Compact Reinforced Concrete) and the first information on this was published in 1981 [3]. This special form of construction is still used frequently today, especially for stairs and balconies and primarily in Denmark.

Bache's ideas were taken up in 1994 by the French contractor Bouygues (*Richard* and *Cheyrezy*) and developed further. Cooperating with Lafarge, a new mix was devised: 'Reactive Powder Concrete', which continues to exist in the form of 'Ductal®'. One early application involved replacing steel beams by ultra high performance concrete ones in the cooling towers of a power station at Cattenom in France. The steel beams had to be replaced because they were corroding in the extremely aggressive environment inside the cooling towers. One important point to note here is that it was not the high strength of the ultra high performance concrete that was decisive in this case, but rather the durability of the material in connection with the anticipated very long service life without maintenance or repairs.

It was the realization that the material can be specified for its other outstanding properties and not just for its high strength that led to the term 'ultra-high-strength concrete' being replaced by 'ultra high performance concrete'. The abbreviation UHPC will be used throughout this book.

As soon as the potential of this new high-performance construction material received more publicity, e.g. through the building of the first footbridge made from this material in Sherbrooke, Canada, in 1997 [4], so architects and engineers began to come forward with a wide range of ideas for new, innovative forms of construction. Current French projects such as MuCEM in Marseille, with tree-like columns and delicate façade elements, or the Jean Bouin Stadium in Paris, which is clad in 3500 prefabricated UHPC elements, show quite aptly the direction in which developments are going. One remarkable structure is the UHPC platform in the open sea which was built for the extension to Haneda Airport in Japan. The slab with an area of 200 000 m² is the largest application of UHPC to date. These projects and many others are described in more detail in Chapter 7.

One first pilot project in Germany was Gärtnerplatz Bridge in Kassel [5], which was opened to the public in 2007 and enabled important experience to be gained with UHPC. A national research programme with a budget of €12 million was launched in Germany in 2005.

The first design rules for UHPC were published in France in 2002. As design methods are lacking elsewhere, this pre-standard has often been used since then outside France as well. Japan's first guideline appeared in 2004. Currently, *fib* Task Group TG 8.6 is working on an international standard for UHPC [6].

Until recently, concrete with a very high strength still met with opposition. Comparing the per m³ cost of producing such a concrete with that of a conventional concrete results in a negative verdict at first sight: up to now, the cost of UHPC per m³ has been four to five times that of a conventional concrete. However, comparisons should take place on the basis of entire projects. An example of this is Sakata Mirai, a Japanese footbridge (Section 7.1.3). The self-weight of this bridge is only 20% of that of a conventional bridge [7]. Therefore, the costs of the foundations were also much lower. According to information supplied by the initiators, the final cost of the project was 10% lower than that of a comparable bridge in conventional concrete.

In the future, design will be based primarily on the design life, see also [8]. Moreover, sustainability considerations will play an ever greater role. For example, in [9] the Gärtnerplatz Bridge in Kassel, a hybrid design with a steel frame, was compared with a conventional prestressed concrete bridge and a wholly UHPC bridge with the same span and load-carrying capacity within the scope of a life cycle assessment [10]. The result was that the production and upkeep of the wholly UHPC solution causes only 40% of the CO₂ emissions of a normal concrete bridge. What this means is that the new construction material UHPC has a good chance of achieving a breakthrough.

2 Principles for the production of UHPC

2.1 Development

Concrete technology has made remarkable advances in recent decades. Whereas the compressive strength classes for concrete in the 1988 edition of DIN 1045 ended at B55, the current edition of DIN EN 206/DIN 1045-2 includes the strength classes C55/C67 to C100/115, the ‘high-strength concretes’. Over the past 15 years, many working in this field have developed ultra-high performance concretes (UHPC) up to a level where they are ready for application – and with compressive strengths from about 150 to 200 N/mm², which are almost the same as those of steel. Reinforced with fine steel fibres with a high tensile strength, such concretes become ductile and reach tensile strengths exceeding 15 N/mm² (really exceptional for concrete) and flexural tensile strengths of up to 50 N/mm² [11]. So this type of concrete can for the first time be designed to accommodate tension, and by using new design principles suited to this material, with or without traditional reinforcement, the result is forms of concrete construction that save materials and are thus especially sustainable. It is not only the strength of UHPC that is high. Compared with conventional normal- and high-strength concretes with their capillary porosity, UHPC exhibits a much denser microstructure. It has virtually no capillary pores and is therefore so impervious to liquids and gases that its corrosion is practically zero; it can serve as the wearing course of a bridge deck without any additional protection against chlorides, alkalis or de-icing salts [12]. Owing to UHPCs good durability, its materials-saving composition and the low maintenance requirement, structures made from UHPC, when properly designed, are also considerably more cost-effective than comparable structures made from normal-strength concrete when the, predictably, longer design life is considered, despite the fact that the concrete itself is more expensive [13, 14].

The basic idea of producing a concrete with a very high strength and especially dense microstructure had already been put forward in the 1980s [3]. But the practical breakthrough came with the development of an especially efficient superplasticizer that enabled the production of concrete with a high proportion of optimally tightly packed ultrafine particles and at the same time an extremely low water/binder ratio of only about 0.20 in an easy-flowing consistency. The optimum combination of these two principles is what gives UHPC its special properties. Originally produced in the majority of cases as a fine-grained concrete with a maximum particle size of 1 mm and an easy-flowing consistency, in the meantime mixes have been developed with up to 60% by vol. 8 or 16 mm coarse aggregate in a mouldable and no-slump consistency with the same hardened concrete properties. Therefore, a wide range of applications can now be covered very economically [16–20].

Key new findings about the special material properties of UHPC and the proper design and construction of components and structures made from this new material were supplied by a programme of research into sustainable building with UHPC (priority programme SPP 1182) funded by the DFG (German Research Foundation) [21], which was concluded in 2012. This book takes into account the results of about 30 research projects in that programme. Besides representing the most extensive practical

experience with a diverse range of UHPC structures in Germany and abroad, the results of the research programme also form the basis for a first set of technical rules currently being drawn up by the German Committee for Reinforced Concrete (DAfStB) which follows on from the state of the art report dating from 2008 [22].

The research programme covered virtually all the issues relevant to the raw materials, production, processing, design, construction details and durability of UHPC and structures made with UHPC.

2.2 Basic material concepts

2.2.1 Microstructure properties

The excellent performance of UHPC – when compared with normal-strength or even high-strength concretes – is predominantly due to its much denser hardened cement matrix with virtually no capillaries. Furthermore, ‘classic’ easy-flowing UHPC is a fine-grained mix, with a maximum particle size of 1 mm. Therefore, its internal microstructure is much more homogeneous than customary, coarse-grained concretes and it is essentially more uniformly stressed by external actions. Together, these two aspects result in the compressive strengths of about 150–200 N/mm² so typical of UHPC. Even in the case of the coarse-grained UHPC that has been developed in the meantime for various applications, the differences in the strengths and deformation behaviours of the matrix and the aggregate are so small that any cracks that do form propagate in a straight line through the matrix and the aggregate. That in turn means that UHPC has a distinctly brittle failure behaviour. Whereas normal-strength concrete exhibits an increasingly (quasi-)ductile behaviour as compressive stresses rise due to changes to the internal microstructure and still retains a loadbearing capacity even after its strength is reached, unreinforced UHPC fails abruptly. Nevertheless, UHPC can still be used to build safe structures provided it is reinforced with fine high-strength steel fibres (and conventional or prestressed reinforcement if required). With a sufficiently high fibre content, the tensile strength of UHPC can be improved and ensured to such an extent that structural components in tension are possible without any further reinforcement [23].

The very dense microstructure and high strength so typical of UHPC are due to its very low water/binder ratio (cement, silica fume and further reactive substances if required) of only about 0.20. The matrix therefore has practically no capillaries and is thus diffusion-resistant. Another factor contributing to the high strength is the fact that the ultrafine particles (grain size <125 µm) consist of various components (cement, quartz powder, silica fume plus further inert or reactive fine fillers if required) that are combined in such a specific way that the ultrafine particles are packed very tightly together. Figure 2.1 compares the composition (by volume) of normal-strength concrete, high-strength concrete, self-compacting concrete (SCC) and fine- and coarse-grained UHPC for various applications.

The use of grading-optimized admixtures made up of several different components leads to a wider concrete technology approach that goes beyond conventional thinking in mass-based water/binder ratios as the key variable determining the strength. The

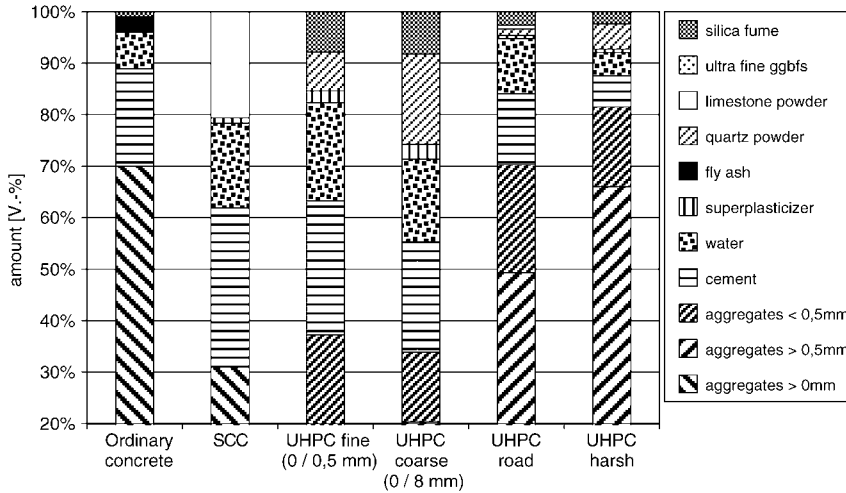


Fig. 2.1 Comparison of mix compositions for normal-strength, high-strength and various UHPCs (see also [24])

volume-based water/ultrafine particles ratio (w/F_v) was therefore introduced in [25] because – as shown schematically in Figure 2.2 – it enables the strength-increasing physical effect of grading-optimized ultrafine particle combinations to be taken into account when predicting the concrete strength and hence when designing UHPC mixes (extended k^+ value).

$$\frac{w}{F_v} = \frac{w}{\sum (c + ultrafine\ particles)_{vol}} \tag{2.1}$$

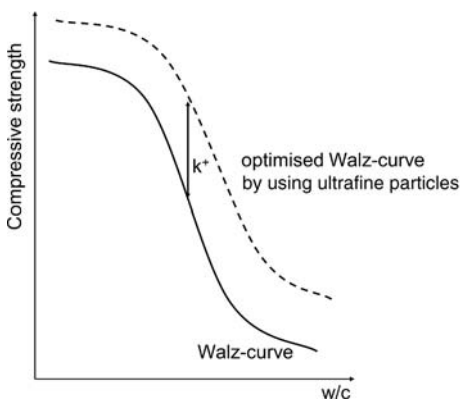


Fig. 2.2 Granulometric coefficient k^+ for assessing how packing-optimized ultrafine particle combinations with various densities influence the compressive strength (optimized *Walz* curve)

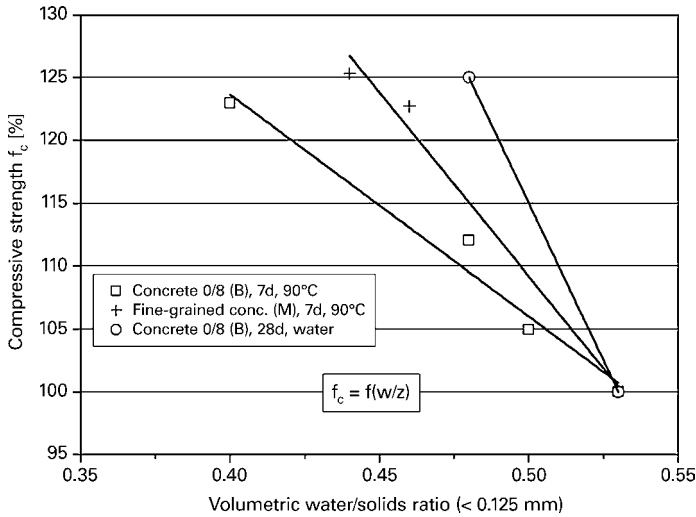


Fig. 2.3 How the volumetric water/solids ratio, as a measure of the packing density, influences the compressive strength of UHPC

Being based on volume, the w/F_v value is also a measure of the quality of the grading of the various ultrafine particles ($<125\ \mu\text{m}$ grain size) and the residual pores between the particles, which must be filled by water, and hence the packing density of the ultrafine particles. It forms the actual basis for optimizing UHPC [26].

As an example, Figure 2.3 shows that the 28-day compressive strengths of the fine- and coarse-grained UHPCs investigated in [11] increased by up to about 30% – for practically the same w/c ratio – when the packing density (and hence the water/ultrafine particles ratio of the mixture of cement, various fine quartz powders and silica fume) was improved by about 3% by vol [27]. Incidentally, optimizing the proportion of ultrafine particles even improves the strength of normal-strength concrete significantly – albeit on a much lower basic level of strength, as is reported in [26, 27].

2.2.2 Grading optimization

One way of achieving optimum packing of the fine particles is through experimentation. Another way is to use numerical modelling to optimize the packing density on the basis of the characteristics of the raw materials measured beforehand.

In experiments it is possible to approach the optimum packing of the grains iteratively, e.g. using the *Puntke* method [28]. However, without exact knowledge of the grading, and possibly the forms of all the particles, and without a numerical model in advance, this method is usually costly and often tedious.

The numerical grading optimization of fine particle combinations for UHPC and their principles have been described in detail in [29] and [30–32]. Most models are based on circular discs, some on spheres. A spheres-based model was used in [33], for example, in order to find a grading curve that enables optimum utilization of the space

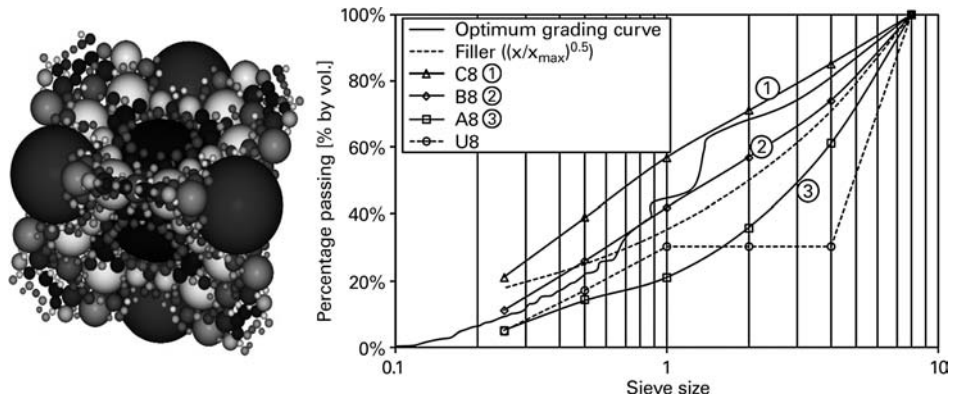


Fig. 2.4 Optimum positioning and sizes for a rhombohedral packing [34]

with grains of aggregate (Figure 2.4). The grading curve shows – as an important prerequisite for use in real UHPC mixes – that several individual grain size ranges are missing. It is this that allows the ‘filler particles’ to reach the spaces allocated to them within the ‘scaffold’ of larger particles.

Where large quantities of fine particles are involved, the form of the particles becomes more important. *Reschke* used empirical factors to take this into account [35]. The determination of the particle form with an optical instrument is described in [29]. Taking the particle form into account means that it is possible to make far better predictions of, for instance, the water requirement of a mixture of fine particles and hence how this influences the workability of a UHPC (in which the water content should hardly be varied if the density of the microstructure is not to be impaired).

Studies of the optimum composition of UHPC undertaken at the University of Kassel resulted in a calculation program. Based on the particle size distribution measured in a laser granulometer and, if applicable, taking into account the form of the fine particles determined in an optical photometer, the program determines the optimum volume proportions of the various ultrafine particles necessary for a high packing density [24, 29, 34].

The grading curve is divided into 120 fractions in this method of calculation. Each of these fractions is set against the other fractions and their influence on the packing density; in each case one fraction is taken as the scaffold, the other as the filling material. This results in more than 14 400 calculation steps. The fine division of the grading curve enables even smaller fluctuations (e.g. in gap grading) to be taken into account which could not be described with the standard values position parameter and slope. Figure 2.6 shows the result of such a calculation for the three fine-grained UHPC ultrafine components cement, W12 quartz powder and silica fume shown in Figure 2.5. More detailed information can be found in [24, 29].

By varying the volume proportions of the individual grains, the packing density rose from an initially low figure of 65% to more than 83%, i.e. the volume of pores could

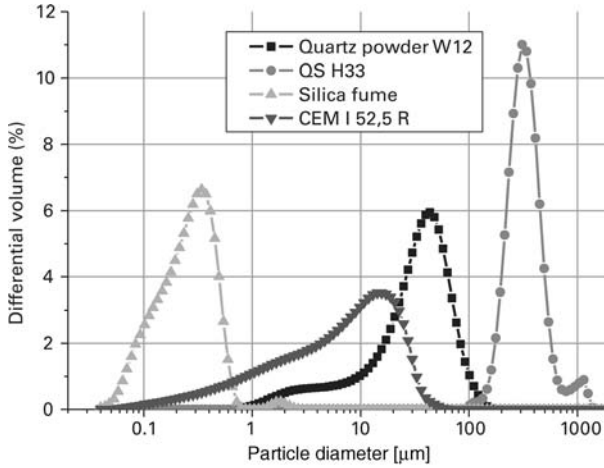


Fig. 2.5 Grading of raw materials for the calculated packing density optimization shown in Figure 2.6

be reduced from 35 to just 17% by vol. This not only increased the strength accordingly (see Figure 2.3), but also significantly reduced the amounts of water and superplasticizer required.

As in the past, the results of the calculations must be validated by experiments. Generally, the values do not agree fully with the pore volumes and packing densities

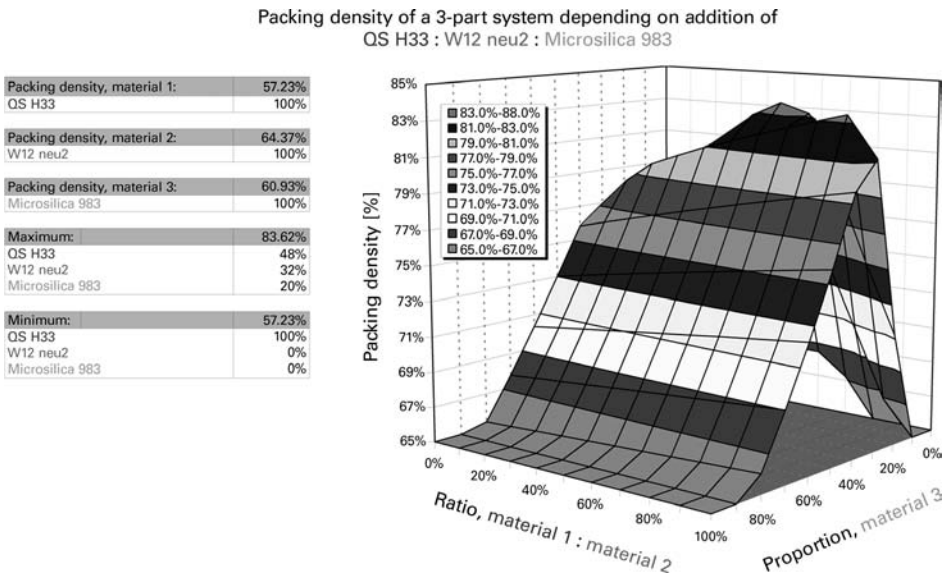


Fig. 2.6 Example of packing density optimization for a three-part system using an optimization program developed by the University of Kassel

determined experimentally using the *Puntke* method [28], for example. One of the reasons for this is the bonding of the water by the first products of hydration. Therefore, the calculated values must be adjusted using a correction factor for the chemical water bonding which is validated experimentally. This factor is in the order of magnitude of 10% of the calculated pore volume.

Workability, however, places limits on optimizing the packing density. On the one hand, with ever better packing density, the pores between the particles, which otherwise must be initially filled with rheologically inactive water, become smaller before water can function as a lubricant between the grains. On the other, the surface area of the filler materials to be wetted increases progressively with the fineness, and that in turn means more water is needed for wetting. In addition, the interparticle forces between the finest particles increase. They agglomerate to form larger ‘particles’ and therefore can no longer act as optimum filler materials as intended. Furthermore, the viscosity of the fresh concrete increases. Figure 2.7 shows the relationship between the principles of filling pores and viscosity using the simple example of two quartz powders with different degrees of fineness.

The conflict between maximum packing density on the one hand and the decrease in workability on the other can be resolved by adding a high-performance superplasticizer based on PCE (polycarboxylate ether). In order to guarantee a sufficient effect, the plasticiser must be selected within the scope of suitability testing; it must deagglomerate and liquefy adequately – not only the particular cement, but also all the other fine particles and especially the silica fume. Practical advice can be found in [36]. In the meantime, specially formulated multi-component superplasticizers with different active polymer components are available for UHPC (see also Section 2.3.4).

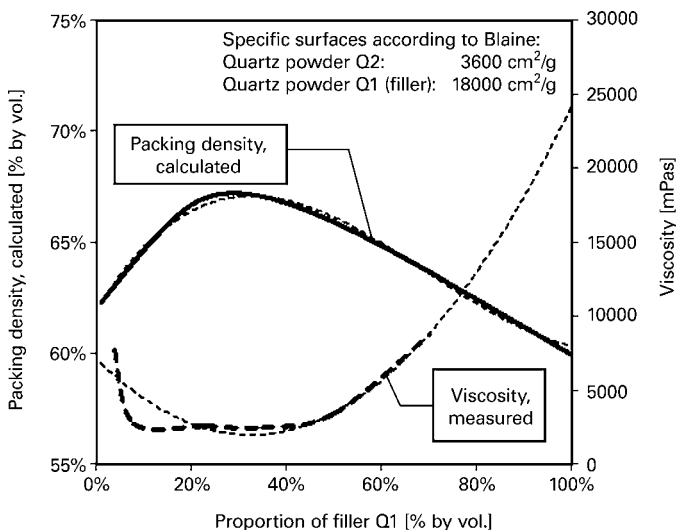


Fig. 2.7 Relationship between the packing density and workability of an inert paste made from two different fine quartz powders (Q1, Q2) when using superplasticizers ($w/F_m = 0.26$) [29]

2.3 Raw materials

2.3.1 Cement

The cements generally used for UHPC are CEM I low-alkali Portland cements of strength classes 42.5 R and 52.5 R according to DIN EN 196, preferably with a high sulphate resistance and low heat of hydration (HS/NA). These cements are advantageous because despite their high strength potential and despite the high cement content of fine-grained UHPC (700–850 kg/m³), the water requirement and the chemical shrinkage are limited and the possibility of an alkali-silica reaction is practically excluded. Nevertheless, when selecting the cement, the individual water requirement should still be considered because the flow behaviour and the amount of superplasticizer required in the UHPC also depend on this.

Blastfurnace slag cement CEM III/A is advantageous for UHPC components cured without heat and particularly at risk of temperature and shrinkage cracking, e.g. thin concrete pavements for roads, or for components exposed to chemicals, e.g. wastewater pipes [16, 17].

Even after intensive heat treatment at 80–90 °C, about 30% of the cement remains unhydrated as a result of the low water content. This is one reason for replacing some of the cement by rheologically similar quartz powder. On the other hand, the high potential for cracks to close themselves is based on this (see Chapter 4).

2.3.2 Reactive admixtures

2.3.2.1 Silica fume

Silica fume acc. to DIN EN 13263-1 [37] essentially functions physically as a micro-filler. According to [38], during UHPC heat treatment at approx. 80–90 °C it contributes partially to the formation of additional strength-forming hydrate phases. As shown in Figure 2.8 the microstructure is free of pores and practically impermeable. However, without heat treatment, the physical filler effect dominates. Figure 2.9

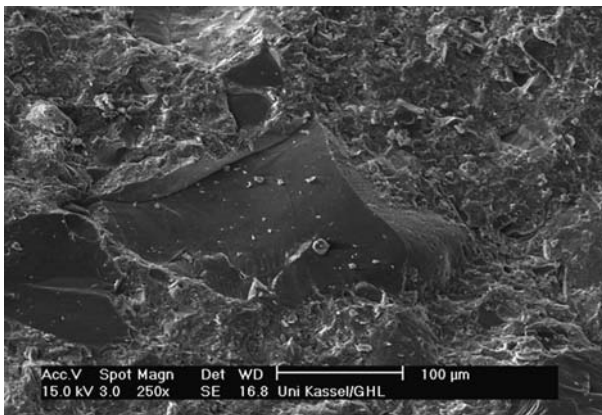


Fig. 2.8 Dense UHPC microstructure with angular aggregate particles

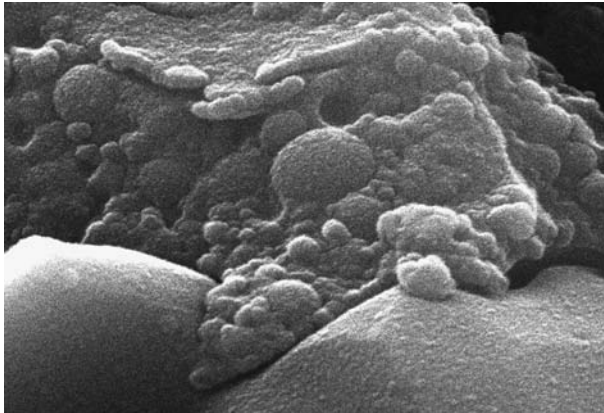


Fig. 2.9 Silica fume particles in a UHPC matrix

shows essentially unhydrated silica fume particles in a dense UHPC matrix. This might be one reason why UHPC stored in water generally exhibits a significantly lower compressive strength (10–20% lower). So far, the proportion of silica fume has been treated like cement with regard to its contribution to strength ($k = 1$), even though the amount used, with respect to the cement, often exceeds 20% by mass. Whether this is actually always justified requires further observation.

Owing to its large specific surface of $100\,000\text{ cm}^2/\text{g}$ and the high interparticle forces, silica fume is the main factor in the determination of water and superplasticizer requirements as well as the rheological properties of the fresh concrete [39]. It should consist of at least 96% by mass of amorphous SiO_2 and contain only little carbon since carbon increases the amount of water and superplasticizer needed. In addition, the quantity should certainly be limited to the minimum quantity required for filling the pores within the scope of the packing density optimization according to Section 2.2 because otherwise the concrete can become sticky and viscous. The superplasticizers used must be able to deagglomerate the usually agglomerated silica fume particles during the mixing process because otherwise all the considerations regarding packing density are meaningless.

2.3.2.2 Ground granulated blast furnace slag

The investigations of *Gerlicher* and *Heinz* [40] revealed that the water and superplasticizer requirements of a UHPC can be reduced further, while retaining the consistency, without having a negative effect on the strength if some of the CEM I is replaced by ground granulated blast furnace slag and the w/c ratio is reduced by the water saved. However, heat treatment caused the reaction of the granulated slag to stop prematurely. Pulverized fly ash (PFA) with particularly favourable rheological properties and a high proportion of spherical, amorphous particles can also be used to a limited extent as a reactive filler and hence as a cement replacement.

2.3.3 Inert admixtures

As a rule, various fine quartz powders are used to achieve the optimum packing of the combination of particles. The important factor is that they should undergo highly selective fractionation. As an example, a powder ground to a fineness of approx. $12\,000\text{ cm}^2/\text{g}$ and a powder with approx. $3\,600\text{ cm}^2/\text{g}$ (i.e. somewhat coarser than the cement used) were used in the investigations carried out within the scope of the German research programme and in other studies [27]. This enabled the ‘filler effect’ of the cement to be partially replaced and the ‘granular gap’ to the fine sand to be bridged over. Quartz powder exhibits a high grain strength on the one hand and, on the other, is readily available in a wide range of well-defined gradings with different degrees of fineness. By contrast, limestone is less suitable because of its lower strength and because the UHPC produced with it is generally even stickier, even more viscous.

2.3.4 Superplasticizers

Effective superplasticizers for UHPC are based on polycarboxylate ethers (PCE) [36]. Many different PCE superplasticizers are now available. However, most have to be optimized for their interaction with the different cements. Experience shows that for UHPC with a high quantity of silica fume, the superplasticizers that are particularly suitable are those that properly deagglomerate both the cement and the other fine particles [41]. Those superplasticizers include types consisting of two components with differently structured polymers. The quantity required to reach a certain consistency in an individual case also depends on the quantity of active substances in the superplasticizer, which, according to experience, lies between about 30 and 45% by mass. Recommendations on the exact amount of superplasticizer can be found in Section 2.4.

2.3.5 Steel fibres

Steel fibres are especially tightly integrated into the very dense, solid and homogeneous microstructure of the fine-grained UHPC matrix. High bond stresses can therefore be transferred. On the other hand, the effect that the fibres have on increasing the ductility is based on the fact that when the matrix ruptures, the static friction between matrix and fibres is overcome without the fibres breaking themselves. Short, slender fibres to DIN EN 14889-1 [42] with a diameter of max. 0.20 mm and length of 9–17 mm made from high-strength steel with a tensile strength $\geq 2000\text{ N/mm}^2$ have proved the best option, also for reasons of better workability. Particularly favourable is a length/diameter ratio of at least 65.

In areas of components potentially at risk of corrosion, stainless steel fibres can be advantageous when larger crack widths are expected (see Chapter 4). The same applies to fair-face concrete where fibres near the surface could rust, which, incidentally, does not affect the durability of the component.

Corrosion-resistant high-strength synthetic fibres, e.g. made from polyvinyl alcohol (PVA) with a modulus of elasticity of approx. $30\,000\text{ N/mm}^2$ and a tensile strength of approx. 1000 N/mm^2 , used alone or in combination with steel fibres, can be employed to

lend concrete the necessary ductility in less heavily stressed components [43]. See Section 3.10 for details of the effects of such fibre combinations.

2.4 Mix composition

Designing a UHPC mix begins with selecting and defining the ultrafine materials required to achieve an optimum packing density. The grading of the fine raw materials is evaluated with a laser granulometer unless the supplier has provided sufficiently accurate information. This is followed by the numerical optimization of the packing density and its experimental validation based on the combination of fine particles, e.g. using the Puntke method according to Section 2.2.2. The aim of this is to achieve a maximum water/fines ratio and at the same time low water and superplasticizer requirements [25]. In contrast to normal-strength concrete, the equivalent water/cement ratio (cement + silica fume) in the mix design cannot be varied because even a small increase beyond the value of about 0.20 (max. w/c ratio approx. 0.24) normal for UHPC leads to the formation of capillary pores, which reduce the characteristic imperviousness of the microstructure and introduce drying shrinkage in addition to autogenous shrinkage [44] (see Section 3.3). On the other hand, even a minor increase in the water content (but still within the aforementioned limits) can improve the effect of the superplasticizer.

Figure 2.1 shows examples of the volumetric composition of different UHPC mixes. The associated mass proportions per m^3 are given in Table 2.1.

2.5 Mixing

In practice, UHPC has been produced with twin-shaft batch mixers, pan mixers and planetary mixers with extra paddles and also intensive mixers. The prerequisite is a sufficiently high mixing energy in order to solubilize the high proportion of ultrafine particles and wet the particles adequately with water and superplasticizer. Single-shaft compulsory mixers are not usually capable of this. When using a pan mixer, it is important to ensure that no ultrafine materials accumulate on the walls and bottom of the mixer because this alters the formulation of the mix. Advantageous are mixers in which the rotational speed can be varied while mixing. Intensive mixers have proved to be particularly good at achieving homogeneous mixing of the combination of fine particles, especially for fine-grained UHPC and in both laboratory and practical applications.

As with normal-strength concrete, first of all the dry materials are put into the mixer – preferably any coarse aggregate first, then the fine powdery constituents – and premixed dry for between about 30 s and 2 min. When using a skip in a precasting plant, it is important to make sure that the free-flowing silica fume does not run out of the skip as it is being tipped. Next, the water plus the superplasticizer (mixed separately with the water beforehand) is added. The mixing time necessary to achieve a stable, workable consistency must be established in each individual case. Experience shows that it can lie between 3 and 15 min. and depends on the type of mixer and mixing action, the size of the batch, the degree of filling of the mixer, the temperature and, above all, the time the superplasticizer needs to produce the necessary fluidity.

Table 2.1 Mass-based composition of selected UHPC mixes.

	UHPC fine (0/0.5 mm) M2Q [45]	UHPC fine (0/0.5 mm) M3Q [46]	UHPC coarse (0/8 mm) B5Q [47]	UHPC roadbuilding [16]	UHPC no- slump [18]
	[kg/m ³]				
Water	166	183	158	107	49
Cement	832	775	650	404	186
Ultrafine granulated blast furnace slag	—	—	—	24	—
Silica fume	135	164	177	54	51
Superplasticizer dosage FMW/b [% by mass] ^{a)}	1.1	1.1	1.2	0.6	1.2
Quartz powder, fine	207	193	325	—	93
Quartz powder, coarse	—	—	131	32	38
Quartz sand 0.125/0.5	975	946	354	541	101
Quartz sand 0/2	—	—	—	—	616
Quartz sand 0.6/2	—	—	—	283	—
Gravel 2/8	—	—	—	—	821
Gravel 8/16	—	—	—	—	616
Basalt 2/8	—	—	597	1123	—
Micro-wire fibres	2.5% by vol.	2.5% by vol.	2.5% by vol.	1.0% by vol.	—

^{a)} Superplasticizer with respect to binder

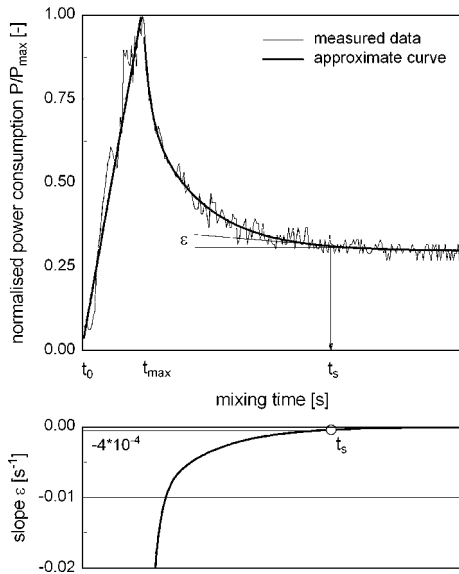


Fig. 2.10 Diagrams of the energy consumption of the mixer for UHPC up to reaching the target consistency (stabilization time t_s) [48]

Further, the mixing time depends on how long it takes to introduce the well-separated fibres into the fluid concrete and mix them in. It must also be ensured that the consistency desired for workability really is stable once mixing has ended and that no further fluidization takes place. The fluidization of the concrete can be speeded up by using a high mixing speed up to fluidization and then continuing to mix at a lower speed as the fibres are added. Figure 2.10 shows the typical energy consumption up to fluidization and until the stable target consistency is finally reached (stabilization time). Detailed information on the mixing of UHPC and how the ultrafine components and the concentration of solids affect the mixing time can be found in [48].

2.6 Curing and heat treatment

The curing of UHPC already begins during its production. As a consequence of its very low water content, the immediate surface dries very quickly and a dense, tough ‘elephant skin’ just a few tenths of a millimetre thick frequently already starts to form during the longer compaction time needed for UHPC. This prevents deaeration of the concrete and also prevents the surface from being levelled further. The skin can be avoided if open concrete surfaces are covered with plastic sheeting immediately after concreting, an effective curing agent is sprayed over the whole surface or water is applied as a fine mist to form a film on the surface.

Components made from UHPC are currently mainly produced in precasting plants. As a rule they are heat treated at about 80–90 °C, after which no more hydration takes place. The high temperatures cause the silica fume to react with the calcium hydroxide in the cement, and additional strength-formation phases ensue [38]. The compressive and flexural tensile strengths are therefore higher and the microstructure denser than

in the case of curing with water or sheeting. In addition, no further shrinkage takes place after the heat treatment and the precast elements are dimensionally accurate and free from shrinkage stresses. Generally, the components, or test specimens, are left in the mould for 24 h and covered with sheeting before being heated for 48 h. Heating for longer has no effect. During the heat treatment, the concrete should be covered airtight and thus protected against drying out completely. It is important to ensure that the components are allowed to cool slowly after the heat treatment, e.g. further storage covered in sheeting (also thermal insulation in the event of low temperatures), in order to prevent microcracks.

2.7 Testing

2.7.1 Fresh concrete

UHPC is produced and worked predominantly in an easy-flowing consistency. Owing to the high content of fine particles and superplasticizer, in the fresh state it is more similar, rheologically, to a self-compacting concrete (SCC) than a normal-strength concrete. However, owing to its high proportion of packing-optimized fine grains, it is more cohesive and more viscous. It flows much slower. Unlike SCC, it is not self-deaerating. Adequate deaeration requires sufficient vibration energy, which must continue for longer than with normal-strength concrete. This applies to both the production of test specimens and for large-scale pours.

Besides a flow table test acc. to DIN EN 12350-5, a slump-flow test acc. to DIN EN 12350-8 is the best way of illustrating the rheological behaviour. The combination of slump-flow measurement for flowability and t_{500} -time as an indirect measure of the viscosity describes the rheological properties of a particular mix more fully than the other DIN EN 12350 consistency testing methods. Figure 2.11 shows the distinctly

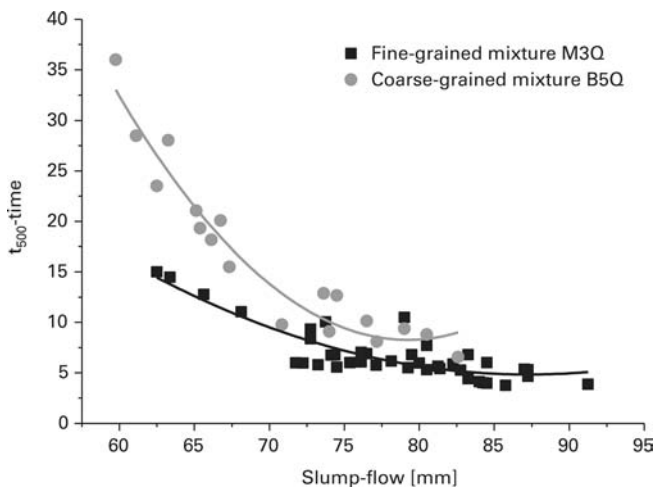


Fig. 2.11 Rheological properties of M3Q and B5Q mixes from Table 2.1 without and with 1.0 or 2.5% by vol. steel fibres, described by the slump-flow measurement SF and the t_{500} time [49]

different plots of both variables for the fine-grained (≤ 0.5 mm) and the coarse-grained (≤ 8 mm) mixes with and without fine steel fibres (1.0 and 2.5% by vol.) given in Table 2.1. Here, values measured decreased as the maximum grain size and fibre content rose, and the t_{500} -time increased. In coarse-grained mixes with fibres, this effect was especially apparent owing to the mutual influence of fibres and aggregate. The coefficient of variation (ratio of standard deviation to mean) was 0.02–0.07 when testing the M3Q mix under repeatability conditions for the slump-flow measurement, and 0.02–0.32 for the t_{500} -time [49].

The slump-flow classes of DIN EN 206-9 [50] can be used to assess the flow behaviour. Easy-flowing UHPC without fibres normally corresponds to consistency classes SF2 or SF3 depending on maximum grain size and composition, but often it is only possible to reach class SF1 with high fibre contents. On the other hand, the DIN EN 206-9 viscosity classes VS1 and VS2, with limits of < 2 s and ≥ 2 s respectively for the t_{500} -time, are not suitable criteria for UHPC, although, as Figure 2.11 shows, the t_{500} -time for fine-grained mixes lies between about 3 and 15 s depending on the flowability, and between about 10 s and as much as 30 s (e.g. for 2.5% by vol. steel fibres) for coarse-grained mixes. The final value of the slump-flow measurement is frequently only reached after more than 1 min.

The flow table test acc. to DIN EN 12350-5 is suitable for UHPC mixes with a plastic to very soft consistency (F2 to F4). The compaction test acc. to DIN EN 12350-4 is suitable for measuring the consistency of stiff-plastic mixes such as those used in roadbuilding. A slump test is not recommended because the concrete adheres to the slump cone.

The tendency of fibre-reinforced UHPC mixes to cause blockages in reinforced components can be assessed with the J-ring test acc. to DIN EN 12350-12 provided the content of short steel fibres does not exceed 2% by vol. To what extent the J-ring classes specified in [50] enable a proper assessment remains to be seen because experience with UHPC components with congested reinforcement is lacking.

One important criterion for the later compressive strength is the proportion of compaction pores remaining in the concrete. Owing to its viscous behaviour, UHPC deaerates more slowly than normal-strength or self-compacting concrete even with intensive vibration. Comparative tests across 10 institutes have shown that when testing with the 8 l capacity air entrainment metre according to the stipulations of DIN EN 12350-7, the air content can show a scatter of 1–6% by vol. for the same UHPC mix when neither the filling of the test equipment nor the vibration time/intensity are defined. This is one explanation for the fact that various institutes obtained significantly different compressive strengths for the same UHPC mix in some instances [47, 49].

As with normal-strength concrete, compaction ends when practically no more air bubbles appear on the surface. In very viscous mixes with a high fibre content, compaction times of up to 5 min. are necessary on a standard laboratory vibrating table. Owing to the much more distinct cohesive-elastic properties of fresh UHPC, lower frequencies and amplitudes than those used for compacting normal-strength concrete are generally more effective. The optimum setting of the compacting equipment must be tried out in each individual case.

During the pouring and compaction of the concrete it is important to make sure that no dry skin forms on the surface of the concrete. Ideally, testing equipment should be filled in a continuous flow with the vibrating table running and already covered during compaction. Incidentally, the same applies to the production of specimens for compressive and flexural tensile strength tests.

2.7.2 Compressive and flexural tensile strengths

UHPC's principal characteristic is its high strength ($>150 \text{ N/mm}^2$). However, so far there has been no unique definition of a compressive strength class for UHPC. In a similar way to DIN 1045-2, the 28-day compressive strength according to DIN EN 12390-3 could be used, tested on 150 mm dia. \times 300 mm high cylinders or 150 mm cubes stored in water. But the fact is that almost all UHPC structural elements are currently heat treated at 80–90 °C. The compressive strength of heat-treated UHPC is generally about 20–30 N/mm^2 higher than otherwise identical components stored in water (see also Section 2.3.2.1). In addition, it must be remembered that the setting of UHPC specimens stored in water is almost complete after 7–10 days because the dense microstructure does not allow any more external moisture to infiltrate the concrete in order to compensate for the internal drying-out due to hydration. These aspects should be taken into account when specifying the performance classes for the compressive strength of UHPC, e.g. in the form of different classes for UHPC with and without heat treatment. Until that happens, it will be necessary to define the desired 'compressive strength' sufficiently accurately in each individual case by including the test specimen dimensions, type of storage and age at testing in the specification.

The same information given for testing the air content in Section 2.7.1 applies to the production of the test specimens. If a larger number of test specimens is to be produced, then making several smaller batches is the better method so that fresh concrete can be used each time. Internal concrete vibrators are unsuitable for compacting test specimens with fibres because they upset the uniform distribution of the fibres in the concrete and can cause an irregular orientation (spaces for vibrator).

Two round robin tests within the scope of the German research programme [49] established that the flatness of loaded surfaces had a significant influence on the measured compressive strength. Even the very smallest unevenness, in the μm range, can lead to load being concentrated at a point; the measured compressive strength for the same UHPC can drop by up to 20–30 N/mm^2 as a result. Round robin tests involving several institutes also revealed that highly precise grinding and polishing of the loaded surfaces can reduce the standard deviation, e.g. for the coarse-grained UHPC B5Q mix to Table 2.1, from 7.4 N/mm^2 (grinding on various machines with different precision) to just 1.0 N/mm^2 when all test specimens were processed on the same precision grinding machine.

UHPC testing machines must comply with the requirements of DIN EN 12390-4 class 1. In addition, it must be ensured that the permissible pressure of the platens per unit area is not exceeded. Testing is generally carried out with load control to DIN EN 12390-3. Low- or zero-fibre UHPCs fail abruptly without cracking upon reaching their maximum load. Protective measures must therefore be provided, e.g. an unbreakable protective

collar around the test specimen. Testing with displacement control is required when determining the post-peak stress–strain curve of a UHPC with fibres. A strain rate as low as possible (in the order of ≤ 0.05 mm/s) should be selected up to reaching the maximum load in order to limit the unavoidable drop in stress that occurs in most machines, even with specimens including fibres, when the matrix ruptures.

The flexural tensile strength of fibre-reinforced UHPC can be determined in either a four-point bending test on unnotched beams ($700 \times 150 \times 150$ mm) based on the DAfStb guideline for steel fibre-reinforced concrete [51] or a three-point bending test on notched beams ($550 \times 150 \times 150$ mm) according to DIN EN 14651 [52] or RILEM TC 162-TDF [53]. In all cases the underside during casting should also be the underside during testing (see also Section 3.3.2). In the four-point bending test, the post-cracking flexural tensile strength at deflections of 0.5 and 3.5 mm should be taken as a measure of the effectiveness of the fibres. The three-point bending test to DIN EN 14651 is preferred when the load–cracking relationship is of interest. It is used to calculate the residual flexural tensile strength. Disruptions to the edge zone, e.g. following heat treatment of the test specimens, are ignored by notching the underside for testing.

The results of tensile and flexural tensile tests on UHPC with fibres essentially depend on the distribution and orientation of the fibres in the concrete. The production of the test specimen has a considerable influence on this. For an easy-flowing consistency, the recommendation is to allow the concrete to flow into the mould freely from one side with the vibrating table switched on. This allows the fibres in the centre of the beam to be aligned distinctly in the longitudinal direction and hence in the direction of the tensile stresses. At the same time, this considerably reduces the scatter of the results for a series of test specimens, as can be seen in Figure 2.12. In the case of coarse-grained UHPC, a

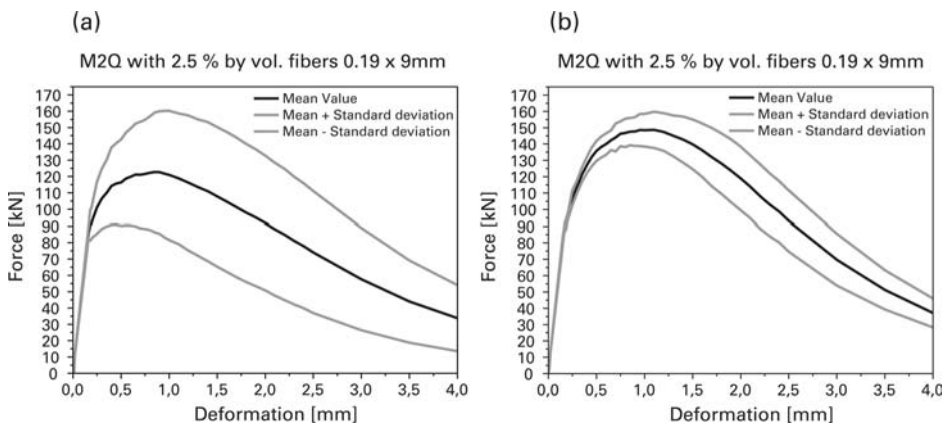


Fig. 2.12 Median and scatter of force–deformation curves for the same easy-flowing UHPC with 2.5% by vol. steel fibres, $L/D = 0.19/9$ mm, measured on $700 \times 150 \times 150$ mm beams in accordance with [51]: a) unregulated filling of the mould, b) allowing the concrete to flow from one side of the mould on the (operating) vibrating table

much lower degree of alignment can be expected because the movement of the fibres is restricted by the coarse particles.

The fibre orientation in the hardened concrete can be ascertained with photo-optical [54, 55] or magnetic methods or by means of X-ray computed tomography [56]. In addition, a distinct scale effect must be taken into account in the flexural tensile tests. It can be seen from [11] that when testing fine-grained UHPC using $160 \times 40 \times 40$ mm prisms, a value approx. 1.5 times greater can be expected for the flexural tensile strength than when testing $700 \times 150 \times 150$ mm beams.

The sensitivity of the testing machine also has a considerable influence on the resulting flexural tensile strength. The increase in deformation is generally controlled via sensors attached to the middle of the beam. At the moment of the first crack in the matrix, a sudden drop in stress can occur which, depending on the degree of deformation and the sensitivity of the sensors, can lead to a severe scattering of the results within a series of tests. This in turn has an effect on the performance classes determined in accordance with the DAfStb guideline, which include the coefficient of variation. The evaluation of a round robin test carried out within the scope of the German research programme [49] resulted in a coefficient of variation between 0.15 and 0.4 for calculating the post-cracking flexural tensile strength at a deflection of 3.5 mm on each of six tested beams made from fine-grained UHPC with 2.5% by vol. 0.19×9 mm steel fibres. Accordingly, the values for performance class 2 determined in the institutes taking part were very different, ranging from 0 to 4.7.

3 Mechanical properties of the hardened concrete

3.1 General

Owing to its dense microstructure, ultra high performance concrete (UHPC) has both a high strength and also a greater stiffness (expressed by the modulus of elasticity) when compared with normal- and high-strength concretes. It is well known that the behaviour of concrete becomes more brittle as its strength increases. This effect is particularly evident with UHPC. However, this disadvantage can be countered effectively by adding fibres, e.g. high-strength steel fibres, which bring about a considerable improvement in the post-peak behaviour in compression and tension, and that in turn means a more favourable response generally and better warnings when failure is pending. Further, the utilizable strength can be increased, especially for tension actions. Compared with the brittle matrix, activating the fibres (basically a form of reinforcement) can also help UHPC handle tension more reliably. Various mechanical properties of the hardened concrete are discussed below in so far as they are relevant, also with respect to the influence of adding fibres. However, the local distribution of the fibres and their orientation must always be considered, see Section 2.7.2. Some of the information below is drawn from the state of the art report on UHPC [22].

3.2 Behaviour in compression

3.2.1 UHPC without fibres

UHPC, compared with normal- and high-strength concrete, is characterized by the fact that, in a uniaxial compression test, it exhibits an essentially linear elastic behaviour for a relatively long time – until shortly before reaching its compressive strength and before the formation of microcracks signal the transition to failure. This effect has been observed essentially irrespective of the maximum grain size. The modulus of elasticity generally lies in the range 45–55 GPa. Adding bauxite can increase this figure significantly, to approx. 70 GPa. Without fibres, brittle failure is the result (see Figure 3.1), which in compression tests – as described in Section 2.7.2 – is very often in the form of a sudden, explosive failure. A similar effect has been observed in UHPC from values as low as about 90 N/mm^2 .

The addition of fibres has very little influence on the ascending portion of the stress–strain diagram. The increase in strength with typical fibre contents of up to approx. 2.5% by vol. is of minor importance, likewise the influence on the modulus of elasticity. However, this and the strain upon reaching the strength clearly depend on the grading of the aggregate. In the case of fine-grained concretes with max. 2 mm particle size, we can typically expect 4.0–4.4% [57, 58], whereas in coarse-grained concretes, figures in the region of 3.5% have been observed.

Generally, the value of the modulus of elasticity of UHPC is underestimated by the equations given in DIN 1045-1 and CEB-FIP Model Code 90 [59]. Following tests carried out at the University of Leipzig [58], the following relationships between the modulus of elasticity E_c and the cylinder compressive strength f_c have been proposed for

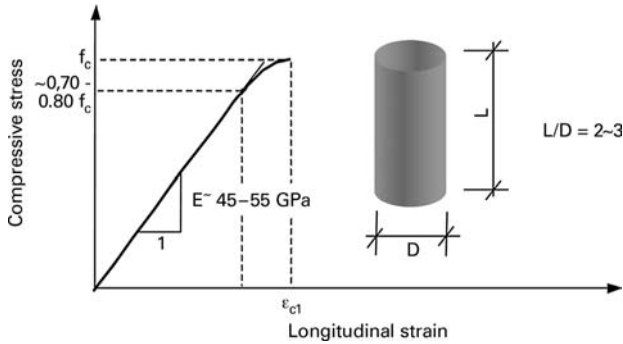


Fig. 3.1 Stress–strain diagram for UHPC without fibres in a uniaxial compression test

fine- and coarse-grained UHPC (see Figure 3.2):

$$\text{Fine-grained UHPC:} \quad E_c = 8800 \cdot f_c^{1/3} \quad (3.1)$$

$$\text{Coarse-grained UHPC with basalt chippings:} \quad E_c = 10\,200 \cdot f_c^{1/3} \quad (3.2)$$

with E_c and f_c in N/mm^2 .

As in EN 1992 [61, 62] and DIN 1045-1,

$$f_c = f_{ck} + 8 \text{ [N/mm}^2\text{]} \quad (3.3)$$

can be assumed.

Poisson's ratio ν was found to lie between 0.18 and 0.19 for fine-grained UHPC in the elastic zone [60] and to be approx. 0.21 for coarse-grained UHPC (basalt chippings with max. 5–8 mm particle size). It is therefore very similar to the figure of 0.2 typically assumed for normal-strength concrete. As can be seen from the stress–strain diagram, a departure from the linear elastic response takes place fairly late due to the formation of microcracks, which is reflected in the late rise in Poisson's ratio (see Figure 3.3). At failure, $\nu = 0.3$ can be assumed unless more accurate data is available for the respective mix.

3.2.2 UHPC with steel fibres

The addition of high-strength steel fibres can bring about a distinct improvement in the post-peak structural behaviour. However, this has hardly any effect on the ascending portion of the stress–strain curve. By contrast, the descending portion of the curve is influenced to a great extent by the following parameters:

- Fibre content
- Fibre geometry (length, diameter), also when compared with the maximum particle size
- Fibre orientation
- Bond between fibre and matrix (surface properties, any profiling, etc.)
- Stiffness of the fibres, specifically in combinations of different fibres.

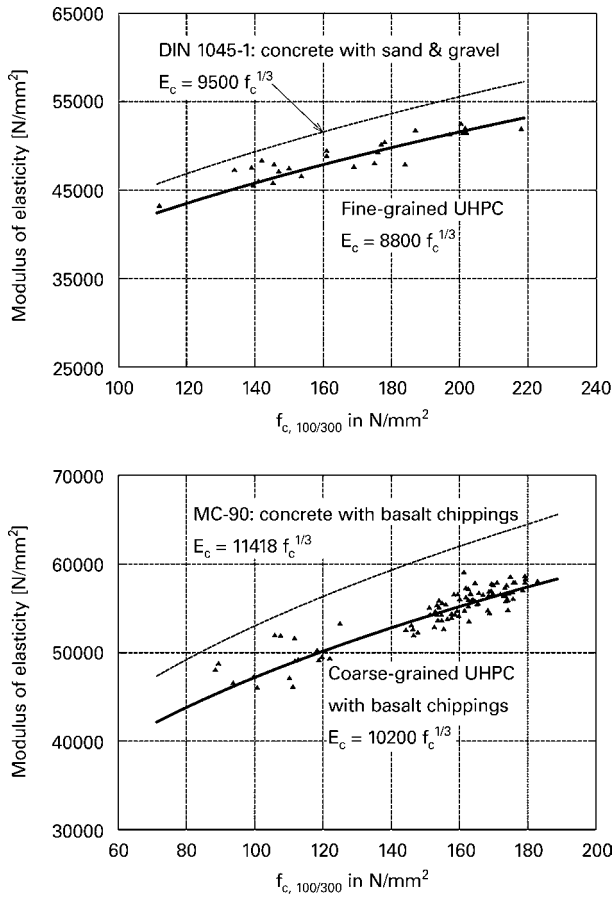


Fig. 3.2 Relationship between modulus of elasticity and cylinder compressive strength [22]

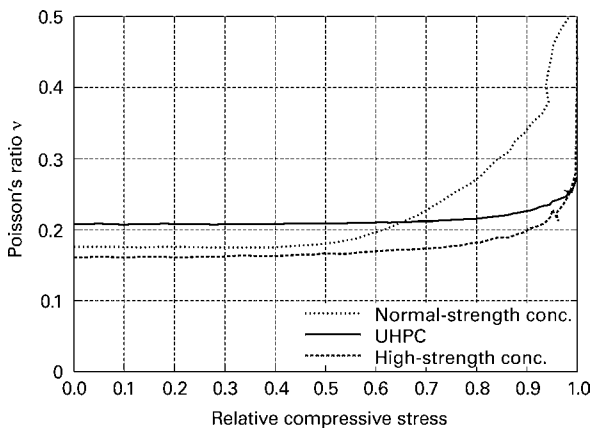


Fig. 3.3 Development of Poisson's ratio ν as the compressive stress increases [22]

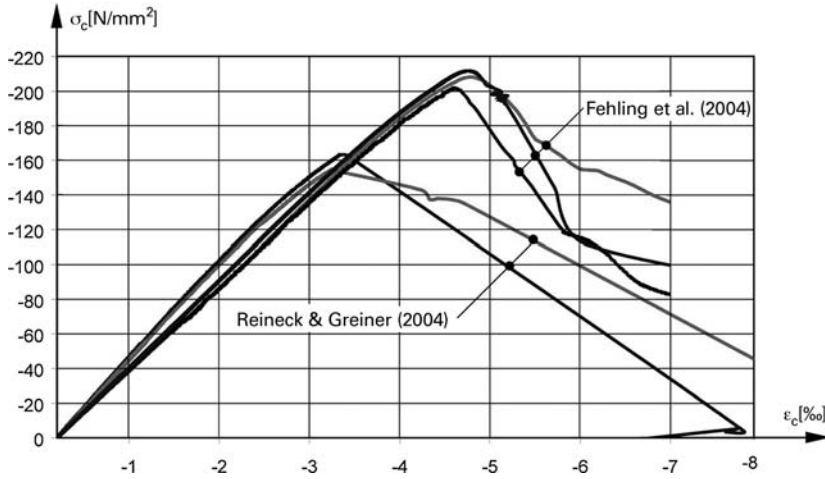


Fig. 3.4 Compression stress–strain relationships for UHPC with fibres [22, 63]

It is, however, hardly possible to predict the course of the descending portion of the stress–strain curve by means of simple relationships. Therefore, appropriate laboratory studies are generally necessary for a certain UHPC. It should also be remembered that the fibre content and fibre orientation in a component can vary locally and be influenced by concreting activities. During concreting, the large majority of the fibres is aligned with the direction of flow, primarily parallel with any nearby formwork surface. As an example, Figure 3.4 shows a number of measured stress–strain curves for Ductal® [63] (measured on $200 \times 100 \times 100$ mm prisms) and according to [11] (measured on $300 \times 150 \times 150$ mm cylinders). The figure clearly shows how the post-peak behaviour can be considerably improved and controlled by adding fibres. However, the measured stress–strain curves for the post-peak range (descending portion of curve) exhibit much more scatter than the ascending portion. This is illustrated schematically in Figure 3.5.

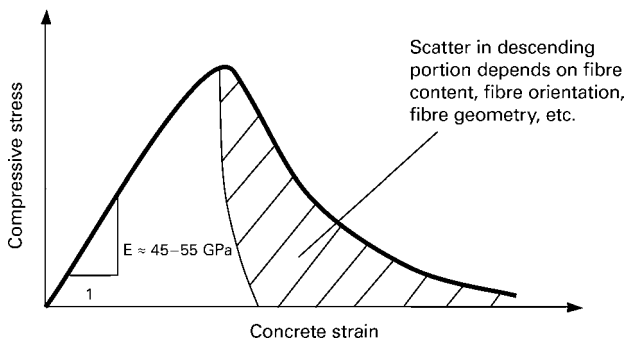


Fig. 3.5 Compression stress–strain diagram (schematic) for UHPC with variation in the behaviour in the descending portion depending on fibre content, fibre type and fibre orientation [22]

Up to about 2% by vol. fibres, no significant influence on the compressive strength was observed. According to [11], a rise in the compressive strength amounting to approx. 15%, compared with an otherwise identical mix without fibres, was noted at a content of 2.5% by vol.

3.2.3 Further factors affecting the compressive strength

3.2.3.1 Geometry of test specimen and test setup

The results available regarding the influences of the test specimen geometry are inconsistent. From the mechanics of materials viewpoint, it is the way the loading platens restrict the lateral strain that is responsible for this. Normally, cylindrical specimens with a slenderness ratio (height/diameter) of 2 should be used to determine the compressive strength. The diameter should be at least 100 mm. The French guideline [64] recommends cylinders with dimensions of 70 mm dia. \times 140 mm high or 110 mm dia. \times 220 mm high.

Quite often, the high strength of UHPC means that the test specimen dimensions have to be chosen to suit the capacity of the testing machine. In the case of UHPC without fibres in particular, it is especially important that the surfaces of the specimen are exactly parallel and that stress concentrations due to misalignment or deformation of the loading platens are avoided.

3.2.3.2 Heat treatment

Curing with the help of heat can increase the strength of UHPC and accelerate the strength development. Temperatures of approx. 80–90 °C are typical, which are applied for 1–2 days. According to [11, 25, 65], heating at only 90 °C for just 48 h leads to higher strengths than storing in water for 28 days at 20 °C. Heat treatment at 250 °C influences not only the reaction rate of the setting process, but also leads to the formation of other mineral phases and hence to a change to the microstructure that results in much higher strengths being reached.

3.3 Behaviour in tension

3.3.1 Axial (concentric) tension loads

Axial tension tests represent a direct way of shedding light on how UHPC behaves in tension. Tests on unnotched specimens are suitable for determining the tensile strength, whereas tests on notched specimens are more appropriate for determining the stress–crack width relationship of fibre-reinforced UHPC. The latter is regarded as characteristic for the response of brittle materials or materials with a softening post-peak behaviour. Typical tensile strength values for UHPC lie in the range 7–11 N/mm². *Fehling et al.* [11] and *Tue/Dehn* [60] did not observe any significant differences between fine- and coarse-grained concretes without fibres. However, the tensile strength is mainly influenced by the addition of silica fume to the mix.

Without fibres, very brittle failure can be expected in tension. It is therefore very difficult to measure any stable descending portion in the force–deformation diagram,

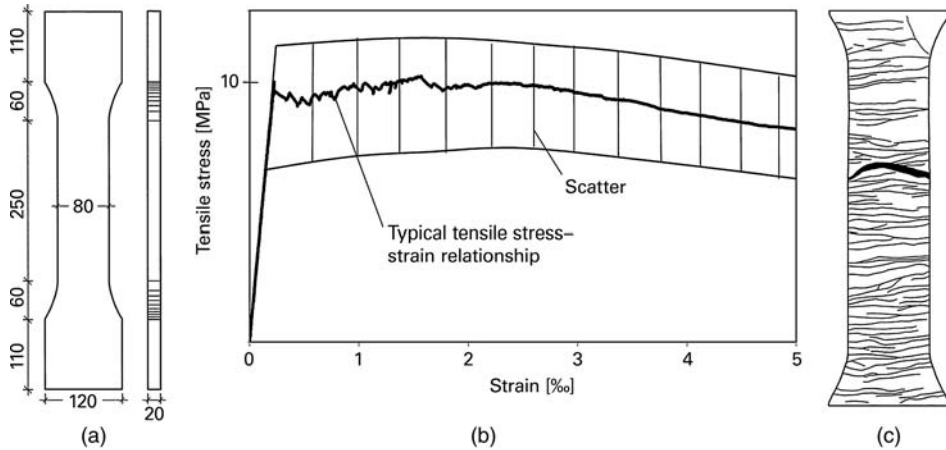


Fig. 3.6 Stress–strain diagram for axial tension for UHPC containing fibres with an initially strain hardening behaviour (Ductal[®], fibre content 2% by vol., after [63]); (a) dimensions, (b) Stress–strain diagram, (c) crack pattern. (Note: $\varepsilon = 1\text{‰}$ corresponds to approx. 0.2 mm elongation)

or stress–crack width diagram. Owing to the high strength of the matrix, cracks typically run through the grains of aggregate as well, and the edges to cracks are very smooth, which means that the interlocking effects typical of normal-strength concrete are virtually absent in UHPC. Therefore, up until complete separation of the crack edges, the specific fracture energy per unit area G_F required is only in the order of magnitude of 50 N/m (fine-grained UHPC) to 100 N/m (coarse-grained UHPC) [66].

However, the addition of fibres results in a higher tensile strength on the one hand and the ability to transfer forces across much wider cracks on the other. The fibres bridge over the cracks in this situation and are able to transfer some of the tensile strength of the matrix, or even higher stresses in favourable conditions. This situation occurs when sufficient numbers of high-strength fibres with a favourable orientation are available. An increase in strength is then possible with respect to the first crack in the matrix, i.e. a strain hardening behaviour is observed (see Figure 3.6). Figure 3.7 shows the development of the stress as the crack widens for cases with a softening behaviour. The dependence of the post-cracking behaviour on the addition of fibres is illustrated in Figure 3.8. In principle, it involves the same parameters as those that determine the post-peak response for compression actions (see above).

Leutbecher [68] has described and carried out further studies of the load-carrying mechanism in cracked fibre-reinforced UHPC. Figure 3.9 shows the results of tests in which the crack widths in notched prisms were measured very accurately. It can be seen that after the matrix cracks, there is initially a drop in the force (concrete stress at crack, for cracks $< 50 \mu\text{m}$ wide) followed by a rise as the steel fibres are activated. Following full activation of the load-carrying effect of the fibres, pull-out of the fibres begins beyond a certain crack width w_0 (from approx. 0.15 mm in this case), with a decrease in the force carried by the fibres.

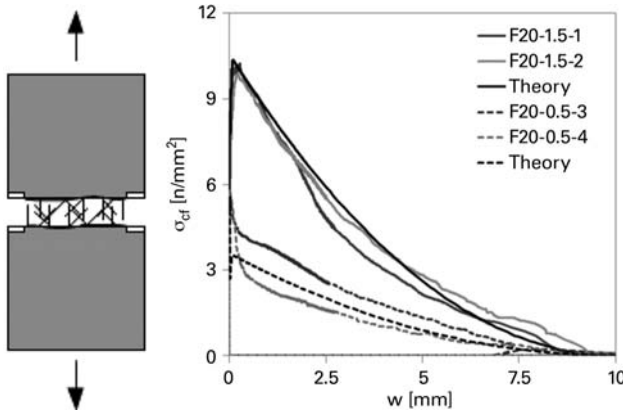


Fig. 3.7 Stress–crack width relationships for fibre contents of 0.5% by vol. without strain hardening behaviour and 1.5% by vol. with an initially strain hardening behaviour; test data for 20 mm long fibres and derived theoretical curve according to Equation 3.5 [67]

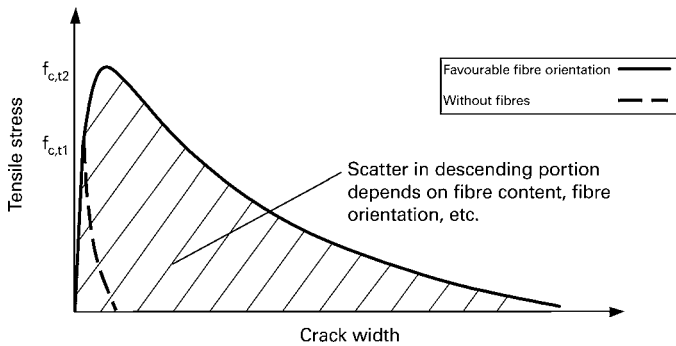


Fig. 3.8 Typical stress–crack width behaviour of UHPC in a tensile test

As long as the force, or stress, possible at full fibre activation exceeds the tensile strength of the matrix (outside the region where the fibres transfer the load), so further cracks can form and strain hardening behaviour is possible. As the crack width increases, so the fibres are pulled out more and more and their embedment length is reduced, which leads to a drop in the force that can be carried by the fibres. What typically happens in an axial tensile test is that one crack opens wide and the stress that can be accommodated drops so that other points along the bar are relieved. Localized deformations are the result. This can limit the ductility considerably in the case of long components.

The crack opening behaviour observed experimentally is explained further in Figure 3.10 and by means of the model described in the following. As the concrete matrix softens (in the figure assumed, for simplicity, to be linear with the concrete stress decreasing as the crack widens), so the load-carrying effect of the fibres is mobilized more and more. If we assume that the bond between the fibre and the matrix has already

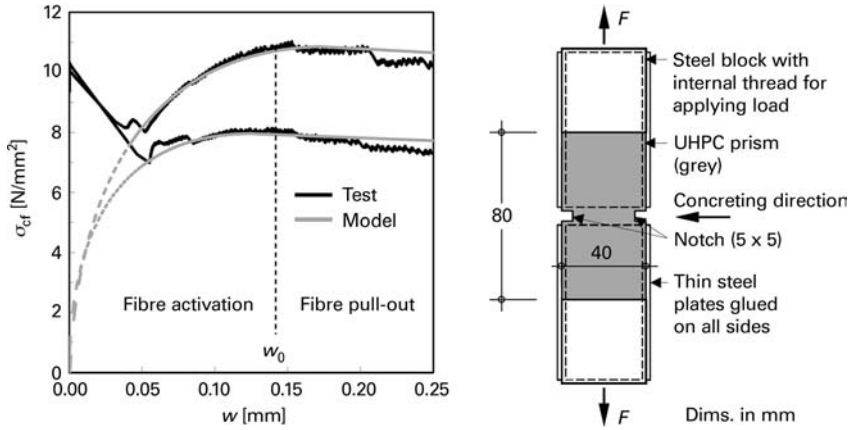


Fig. 3.9 Phases of the load-carrying behaviour: following matrix softening, fibre activation followed by fibre pull-out, illustrated for two different fibre efficiency values [68]

been overcome, then slip starts to occur over a successively longer length of the fibre and frictional bond stresses are mobilized. This results in a rise in the force carried by the fibres in accordance with a root function up until the maximum possible embedment length is activated:

$$\sigma_{cf} = \sigma_{cf0} \left(2 \sqrt{\frac{w}{w_0}} - \frac{w}{w_0} \right) \tag{3.4}$$

where

- σ_{cf0} fibre efficiency
- w current crack width
- w_0 crack width upon reaching fibre efficiency.

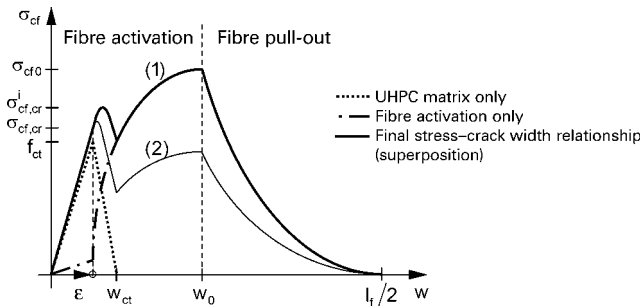


Fig. 3.10 Example of the superposition of matrix softening and fibre activation [68] (1) Fibre-reinforced UHPC with hardening behaviour following formation of first crack ($\sigma_{cf0} > \sigma_{cf,cr}^i$) (2) Fibre-reinforced UHPC with softening behaviour following formation of first crack. ($\sigma_{cf0} < \sigma_{cf,cr}^i$)

A constant frictional bond stress is presumed here (rigid-plastic bond). The gross concrete stress currently transferred by the fibres is σ_{cf} , and σ_{cf0} is the fibre efficiency, i.e. the maximum gross concrete compressive stress made possible by the fibres. This expression is based on the work of *Pfyl* [69] on the modelling of fibre-reinforced concrete. The term ‘post-cracking strength’ is also common, which originally comes from fibre-reinforced normal-strength concrete, where the effect of fibres added in typical amounts is generally insufficient to keep the stress at the level of the tensile strength of the matrix. Figure 3.10 also shows that by superposing matrix softening and fibre activation, which results in a severe increase in stresses for small crack widths, a maximum stress $\sigma_{cf,cr}^i$ can exist. Similar behaviour was observed by *Holmberg* [70, 71], who was able to establish a more severe rise in the cracking force in heavily reinforced concrete tension members than can be explained by the ratio between the ideal and the net cross-sectional areas.

For a fibre that crosses the crack at a right-angle at half its length, the maximum available embedment length is equal to half the length of the fibre l_f . This is called the model fibre in the following. As a crack opens further, so the model fibre begins to be pulled out of the matrix. The consequence of this is a linear decrease in the fibre stress over the remaining pull-out distance (slip), with the bond stress on the fibre surface presumed to be constant. If we assume that the embedment length on one side is minimally smaller than that on the other, so the fibre will pull out from the shorter side, while remaining anchored in the matrix on the somewhat longer side. So the limit case, the point at which the fibre no longer has any effect, is for a crack width equal to half the length of a fibre, i.e. $\sigma_{cf} (w = l_f/2) = 0$.

However, in the case of fibre-reinforced concrete it is not just the behaviour of the model fibre that is decisive, but rather the behaviour of all the fibres that cross the crack at various angles and with various embedment lengths on both sides of the crack. Therefore, as the fibres begin to be pulled out, there is a considerable drop in force as the crack widens, whereas at large crack widths, many fibres have already been fully pulled out from one side of the crack. So at large crack widths, no great changes to σ_{cf} are to be expected. This can be expressed by a quadratic decrease in the gross concrete stress σ_{cf} as the crack widens, which is attributed to the fibre efficiency:

$$\sigma_{cf} = \sigma_{cf0} \left(1 - \frac{2w}{l_f} \right)^2 \quad (3.5)$$

Equations 3.4 and 3.5 are found in the studies of *Li* [72], *Pfyl* [69], *Behloul* [73, 74], *Jungwirth* [75] and *Leutbecher* [68], and are valid for fibre-reinforced concrete in general but fibre-reinforced UHPC in particular. It has been shown that the stress–crack width relationship originally derived for fibres exclusively aligned in the tension direction, and hence the form of the curve shown in Figure 3.10, also applies, in principle, to the effect of all the fibres crossing the crack at any angle. However, the value of the fibre efficiency σ_{cf0} must be adjusted accordingly, which is best carried out on the basis of test results.

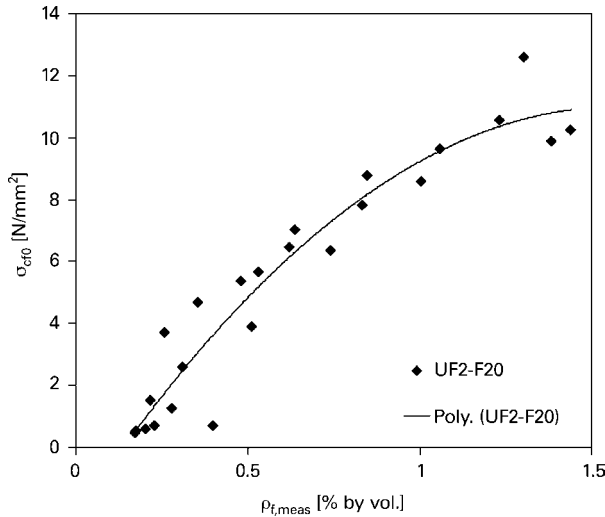


Fig. 3.11 Fibre efficiency plotted against fibre content measured using optical analysis (fibres $l_f/d_f = 20/0.25$ mm) [67]

Test results from Delft [76] and Kassel [68, 77] prove that the fibre efficiency changes little in the range of a $0\text{--}60^\circ$ deviation from a normal to the crack. This can be explained by the fact that the fibres in the crack become aligned in the deformation direction as the crack widens and are bent at the edges of the crack. The additional friction as a result of the contact pressure between the surface of the fibre and the matrix in the region of the bend can even result in a higher stress being possible provided the matrix has not been damaged by local spalling. The latter also seems to play a role with respect to the disproportionate increase in the fibre efficiency as fibre content increases (see Figure 3.11).

3.3.2 Flexural tensile strength

Flexural tensile tests are often preferred for determining the tensile strength properties because they are also easily carried out with a compression testing machine and do not require any elaborate arrangements to introduce the load. Section 2.7.2 contains advice on the production of test specimens and testing.

Tests carried out in Kassel [25] with unnotched specimens made from UHPC without fibres established that the flexural tensile strength for prisms measuring $160 \times 40 \times 40$ mm can reach $13\text{--}17$ N/mm², whereas the same mix only reached values of $7\text{--}10$ N/mm² for beams in bending measuring $700 \times 150 \times 150$ mm [11, 78]. A significant scale effect can therefore be observed, which in the first place can be attributed to fracture mechanics effects.

When fibres are added, the behaviour after crack formation is on the whole less brittle, almost plastic, which leads to a more favourable distribution of flexural stresses. A higher measured flexural tensile strength $f_{ct,fl} = M_u/W$ is the result. Depending on the

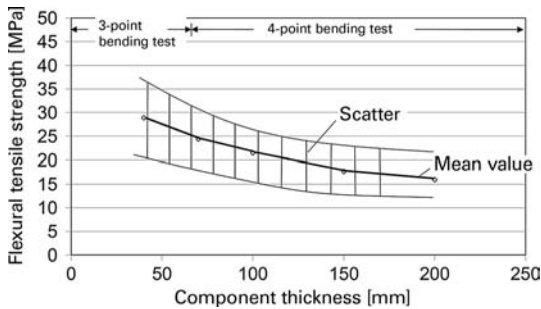


Fig. 3.12 Relationship between flexural tensile strength and component thickness for UHPC with 2% by vol. fibre content, $f_{ck} = 160\text{--}180\text{ N/mm}^2$ (after [79])

mix, values in the range $15\text{--}40\text{ N/mm}^2$ have been measured. Here, the influence of the fibre orientation due to the proximity of formwork surfaces, which can have a noticeable effect on test specimens with small dimensions, is superposed on the scale effect due to fracture mechanics.

For prisms with a square cross-section, Equation 3.6 expresses this relationship for the results on which Figure 3.12 is based:

$$f_{ct,fl} = 15 \cdot \left(\frac{200}{h}\right)^{0.45} \quad \text{for } h \leq 200 \text{ mm} \quad (3.6)$$

where

h thickness of test specimen (square cross-section) [mm]

$f_{ct,fl}$ flexural tensile strength [N/mm^2].

Also conceivable in principle is transferring this relationship to other fibre-reinforced UHPCs provided the tensile strength is scaled to suit the particular component thickness.

Determining the flexural tensile strength is best carried out with unnotched test specimens; notched specimens are suitable for determining the stress–crack width relationship. The French guideline [64] recommends the following when determining the tensile strength properties of UHPC:

- Four-point bending tests on unnotched specimens for determining the flexural tensile strength. The axial (concentric) tensile strength can be determined with the help of a correction factor to take account of the scale effect.
- Three-point bending tests on notched specimens for determining the contribution of the fibres in a cracked cross-section. The French guideline also specifies a method for backward identification in order to back-calculate to a stress–crack width relationship.

Prisms with a square cross-section are recommended in the French guideline, with a length equal to four times the cross-section thickness ($L = 4a$). The span should be $3a$. The thickness of the zone with the fibre orientation preferably parallel with the edge

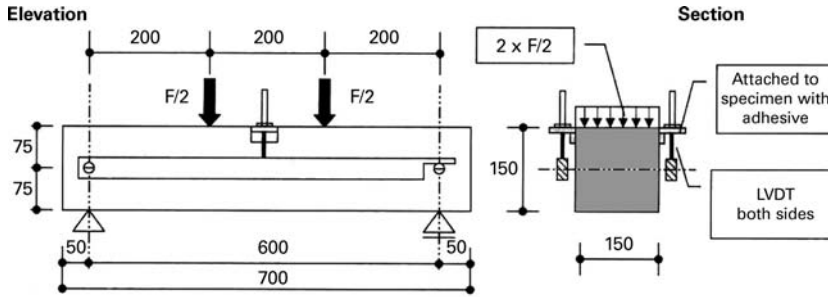


Fig. 3.13 Standard test according to DAfStb guideline for steel fibre-reinforced concrete [51]

increases with the fibre length l_f , so the choice of specimen thickness depends on this, and the recommendations are:

- 280 × 70 × 70 mm prisms for $l_f \leq 15$ mm
- 400 × 100 × 100 mm prisms for $15 < l_f \leq 20$ mm
- 560 × 140 × 140 mm prisms for $20 < l_f \leq 25$ mm
- Prisms with width and height $a > 5 l_f$ for $l_f > 25$ mm

The DAfStb guideline for steel fibre-reinforced concrete [51] uses a four-point bending test with beam dimensions of 700 × 150 × 150 mm ($L \times W \times D$) (see Figure 3.13).

When it comes to the residual tensile strength, the evaluation of the tests according to the DAfStb guideline is based on conversion factors that permit the concentric post-cracking tensile strength to be estimated from the post-cracking flexural tensile strength. As cross-section thicknesses much smaller than 15 cm are very common for UHPC, the use of correspondingly thinner test specimens is sensible in these cases. The influence of the fibre orientation parallel with the formwork in the perimeter zones is very important for the flexural tensile strength in particular.

The interaction of fibres with different geometries or made from different materials (e.g. PVA instead of steel) in ‘fibre cocktails’ can have advantages when it comes to the flexural tensile strength and the fracture energy. Fibres that are activated in different deformation ranges can usefully complement each other [43, 76, 78, 80]. For example, PVA fibres with their lower strain stiffness are effective at greater crack widths, whereas steel fibres are already active at small crack widths (Figure 3.14), see also Section 3.10.

3.3.3 Derivation of axial tensile strength from compressive strength

EN 1992 specifies more cautious relationships for concretes with a higher strength (C50/60 and higher) than for normal-strength concretes. However, the results obtained for UHPC so far justify the use of the following relationships:

$$f_{ctm} = 0.3 \cdot f_{ck}^{(2/3)} \quad (3.7)$$

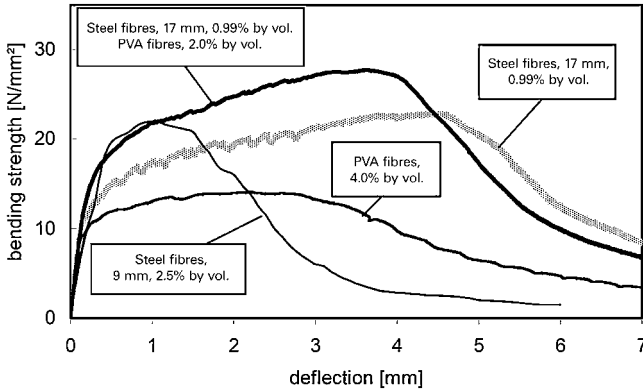


Fig. 3.14 How steel and PVA fibres interact and influence the post-cracking behaviour [78]

and

$$f_{ctk,0.05} = 0.7 f_{ctm} \quad (3.8)$$

as for normal-strength concrete. The tensile strength determined in this way is related to the tensile strength of the matrix. In fibre-reinforced concrete with a sufficiently large fibre content, however, the fibre efficiency can lie well above the tensile strength of the matrix.

3.3.4 Derivation of axial tensile strength from bending tests

The French guideline [64] uses a slightly modified relationship taken from Model Code 90 to derive the axial tensile strength from the flexural tensile strength:

$$f_{ct} = f_{ct,fl,el} \cdot \frac{2 \cdot \left(\frac{h}{h_0}\right)^{0.7}}{1 + 2 \cdot \left(\frac{h}{h_0}\right)^{0.7}} \quad (3.9)$$

where

$h_0 = 100$ mm

h_0 height of prism [mm]

$f_{ct,fl,el}$ extreme fibre stress upon formation of flexural crack (elastic limit) [N/mm²].

Equation 3.9 uses the extreme fibre stress upon formation of the first crack, or rather the elastic limit. It is therefore based on the capacity of the concrete matrix, but was originally derived for the flexural tensile strength, i.e. the nominal bending stress upon reaching the maximum bending moment.

In UHPC with sufficiently strong fibre reinforcement, the effect of the fibres can determine the flexural tensile strength. However, the same fracture mechanics scale effect is not to be expected; other conversion factors should be applied. The DAfStb

guideline for fibre-reinforced concrete can be used here. A conversion factor of 0.37 is specified in that guideline, and the post-cracking flexural tensile strength should be multiplied by that figure.

3.3.5 Splitting tensile strength

Cylinders with a slenderness $\lambda = d/h = 2$ and min. 100 mm diameter should be used for determining the tensile strength from tensile splitting tests.

In the light of the results obtained hitherto, it can be said that the splitting tensile strength of UHPC without fibres roughly corresponds to the axial tensile strength. Only a few results are available so far for UHPC with fibres [81].

3.3.6 How fibre geometry and orientation influence the behaviour of UHPC in tension

As already discussed, the post-cracking behaviour of UHPC depends on fibre content, fibre geometry and fibre orientation. The fibre content and orientation can vary locally within a component, which in the first place is connected with the concreting procedure (concreting direction and progress, the flow of the concrete within the formwork). The proper choice of formwork and concreting procedures also provides a chance to influence the fibre distribution and orientation in the component in such a way that the fibres make an optimum contribution to carrying the loads, see also Section 2.7.2.

Flexural tensile tests carried out at the Institute of Construction Materials, Concrete Construction & Fire Protection in Braunschweig [82] included studies comparing the behaviour of UHPC with long fibres (30 mm) and short fibres (approx. 13 mm). A coarse-grained concrete with max. 8 mm particle size and fibre contents between 80 and 120 kg/m³ was used in the tests (see Figure 3.15). Whereas in the range of small deformations, similar, good values for both types of fibre were obtained, the tensile capacity of short fibres decreased faster as the deformations (and hence the crack widths) increased.

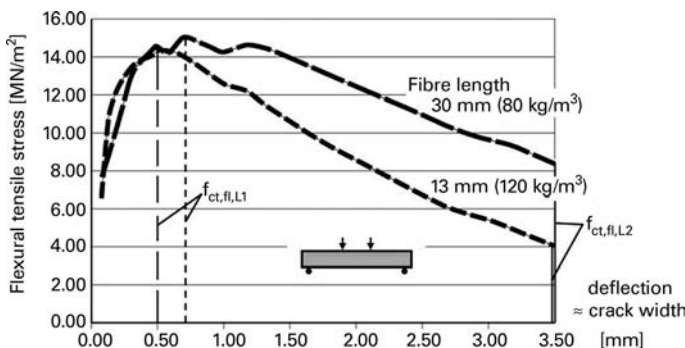


Fig. 3.15 Stress–deflection diagram for UHPC beam in bending with short and long fibres

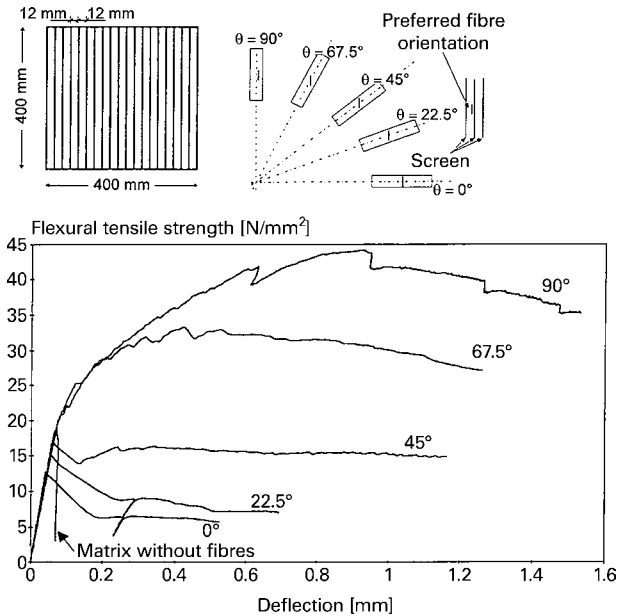


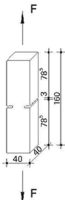
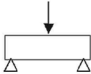
Fig. 3.16 How fibre orientation influences flexural tensile strength and ductility (after [83])

Bernier and Behloul [83] investigated the influence of fibre orientation on the flexural tensile strength and post-cracking behaviour of UHPC by forcing the concrete to flow through screens during casting and thus achieving the preferred fibre orientation. It is clear from the results shown in Figure 3.16 that the maximum flexural tensile strength is reached when $\theta = 90^\circ$ (practically all the fibres aligned in the tension direction), whereas in the most unfavourable case of $\theta = 0^\circ$ (fibres perpendicular to tension direction), the fibres even had a separating effect. In the latter case, the flexural tensile strength was even below that of a plain concrete matrix.

The effect of fibre orientation after passing the fibre-reinforced concrete through screens can explain the preferred orientation parallel with the formwork in the proximity of the formwork. Another consequence is that, on the whole, a preferred orientation parallel with the formwork can ensue with small test specimen thicknesses/widths.

Table 3.1 shows the results of tests [11] on UHPC with almost self-compacting properties. The fibres align themselves mostly horizontally in such concretes. The orientation of the test specimens during concreting was varied in this series of tests. Considerable differences for the different positions during concreting can be seen in Table 3.1 because in the specimens concreted vertically, the fibres were primarily aligned perpendicular to the forces during loading. As shown above, a lower (flexural) tensile strength is to be expected when loads are applied perpendicular to the prevailing fibre orientation than when the fibres are mainly aligned in the loading direction. Besides the tensile strength, the specific fracture energy $G_{f,10\%}$ was also ascertained. For this parameter, the area beneath the stress–crack width curve was evaluated up to a residual strength of 10%.

Table 3.1 Tensile strength and fracture energy depending on specimen orientation during concreting [11].

Test specimen	Age of specimen	Uniaxial tension		Flexural tension			
				Prism 160 × 40 × 40 mm			Beam 700 × 150 × 150 mm
Curing		90°		90°		90°	
Concreting direction		horizontal	vertical	horizontal	vertical	horizontal	vertical
Fracture energy $G_F, 10\%$ [N/m] ^{b)}	7d 28d 28d ^{a)}	16 757 14 555 17 014	9993	20 100 18 052 19 820	15 097	20 355 19 892	14 543
Tensile strength f_{ct} [N/mm ²]	7d 28d 56d	14.2 13.3 17.7	7.86	34.0 35.7 36.3	22.51	22.1 22.2 22.1	17.6

a) Specimens with 25 days of heat treatment at 90 °C

b) Fracture energy for integration up to reaching a residual load-carrying capacity equal to 10% of the maximum capacity

So apart from the geometry of the test specimen, or component, the orientation of the component during concreting and the complete production process are always important, especially with respect to the direction of flow during concreting. This information should therefore always be specified because otherwise there is no chance of reproducing results and making comparisons.

3.3.7 Converting the stress–crack width relationship into a stress–strain diagram

With softening behaviour, the stress–strain line for axial tension is no longer obvious owing to the localization of the deformations taking place at a severely widening crack. For example, for the same fibre-reinforced concrete, or generally the same material, the line would depend on the reference length. The longer the component, the less a local deformation (elongation) can determine the overall behaviour. Consequently, it is not possible to specify a clear stress–strain line for fibre-reinforced concretes with a softening behaviour. For materials with a strain hardening behaviour, a clear stress–strain line only exists up to the onset of softening.

Nevertheless, in order to be able to define UHPC, and especially fibre-reinforced UHPC, it is possible to specify a stress–crack width relationship. By providing a reference to the length l_{st} relevant to the particular case, however, this relationship can be converted to a stress–strain line. Apart from the crack width, the strains that exist within the length l_{st} , but outside the crack, are also included. The strains at the edge of the crack can be determined from the stress as a result of the fibre effect σ_{cf} in the crack and at the end of distance l_{st} , and a mean strain can be estimated:

$$\varepsilon_{cm}(\sigma_{cf}(w)) = \frac{w}{l_{st}} + \varepsilon_{c,st} \quad (3.10)$$

where

ε_{cm} mean equivalent strain in fibre-reinforced concrete within length l_{st}

$\varepsilon_{c,st}$ mean equivalent strain in fibre-reinforced concrete within length l_{st} but outside the crack

$$\varepsilon_{c,st} = \frac{1}{E_{c,sec}} [\beta_{st} \cdot \sigma_{ce} + (1 - \beta_{st}) \cdot \sigma_{cf}(w)] \quad (3.11)$$

$\sigma_{cf}(w)$ nominal (concrete) stress as a result of the force transfer by the fibre effect in the crack $\sigma_{cf}(w)$ depending on crack width w

l_{st} relevant structural length

$E_{c,sec}$ secant modulus (from relief after tension loading)

β_{st} solidity coefficient of stress distribution over the length, which may normally be taken to be $\beta_{st} = 0.6$ (see Figure 3.17)

σ_{ce} stress at end of relevant length l_{st} or at a distance of $l_{st}/2$ from the crack.

In the case of a beam in bending, the change in stress between the value at the crack σ_{cf} and that at the end of the discontinuity region follows from the in-plane stress state

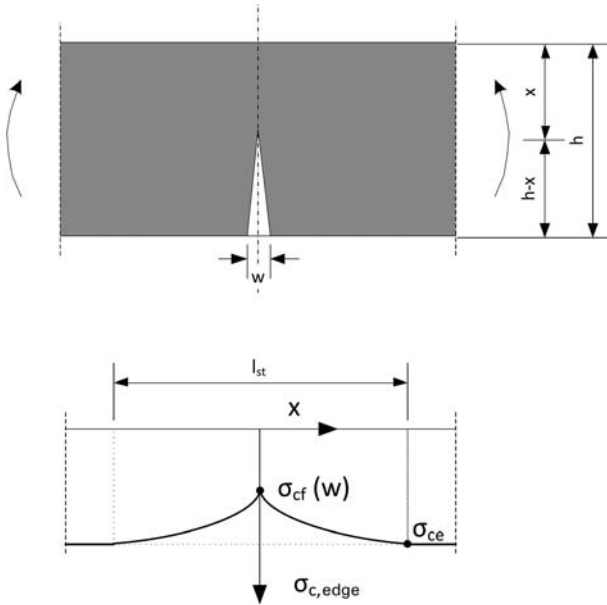


Fig. 3.17 Schematic view of the progress of concrete stresses at the extreme fibres in the vicinity of a crack in fibre-reinforced concrete, based on the example of a beam in bending

adjacent to the crack. When using a combination of steel bars and fibres as the reinforcement, the rebars also transfer stresses, although this requires a certain short transfer length in the millimetre range for UHPC.

Different lengths should be assumed for l_{st} depending on the situation. For components without reinforcing bars, the total length of the discontinuity regions on both sides of the crack can be based on the principle of Saint-Venant:

$$l_{st} \leq 2 \cdot h \quad (3.12)$$

where

h thickness of cross-section.

For components with a combination of reinforcing bars and fibres, the mean crack spacing governs:

$$l_{st} = s_{rm} \quad (3.13)$$

where

s_{rm} mean crack spacing.

When it is necessary to consider localization of deformations at a crack after the onset of yielding of the reinforcement, the structural length l_{st} can be chosen depending on the modelling used (discrete or smeared cracks).

Where there is a constant distribution of the stresses in the longitudinal direction, then it follows that $\sigma_{ce} = \sigma_{cf}(w)$, i.e.

$$\varepsilon_{c,st} = \frac{\sigma_{cf}(w)}{E_{c,sec}} \quad (3.14)$$

3.3.8 Interaction of fibres and bar reinforcement

Provided the thickness of the component permits it, combining reinforcing bars and fibre reinforcement is interesting from the economic and ecological viewpoints because the energy and drawing plant needed to produce thin fibres are considerable. *Leutbecher* [68] has shown that this approach with a limited fibre content ($\leq 1\%$ by vol.) and moderate use of steel reinforcing bars can achieve favourable behaviour in tension members and limit crack widths to <0.1 mm.

A mechanical model [68] based on compatibility and equilibrium at the cracked cross-section permits a reliable determination of the crack widths and the forces that can be accommodated with combined reinforcement in UHPC cross-sections. The load–deformation behaviour exhibits a practically constant contribution of the fibre-reinforced concrete over large ranges and this contribution is more distinct than that of the known contribution of the concrete between the cracks in reinforced concrete without fibres (see Figure 3.18).

Components with combined bar/fibre reinforcement therefore exhibit ‘plastic’ behaviour to a certain extent although the steel reinforcing bars have not yet begun to yield. Owing to the smaller crack widths, a pronounced localization of deformations at a crack is not normally to be expected. Up to the yield point, which in the case of high-strength steels can be way over 5% , this type of behaviour is observed virtually every time. The unavoidable scatter with respect to fibre distribution and orientation are

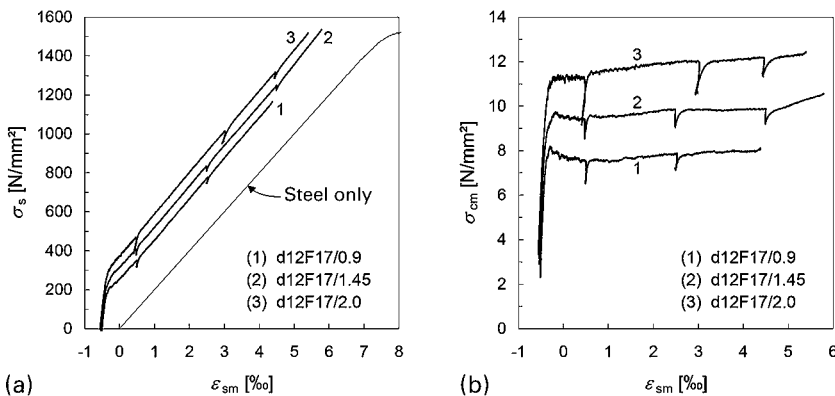


Fig. 3.18 Load–deformation behaviour of UHPC tension members reinforced with high-strength steel bars (grade St 1470/1620, $d_s = 12$ mm) and 17 mm long fibres (fibre contents: 0.9, 1.45 and 2.0% by vol.): a) steel stress–strain relationship, b) contribution of fibre-reinforced concrete

therefore far less noticeable in long components in particular than in fibre-reinforced concrete without steel reinforcing bars, where a local weakness could very quickly limit the extensibility of a long component.

After the onset of yield in the steel rebars, localization of deformation at a single crack can take place more easily if the negative tangent stiffness of the fibre-reinforced concrete as the fibres are pulled out (descending portion of stress–crack width diagram) can no longer be compensated for by a sufficiently large stiffness of the – now plastic – steel reinforcement.

3.4 Shrinkage

The shrinkage of the reference concretes M2Q (fine-grained) and B5Q (coarse-grained) from the German research programme (see Table 2.1) was compared with that of conserved specimens and specimens that were able to dry out naturally in a climate chamber at 20 °C and 65% RH. The results are shown Figure 3.19. Measuring started one day after production.

For the fine-grained UHPC with a w/c ratio of 0.20 and a w/b ratio (equivalent w/c ratio) of 0.17, the shrinkage progression and the total shrinkage strain for the two differently stored series were identical (about 0.35 mm/m). This means that the measured deformation for this w/b ratio was due exclusively to the hydration-related autogenous shrinkage.

The shrinkage progression and the shrinkage strain of the conserved coarse-grained UHPC were similar to those of the fine-grained M2Q mix up to an age of 200 days. If the specimens were able to dry out, so a significant proportion of drying shrinkage was added to the autogenous shrinkage. This may well be due to the higher w/c ratio of this mix (0.24). This also confirms that the silica fume primarily acts only physically as a filler in the case of storage in water. In addition, the results indicate that the first

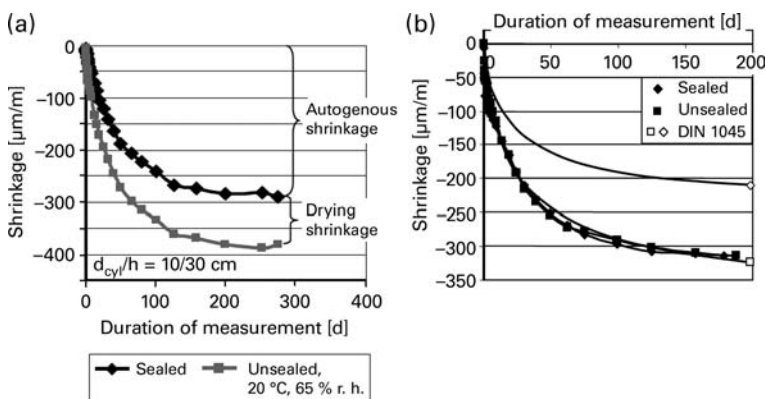


Fig. 3.19 Shrinkage of the a) coarse-grained UHPC B5Q mix [84], and b) fine-grained UHPC M2Q mix [85], measured on conserved specimens and specimens able to dry out naturally at 20 °C/65% r.h

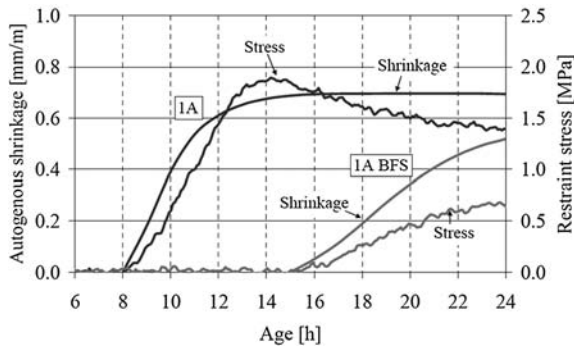


Fig. 3.20 Shrinkage progression and shrinkage stresses over the first 24 h established in a shrinkage ring test carried out on a fine-grained UHPC (after [84])

capillary pores already start to form at this w/c ratio and hence reduce a key feature of UHPC – its very high diffusion resistance.

The foregoing measurements began one day after producing the test specimens. This is usual with normal-strength concrete because the hydration proceeds much more slowly. But with UHPC a compressive strength of 50–60 N/mm² has already been reached after this time, i.e. the reaction and hence the correlating autogenous shrinkage proceed much faster. The shrinkage from the start of hydration was followed in [84] in a ‘shrinkage ring test’. As an example, Figure 3.20 shows the shrinkage progression and shrinkage stresses measured over the first 24 h. A shrinkage contraction of approx. 0.7 mm/m was measured on mix M2Q (mix 1A in Figure 3.20) after just one day.

Depending on cement content and mix design, a total shrinkage strain of about 0.6–0.9 mm/m can be assumed for the design of components made from non-heat-treated, low-capillaries UHPC (w/c ratio ≤ 0.25).

3.5 Creep

In a similar way to shrinkage, creep can be significantly reduced through prior heat treatment. As a first rough approximation, the following orders of magnitude can be specified:

- Final creep coefficient for UHPC without heat treatment: $\varphi = 0.6 \dots 1.4$
- Final creep coefficient for UHPC with heat treatment (approx. 70–90 °C): $\varphi = 0.2 \dots 0.4$

Studies carried out in *Leipzig* [86] and *Karlsruhe* [85] demonstrated that UHPC without heat treatment had much higher creep values than those that might be expected according to acknowledged creep theories. On the other hand, the creep of UHPC is

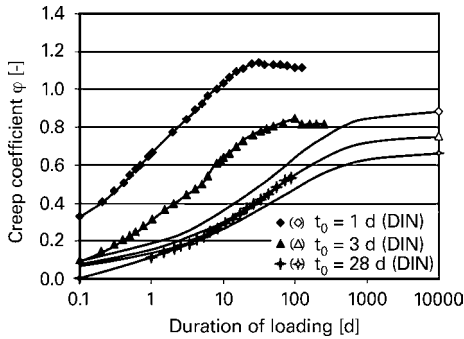


Fig. 3.21 Creep figures for UHPC depending on concrete age at start of loading compared with predictions according to DIN 1045-1

much lower than that of high-strength concrete. Figure 3.21 compares the results obtained with unsealed 100 mm dia. test cylinders (standard climate, loading level equal to 30% of the short-term strength, onset of loading at various concrete ages) with the predictions according to DIN 1045-1.

According to [86], the drying creep proportion is low when compared with concrete with a lower strength, which is probably due to the fact that the dense microstructure represents a considerable obstruction to the transport of capillary water. Another reason could be the pronounced self-drying-out effect of UHPC.

Linear creep up to approx. 60% of the short-term strength (concrete 28 days old at onset of loading) was observed in [85], whereas distinct non-linearity has already been noted at this stress utilization when the onset of loading was earlier. Apparently, however, this can be attributed to the fact that the concrete strength is not yet fully developed in these early phases.

3.6 Multi-axial stresses

Interesting tests were carried out in a multi-axial test rig to determine the biaxial and triaxial strengths (Figure 3.22). The loading was applied via brushes in order to minimize the obstruction to lateral strain. The test results show that the increase in strength for biaxial compression is less pronounced than with normal-strength concrete. Consequently, the approaches customarily used for normal-strength concrete, which are based on an increase in strength for multi-axial loading, may not be used automatically for UHPC (see Figure 3.23a). In the case of triaxial loading, as compression increases in the third direction (from about 6–9%), so there is a transition from brittle to ductile behaviour, as Figure 3.23b shows [87].

3.7 Fatigue behaviour

Extensive results from various sources regarding fatigue behaviour are now available. The studies carried out on fibre-reinforced UHPC by *Bunje* [11, 57] are shown in Figure 3.24 and compared with the results of *Klausen* [88] for normal-strength concrete.

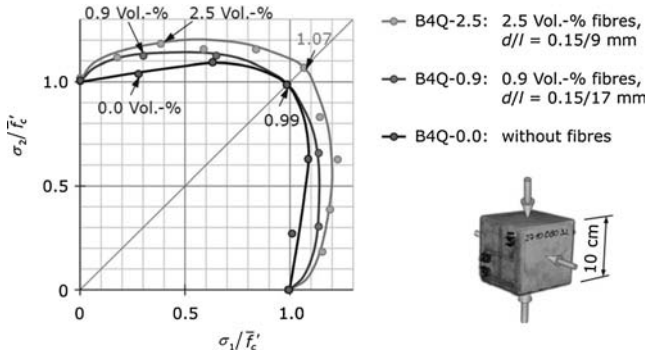
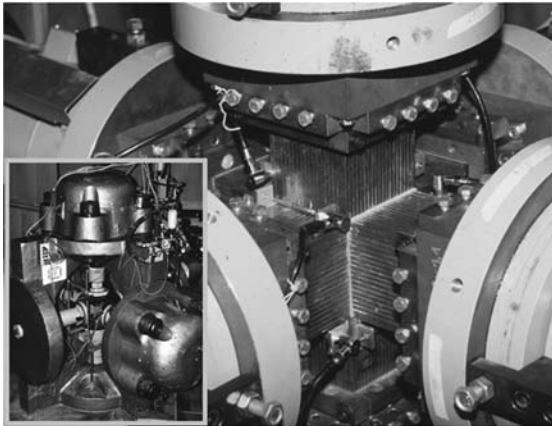
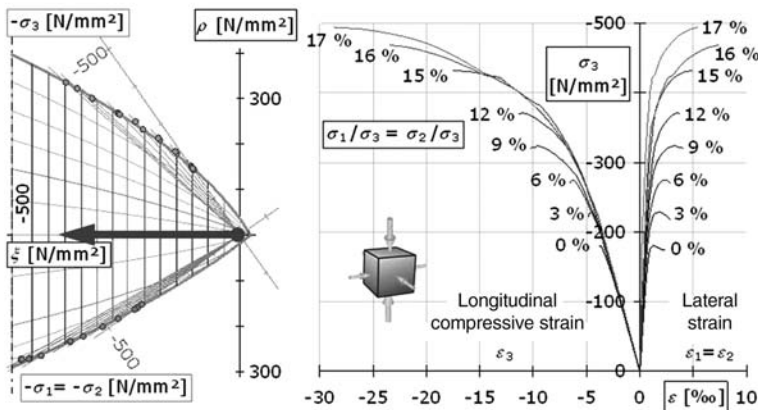


Fig. 3.22 Behaviour of various concretes in the compression-compression zone [87]



(a)

Influence of hydrostatic pressure



(b)

Fig. 3.23 a) Triaxial testing machine, b) fracture values in the Rendulic plane and stress–strain behaviour on the compressive meridian [87]

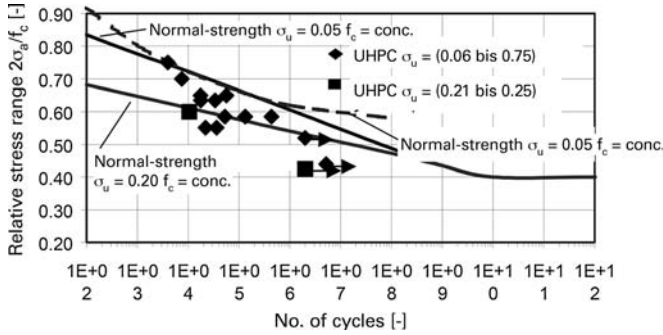


Fig. 3.24 S-N curve for coarse-grained UHPC with fibres [11, 57]

The outcome was no significant difference between UHPC and normal-strength concrete when it came to the admissible, standardized stress ranges (related to the short-term strength). Although further tests on UHPC without fibres did reveal a similar behaviour, there was greater scatter.

More recent investigations by *Wefer* [89] in Hannover involving approx. 200 single-stage S-N tests resulted in similar yet slightly more favourable results. No significant difference between UHPC with fibres (2.5% by vol., 9 mm long, $l/d = 60$) and without fibres could be established. Some 88 tests were evaluated for a lower stress level $S_u = 0.05$, as Figure 3.25 shows. Instead of a direct regression of the means of the tests, *Wefer* suggests using a linear approximation passing through the relative upper stress

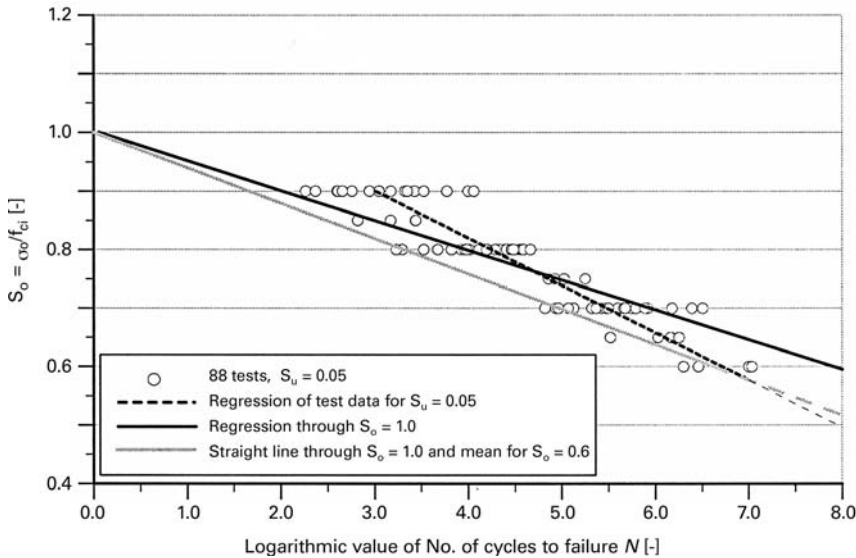


Fig. 3.25 Approximation of test results for the range $\log N_f < 8$ and $\log N_f < 9$ using the example of the regression line for a relative lower stress level $S_u = 0.05$ (after [89])

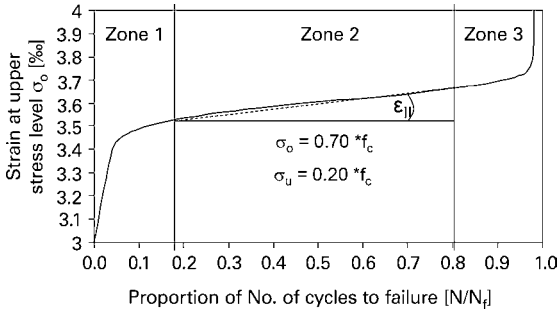


Fig. 3.26 Typical example of development of strains at upper stress level σ_0 plotted against number of load cycles

level $S_0 = 1.0$ at $\log N_f = 0$ and through the value of the regression line for $S_0(N_f > 10^7)$ for a reasonable value of number of cycles to failure N_f exceeding 10^7 . The reason for this is that, on the one hand, no indications for a deviation from the linear progression could be observed up to $N_f = 10^8$. On the other, such an approach lies on the safe side for smaller numbers of cycles to failure. With respect to the question as to whether there is a limit to the fatigue strength, *Wefer* argues that taking the logarithm of the increase in damage $\log \epsilon^{II}$ does not show any deviation from linear behaviour up to 10^6 , and has a very good coefficient of determination for the regression (see Figures 3.26 and 3.27).

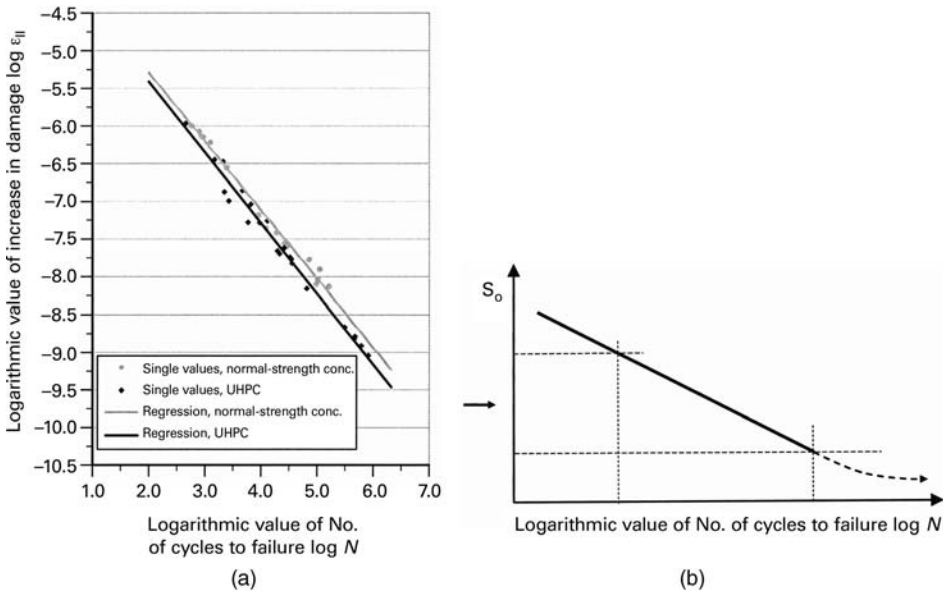


Fig. 3.27 a) Interpretation of relationship between increase in damage $\log \epsilon_{II}$ and taking the logarithm of the number of load cycles to failure $\log N$, and b) in relation to the course of the S-N curve (after *Wefer* [89])

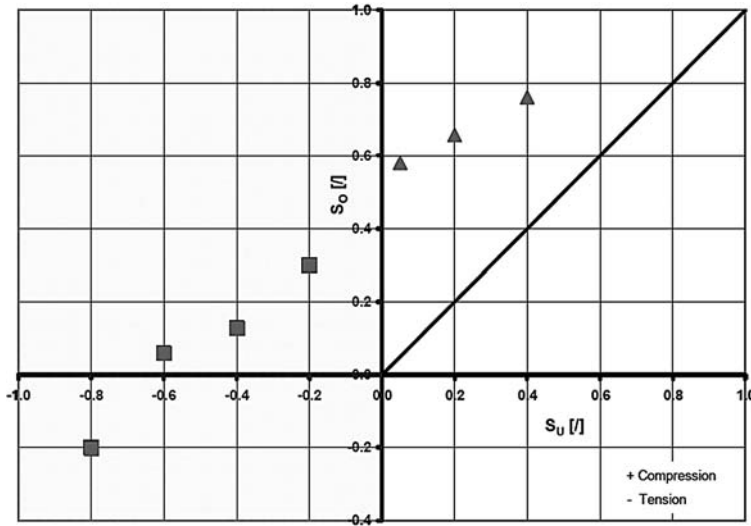


Fig. 3.28 Summary of tests from Munich (squares) and Hannover (triangles) for 10^7 load cycles in a modified Goodman diagram [90, 175]

The $\log \epsilon^{\text{II}}$ value describes the gradient of the line of the strains for the upper stress level in the secondary range of the development of the axial strain up to the number of cycles to failure (see Figure 3.26) and could possibly serve as a good forecast for the range $N_f > 10^8$. Accordingly, it could be suspected that there is no distinct fatigue strength. The linear progression then lies on the safe side for high numbers of cycles to failure as well. These deliberations can be used as a starting point for a design approach, which is discussed in Chapter 5.

For reversed and compressive fluctuating loads, fatigue tests were carried out on dog-bone specimens and test cylinders in Munich and Hannover. A summary of the results is given in Figure 3.28 in the form of a modified Goodman diagram.

For multi-axial loading, the results must be modified according to the failure envelopes in the principal stress space: see Figure 3.29 for compressive fluctuating loads with rotationally symmetric transverse compression, and Figure 3.30 for transverse tension. The latter were obtained using cone-shaped specimens. Detailed information on this can be found in [90–92].

Figure 3.31 shows an overview of the results obtained at various universities for general triaxial loading.

A research project to investigate the fatigue behaviour of UHPC was also carried out at Delft University of Technology [93]. Three different concrete mixes were compared (Figure 3.32). The concrete with the highest strength was a BSI/Ceracem. This concrete had a relatively large maximum grain size (7 mm) and contained 2.5% by vol. steel fibres (200 kg/m^3 , 20/0.3 mm). The mean compressive strength was 220 N/mm^2 .

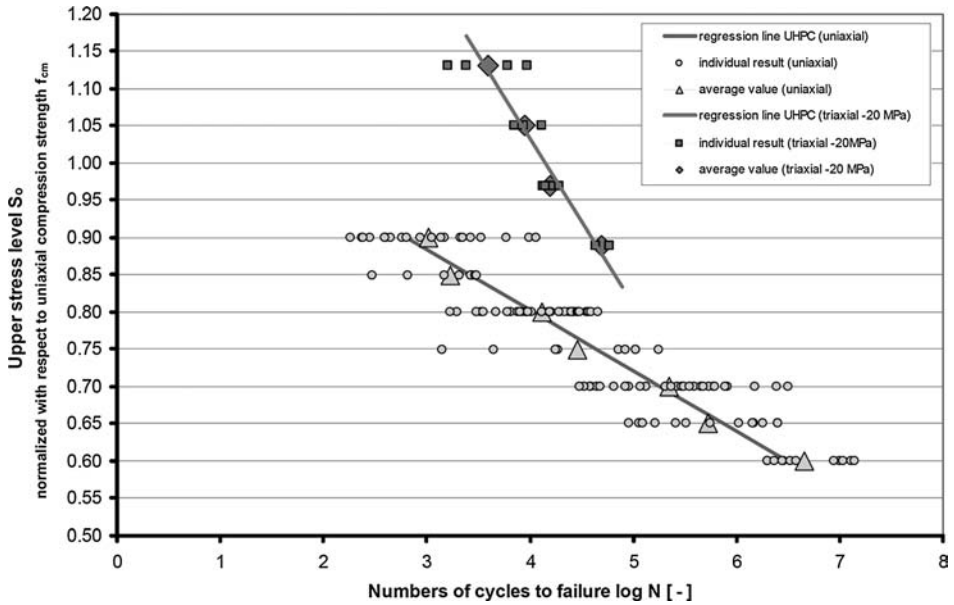


Fig. 3.29 Triaxial and uniaxial S-N curves for UHPC (with transverse compression, after [90])

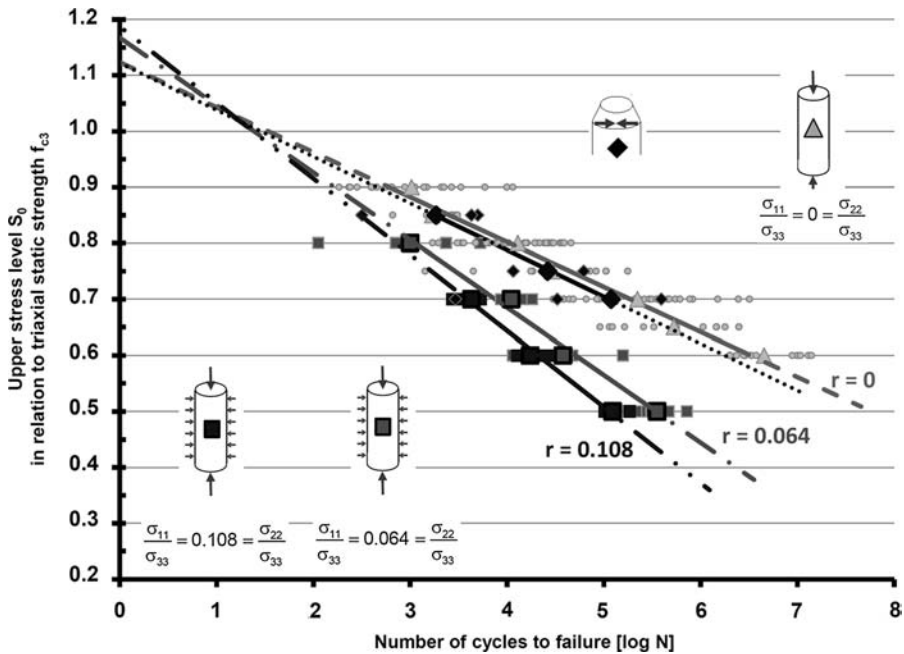


Fig. 3.30 Triaxial and uniaxial S-N curves for UHPC (with transverse compression, after [92])

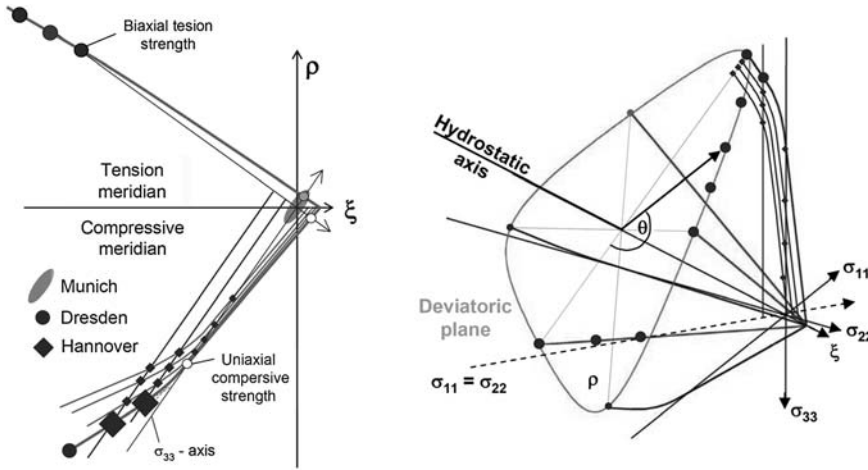


Fig. 3.31 Overview of fatigue tests carried out so far in the meridian intersection and the deviatoric plane [90]

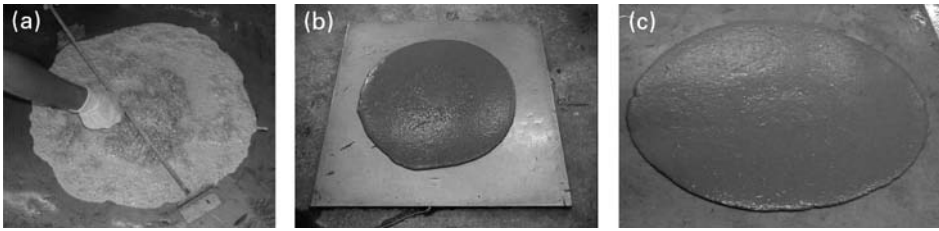


Fig. 3.32 Flow table measurements for three UHPC mixes tested for fatigue: a) BSI/Ceracem, compressive strength = 220 N/mm², $V_f = 2.5\%$ by vol. b) HSFRC, compressive strength = 145 N/mm², $V_f = 1.6\%$ by vol. c) Hybrid HSFRC, compressive strength = 130 N/mm²

Another mix, denoted ‘HSFRC’, had been developed previously at the university by *Grünewald* [94]. This mix contained 1.6% by vol. 13/0.16 mm steel fibres; the mean compressive strength was 145 N/mm². The third mix was a hybrid UHPC (denoted ‘hybrid HSFRC’) and contained 0.5% by vol. short fibres ($l = 13$ mm, $d_f = 0.2$ mm) and 1% by vol. long fibres with hooked ends ($l = 60$ mm, $d_f = 0.75$ mm) after *Markovic* [76]; the compressive strength was about 120 N/mm². Beams measuring 1000 × 125 × 125 mm were cast from all three mixes and then tested in four-point bending tests. Both static and fatigue tests were carried out. Figure 3.33 shows the relationship between the calculated flexural tensile stress and the deflection under static loading. The strain hardening part, an indicator of a good mix, is readily apparent.

Figure 3.34 shows the results of the fatigue tests. The HSFRC mix exhibited the best behaviour. It turned out that, on the one hand, the scatter of the results decreased when the workability improved and that, on the other, the S-N relationships for UHPC agree well with the relationships for concrete without fibres.

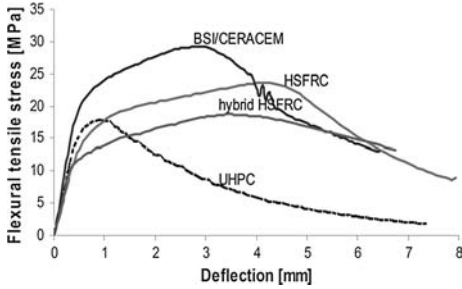


Fig. 3.33 Relationship between flexural tensile stress and deflection for three different UHPC mixes under static loading (after *Lappa* [93])

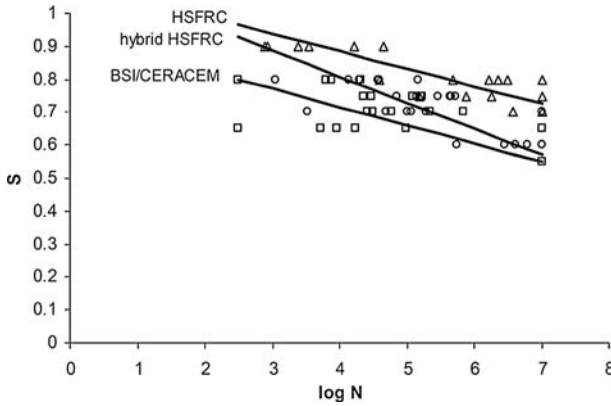


Fig. 3.34 Results of fatigue tests on beams in bending made from various UHPC mixes (after *Lappa* [93])

3.8 Dynamic actions

At high strain rates, i.e. with a very fast increase in strain over time, an increase in the tensile and compressive strengths has been observed for concrete in general. *Millon* and *Nöldgen* [95] investigated UHPC under an extremely fast tension loading rate within the scope of tests on the split Hopkinson bar. With values 5–6 at strain rate of 100 [1/s], the dynamic increase factors (DIF) observed for UHPC (see Figure 3.35) are slightly below those that are observed for normal-strength concrete.

According to the test results obtained so far, this increase in strength should be assigned to the matrix, whereas after crack formation, the effectiveness of the fibres upon pull-out exhibits no comparable increase in stress (see Figure 3.36). Nevertheless, fibre reinforcement has proved to be very effective in slab impact tests [96]. Moreover, the very high compressive strength of UHPC is particularly important when it comes to impact loads. A good overview of the behaviour of UHPC under

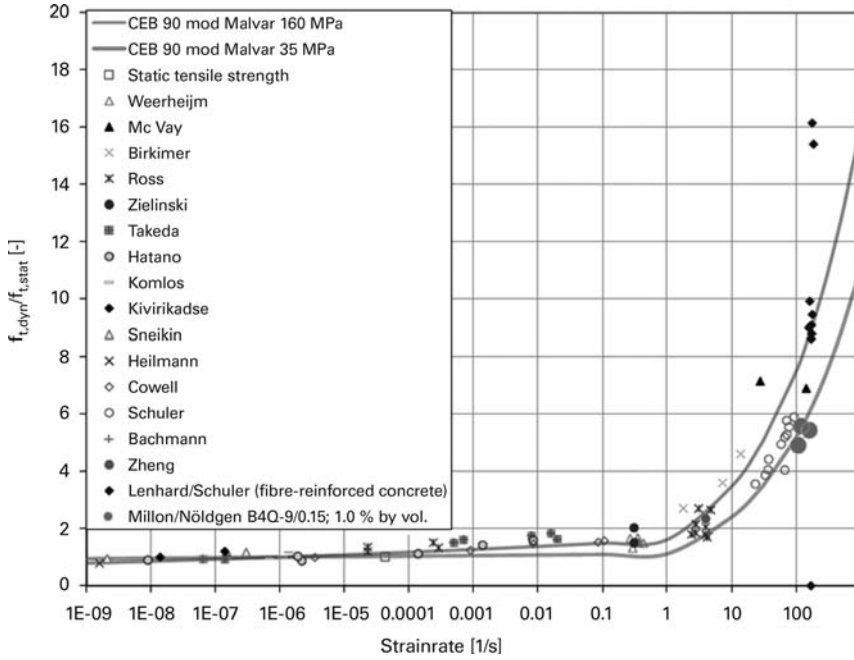


Fig. 3.35 Dynamic increase factors for UHPC (after [95])

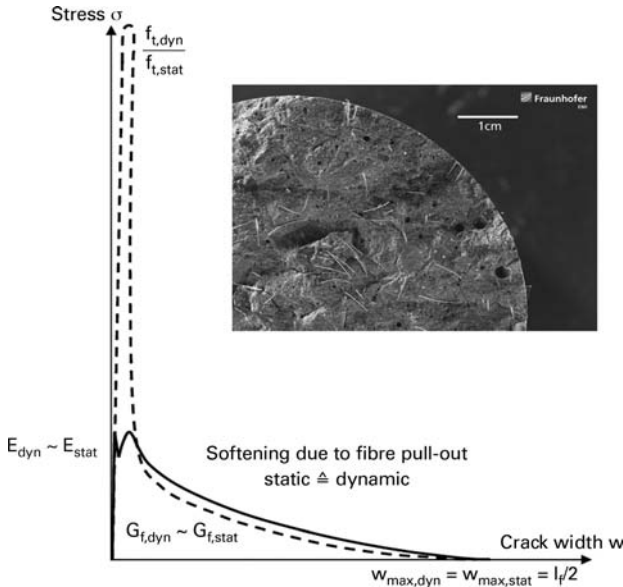


Fig. 3.36 Scheme for increasing the strength of UHPC in the case of highly dynamic tension loads

highly dynamic loads, its modelling and the application to building design to resist impact loads can be found in [96].

3.9 Fire resistance

As already known from high-strength concrete, spalling can begin even during the early stages of a fire because the dense microstructure prevents the dissipation of vapour pressure caused by the elevated temperature. It was this that motivated investigations of the behaviour of UHPC under high thermal loads, i.e. in fire (see Table 3.2). The positive effect of adding polypropylene (PP) fibres is very clear. Likewise, the use of basalt sand instead of quartz sand prevented the damage due to the volume increase as a result of the quartz inversion above 573 °C, which had a positive effect.

More recent investigations by *Hosser et al.* [98] confirm the results and add the fundamental material characteristics to our knowledge of UHPC's behaviour in fire. Such characteristics are needed for modelling and assessing behaviour in fire. Figure 3.37 shows the state of test specimens after 90 min exposure to fire (standard time-temperature curve).

The tests also established that the test specimens made from UHPC heat up faster than would be expected when performing calculations with the thermal conductivity and specific heat capacity values for normal-strength concrete. Figure 3.38 compares the thermal conductivity values for UHPC with those for high-strength concrete and the Eurocode 2 figures.

Also interesting is the strength reduction for UHPC, which is much lower at high temperatures although initially a temporary drop is observed below 200 °C (see Figure 3.39).

Further parameters can be found in [98], others are still being determined. This represents a good starting point for developing material models for use in finite element modelling to simulate the behaviour in fire. According to appropriate calculations, fire tests should be carried out in order to validate the models or gain further knowledge.

3.10 UHPC with combinations of fibres ('fibre cocktails')

Generally, there exist different opinions regarding the role of fibres in fibre-reinforced concrete. In conventional fibre-reinforced concrete, the fibres are relatively large compared with the grains of aggregate. When a macrocrack forms in the concrete, the fibres are activated, i.e. they bridge over the crack and resist the further opening and propagation of the crack. Seen in this way, they function similarly to classic steel reinforcing bars. But the fibres used in UHPC are much finer, which is why they are activated as early as the microcrack formation phase. So the question is whether they should be considered as reinforcement or as part of the composite material. *Markovic* [76] combined short and long fibres (Figure 3.40). The short fibres react as soon as microcracks start to form in the concrete, with the development of the cracks being halted immediately by the fibres. The concrete therefore behaves quasi elastically. If as a result of a further increase in load macrocracks eventually form, then the long fibres are activated.

Table 3.2 Overview of the results of fire tests [97].

Mix	Unit	M3Q					B1Q	B4B Basalt sand
		M1Q						
Steel fibres	% by vol.	4.0	2.5	2.5	2.5	2.5	4.0	2.5
PP fibres	% by vol.	without	without	0.30	0.60	0.60	without	0.30
Storage		28d W	28d W	28d W	28d W	90°C	28d W	90°C
Load		STT 90 min	STT 90 min	STT 90 min	STT 90 min	STT 45 min	STT 90 min	STT 45 min
Degree of damage		--	--	+	++	+	-/+	++
Compressive strength after loading	N/mm ²	could not be tested	could not be tested	could not be tested	126	102/144 (108)	59	147/149 (148)
Proportion of starting value					~96%	~60%	~30%	~77%

-- very severe damage; - severe damage; + light damage; ++ no damage; W stored in water; HT heat treatment; STT standard time-temperature curve.

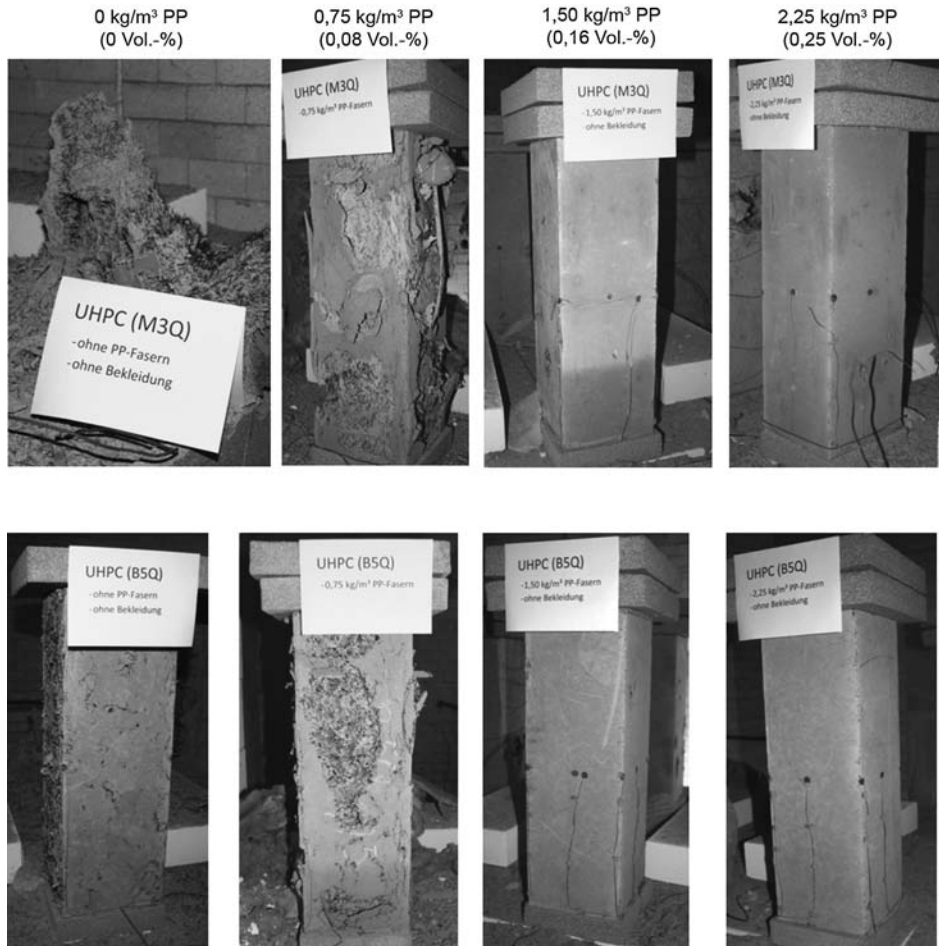


Fig. 3.37 Tests to establish the spalling behaviour of $60 \times 20 \times 20$ cm prisms with different PP fibre contents for the UHPC mixes M3Q (top) and B5Q (bottom), after [98]

Figure 3.41 shows the results of bending tests on beams made from UHPC with combinations of fibres. The tests were carried out as three-point bending tests on notched beams according to the RILEM method [53]. The beams measured $600 \times 150 \times 150$ mm and spanned 500 mm; they had a 25 mm deep sawcut in the middle of the tension side. Various combinations of long fibres with hooked ends ($l = 40$ mm with $d_f = 0.5$ mm, or $l = 60$ mm with $d_f = 0.7$ mm) and short straight steel fibres ($l = 13$ mm, $d_f = 0.20$ mm) were used. The flexural tensile strength reached values of up to 45 N/mm^2 . The compressive strength of the concrete was approx. 120 N/mm^2 . It turned out that there are considerable differences between concretes reinforced with just one type of fibre and concretes reinforced with a combination of short and long fibres. Figure 3.41 shows the flexural tensile strength calculated from the test results as a function of the fibre volume for different fibre combinations.

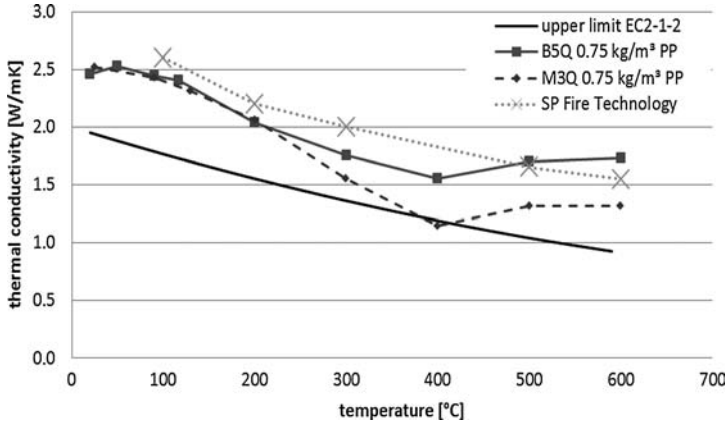


Fig. 3.38 Temperature-dependent development of thermal conductivity of B5Q and M3Q mixes with PP fibre contents of 0.75 kg/m^3 (0.08% by vol.) compared with the upper bound for normal-strength concrete to EC 2-1-2 and measured results (SP Fire Technology) for high-strength concrete

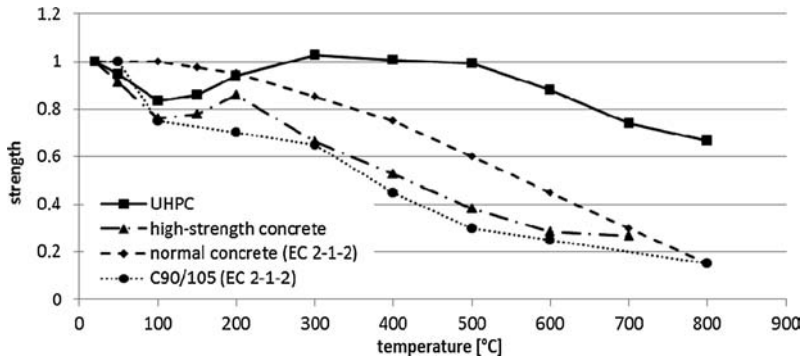


Fig. 3.39 Temperature-dependent compressive strength of UHPC (after [98])

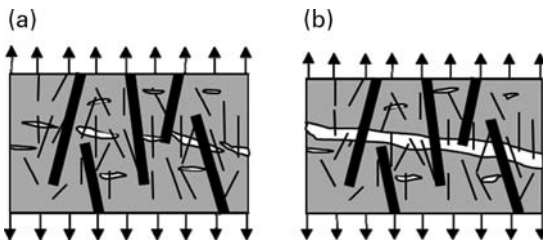


Fig. 3.40 Combination of short and long steel fibres, where a) the short fibres already react to the formation of microcracks, and b) the long fibres do not react until macrocracks start to form [76]

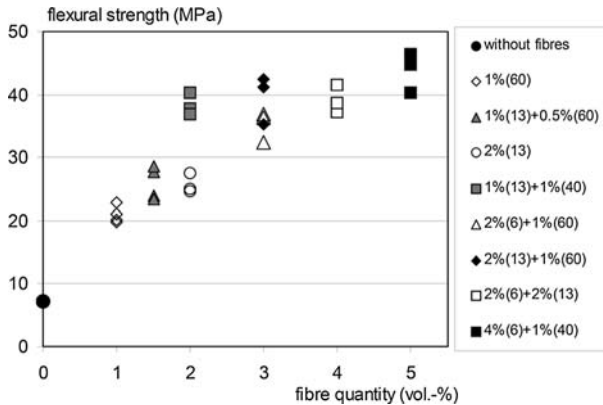


Fig. 3.41 Flexural tensile strength as a function of fibre content and fibre type for concrete with combinations of fibres ('fibre cocktails') [76]

The diagram shows that a mix with 2% by vol. fibres (155 kg/m^3) of length $l = 13 \text{ mm}$ has a flexural tensile strength of 25 N/mm^2 , whereas a mix with 1% by vol. fibres of length $l = 13 \text{ mm}$ plus 1% by vol. fibres of length $l = 40 \text{ mm}$ reaches a flexural tensile strength of 40 N/mm^2 . The diagram also shows that 1% by vol. short fibres (13 mm) combined with 0.5% by vol. long fibres (40 mm) leads to the same flexural tensile strength as 2% by vol. short fibres. In other words, the mechanical properties can be optimized by combining different types and quantities of fibres.

4 Durability

4.1 Microstructure

Owing to its ceramic-like, dense microstructure, ultra high performance concrete (UHPC) exhibits a much higher resistance to substances that attack and damage concrete or reinforcement than is the case with normal- or high-strength concrete. The effect of the high packing density in conjunction with the very low w/b ratio of only approx. 0.20 (see also Chapter 2 and Figure 4.1) is that such a UHPC has practically no capillary pores. Figure 4.1 shows the pore radius distribution, measured using high-pressure mercury porosimetry, of a high-quality class C45/55 normal-strength concrete, a class C90/105 high-strength concrete and two UHPC mixes (90 °C heat treatment, coarse- and fine-grained mixes) [11]. After storage in a standard climate for one year, carbonation of the UHPC extended only approx. 1 mm into the concrete because practically no CO₂ could infiltrate the material.

However, the shrinkage test results presented in Section 3.4 and Figure 3.19 [84] lead us to suspect that UHPC without heat treatment is only totally free from capillary pores, and hence impermeable to gases and liquids, when the w/c ratio is no higher than 0.22. Despite a low w/b ratio (equivalent w/c ratio) of 0.19, drying shrinkage was already measured at a w/c ratio of 0.24 and higher, and such shrinkage is generally associated with the formation of capillary pores. This finding is confirmed by the pore radius distribution of the same coarse-grained UHPC in Figure 4.1. Here, too, an – albeit small – number of pores with a capillary effect is evident. To what extent this has a practical effect on the durability aspects discussed below has not yet been fully clarified, however.

4.2 Resistance to aggressive media

As a result of UHPCs very dense microstructure, its resistance to the diffusion of chloride ions originating from de-icing salts or occurring in marine environments is significantly higher than that of normal-strength concrete. Hence, a concrete cover of UHPC provides the reinforcement with much better protection against corrosion. Figure 4.2 shows the charge and the infiltration depth of the chloride ions established in a rapid chloride migration (RCM) test [99]. Measurements were carried out on 3.5 cm thick disc-shaped specimens made from class C45/55 normal-strength concrete (C1 without and C2 with hydrophobic agent) and a coarse-grained UHPC mix (B3Q from [11]), whose capillary porosity is shown in Figure 4.1.

Figure 4.2 shows the relationship between the charge transmitted and the infiltration depth of the chloride ions. Clearly evident in the figure is the fact that the highest chloride ion infiltration was measured on the normal-strength concrete specimen without hydrophobic agent (C1), a lower infiltration of 0.9 mm on the specimen with hydrophobic agent (C2) and virtually no infiltration on the UHPC specimen. The measurements collected over 6 h were carried out with a 3% NaCl solution and an applied DC voltage of 40 V.

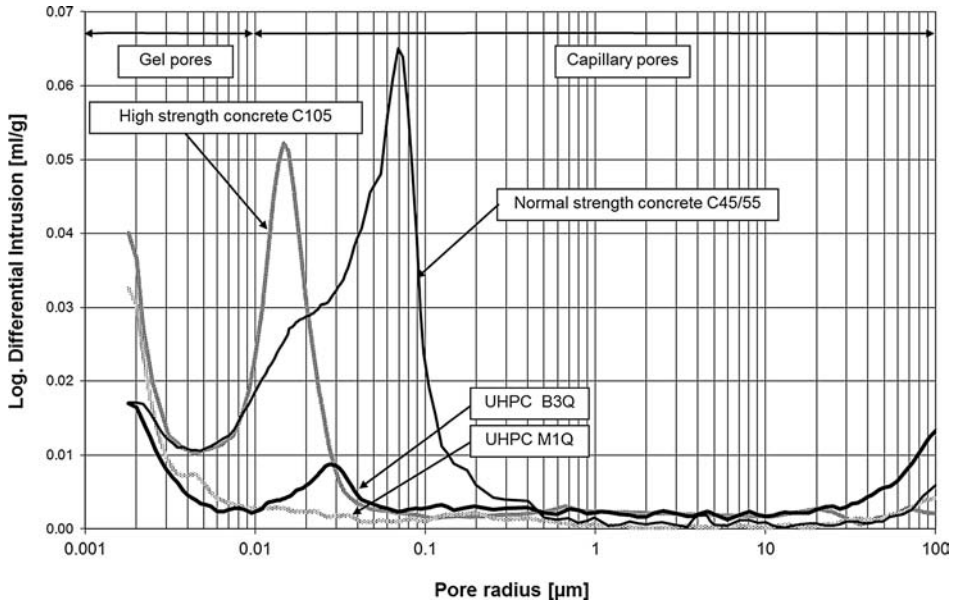


Fig. 4.1 Distribution of pore radius in C45/55 normal-strength concrete, C90/105 high-strength concrete, and fine- (M1Q) and coarse-grained (B3Q) UHPC mixes, after [11]

These findings, in the meantime backed up by the results of further studies [100], allow us to conclude that when using UHPC it is generally possible to reduce the cover depths of DIN 1045-1, which are based on the diffusion resistance of normal-strength concrete. Furthermore, the results imply that components directly exposed to chloride ions from

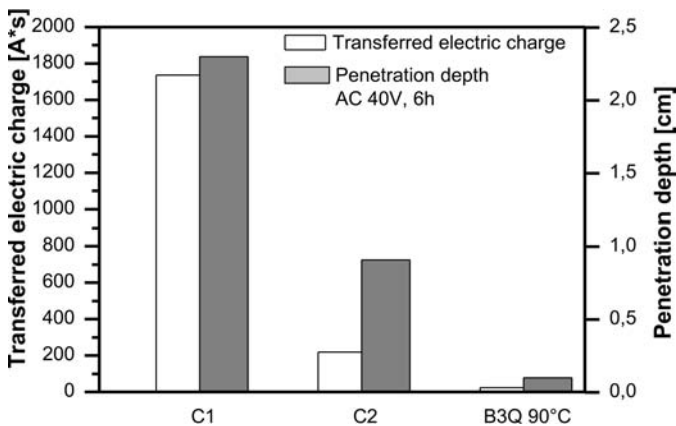


Fig. 4.2 Chloride ion diffusion depths (right) and transmitted charge (left) of normal-strength concrete (with – C2 - and without hydrophobic agent) and coarse-grained, heat-treated UHPC (RCM test) [11]

de-icing salts, i.e. exposure class XD3, can be designed without any additional protective measures; e.g. parking decks or bridge decks can manage without an insolation layer or without a separate water and chloride tight wearing courses respectively [12]. The prerequisite is a sufficiently well-defined limit to the calculated crack width on the surface of the component. According to extensive investigations in [101], depending on the environmental conditions near-surface cracks with a mean width of 0.05 to app. 0.1 mm close themselves completely owing to the high proportion of unhydrated cement. In UHPC with fibres, the beneficial contribution of the fibres can be taken into account when specifying the reinforcement required due to the practical experience that only fibres at the very surface corrode.

Resistance to acids is also better. UHPC is therefore particularly suitable for the production of lightweight pipes with a reduced wall thickness or linings with an improved resistance to industrial wastewater. Prototypes of such pipes made from low-matrix, aggregate-rich, no-slump UHPC (see Table 2.1) have already been produced within the scope of a research project and been approved in a production plant [18]. Figure 2.1 shows the volumetric composition. Further improvements to the chemical resistance can be expected in the future once acid-resistant mineral binders – currently undergoing development [19] – become available.

In [102], the fine- and coarse-grained Portland cement UHPCs of the German research programme plus a further mix with about 220 kg Portland cement, about 600 kg ground granulated blast furnace slag and 145 kg silica fume as a binder were investigated for their corrosion resistance after storage for 4000 h in sulphuric acid (pH 3 and 4) and lactic acid (pH 4). Their resistance to ammonium nitrate and sodium sulphate based on static and cyclic storage was also studied. The w/b ratio of the mix with ground granulated blast furnace slag was 0.24. The UHPC mixes with their w/c ratios of up to 0.24 and w/b ratios of 0.19 and 0.20 were also compared with a reference mortar (512 kg/m³ CEM I 42.5 R, w/c ratio 0.45), which apart from the lack of coarse aggregate complied with the requirements of DIN 1045-2 exposure class XA3. Owing to the low w/c ratio and the packing optimization for the ultrafine constituents, the proportion of transport-relevant capillary pores in the UHPC tested was max. 0.7% by vol. and thus about one power of 10 lower than that of the reference mortar (approx. 10% by vol.). This also corresponds to the capillary pore proportions of normal-strength concrete, high-strength concrete and UHPC shown in Figure 4.1.

The lack of capillary pores is reflected in the much lower water absorption, especially for the UHPC with heat treatment and ground granulated blast furnace slag used in the German research programme (M2Q, B4Q), which is shown in Figure 4.3.

Accordingly, distinctly different corrosion rates were also found for storage tests involving 160 × 40 × 40 mm prisms. Figure 4.4 shows this using the example of exposure to ammonia solution. The corrosion rate of the reference mortar was in each case more than twice as high. Similar differences were found in the other storage tests as well, as with equally long storage in sulphuric acid (pH 3). There was practically no corrosion on the UHPC mix with ground granulated blast furnace slag when stored in sulphuric acid and lactic acid, likewise the heat-treated fine-grained mix made from CEM I (M2Q) in sulphuric acid, in all cases with pH 4.

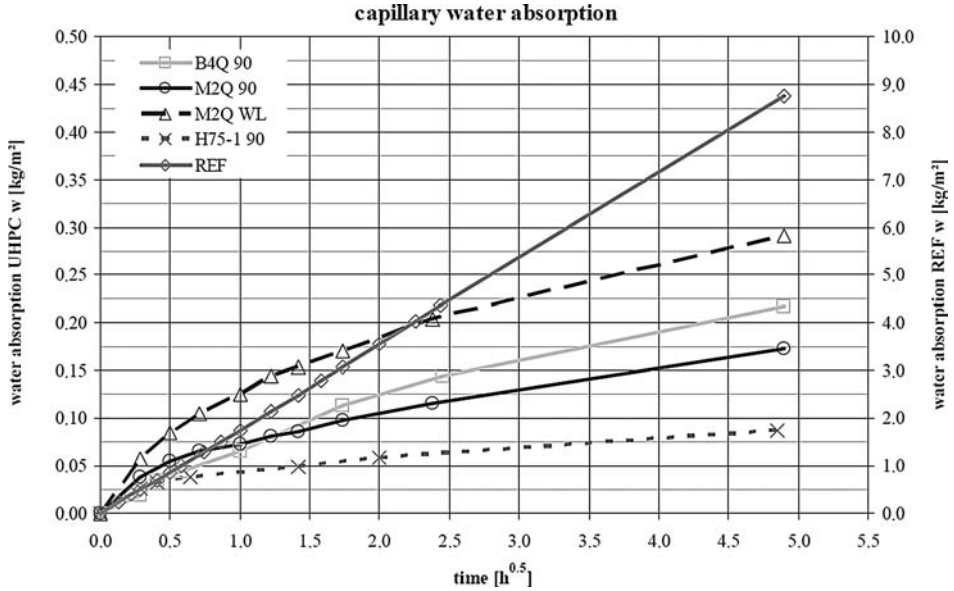


Fig. 4.3 Water absorption of UHPC over time made with Portland cement (M2Q with and without heat treatment and B4Q from the German research programme), a heat-treated UHPC made with ground granulated blast furnace slag (H75) and a reference mortar for exposure class XA3 [102]

As a result of their studies, the authors recommend classifying UHPC with verified low capillary porosity in exposure class XA3 without having to provide the additional protective measures normally required.

For components directly exposed to de-icing salts, including, for example, bridge decks without a water and chloride-tight wearing course, UHPC is not only particularly

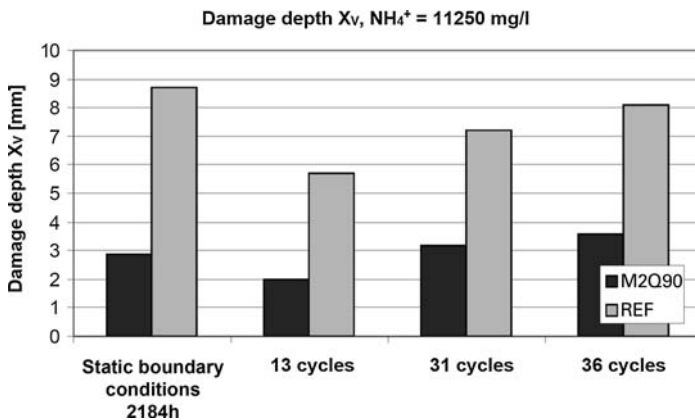


Fig. 4.4 Depth of corrosion X_v for static and cyclic storage in ammonium nitrate solution (NH_4NO_3) [102]

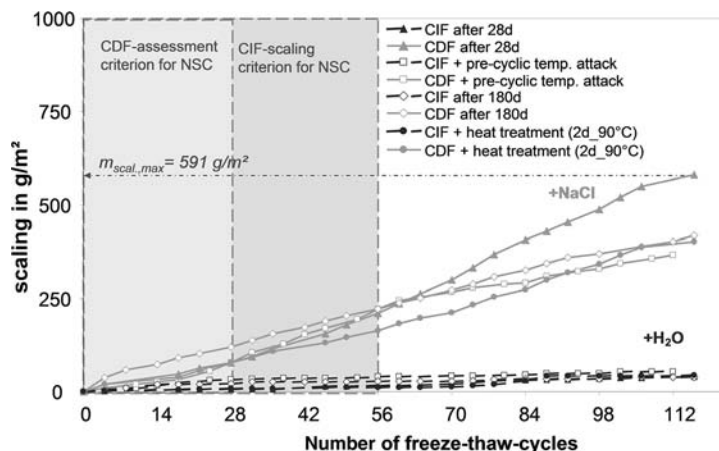


Fig. 4.5 Freeze-thaw and freezing/de-icing salt resistance of UHPC measured using the fine-grained mix M2Q with variations in the methods of curing [103]

suitable because of its especially high resistance to diffusion of chloride ions, but also because of its high freezing/de-icing salt resistance without the addition of an air entrainer. Figure 4.5 shows the erosion that was found for mix M2Q from the German research programme (Table 2.1) with and without heat treatment in the CIF test (freeze-thaw cycle in water) and in the CDF test (freeze-thaw cycle in 3% de-icing salt solution). Practically no erosion occurred in water. The erosion in the CDF test was likewise minimal when comparing the measurements after 28 cycles with the acceptance criteria for high freezing/de-icing salt resistance valid for normal-weight concrete when using this method.

4.3 Classification in exposure classes

In the light of the knowledge gained so far, UHPC produced properly according to Chapter 2 always satisfies the highest exposure class of DIN EN 206/DIN 1045-2. Assuming that no further detrimental capillary pores can be verified and that the concrete is therefore practically impervious to the gases and liquids specified in the standards as damaging to concrete or reinforcement, then the application rules can be revised to take into account UHPCs special capabilities. To begin with conservatively, these rules apply for UHPC not being heat treated when its w/c ratio does not exceed 0.22. For heat treated UHPC due to its higher degree of hydration the same may be true from an effective w/c ratio of 0.22 meaning that the min. w/c ratio may rise to 0.25. If one or both values are higher for a specific mix, then the distribution of the pores, and specifically the proportion of pores with capillary action, must be determined or the respective durability criterion checked directly using a recognized performance test method.

Heat-treated UHPC in particular absorbs no appreciable amounts of water and suffers practically no carbonation over the long term. This means that exposure classes XC4 and XF4 are automatically satisfied, the latter without the addition of an air entrainer.

According to the findings so far, UHPC is also suitable for reinforced components directly exposed to de-icing salt solutions. According to [101], this also applies when the solution is lying around for a longer period of time, e.g. on bridge decks without a wearing course or on open parking decks, which would otherwise have to be provided with some form of protective system or for which a maintenance schedule would have to be drawn up. There is an opportunity here to formulate an additional exposure class, XD4, within the scope of future technical rules for UHPC taking into account the aforementioned boundary conditions (w/c ratio, with/without heat treatment).

The same applies to the chemical resistance. It has already been proposed in [102] that where components require additional protective measures to comply with DIN EN 206/DIN 1045-2 exposure class XA3 because of the anticipated exposure, such protective measures can be omitted. This would be possible in many cases, e.g. components for wastewater systems without elaborate and expensive inner pipes or linings made from synthetic materials. The studies of an ongoing research project sponsored by Germany's Federal Ministry of Education & Research [18] have – in accordance with the results in [102] – identified that UHPC can also withstand longer-term exposure to acid with a pH value of 3.0. This would justify a new, additional exposure class for UHPC – XA4, although the chemical substances for which the class would apply, and their concentration limits, would still have to be defined.

Further, the concrete cover to the reinforcement can be reduced significantly in most cases, which also facilitates the construction of especially delicate but nevertheless durable structures in UHPC. In such designs, as explained above, the widths of cracks near the surface must be restricted adequately. Construction design rules have yet to be drawn up for this.

5 Design principles

5.1 Influence of fibre distribution and fibre orientation

The loadbearing behaviour of fibre-reinforced UHPC, like that of fibre-reinforced concrete in general, is essentially influenced by the orientation and distribution of the fibres. This particularly applies to its response to tension actions.

The causes of the scatters observed are primarily the changing mixing and concreting methods. There are systematic influences as well, e.g. in close proximity to formwork surfaces. The latter also aggravates the derivation of universally applicable material parameters because, strictly speaking, the – normally small-format – specimens (prisms, short beams) used in tests on materials can only determine the ‘component properties’ valid for the respective specimen geometry.

Irrespective of the statistical evaluation of the results of the tests on such building materials, it is also necessary to carry out a conversion in order to take account of the different responses of the specimens produced in the laboratory and the fibre-reinforced UHPC in the real components cast at a later date.

In the end, an ‘exact’ determination of the corresponding conversion factors is only possible on the basis of a representative (full-scale) model produced in exactly the same manner as the later loadbearing structure, and from which comparative samples can be taken from various areas and for various directions (e.g. for shear force perpendicular to a shear crack). Using the comparative samples, it is possible to ‘calibrate’ the results of the other specimens produced in the traditional way. It might be that different local conversion factors are needed for different parts of one member. As an alternative, empirical values can be used for similar geometries and production methods [64].

The draft of the *fib* Bulletin ‘Ultra High Performance Fibre Reinforced Concrete’ [6] specifies the fibre efficiency, in the form of a characteristic or mean value, as the basis for the further calculations. Fibre efficiency is calculated as follows:

$$\sigma_{cf0k} = \sigma_{cf0k}^{\text{test}} / K \quad (5.1a)$$

$$\sigma_{cf0m} = \sigma_{cf0m}^{\text{test}} / K \quad (5.1b)$$

where

$\sigma_{cf0k}^{\text{test}}$, $\sigma_{cf0m}^{\text{test}}$ characteristic or mean value of fibre efficiency determined in tests on the material

K conversion factor to allow for the different fibre orientation and distribution in the moulded standard test specimen and in the real component/structure [64].

Alternatively, for smaller components, the theoretical assumptions can also be validated by way of full-scale loading tests.

5.2 Analyses for the ultimate limit state

5.2.1 Safety concept

When designing loadbearing structures made from UHPC, it is important to take account of a number of characteristics of this material when applying the methods of analysis with partial safety factors common in structural engineering. Consequently, adjustments are chiefly necessary on the resistance side, whereas the usual partial safety and combination factors for actions apply to UHPC as well.

These special characteristics of UHPC concern the following in particular:

1. The material's high sensitivity with respect to changes to the composition of the mix, the mixing and concreting methods and the climatic boundary conditions.
2. Its greater brittleness compared with normal-strength concretes.
3. The use of fibres as structural reinforcement.

Point 1 leads to high demands being placed on the quality of the mixing and concreting processes. With its higher quality standards with respect to production and monitoring (and also the exclusion of the effects of the weather to a large extent), precast concrete construction would seem to promise advantages over using UHPC as *in situ* concrete. However, the drawbacks of *in situ* concreting can be largely compensated for by employing comprehensive quality assurance measures and by selecting suitably qualified contractors.

Studies of the level of safety for high-strength concrete show that by adhering to appropriate quality standards, the coefficient of variation of the compressive strength decreases as the compressive strength rises [104]. In other words, taking into account the much higher compressive strength of UHPC, the scatter is even smaller. And that in turn would justify reducing the partial safety factor. However, when using UHPC, and depending on the quality standards that are feasible, designers are recommended to use the γ_c values for compression which apply to normal- and high-strength concretes (see Table 5.1). This means that $\gamma_c = 1.35$ can be used for precast concrete components produced in fully controlled mixing and concreting processes, but otherwise $\gamma_c = 1.5$.

The greater brittleness of the material (point 2) is generally transformed into some degree of ductile behaviour by adding fibres or including confining reinforcement. A ductility criterion is needed to differentiate 'brittle' and 'sufficiently ductile' post-peak behaviour. For example, it is possible to use the fibre efficiency (post-cracking axial tensile strength) of the fibre-reinforced UHPC related to the compressive strength. Also conceivable is a minimum reinforcement criterion (see Section 5.3.2).

If the required ductility, i.e. a ductility adequate for normal-strength concrete, is not reached, the recommendation (in line with the former concept for high-strength concretes) is to include an additional partial safety factor γ'_c when calculating the design value of the concrete compressive strength. By specifying $\gamma'_c = 1.2$, the level of safety achieved is the same as that for unreinforced normal-strength concrete.

If fibres are considered to act as structural reinforcement (point 3), this presumes a very uniform distribution of those fibres. The formation of 'hedgehogs', i.e. lumps of fibres,

Table 5.1 Partial safety factors γ_M for determining the ultimate resistance at the ultimate limit state.

	Design situation	
	Persistent and transient	Accidental
UHPC in compression		
High quality standard	$\gamma_c = 1.35$	$\gamma_c = 1.15$
Normal quality standard	$\gamma_c = 1.5$	$\gamma_c = 1.3$
If ductility criterion not satisfied, then also	$\gamma'_c = 1.2$	
UHPC in tension		
Fibre efficiency, σ_{cf0} (use with high quality standard only)		
Generally	$\gamma_{cf} = 1.5$	$\gamma_{cf} = 1.3$
For local analyses only	$\gamma_{cf} = 2.1$	$\gamma_{cf} = 1.5$
Reinforcing or prestressing steel	$\gamma_s = 1.15$	$\gamma_s = 1.0$

must be avoided at all costs. How the concrete is placed in the formwork must be specified exactly and monitored in order to achieve a uniform distribution and the desired fibre orientation. Therefore, counting the fibres as part of the reinforcement in analyses for the ultimate and serviceability limit states is only permitted when the mixing and concreting methods are monitored intensively.

Furthermore, in the light of the desirable level of safety, it is necessary to distinguish between those members, or types of action, for which the presence of local weaknesses can result in immediate failure (e.g. anchorage zone of an anchor) and those that open up alternative load paths (e.g. bending in slabs). Even when taking great care, scatter in the distribution of the fibres is inevitable and therefore an appropriate, higher partial safety factor should be used for local analyses.

Table 5.1 lists the partial safety factors recommended by the authors for the design of UHPC components.

5.2.2 Simplified stress–strain curve for design

5.2.2.1 Compression actions

For simplicity, the stress–strain curve for UHPC in compression – neglecting a low non-linearity observed in tests above a level of stress of about 85–90% of the concrete compressive strength – can be assumed to be linear elastic up to reaching the design value of the concrete compressive strength (Figure 5.1).

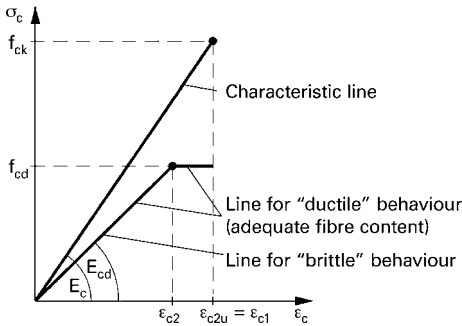


Fig. 5.1 Stress–strain diagram for UHPC for compression design [6]

The following applies:

$$f_{cd} = \alpha_{cc} \cdot f_{ck} / (\gamma_c \cdot \gamma'_c) \quad (5.2)$$

where

- f_{ck} characteristic value of cylinder compressive strength
- γ_c safety factor for UHPC subjected to compression action (see Table 5.1)
- γ'_c additional safety factor for UHPC that does not satisfy the ductility criterion (see Table 5.1)
- α_{cc} factor to allow for long-term effects on the concrete compressive strength and to convert between cylinder and component compressive strengths
- $\alpha_{cc} = 0.85$ for long-term or repeated loading (similar to normal- and high-strength concrete)
- $\alpha_{cc} = 0.95$ for short-term loading to convert between cylinder and component compressive strengths.

In a similar way to the rules applicable for normal- and high-strength concrete, the ascending portion of the stress–strain curve for design is chosen to be shallower than the curve determined with the mean or characteristic values of the material properties. The reason for this is to take into account creep effects (long-term loading) and also to reflect the correlation between the compressive strength and modulus of elasticity of the concrete. The value according to Equation 5.3 is proposed as the design value of the modulus of elasticity [6]:

$$E_{cd} = E_{cm} / 1.3 \quad (5.3)$$

where

E_{cm} mean value of modulus of elasticity.

It is not necessary to distinguish between the secant and tangent modulus of elasticity when it comes to UHPC.

The compressive strain at maximum load ϵ_{c2} can be directly derived from the design values of the compressive strength and the modulus of elasticity:

$$\varepsilon_{c2} = f_{cd}/E_{cd} \quad (5.4)$$

Owing to UHPC's very brittle behaviour, especially without fibres, but also mixes with a low fibre content, failure upon reaching the design value of the concrete compressive strength should be assumed for these cases. Softening behaviour with consideration of the stresses at strains in the post-peak region beyond ε_{c2} may be taken into account in the design of the section only when the UHPC exhibits a sufficiently ductile post-peak behaviour (see 'ductility criterion' in Section 5.2.1). The approach illustrated in Figure 5.1 adds a plastic portion to the stress–strain curve, the end of which is reached at a compressive strain ε_{c2u} according to Equation 5.5:

$$\varepsilon_{c2u} = f_{ck}/E_c \quad (5.5)$$

The plastic portion of the stress–strain curve does not reflect the actual behaviour of the material when it comes to UHPC. This is not a disadvantage, however, because the parameters needed for designing the cross-section are determined by integrating the stress–strain curve (cf. parabolic–rectangular diagram for normal- and high-strength concrete). Generally limiting the compressive strain to a value $\varepsilon_{c2u} = \varepsilon_{c1}$ validated in tests on the material seems rather conservative.

As an alternative to the numerical model of Figure 5.1, which is easy to deal with mathematically, it is also possible to use stress–strain curves that take into account the post-peak behaviour more realistically, e.g. by way of a linear softening portion [6]. In this case the ultimate compressive strain ε_{c2u} can be specified individually depending on the fracture energy.

The linear elastic–linear softening stress–strain curve according to Figure 5.2 can in turn be transformed into a linear elastic–ideal plastic curve (Figure 5.3a), which is equivalent in terms of determining the internal forces. In Figure 5.3a, ε_{c3} corresponds to the compressive strain at maximum load ε_{c2} from Figure 5.2 and ε_{cu} to the ultimate compressive strain ε_{c2u} , likewise according to Figure 5.2. Figure 5.3b can be used to

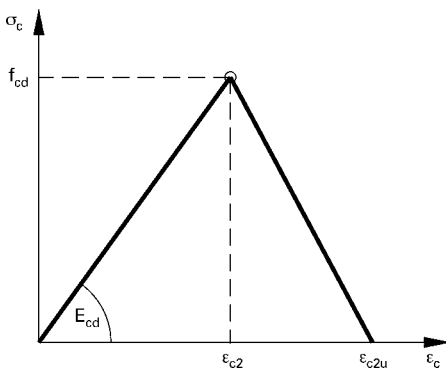


Fig. 5.2 Stress–strain diagram for UHPC with a linear softening portion for compression design [6]

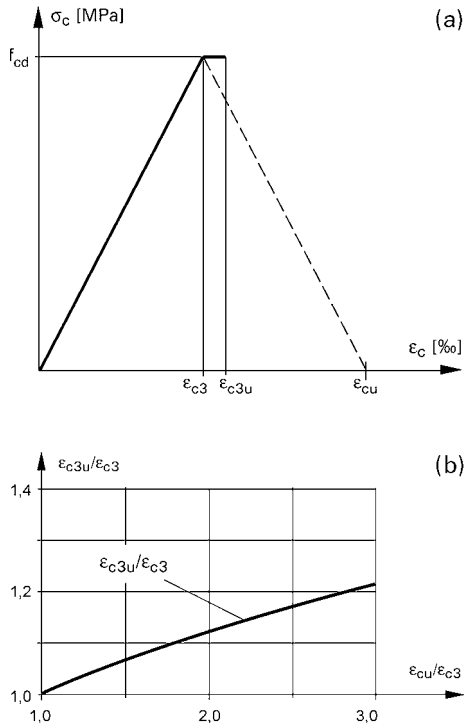


Fig. 5.3 Stress–strain diagram for UHPC with a linear softening portion for compression design [6]: a) stress–strain curve, b) determining the compressive strain at failure ϵ_{c3u}

determine the ultimate compressive strain ϵ_{c3u} equivalent to ϵ_{cu} depending on the $\epsilon_{cu}/\epsilon_{c3}$ ratio.

5.2.2.2 Tension actions

Looking at the contribution of the (fibre-reinforced) UHPC in tension, in line with the philosophy of reinforced concrete, it is necessary to distinguish between the uncracked and cracked states. The cracked state is generally assumed for analyses for the ultimate limit state (e.g. bending and axial force analyses), with the tensile strength of the concrete matrix being ignored. This principle is applied to UHPC as well. However, here ‘tensile strength’ applies to the strength of the matrix and the fibres added to the concrete mix are understood to correspond to reinforcing bars.

Accordingly, UHPC without fibres can be designed like reinforced concrete. Based on Section 3.3, a stress–crack width relationship according to Figure 5.4 can be formulated for the fibre-reinforced UHPC subjected to tension actions. Here, the non-linear, ascending portion describes the fibre activation phase and can be calculated with Equation 5.6 (see Section 3.3.1):

$$\sigma_{cf} = \sigma_{cf0} \left(2\sqrt{\frac{w}{w_0}} - \frac{w}{w_0} \right) \quad (5.6)$$

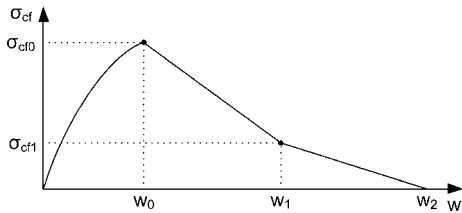


Fig. 5.4 Stress–crack width relationship for cracked UHPC under tension actions [105]

where

σ_{cf} effective stress in fibre-reinforced concrete in a crack

σ_{cf0} fibre efficiency, calculated as design value σ_{cf0d} with Equation 5.7 for analyses for the ultimate limit state

w_0 crack width upon reaching fibre efficiency.

The design value of the fibre efficiency can be calculated from the characteristic value of the fibre efficiency as follows [6]:

$$\sigma_{cf0d} = \alpha_{ct} \cdot \frac{\sigma_{cf0k}}{\gamma_{cf}} \quad (5.7)$$

where

σ_{cf0k} characteristic value of fibre efficiency determined from a statistical evaluation of test results

γ_{cf} partial safety factor for UHPC under tension actions (see Section 5.2.1)

α_{ct} factor to allow for long-term effects on the concrete tensile strength.

No verified findings have yet been published regarding how long-term or repeated loading might affect the fibre efficiency.

For ultimate limit state calculations, the fibre pull-out phase ($w > w_0$) can generally be approximated sufficiently accurately by a bilinear line at least. It is advisable to specify intermediate points between $(w_0; \sigma_{cf0})$ and $(w_2; 0)$ on the basis of test results. The same applies to the crack width w_2 . However, no value $> l_f/2$ may be used, which, theoretically, is the value obtained for a fibre intersected by the crack at half of its length.

The crack width w_0 can either be determined experimentally or, if measurements are unavailable, estimated roughly with the help of Equation 5.8 [68, 69]:

$$w_0 = \frac{\tau_{fm} \cdot l_f^2}{E_f \cdot d_f} \quad (5.8)$$

where

τ_{fm} mean fibre bond strength assuming a rigid–plastic bond relationship

l_f fibre length

d_f fibre diameter

E_f modulus of elasticity of fibre material.

Based on the results of experiments [74, 104], τ_{fm} can be taken as $1.3 f_{ctm}$ for plain, straight steel fibres.

Strictly speaking, Equation 5.8 only applies to fibres aligned in the tension direction. In fibre-reinforced concretes with random fibre orientations, the fibres at the crack which are at an angle to the tension direction will initially be pulled straight. Therefore, Equation 5.8 generally underestimates the crack width w_0 observed in tests.

5.2.3 Design for bending and normal force

Traditionally, designing for bending and normal force in reinforced and prestressed concrete is carried out under the assumption that plane sections remain plane and that there is a rigid bond between the concrete and the reinforcement. The tensile strength of the concrete (matrix) is ignored. The corresponding stress–strain curves are used in the design of the cross-section for concrete in compression and for the reinforcement.

Including fibres as additional reinforcement means that these design principles must be extended. The first difficulties are that a stress–crack width relationship (instead of a stress–strain curve) based on tests is available for the fibre reinforcement as a constitutive model (see Sections 3.2.2 and 3.3) and that the apportionment of the forces between the fibre reinforcement and the (bar-type) conventional or prestressed reinforcement that is frequently also present is derived from a compatibility condition (see Section 3.2.3). However, the following parametric study presents a simple, generally sufficiently accurate solution of this problem.

Figure 5.5 is a schematic view of the stress distributions and ensuing internal forces acting on the cross-section. The concrete compressive stresses are shown simplified without taking into account any horizontal portion of the stress–strain relationship which may be permissible. The stress resultant F_{cd} for a cross-section with a rectangular concrete compression zone therefore lies at the one-third point from top. The resultant tensile force in the steel F_{sd} acts at the level of the centroid of the reinforcement. Acting in addition to this couple is the resultant of the stress in the fibre-reinforced concrete F_{fd} .

The distribution of the tensile stresses transferred across the crack by the fibres can be read off directly from the stress–crack width diagram depending on the actual local crack width. Assuming a crack width that varies linearly over the depth of the crack (analogy: plane sections remain plane), a segment of the stress–crack width relationship of Figure 5.4 represents the stresses in concrete tension zone.

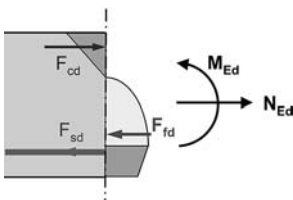


Fig. 5.5 Stress distribution and resultant internal forces for the cracked cross-section [105]

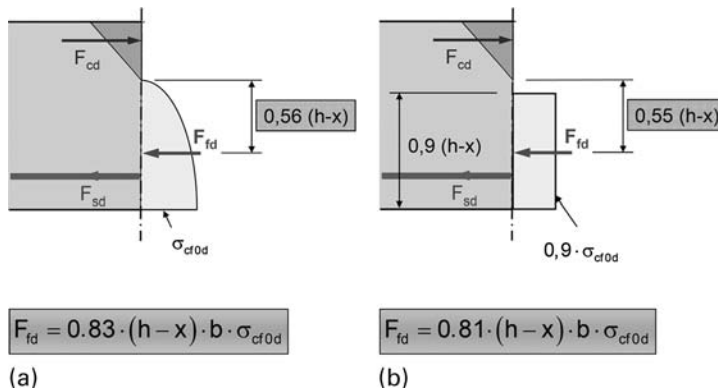


Fig. 5.6 Assumed stress distribution and resultant tensile force carried by the fibres upon reaching the ultimate limit state [105]: a) realistic stress distribution, b) stress block equivalent to a)

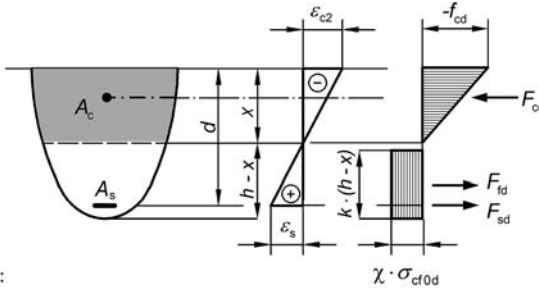
Once the yield point of the reinforcement at a crack is reached, there is a rapid increase in the crack width for an approximately constant level of load. Provided the crack width w_0 has not been reached within the elastic range of the steel, the transition from the fibre activation to the fibre pull-out phase takes place, at the latest, at the onset of yield. Consequently, as an approximation and without considering compatibility accurately, a minimum value $w = w_0$ can be assumed for the crack width at the onset of yield.

Integrating the stress distribution according to Equation 5.6 for $w = w_0$ on the tension side of the cross-section for a rectangular concrete tension zone results in a stress factor of 0.83 for solidity and a centroid factor 0.56 for the position of the stress resultant (Figure 5.6a).

As the softening portion of the stress–crack width diagram is significantly shallower for the fibre pull-out phase ($w > w_0$) than the ascending portion for the fibre activation phase ($w \leq w_0$), the stress block parameters for the stress distribution change only marginally, and also in the opposite directions at first, as the crack widens on the tension side of the cross-section. So as the solidity approaches the rectangle, the stress resultant migrates in the direction of the centroid of the cross-sectional area in tension. As comparative calculations show, with $w = w_0$ on the tension side of the cross-section, the moment capacity is generally represented very well [106].

From the point of view of simplifying the mathematics, for cross-sections with a non-rectangular concrete compression zone as well, the ‘more exact’ stress distribution of Figure 5.6a can be converted to an equivalent stress block (Figure 5.6b) with regard to the moment capacity.

In order that the stress block does not overestimate the effect of the fibres, $0,85 \sigma_{cf0d}$ (instead of $0,9 \sigma_{cf0d}$) is recommended as the stress factor of the fibre-reinforced concrete in the tension zone for the case where the width of the cross-section decreases towards the tension side.



Legend:

$k = 0.9$

$\chi = 0.9$ Generally

$\chi = 0.85$ If width of cross-section reduces towards tension side

Fig. 5.7 Simple model for design for bending and axial force [105]

For simplicity, the design value of the concrete compressive strength f_{cd} can be used as the concrete stress on the compression side of the cross-section (cf. stress block for the design of normal- and high-strength concrete).

As reaching the elastic limit for steel reinforcement with a distinctive yield point generally initially leads to a localization of further deformations at the crack governing the load-carrying capacity, the stress in the reinforcing steel when applying the proposed design model should be limited to the design value of the yield point f_{yd} . Alternatively, when exploiting the strain hardening of the reinforcing steel up to its tensile strength, owing to the already very wide cracks, the contribution of the fibres can be ignored, which is on the safe side.

Figure 5.7 summarizes the proposed simple model for designing for bending and normal force.

We get the following internal forces for the rectangular cross-section:

$$F_{cd} = 0.5 \cdot b \cdot x \cdot f_{cd} \quad (5.9a)$$

$$F_{sd} = A_s \cdot f_{yd} \quad (5.9b)$$

$$F_{fd} = 0.81 \cdot b \cdot (h - x) \cdot \sigma_{cf0d} \quad (5.9c)$$

The equilibrium conditions known from reinforced concrete design are as follows when taking the contribution of the fibres into account:

Equilibrium of forces:

$$\Sigma H = 0 = N_{Ed} - F_{sd} + F_{cd} - F_{fd} \quad (5.10a)$$

Equilibrium of moments:

$$\Sigma M = 0 = M_{Eds} - F_{cd} \cdot (d - x/3) + F_{fd} \cdot (d - 0.45 \cdot x - 0.55 \cdot h) \quad (5.10b)$$

5.2.4 Design for shear

According to EN 1992-1-1 [61], a distinction must be made between planar components (slabs) and linear components (beams) when analysing the shear capacity. Owing to their large size, slabs present redistribution options for local overstressing and therefore may be built without shear reinforcement provided they do not exceed defined limits. Such options are not available in linear components, where minimum shear reinforcement should always be provided. These principles known from normal-strength concrete also apply to UHPC members.

5.2.4.1 Tests at the University of Kassel

Four-point bending tests were carried out on beams at the University of Kassel in order to determine the shear capacity of UHPC members.

In a first series of tests (beams S1 to S4), *Fehling/Bunje* investigated beams without shear reinforcement and without fibre reinforcement [107]. The beams involved were rectangular sections and contained various amounts of longitudinal reinforcement (Figure 5.8). Shear failure occurred in all the specimens (Figure 5.9). The values obtained from the tests are very easy to understand when applying the model according to *Zink* [108]. This model is essentially based on the shear capacity of the flexural compression zone, as Figure 5.10 shows.

In order to determine the shear capacity $V_{u,ct}$, Equation 5.11 also includes the fracture mechanics influence of the transfer of tensile stresses in the region of the tip of the crack and a term that allows for the shear slenderness a/d :

$$V_{u,ct} = \frac{2}{3} \cdot b_w \cdot k_x \cdot d \cdot f_{ct} \cdot \left(\frac{4 \cdot d}{a} \right)^{1/4} \cdot \left(\frac{5 \cdot l_{ch}}{d} \right)^{1/4} \quad (5.11)$$

where

b_w web thickness

k_x relative depth of compression zone x/d

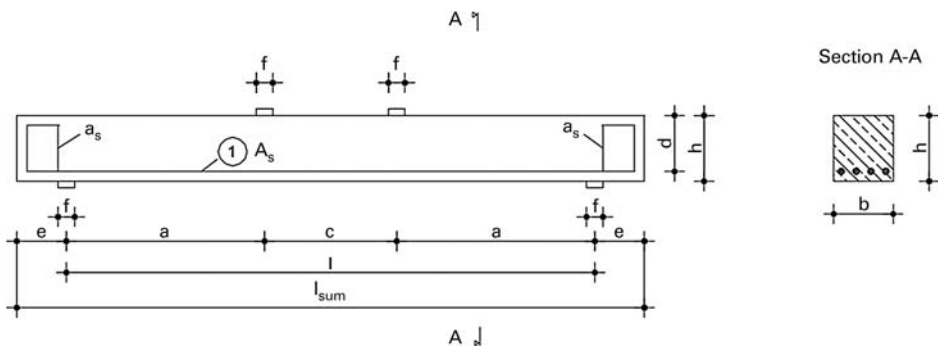


Fig. 5.8 Sketch of reinforcement in test beams [109]

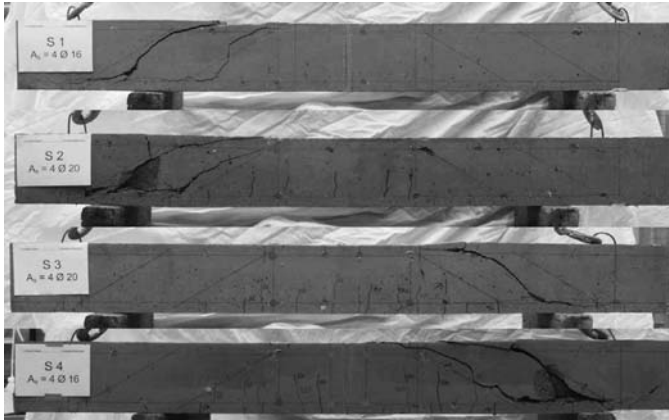


Fig. 5.9 Photographs of failures of first series of test beams without shear reinforcement and without fibre reinforcement [109]

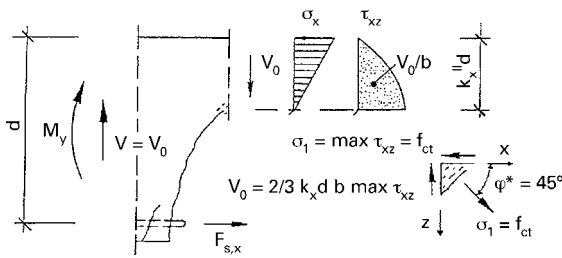


Fig. 5.10 Shear force model after Zink [108]

d effective depth

f_{ct} tensile strength of concrete matrix

a distance of applied point load from support

$$l_{ch} = \frac{E_c \cdot G_f}{f_{ct}^2} \text{ characteristic length after Hillerborg [110]} \quad (5.12)$$

As an estimate when re-analysing the tests, $G_f = 143 \text{ N/m}$ was assumed for UHPC without fibres – a figure based on the values according to *Rommel* [111] and *Grimm* [112] for high-strength concrete. Figure 5.11 shows good agreement with the test results. As the depth of the compression zone is essentially determined by the longitudinal reinforcement ratio ρ_1 , this is used as the abscissa in Figure 5.11.

Results similar to those obtained using the *Zink* model are obtained for the design value of the shear capacity for members reinforced for bending but without shear reinforcement in accordance with EN 1992-1-1 [61], considering DIN EN 1992-1-1/NA [62]:

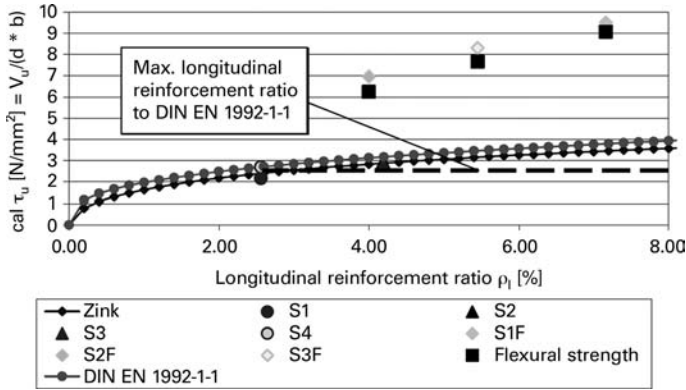


Fig. 5.11 Shear capacity depending on amount of longitudinal reinforcement [109]

$$V_{Rd,c} = \left[0.1 \cdot k \cdot (100 \cdot \rho_l \cdot f_{ck})^{1/3} + 0.12 \cdot \sigma_{cp} \right] \cdot b_w \cdot d \quad (5.13)$$

where

f_{ck} characteristic concrete compressive strength

k scale factor

$$k = 1 + \sqrt{\frac{200}{d}} \leq 2.0 \quad (5.14)$$

ρ_l longitudinal reinforcement ratio in tension zone

σ_{cp} concrete stress due to axial force, $\sigma_{cp} = N_{Ed}/A_c$ ($N_{Ed} > 0$ for compression).

In a second series of tests, *Fehling/Bunje* investigated beams made from fibre-reinforced UHPC without shear reinforcement (beams S1 F to S4 F). Their dimensions were the same as those of the first series [107].

The beams in these tests turned out to have a much higher load-carrying capacity than those of the comparable test specimens in the first series. The full bending capacity was reached in all tests and a pronounced ductile behaviour was observed. Only in the case of beam S1 F, with a very high longitudinal reinforcement ratio $\rho_l = 7.2\%$, did a combined bending/shear failure take place (Figure 5.12).

As part of the German programme of research into sustainable building with UHPC (priority programme SPP 1182), *Fehling/Thiemicke* [113] investigated the shear behaviour of fibre-reinforced, fine-grained UHPC beams with and without bar-type shear reinforcement. In order to force a shear failure, the test beams had a very pronounced I-shaped cross-section in the zone being investigated (Figure 5.13). The web of the I-section was 30 mm thick, the total web zone measured about 1.16×0.20 m.

Identical flexural tension reinforcement made up of grade B 500 steel bars ($f_y = 500$ N/mm²) was provided in all the test beams (Figure 5.14). The reinforcement in the beams

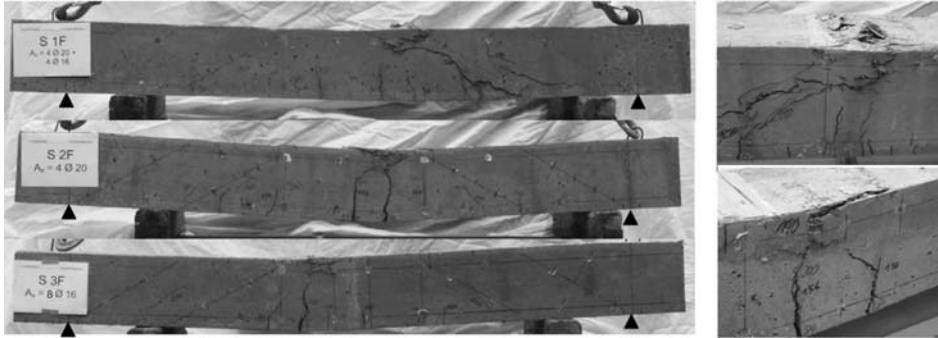


Fig. 5.12 Photographs of failures of the second series (left) and close-ups of the shear failure (top right) and the combined bending/shear failure (bottom right) [109]

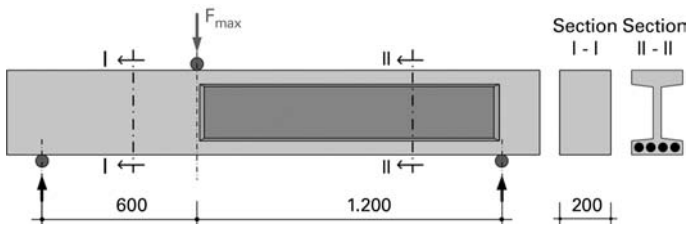


Fig. 5.13 Geometry of test beams [113]

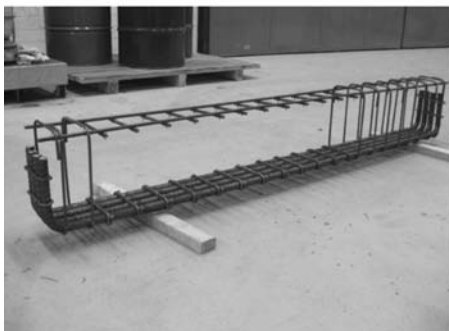
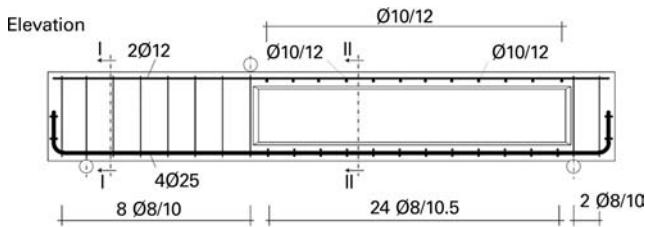
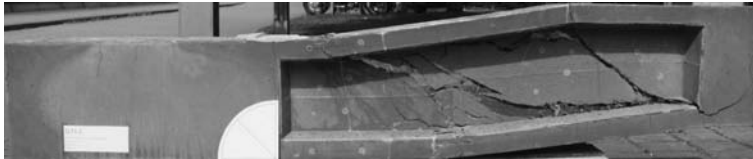


Fig. 5.14 Basic reinforcement [113]

Table 5.2 Variation in shear reinforcement [113].

Shear reinforcement	Q	Q-B1	Q-F1	Q-F1-B1
Shear links, \varnothing 5 mm, 105 mm c/c spacing	–	+	–	+
1% by vol. steel fibres, \varnothing 0.175 mm, 13 mm long	–	–	+	+

**Fig. 5.15** Failure of fibre-reinforced UHPC beam without shear links [113]

differed only in the amount of the high-strength steel fibres ($f_t = 2500 \text{ N/mm}^2$) added to the mix and the provision of bar-type shear reinforcement (Table 5.2).

The accompanying materials tests established compressive strengths of $185\text{--}224 \text{ N/mm}^2$ and flexural tensile strengths of 7.4 N/mm^2 for UHPC without fibres and 23.2 N/mm^2 for UHPC with fibres. A modulus of elasticity $45\,000\text{--}50\,000 \text{ N/mm}^2$ was determined.

The beams were tested in three-point bending tests with displacement control. In every test beam, the shear failure took place within the web. The shear cracks observed in the tests on beams without fibre reinforcement were spaced further apart and were wider, whereas those beams with fibre reinforcement developed a larger number of narrower cracks at a closer spacing, and two much wider failure cracks were only seen shortly before reaching the ultimate load (Figure 5.15). The beams containing shear links cracked upon reaching the maximum load.

When fibres were added or shear links included, the ultimate load attained initially increased beyond that of the test beams without shear reinforcement, and rose again for beams with fibres and shear links (Figure 5.16).

5.2.4.2 Tests at RWTH Aachen University

Again within the scope of the German research programme, *Hegger/Bertram* investigated the shear behaviour of prestressed UHPC beams [114, 115].

The concretes used were based on the mix recommendations of the German research programme. The basic mix (M0) had a fibre content of 2.5% by vol. For reasons of sustainability, lower fibre contents were also investigated. Reference tests without fibres were also carried out. All the fibres used were plain, without hooks, and had tensile strengths $>2000 \text{ N/mm}^2$.

Beams with solid webs and beams with web openings were tested. The key test parameters were the fibre content, the prestress and the shear slenderness. The overhang

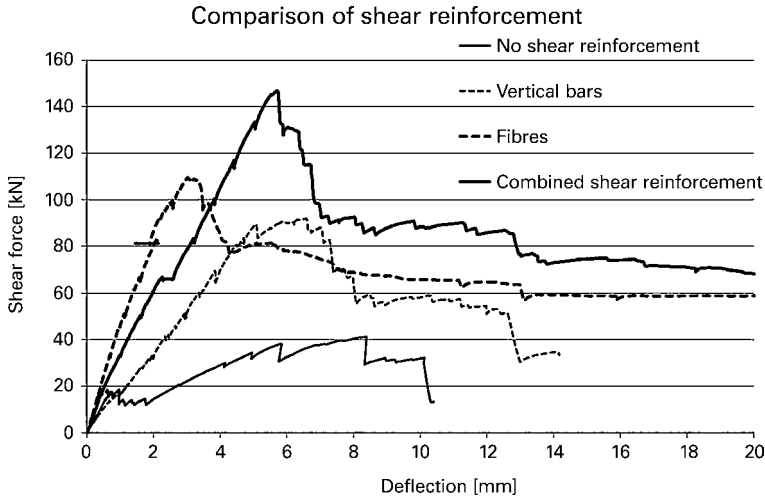


Fig. 5.16 Load–deflection curves for beams with different types of reinforcement [113]

at the supports was the same in all tests, i.e. 15 cm. The key parameters for the beams with web openings were the number of openings and the distances between support and opening and between openings, and these parameters were varied. The cross-section was the same in all tests (Figure 5.17). Two shear tests were carried out on each beam.

The prestress makes a major contribution to the shear capacity. The prestress component introduced right at the support reinforces the arch action (Figure 5.18). If the transfer length is longer than the support overhang, only a certain proportion of the prestress is

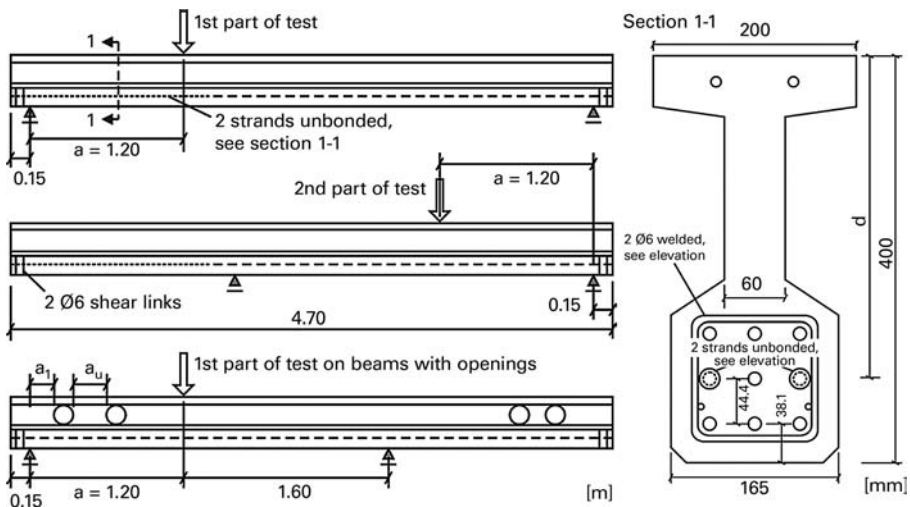


Fig. 5.17 Test setup and beam cross-section [115]

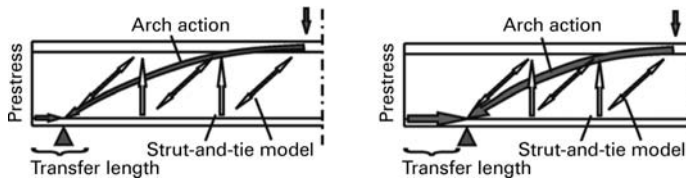


Fig. 5.18 How the prestressing force influences arch action [115]

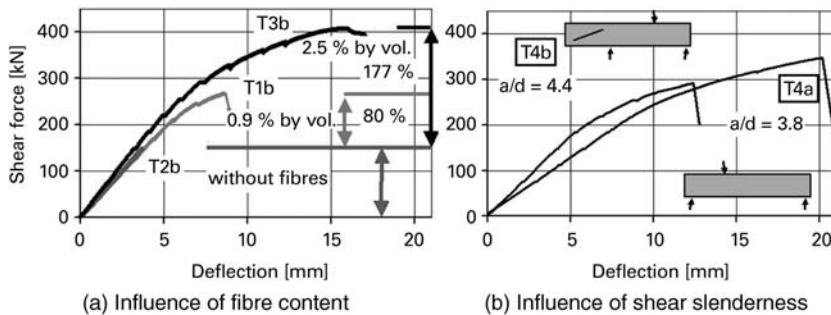


Fig. 5.19 Influence of fibre content and shear slenderness on shear capacity [115]

available. The course of the bond stresses and the resulting transfer length are therefore fundamental for determining the arch action component. Studies of the bond behaviour were therefore carried out prior to the shear tests [116].

Very stiff load–deformation behaviour was observed in all the shear tests. The shear forces reached by the solid web beams are plotted against the deflection at the load application point in Figure 5.19.

The curves in Figure 5.19a show very effectively how different fibre contents affect the shear capacity for the same prestress. The angle of the failure cracks was between 20° and 24° . Besides increasing the load-carrying capacity, ductile failure and advance warnings of failure are the main advantages of adding steel fibres.

Compared with that, the rapid loss of stiffness in the beams without fibres is conspicuous (Figure 5.20). Pronounced, abrupt changes in stiffness occur, which are caused by localized cracking.

The influence of steel fibres is even more noticeable in the beams with web openings than it is in the beams without openings. The loadbearing effect of the fibres declines as the shear cracks widen. Only at the end of the plastic portion of the diagram does the loadbearing effect of the fibres fail completely and the load drop significantly.

5.2.4.3 Tests at Delft University of Technology

In 2004 a series of tests was carried out on three beams within the scope of a research programme at Delft University of Technology [117]. The dimensions of the beams are shown in Figure 5.21. The mean concrete compressive strength was 140 N/mm^2 and the

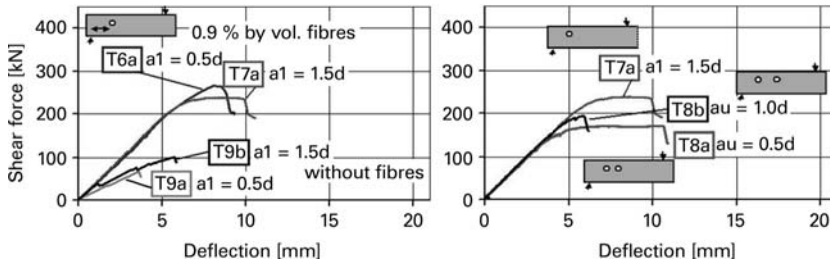


Fig. 5.20 Influence of prestressing force on arch action [115]

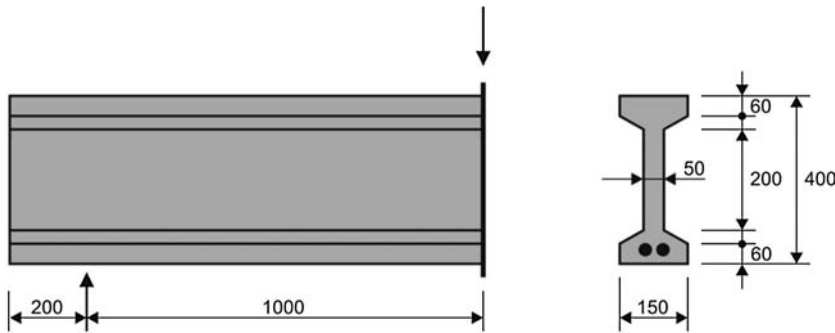


Fig. 5.21 UHPC beam used in shear tests at Delft University of Technology [117]

concrete contained 0, 0.8 and 1.6% by vol. straight steel fibres, 13 mm/0.16 mm. The bending reinforcement consisted of two bars, $\phi = 25$ mm. Again, there was no shear reinforcement. All the beams failed in shear. Figure 5.22 shows the crack patterns.

The different failure loads given in Figure 5.22 and their associated crack patterns revealed that the fibres had a considerable influence on the shear behaviour. The shear capacities were compared with the theoretical capacities calculated with EN 1992-1-1 [61], which uses the variable strut inclination method to calculate the shear capacity of beams with shear reinforcement. According to this method, any strut inclination θ in the range $1 \leq \cot \theta \leq 2.5$ may be chosen. The shear reinforcement activated at this angle contributes to the shear capacity. The shear capacity then follows from

$$V_u = b_w \cdot d \cdot \cot \theta \cdot \frac{A_{sw}}{t} \cdot f_{sy} \quad (5.15)$$

where

- b_w web thickness
- d effective depth
- θ strut inclination
- A_{sw} cross-sectional area of one shear link
- t spacing of shear links
- f_{sy} yield stress of shear link steel.

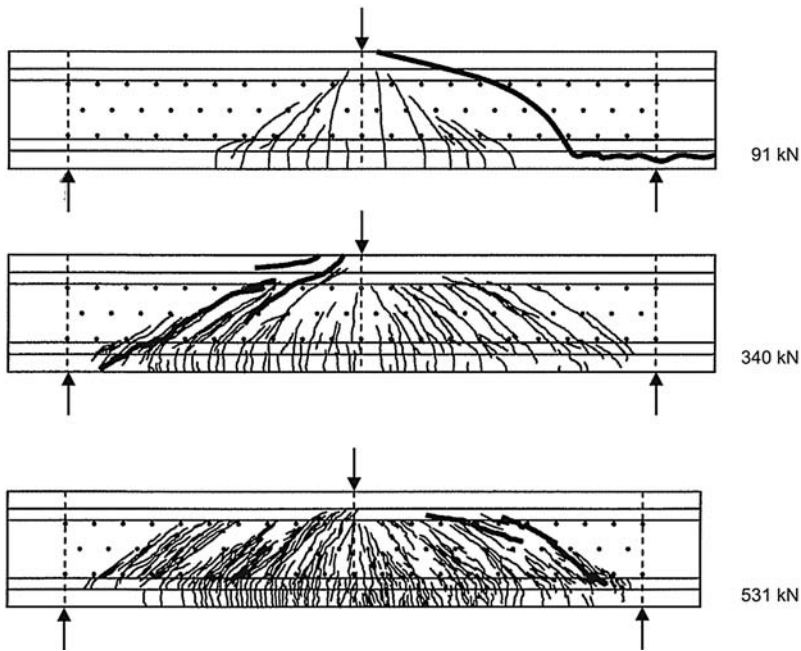


Fig. 5.22 Crack patterns of UHPC beams with (from top to bottom) 0, 0.8 and 1.6% by vol. fibre reinforcement [117]

The following approach may be used when employing fibres as shear reinforcement:

$$V_u = b_w \cdot h \cdot \cot \theta \cdot \sigma_{pf} \quad (5.16)$$

where

h maximum depth of cross-section

σ_{pf} post-cracking tensile strength (fibre efficiency) (a constant stress level is assumed).

Equation 5.16 uses the depth of the cross-section h instead of the effective depth d because it is to be expected that the fibres below the longitudinal reinforcement also contribute to the shear capacity. It is no surprise that the fibres also have a positive influence on the rotation capacity of the struts and therefore it is assumed that the limits to the strut inclination, can be extended to $1 \leq \cot \theta \leq 3$.

The post-cracking tensile strength was determined in axial tensile tests. The corresponding values are $\sigma_{pf} = 5.6$ and 9.0 N/mm^2 for fibre contents of 0.8 and 1.6% by vol. respectively. A further assumption, $\cot \theta = 3$, results in adequate agreement between the shear forces calculated in this way and the tests (see Table 5.3).

Of course, these results can only be regarded as provisional. The comparison shows, however, that expanding the known relationships to UHPC represents an interesting option.

Table 5.3 Shear capacity determined in tests in comparison with values calculated using Equation 5.16 and $\cot \theta = 3$ [117].

	V_f (%)	σ_{pf} (N/mm ²)	$V_{u,theor}$ (kN)	$V_{u,test}$ (kN)
Beam 2	0.8	5.6	311	340
Beam 3	1.6	9.0	500	531

5.2.5 Punching shear

The ultimate resistance to punching shear in thin fibre-reinforced UHPC slabs with and without additional conventional steel reinforcement has been investigated at the University of Applied Sciences, Fribourg, Switzerland [118] (Figure 5.23). The depth of the slabs was 30–80 mm. Each test specimen was supported on eight steel rods, which permitted rotation, arranged in a circle. The load was applied by a hydraulic cylinder via an 80 mm diameter punch in the centre.

The slabs with fibre reinforcement only all failed in bending. The slabs with steel reinforcing bars could be loaded until the flexural tension reinforcement yielded; they subsequently failed in punching shear.

The following expressions can be used to calculate the punching shear resistance [118]:

Contribution of concrete [119]:

$$\frac{V_{R,c}}{b_0 \cdot d \cdot \sqrt{f_c}} = \frac{3/4}{1 + 15 \cdot \frac{\psi \cdot d}{16 + d_g}} \quad (5.17)$$

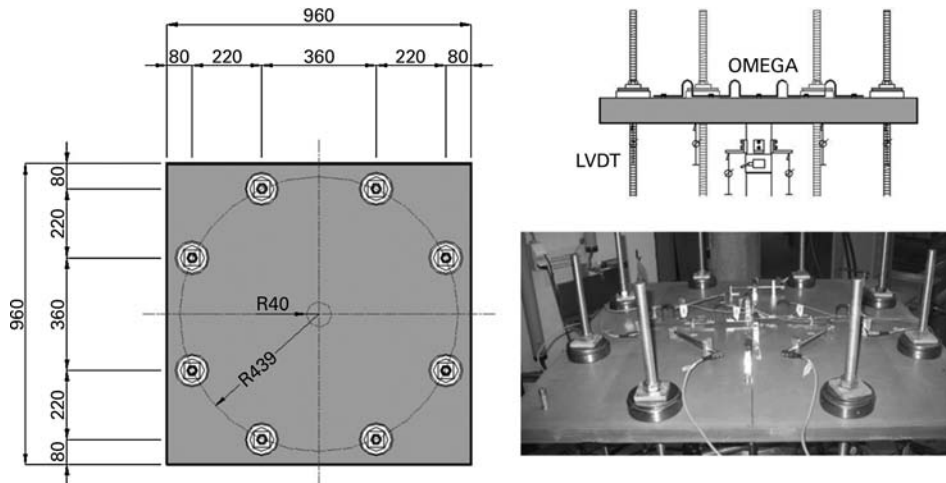


Fig. 5.23 Test setup for punching shear tests on thin UHPC slabs [118]

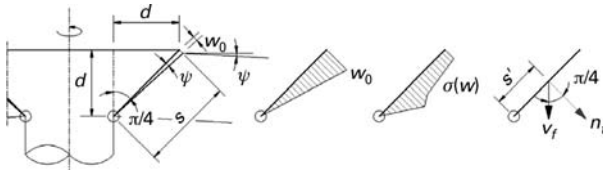


Fig. 5.24 Mechanics-based model for determining contribution of fibres [118]

where

b_0 perimeter of critical section at distance $d/2$ from edge of loaded area

d effective depth

f_c compressive strength of UHPC

ψ angle of rotation of slab around the supported area (see Figure 5.24)

d_g maximum aggregate size, assumed to be zero for UHPC.

Contribution of fibres:

$$V_{R,f} = \frac{1}{K} \cdot \int_{A_p} \sigma_f(w) \cdot dA_p \tag{5.18}$$

K factor to allow for fibre orientation

$\sigma_f(w)$ stress–crack width relationship of fibre-reinforced UHPC

A_p cracked surface area of punching shear cone.

An evaluation of Equation 5.17 calls for knowledge of the relationship between shear force and rotation, which at first has to be calculated theoretically [119]. As the contribution due to matrix softening (aggregate interlock) is already included in the concrete matrix contribution, it is not considered in the stress–crack width relationship of the fibre-reinforced concrete $\sigma_f(w)$. The total ultimate resistance then results from adding together the contributions of the concrete matrix and the fibres.

Figure 5.25 compares the test results of selected slabs with the failure criterion according to Equations 5.17 and 5.18. The solid black line represents the ultimate resistance of the concrete without fibres and the dashed lines represent the fibre contributions. Adding these together results in the solid grey lines. Bending failure governs for those test specimens that do not reach the failure envelope.

5.2.6 Strut-and-tie models

Strut-and-tie (or truss) models consist of concrete struts, ties and the intervening nodes. In pure reinforced concrete construction, the reinforcing bars represent the ties.

Equilibrium must be taken into account when determining the forces in the struts of the strut-and-tie model. Further, in order to guarantee the compatibility of the deformations for the member, the linear elastic determination of the distribution of the tensile and compressive stresses should be represented as accurately as possible by the arrangement of the ties and struts.

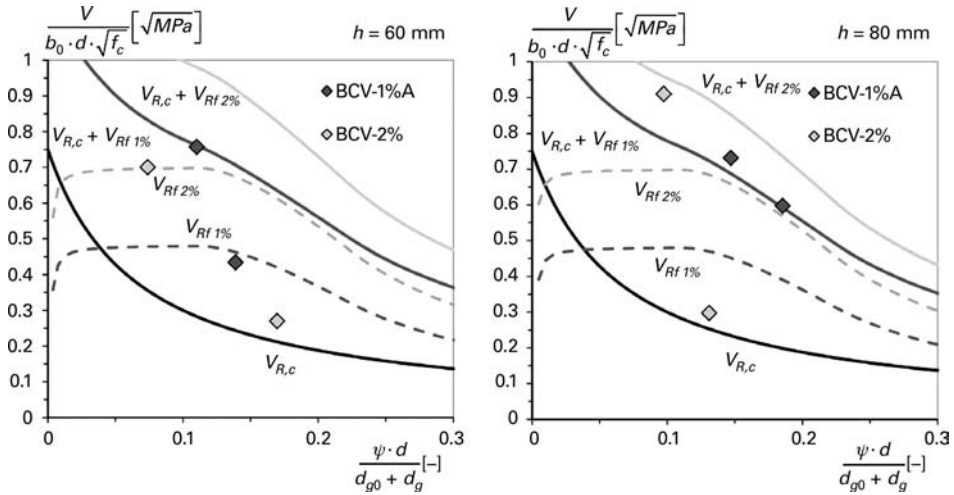


Fig. 5.25 Comparison of failure criterion and test results [118]

In principle, the approach to designing a strut-and-tie model can also be retained when planning a combination of reinforcing bars and fibres. In the design, the fibres may count towards the load-carrying capacity of the ties.

Designing on the basis of a linear elastic or non-linear finite element calculation appears to be better suited to UHPC with fibre reinforcement only.

5.2.6.1 Load-carrying capacity of struts

Tests to establish the compression-tension strength of cracked UHPC with rebars but without fibres were carried out on panel-type specimens [120]. The case of cracks parallel with the compression direction resulted in a reduction in the load-carrying capacity of up to 50% compared with the uniaxial compressive strength for large lateral strains, or rather crack widths. The addition of 1.0% by vol. fibres resulted in a maximum reduction of only 30%.

Based on this, the proposal is to limit the design value of the strength of the strut as follows:

$$\sigma_{Rd,max} = \nu \cdot f_{cd} \quad (5.19)$$

where

f_{cd} design value of uniaxial compressive strength of UHPC

ν reduction factor to allow for the influence of transverse tension action and cracking on the design value of the strength of the strut.

The following ν factors are recommended for ‘sufficiently ductile’ (see Section 5.2.1) fibre-reinforced UHPC:

- $\nu = 1.0$ for uncracked struts subjected to transverse tension
- $\nu = 0.70$ for struts parallel with cracks
- $\nu = 0.50$ for struts that intersect cracks

Conservative ν factors should be assumed for UHPC without sufficient ductility:

- $\nu = 0.85$ for uncracked struts subjected to transverse tension
- $\nu = 0.50$ for struts parallel with cracks
- $\nu = 0.40$ for struts that intersect cracks

5.2.6.2 Load-carrying capacity of ties

With combined reinforcement (rebars + fibres), the contribution of the fibres in a reasonable area around the steel reinforcement may be counted towards the load-carrying capacity of the ties. The design value of the tie capacity is then calculated as follows:

$$F_{Rd} = A_s \cdot f_{yd} + A_{c,ef} \cdot \sigma_{cf0d} \quad (5.20)$$

where

- A_s cross-sectional area of steel rebar, represented by the tie
- f_{yd} design value of yield point of steel rebar
- $A_{c,ef}$ effective cross-sectional area of concrete that can be assigned to the tie (area around steel rebar), which must be specified realistically in each case
- σ_{cf0d} design value of fibre efficiency.

5.2.6.3 Load-carrying capacity of nodes

Work has been carried out by *Curbach/Speck* [121] to establish the multi-axial strength of UHPC. They discovered that the load-carrying capacity under biaxial compression-compression loading in the coplanar stress state climbs to a much lesser extent – compared with the uniaxial compressive strength – than is the case with normal-strength concrete. Whereas $\sigma_1 = \sigma_2$ is valid for the principal stresses, only the uniaxial strength is reached in UHPC without fibres. Only by adding 2.5% by vol. fibres was it possible to achieve an increase in strength amounting to about 7%.

So, even for fibre-reinforced UHPC, the design value of the node load-carrying capacity should be estimated very cautiously. Based on Equation 5.19, the following values are recommended for the factor ν :

- $\nu = 1.0$ for compression-compression nodes (without tie anchorage)
- $\nu = 0.70$ for compression-tension nodes (with tie anchorage) in fibre-reinforced UHPC with ‘sufficient ductility’
- $\nu = 0.50$ for compression-tension nodes (with tie anchorage) in fibre-reinforced UHPC without ‘sufficient ductility’

5.2.7 Partially loaded areas

Tests on partially loaded areas to determine the load-carrying capacity of fine- and coarse-grained UHPC were carried out by *Klotz/Holschemacher* [122]. Test specimens measuring 20 cm × 20 cm × 40 cm and 20 cm × 20 cm × 20 cm, some unreinforced and some with helical and longitudinal reinforcing bars, were loaded via circular punches with diameters of 30 and 50 mm. The unreinforced specimens carried compressive stresses in the order of 2.0–3.7 times the uniaxial compressive strength; failure varied from brittle to splitting. The confining effect of the helical reinforcement resulted in a rise in the load-carrying capacity of up to 5.5 times the uniaxial compressive strength.

Klotz/Holschemacher propose in [122] that for unreinforced coarse-grained UHPC, the admissible partial loading force F_{Rd} should be limited to 75% of the value given in EN 1992-1-1 [61]. A factor of 2/3 can be derived for fine-grained UHPC.

It is frequently the case that a concentrated force transfer leads to the formation of a bottle-shaped compression field in the concrete and the transverse tensile stresses associated with this cannot be accommodated by reinforcement, or rather confinement. Splitting of the concrete can then take place at stresses well below the uniaxial compressive stress, which limits the load that can be carried by the partially loaded areas [80].

Owing to the less favourable tensile/compressive strength ratio in UHPC when compared with normal-strength concrete, experimental investigations of the bottle-shaped compression field [123] resulted in a much lower bearing pressure at the partially loaded area with respect to the uniaxial compressive strength. Figure 5.26 shows the results for different types of concrete. The way of presenting this is that specified by *Schlaich and Schäfer* [80] for the theoretical cracking load of two-dimensional bottle-shaped compression fields. Whereas normal-strength concrete can be assigned roughly to the line $\omega = 0.09$, a relative admissible partial-load bearing pressure < 1 ($\omega = 0.04$ or $\omega = 0.03$) was determined for the high-strength concrete and the UHPC without fibres – almost without exception.

Adding fibres to UHPC raised the load-carrying capacity of the bottle-shaped compression fields significantly. The admissible partial-load bearing pressure was more than doubled with a fibre content of just 1.0% by vol. However, splitting remained the critical failure mode because a compression failure under the load application area was practically ruled out owing to the fact that lateral strain is prevented here.

5.2.8 Fatigue

Based on the research results given in [89], a proposal is made in [124] to determine the design value of the fatigue strength by modifying the method given in CEB-FIP Model Code 90 [59]:

$$f_{cd, \text{fat}} = 0.85 \cdot \beta_{cc}(t) \cdot f_{ck} \cdot (1 - f_{ck}/40f_{ck0})/\gamma_c \quad (5.21)$$

where

$$f_{cf0} = 10 \text{ MN/m}^2$$

$\beta_{cc}(t)$ factor to allow for the increase in strength as hydration progresses

γ_c partial safety factor for UHPC under compression actions.

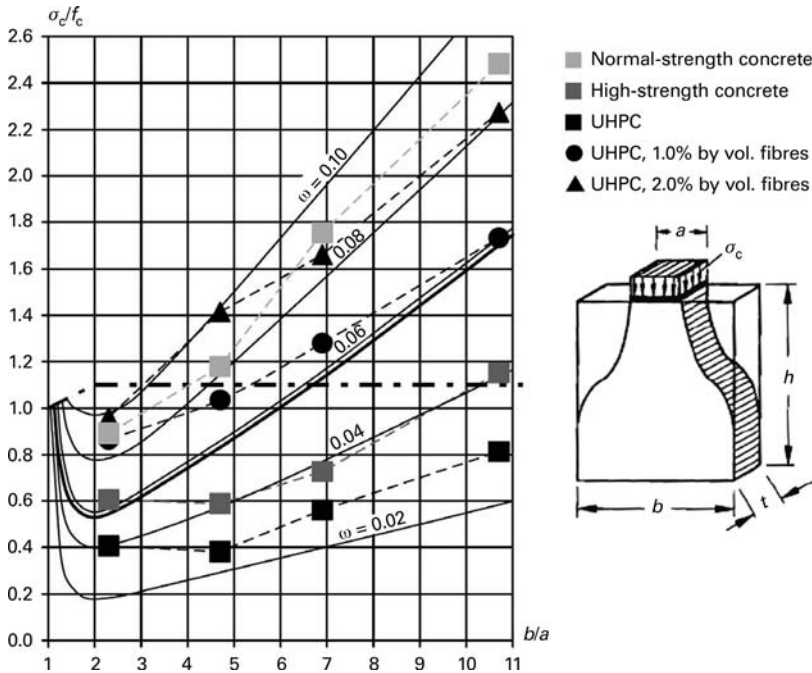


Fig. 5.26 Comparison of theoretical cracking stresses after *Schlaich/Schäfer* [80] with the admissible partial-load bearing pressure (related to the uniaxial compressive strength) found in tests [123]

Compared with Model Code 90, the prefactor of f_{ck0} has been raised from 25 to 40. This modification was necessary because applying the Model Code 90 approach would otherwise have led to a reduction in the fatigue strength design value for strengths of $f_{ck} = 125 \text{ N/mm}^2$ and higher.

Ref. [89] derives a partial safety factor $\gamma_c = 1.5$ for UHPC.

5.3 Analyses for the serviceability limit state

5.3.1 Limiting crack widths

When checking crack widths, it is important to distinguish between exclusively fibre-reinforced components and components with a combination of fibres and conventional reinforcing or prestressing steel.

In the former case, the crack width can be determined directly with the help of the stress–crack width relationship depending on the actual stress level due to external actions. However, owing to the uncertainties with regard to the distribution and orientation of the fibres, the effect of the fibres should be gauged very cautiously.

No verified findings are currently available regarding the effects of long-term or repeated actions on the loadbearing behaviour of cracked fibre-reinforced UHPC.

Therefore, when it comes to durability, the aim is to prevent cracking under service loads (rare combination of actions) if at all possible. This situation frequently arises automatically because designing for the ultimate limit state requires certain reserves since a correspondingly higher level of safety is to be attained.

Notwithstanding, cracking can also be permitted under service loads if the fibre-reinforced UHPC still exhibits a strain hardening post-cracking behaviour in axial tension tests even when taking into account the characteristic value of the fibre efficiency. This is because the crack widths to be expected in this case are not detrimental to the durability. This also applies, of course, to the case where such concretes are reinforced with continuous reinforcing elements.

Mostly, however, only moderate fibre contents are used in combination with reinforcing or prestressing steel, which means that fibre-reinforced UHPC itself does not exhibit strain hardening behaviour. In this case, the development of the crack widths in the serviceability limit state should be investigated more closely.

Our starting point here is the general equation for determining the characteristic value of the crack width w_k well known from reinforced concrete:

$$w_k = s_{r,max} \cdot (\varepsilon_{sm} - \varepsilon_{cm}) \quad (5.22)$$

where

$s_{r,max}$ maximum crack spacing in stabilized cracking state (maximum length over which slip between steel and concrete occurs); for single cracks, $s_{r,max}$ is equal to twice the load transfer length l_{es} of the bar reinforcement

ε_{sm} steel strain averaged over $s_{r,max}$

ε_{cm} concrete strain averaged over $s_{r,max}$.

Figure 5.27 shows the qualitative strain distribution diagrams for the bar reinforcement and the concrete (matrix) for the (substitute) tension bar in the region of a single crack (a) and for the stabilized cracking state (b). The influence of UHPCs comparatively high shrinkage strain on the distributions has been allowed for.

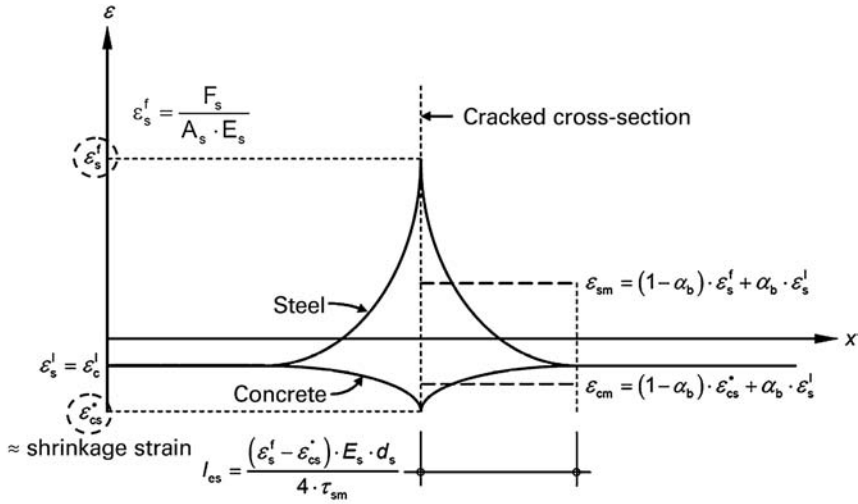
The force in the steel F_s has to be calculated taking into account the contribution of the fibres. This will be described later. The force is therefore smaller than with normal reinforced concrete. The fibres relieve the load on the bar reinforcement and this has a positive effect on the load transfer length, or rather the crack spacing. Now, in order to create a new crack, only the cracking stress of the fibre-reinforced UHPC f_{ctfm} , reduced by the fibre-reinforced concrete stress σ_{cf} , has to be transferred by the contribution of the steel reinforcing bar.

Based on Figure 5.27, the mean strain difference between bar reinforcement and concrete matrix can be expressed as follows [125, 173, 174]:

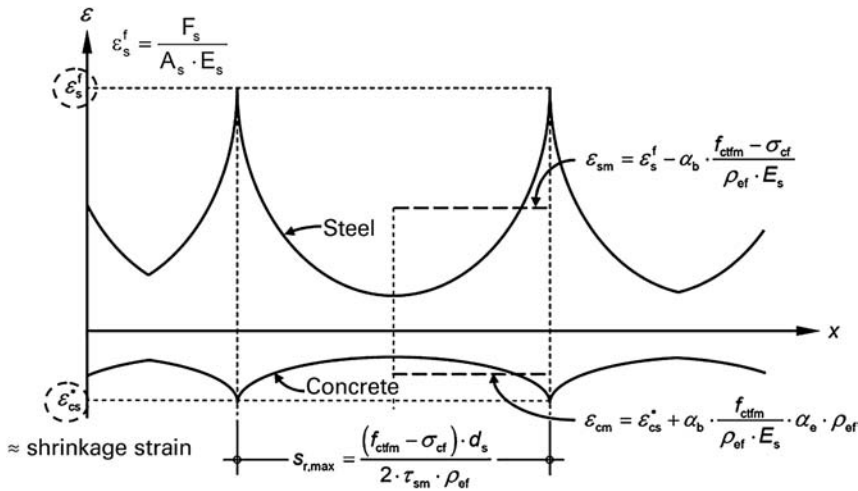
$$\varepsilon_{sm} - \varepsilon_{cm} = \varepsilon_s^f - \varepsilon_{cs}^* - \alpha_b \cdot \frac{f_{ctfm} \cdot (1 + \alpha_e \cdot \rho_{ef}) - \sigma_{cf}}{\rho_{eff} \cdot E_s} \geq (1 - \alpha_b) \cdot (\varepsilon_s^f - \varepsilon_{cs}^*) \quad (5.23)$$

where

ε_s^f steel strain at crack taking into account the fibres (cross-section in equilibrium)



(a) Single crack



(b) Stabilised cracking

Fig. 5.27 Qualitative distribution of strains in bar reinforcement and concrete matrix taking into account concrete shrinkage [125, 173, 174]: a) single crack, b) stabilized cracking

α_b shape coefficient for strain distribution diagrams $\alpha_b = 0.6$ for short-term loads
 $\alpha_b = 0.4$ for long-term and repeated loads

f_{ctfm} mean value of cracking stress in fibre-reinforced UHPC (concrete matrix + fibre effect)

ρ_{eff} effective reinforcement ratio of bar reinforcement, $\rho_{eff} = A_s / A_{c,ef}$

A_s cross-sectional area of bar reinforcement

$A_{c,ef}$ effective tension area for taking into account the non-linear stress distribution in the concrete tension zone at the end of the load transfer length of the bar reinforcement

σ_{ct} tensile stress transferred by fibres at crack (see below)

ε_{cs}^* post-cracking shrinkage strain in concrete at edge of crack; when shrinkage and creep develop similarly to each other, this value can be calculated as follows:

$$\varepsilon_{cs}^* = \frac{\varepsilon_{cs} \cdot (1 + \alpha_e \cdot \rho_{eff})}{1 + \alpha_e \cdot \rho_{eff} \cdot (1 + \rho \cdot \varphi)} \quad (5.24)$$

(To be on the safe side, ε_{cs}^* can be assumed to be equal to the free shrinkage strain of the concrete ε_{cs} .)

α_e modular ratio, $\alpha_e = E_s/E_c$

φ creep of UHPC

ρ relaxation factor, which can be estimated with $\rho = 0.8$.

The first term on the right-hand side of Equation 5.23 represents the stabilized crack pattern, the second one the single crack.

The effective stress in the fibre-reinforced concrete at the crack can be determined with the help of the stress–crack width relationship. During the fibre activation phase, the equation in Section 5.2.2.2 can be used, with the characteristic value of the fibre efficiency being taken as the maximum value instead of the design value:

$$\sigma_{cf} = \sigma_{cf0k} \cdot \left(2 \cdot \sqrt{\frac{w_k}{w_0}} - \frac{w_k}{w_0} \right) \quad (5.25)$$

where

σ_{cf0k} characteristic value of fibre efficiency.

As the stress in the fibre-reinforced concrete during the pull-out phase initially drops only marginally, the following may be assumed for simplicity when checking the crack width for $w_k > w_0$:

$$\sigma_{cf} = \sigma_{cf0k} \quad (5.26)$$

Twice the load transfer length, or rather the maximum crack spacing $s_{r,max}$, is obtained as follows [125, 173, 174]:

$$s_{r,max} = \frac{(f_{ctfm} - \sigma_{cf}) \cdot d_s}{2 \cdot \tau_{sm} \cdot \rho_{ef}} \leq \frac{(\varepsilon_s^f - \varepsilon_{cs}^*) \cdot E_s \cdot \delta_s}{2 \cdot \tau_{sm}} \quad (5.27)$$

where

δ_s diameter of reinforcing bar

τ_{sm} average bond stress of reinforcing bar within $s_{r,max}$.

Reference values for the mean bond stress τ_{sm} can be found in Table 5.4 and Figure 5.28. These figures were derived by analysis (although based on the results of pull-out tests) for use in checking crack widths [68, 125, 173, 174].

The steel strain ε_s^f at the crack required to evaluate Equations 5.23 and 5.27 is to be determined taking into account the force transfer of the fibres at the crack cross-section.

Table 5.4 Reference values for mean bond stress τ_{sm} .

Characteristic value of crack width w_k	Average bond stress τ_{sm} for a projected rib area of	
	$f_R = 0.024$	$f_R = 0.072$
0.05 mm	$1.2 f_{ctm}$	$2.0 f_{ctm}$
0.10 mm	$1.7 f_{ctm}$	$3.3 f_{ctm}$

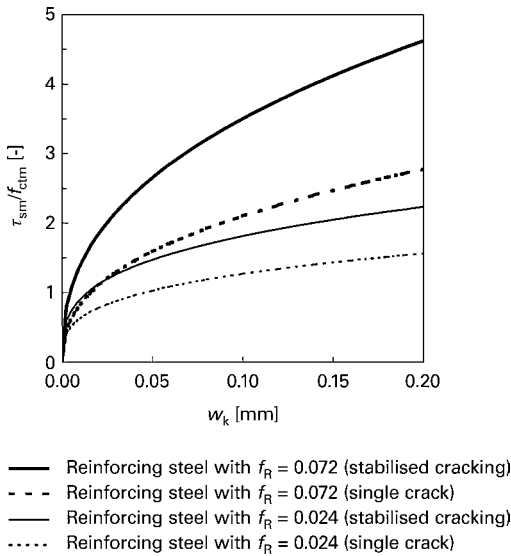


Fig. 5.28 Relative mean bond stress τ_{sm}/f_{ctm} as a function of crack width w_k [68]

For reasons of equilibrium, the following applies for test specimens subjected to axial tension (Figure 5.29):

$$F_s = N - F_f = N - \sigma_{cf} \cdot A_c \tag{5.28}$$

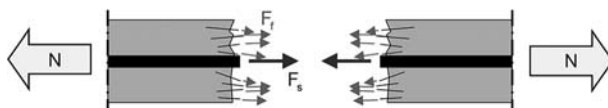


Fig. 5.29 Equilibrium of internal and external forces at crack for axial tension [105]

The tensile stress σ_{cf} transferred by the fibres at the crack is to be determined depending on the crack width using Equations 5.25 and 5.26.

Calculating the force in the steel F_s turns out to be more difficult for cross-sections subjected to bending and axial force because besides stresses in the fibre-reinforced concrete in the tension zone, stresses are also activated in the flexural compression zone. In a similar way to designing for bending and axial force, checking crack widths by considering limit cases can also lead to an approximate solution for rectangular cross-sections without having to consider the compatibility condition exactly.

The starting point for deliberations is again the potential distribution of the stresses in the fibre-reinforced concrete and the internal forces at the cracked cross-section. For the serviceability limit state it can be assumed that the fibre-reinforced concrete is very likely still in the fibre activation phase, or even if fibre efficiency has been reached, the crack width w_0 on the tension side of the cross-section has been exceeded by an insignificant amount only. For the limit case of complete fibre activation, the stress block parameters (hereinafter denoted α_R and k_a) for the ensuing stress distribution have already been given in Section 5.2.3. Figure 5.30 shows the development of these two variables for crack widths $w < w_0$. It can be seen that the stress block parameters vary between 0.67 and 0.83 for solidity and between 0.60 and 0.56 for the position of the resultant, although the values in the vicinity of $w/w_0 = 0$ are irrelevant for practical construction.

From equilibrium of forces it follows that:

$$F_c = -N_{Ed} + F_s + F_f \quad (5.29)$$

From equilibrium of moments it follows that:

$$\sum M = 0 = M_{Eds} - F_{cd} \cdot (d - x/3) + F_{fd} \cdot [d - x - k_a \cdot (h - x)] \quad (5.30)$$

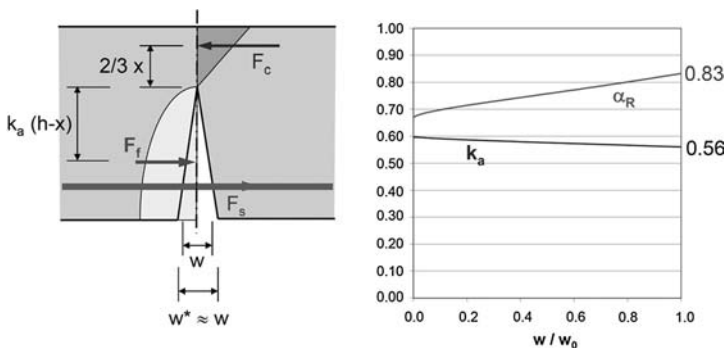


Fig. 5.30 Equilibrium of internal and external forces at crack for bending and axial force [105]

Substituting Equations 5.29 in 5.30 and solving for F_s gives us

$$\begin{aligned}
 F_s &= \frac{M_{Eds}}{z} + N_{Ed} - F_f \cdot \frac{\frac{2}{3} \cdot \frac{x}{d} + k_a \cdot \left(\frac{h-x}{d}\right)}{1 - \frac{x}{3 \cdot d}} \\
 &= \frac{M_{Eds}}{z} + N_{Ed} - \sigma_{cf0} \cdot b \cdot h \cdot \left[\alpha_R \cdot \left(1 - \frac{x}{h}\right) \cdot \frac{\frac{2}{3} \cdot \frac{x}{d} + k_a \cdot \left(\frac{h-x}{d}\right)}{1 - \frac{x}{3 \cdot d}} \right] \\
 &= \frac{M_{Eds}}{z} + N_{Ed} - \alpha_f \cdot \sigma_{cf0} \cdot A_c
 \end{aligned} \tag{5.31a}$$

where

$$\alpha_f = \alpha_R \cdot \left(1 - \frac{x}{h}\right) \cdot \frac{\frac{2}{3} \cdot \frac{x}{d} + k_a \cdot \left(\frac{h-x}{d}\right)}{1 - \frac{x}{3 \cdot d}} \tag{5.31b}$$

The term $(M_{Eds}/z + N_{Ed})$ corresponds to the known solution for equilibrium conditions for reinforced concrete. The expression $\alpha_f \cdot \sigma_{cf0} \cdot A_c$ describes the proportion of the force by which the fibres relieve the reinforcing steel.

The depth of the crack, or rather the depth of the compression zone, must be known in order to calculate the α_f parameter. That means the stress–strain curve of the UHPC valid for the compression zone and the stress–crack width relationship of the fibre-reinforced concrete in the tension zone must be combined while taking into account the compatibility of the deformations. This matter is discussed in [106]. Alternatively, an approximate solution can be found by considering a limit case, as mentioned earlier.

To do this, the case of a very large relative compression zone depth with $x/d=0.5$ and the limit case $x=0$ will be investigated; in addition, $d/h=5/6$ will be assumed. The evaluation of Equation 5.31b supplies values between about $\alpha_f=0.35$ and 0.56 for this (Figure 5.31). As an approximation, $\alpha_f=0.4$ seems to be appropriate. Using the same approach, it is possible to estimate α_f for other d/h ratios.

In the end, the steel strain ϵ_s^f at the crack is calculated with Equation 5.32:

$$\epsilon_s^f = F_s / (A_s \cdot E_s) \tag{5.32}$$

The disadvantage of calculating the crack width with Equation 5.22 or by evaluating Equations 5.23 and 5.27 seems to be that the stress in the fibre-reinforced concrete σ_{cf} is itself dependent on the crack width w_k , and therefore w_k can only be found iteratively.

For the design case, where the cross-sectional area of reinforcing steel required to limit crack widths to a certain theoretical value is to be determined, Equations 5.23 and 5.27 can be substituted in Equation 5.22 and solved for the reinforcement required A_s [68]. Neglecting the concrete strain due to external actions, we get the following:

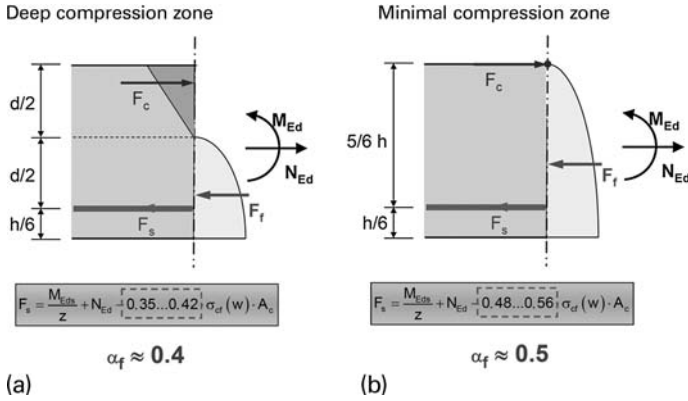


Fig. 5.31 Rough evaluation of the equilibrium conditions by way of considering limit cases [105]: a) large relative compression zone depth with $x/d = 0.5$, b) small (point-like) compression zone with $x = 0$

a) Single crack:

$$A_s = \frac{F_s}{\sqrt{\frac{2 \cdot E_s \cdot \tau_{sm} \cdot w_k}{(1 - \alpha_b) \cdot d_s} + \varepsilon_{cs}^* \cdot E_s}} \quad (5.33)$$

b) Stabilized cracking:

$$A_s = \Omega^f \cdot \left(-\varepsilon_{cs}^* + \sqrt{\varepsilon_{cs}^{*2} + 2 \cdot \frac{F_s - \alpha_b \cdot (F_{f,cr,ef} - F_{f,ef})}{\Omega^f \cdot E_s}} \right) \quad (5.34)$$

where

$$\Omega^f = \frac{(F_{f,cr,ef} - F_{f,ef}) \cdot d_s}{4 \cdot w_k \cdot \tau_{sm}} \quad (5.35)$$

$F_{f,ef}$ tensile force transferred by the fibres at the crack within the area of influence of the reinforcement:

$$F_{f,ef} = A_{c,ef} \cdot \sigma_{cf}$$

$F_{f,cr,ef}$ cracking force of area of influence of reinforcement:

$$F_{f,cr,ef} = A_{c,ef} \cdot f_{ctfm}$$

If reinforcing and prestressing steel are both being used, then it is known that the different bond behaviours of the two types of reinforcement must be taken into account.

In this situation the steel strain ϵ_s^f in Equations 5.23 and 5.27 must be calculated on the basis of the modified stress in the reinforcing steel:

a) Single crack:

$$\sigma_{s2}^f = \frac{F_{s+p}}{A_s + \xi_1 \cdot A_p} \quad (5.36)$$

b) Stabilized cracking:

$$\sigma_{s2}^f = \frac{F_{s+p}}{A_s + A_p} + \alpha_b \cdot (f_{ctfk} - \sigma_{cf}) \cdot \left(\frac{1}{\rho_{ef}} - \frac{1}{\rho_{s+p}} \right) \quad (5.37)$$

where

F_{s+p} sum of tensile force at crack carried by reinforcing and prestressing steel, calculated taking into account the contribution of the fibres

ξ_1 ratio of mean bond stresses for reinforcing and prestressing steel taking into account the different diameters:

$$\xi_1 = \sqrt{\frac{\tau_{pm} \cdot d_s}{\tau_{sm} \cdot d_p}} \quad (5.38)$$

ρ_{ef} effective reinforcement ratio of reinforcing plus prestressing steel:

$$\rho_{ef} = (A_s + \xi_1^2 \cdot A_p) / A_{c,ef} \quad (5.39)$$

ρ_{s+p} geometric reinforcement ratio of reinforcing plus prestressing steel:

$$\rho_{s+p} = (A_s + A_p) / A_{c,ef} \quad (5.40)$$

5.3.2 Minimum reinforcement

The purpose of minimum reinforcement is to prevent brittle failure of a member without prior warning. In UHPC such reinforcement can consist of fibres, reinforcing steel, prestressing steel or a combination of these types of reinforcement.

When dealing with members loaded primarily in bending, taking the simplified equilibrium approach of the preceding section as our basis allows us to apply the following approximation to determine the minimum reinforcement [105]:

$$\sigma_{cf} + \frac{A_s}{A_{ct}} \cdot \sigma_{s2}^f \geq k_c \cdot f_{ctfm} \quad (5.41)$$

where

σ_{cf} tensile stress transferred by the fibres at the crack – the characteristic value of the fibre efficiency σ_{cf0k} can be assumed here for σ_{cf} , but a lower value may be necessary to limit crack widths (see Section 5.3.1)

A_s cross-sectional area of reinforcing steel in tension zone

A_{ct} cross-sectional area of tension zone in uncracked state immediately prior to cracking

σ_{s2}^f steel stress directly after cracking taking into account the contribution of the fibres – the characteristic value of the yield point f_{yk} can be assumed here for σ_{s2}^f , but a lower value may be necessary to limit crack widths (see Section 5.3.1)

k_c factor to allow for the distribution of the tensile stresses and the change to the internal lever arm at the transition from the uncracked to the cracked state, with the following approximation applying for combined bending and tension actions:

$$k_c = 0.4 \cdot \left[1 + \frac{\sigma_c}{2/3 \cdot f_{ctfm}} \right] \leq 1.0 \quad (5.42)$$

σ_c concrete stress at the level of the centroid axis of the cross-section in the uncracked state immediately prior to cracking

f_{ctfm} mean value of cracking stress of UHPC.

Equation 5.41 can be expressed as follows for the limit case of axial tension:

$$\sigma_{cf0k} \cdot A_c + A_s \cdot f_{yk} \geq f_{ctfm} \cdot A_c \quad (5.43)$$

where

$$\sigma_{cf} = \sigma_{cf0k}; \sigma_{s2}^f = f_{yk}; A_{ct} = A_c; k_c = 1.0$$

The first term in the equilibrium condition describes the contribution of the fibres upon reaching fibre efficiency, the second term the contribution of the bar reinforcement upon reaching the yield point. Adding the two terms together assumes that fibre efficiency and yielding of the steel reinforcement are reached simultaneously. And as the stress in the fibre-reinforced concrete only decreases gradually at the start of the fibre pull-out phase, this assumption is justified as an approximation. The term on the right-hand side of the inequality corresponds to the cracking force for the cross-section subjected to axial tension.

For the limit case of pure bending, Equation 5.41 gives us

$$0.5 \cdot \sigma_{cf0k} \cdot A_c + A_s \cdot f_{yk} \geq 0.2 \cdot f_{ctfm} \cdot A_c \quad (5.44)$$

where

$$\sigma_{cf} = \sigma_{cf0k}; \sigma_{s2}^f = f_{yk}; A_{ct} = 0.5 \cdot A_c; k_c = 0.4$$

The expression $A_s \cdot f_{yk} \geq 0.2 \cdot f_{ctfm} \cdot A_c$ corresponds to the minimum reinforcement criterion for reinforced concrete. This formula, which originates from considering equilibrium, is extended by the contribution of the fibres: $0.5 \cdot \sigma_{cf0k} \cdot A_c$. Here, the value

0.5 corresponds to the factor α_f , which was derived in Section 5.3.1 for the case of very small compression zones (Figure 5.31b). This assumption seems to be justified for cross-sections with small amounts of reinforcement.

Interpolation between the two limit cases of axial tension and pure bending, with the help of Equation 5.42, is necessary for combined tension and bending.

5.3.3 Calculating deformations

Compared with normal-strength concrete, it is possible to build very slender loadbearing structures from UHPC owing to the high compressive stresses that UHPC can carry. However, we should not lose sight of the deformations.

For prestressed concrete structures, the modulus of elasticity is the material parameter that governs the deformation calculations. The modulus of elasticity does not increase in proportion to the compressive strength, but instead in the case of UHPC is only about 50% higher than that of normal-strength concrete. What this means for a rectangular cross-section subjected to bending is that with UHPC, the depth of the cross-section, compared with normal-strength concrete, may only be reduced by about 15% at first if we wish to preserve the same elastic deformations.

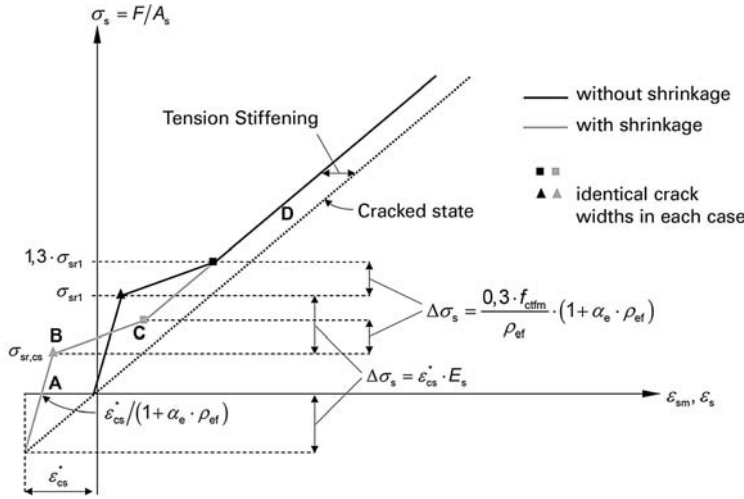
Heat-treated UHPC results in further advantages in terms of the long-term development of deformations due to the – compared with normal-strength concrete – much lower creep coefficient (see Section 3.4).

For non-prestressed concrete structures, calculating deformations is more difficult because we have to assume a cracked state for some areas at least. The contribution of the fibres at the cracks results in additional strain hardening compared with reinforced concrete. The influence of the comparatively high shrinkage strain of UHPC needs to be given special attention when dealing with members in tension and also in bending.

In test specimens, the contribution of the concrete between the cracks leads to the known strain hardening compared with the curve of steel alone (cracked state). The combination with fibres also leads to the strain in the steel reinforcement decreasing at the crack due to the force carried by the fibres, Equations 5.28 and 5.31a.

Figure 5.32 is a qualitative representation of the mean stress–strain curve for a (fibre-reinforced) UHPC tension member. The effects of shrinkage on the mean steel stress or strain are also shown [68].

As shrinkage is impeded by the reinforcement, an internal restraint ensues which causes a negative ‘prestrain’ in the steel and compressive stresses (‘A’ in Figure 5.32). The concrete is already in tension even without the effects of external actions, which reduces the cracking load level (‘B’ in Figure 5.32). The conclusion of the single crack formation phase (‘C’ in Figure 5.32) is then just reached when the force necessary to generate a new crack can just be transferred again between two cracks, i.e. some parts of the member are still in the uncracked state. At this point the internal restraint still has an effect on the cracking force. The scatter of the cracking stress for UHPC over the length of the element is taken into account in Figure 5.32 by a steel stress that is



Influence of shrinkage:
 A: Negative “prestrain” (internal restraint due to shrinkage)
 B: Reduced cracking load level due to residual stress state
 C: Stabilised crack pattern reached at lower level of load due to residual stress state
 D: Shrinkage has no appreciable influence on tension stiffening with a stabilised crack pattern, but does affect crack widths

Fig. 5.32 Mean stress–strain curve for (fibre-reinforced) UHPC [68]

30% higher at the end of the single crack formation phase compared with the formation of the first crack.

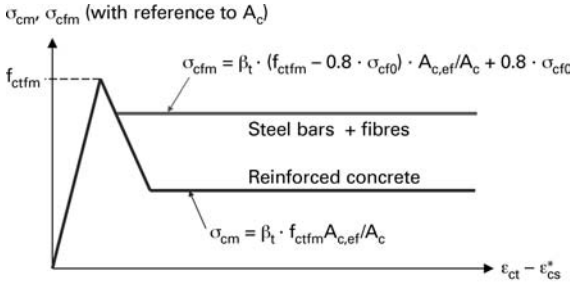
During the stabilized cracking phase, shrinkage has practically no influence on tension stiffening, shown here as constant as an approximation (‘D’ in Figure 5.32), because in this case a difference in strains between steel reinforcement and concrete exists everywhere. At this stage the internal restraint caused by shrinkage is thus no longer effective. However, shrinkage has an effect on the crack widths.

We get the following expression for the mean steel strain in the stabilized cracking phase [105]:

$$\epsilon_{sm}^f = \epsilon_s - \left(\frac{\beta_t \cdot (f_{ctfm} - \sigma_{cfm})}{\rho_{ef}} + \frac{\sigma_{cfm}}{\rho_s} \right) / E_s \tag{5.45}$$

where

- $f_{ctfm} - \sigma_{cfm} \geq 0$
- ϵ_s strain in reinforcing steel at crack but neglecting the contribution of the fibres
- β_t shape factor to allow for the course of the steel strains due to the contribution of the matrix between the cracks: $\beta_t = 0.4$ for short-term loading $\beta_t = 0.25$ for long-term or repeated loading
- f_{ctfm} mean value of cracking stress of (fibre-reinforced) UHPC
- ρ_s geometric reinforcement ratio, $\rho_s = A_s/A_c$



$\beta_t = 0.4$ for short-term loading
 $\beta_t = 0.25$ for long-term/repeated loading

Fig. 5.33 Considering the contribution of (fibre-reinforced) UHPC to tension at and between the cracks for the curve for concrete [105]

ρ_{ef} effective reinforcement ratio, $\rho_{ef} = A_s/A_{c,ef}$
 σ_{cfm} stress in fibre-reinforced concrete according to Equations 5.25 and 5.26 for a crack width w_m averaged over all cracks and, if applicable, taking into account the influence of long-term and repeated loading – fibre efficiency here may be taken into account with its mean value σ_{cf0m} .

The expression $\beta_t \cdot (f_{ctfm} - \sigma_{cfm})/\rho_{ef}$ allows for the reduction in the steel stress compared with the pure cracked state, which results from the contribution of the concrete matrix between the cracks. As is known from reinforced concrete, this contribution depends on the size of the effective area of concrete in tension and therefore must be calculated using the effective reinforcement ratio ρ_{ef} . As the crack spacing decreases, so the value of this expression approaches zero.

The term σ_{cfm}/ρ_s takes into account the reduction in the steel stress at the crack (and, consequently, between the cracks as well) compared with the pure cracked state, which results from the fibre’s contribution to carrying the force. This proportion follows directly from considering the equilibrium at the cracked cross-section and should therefore be determined using the geometric reinforcement ratio ρ_s .

As an alternative to considering tension stiffening in the stress–strain diagram for the reinforcing steel, it is also possible to modify the curve for the concrete. Taking Equation 5.45 as our basis, we get the following mean concrete stress for the stabilized cracking phase:

$$\sigma_{cm} = \beta_t \cdot (f_{ctfm} - \sigma_{cfm}) \cdot A_{c,ef}/A_c + \sigma_{cfm} \tag{5.46}$$

Figure 5.33 shows the corresponding constitutive model without the effect of shrinkage and compares this with the known approach for reinforced concrete. Again, tension stiffening has been approximated as constant.

Figure 5.34a shows the stress–strain curves determined in axial tension tests on specimens with combined reinforcement and different fibre contents. Figure 5.34b compares the respective contribution of the concrete (difference between stress–strain

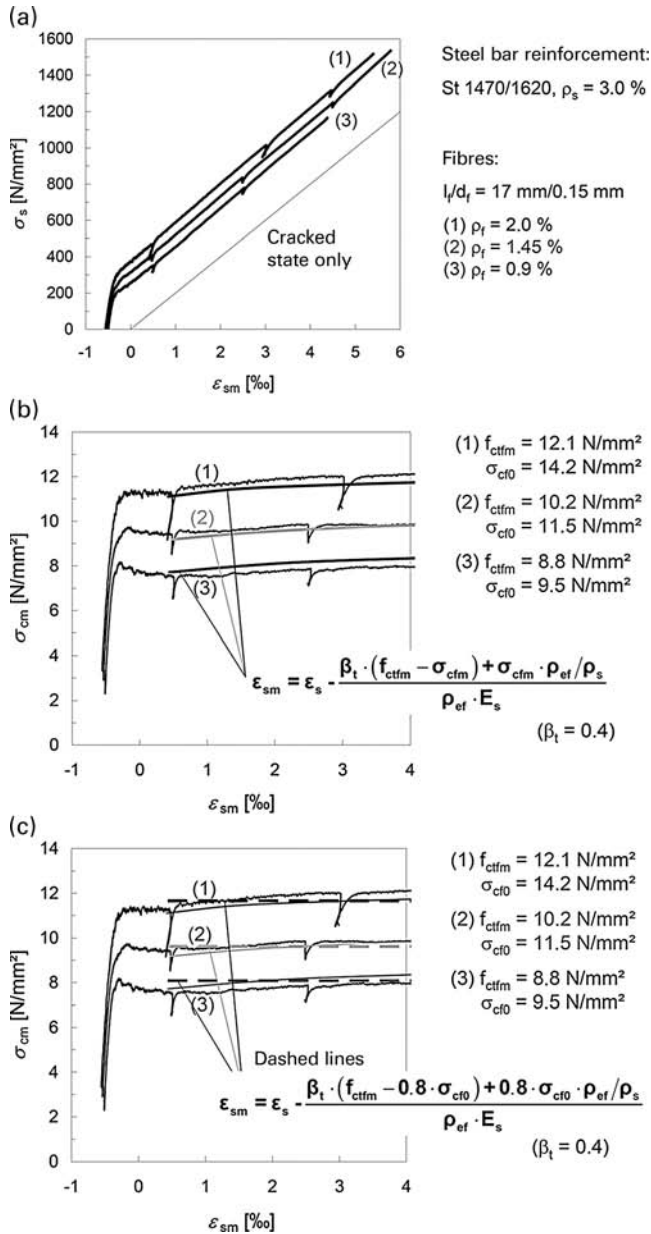


Fig. 5.34 Comparison of test results and deformation calculations: a) stress–strain curves for test specimens with combined reinforcement and different fibre contents [105], b) contribution of fibre-reinforced concrete shown separately as the difference between the stress–strain curve of the respective test specimen and the pure cracked state and a comparison with the results according to Equation 5.46, c) as for b) but a comparison with the approximation according to Equation 5.47

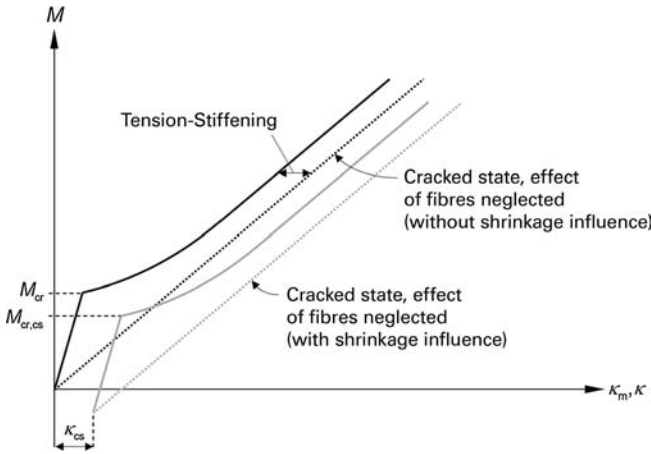


Fig. 5.35 Qualitative course of the moment–curvature relationship taking into account the influence of shrinkage [105]

curve of test specimen and pure cracked state) and the results according to Equation 5.46. Figure 5.34c shows that a similar, good agreement is achieved when the actual increase in tension stiffening with the mean crack width is ignored and, instead, is calculated using a constant stress in the fibre-reinforced concrete σ_{cfm} on the level of 80% of the mean fibre efficiency, i.e.

$$\sigma_{cfm} = 0.8 \cdot \sigma_{cf0m} = \text{const} \quad (5.47)$$

Based on considering the equilibrium at the flexural crack in Section 5.3.1 and the thoughts regarding the load–deformation behaviour of the test specimen, it is possible to apply the proposed model to members in bending as well. However, in order to obtain realistic deflections, the compatibility of the deformations between tension and compression zones must be taken account of exactly when calculating the curvature, and the influence of shrinkage must be considered for both the cracked and uncracked states. As with prestressed concrete, this can be done, for example, by applying a ‘negative prestrain’ to the bar reinforcement as a result of the residual stress state.

Figure 5.35 is a qualitative representation of how shrinkage affects the course of the moment–curvature relationship. With unequal reinforcement cross-sections at the two surfaces of the member, shrinkage already causes a curvature in the uncracked state irrespective of the load. In the cracked state, this is the case even with a symmetrical arrangement of reinforcement. Owing to the residual stress state, the cracking moment continues to decrease compared with the zero-shrinkage case.

6 Connections

6.1 General

UHPC components are often precast. The advantage of this is that the elements can be produced under readily controlled conditions. On the building site, the individual parts are then joined together to form a complete loadbearing structure. There are different ways of connecting the parts: dry joints, wet joints and glued joints. In many structures, UHPC is part of a hybrid system. What this means is that shear forces, possibly in combination with normal forces, have to be transferred via large surface areas in direct contact. Examples of this are UHPC bridge decks supported on conventional concrete beams or a loadbearing steel deck. In structures made up of segments, structural shear joints ensure that, on the one hand, the shear capacity is guaranteed and, on the other, dimensional tolerances can be compensated for. In offshore structures, forces are transferred to the foundations via tubular steel segments; UHPC presents interesting options here. This chapter deals with joints and connections.

6.2 Dry joints



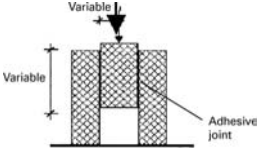
Dry joints can be employed to transfer shear forces. However, such a joint is only able to transfer significant shear forces when the surfaces in contact are compressed over their full area. In a series of tests carried out by *Tue et al.* [126], slab elements measuring $300 \times 200 \times 80$ mm were pressed against each other using different normal compression forces. The elements made from a coarse-grained concrete with 1.0% by vol. steel fibres had a compressive strength of 150 N/mm^2 . The surfaces in contact were either left untreated or ground. It turned out that the untreated surfaces had friction coefficients of 0.75–0.85 for a shear displacement of up to 0.2 mm, the ground surfaces a coefficient of about 0.6. The friction coefficient increased with the shear displacement in all tests, even up to a displacement of 20 mm.

6.3 Glued joints

In structural engineering, joining components with adhesive is a technique that up until now has always met with some reticence. This was due to the performance of glued joints over time, which was regarded as uncertain. On the one hand, the joint is subjected to stresses due to the regular loads of the structure. On the other, there are also the effects of restraint stresses due to temperature and moisture gradients and the loads caused by freezing and de-icing salts. In addition, there is also the low near-surface tensile strength of normal- and high-strength concrete.

Therefore, extensive testing was carried out prior to the first application of adhesives for a UHPC structure in Germany – the Gärtnerplatz Bridge in Kassel. On this bridge (see also Section 7.1.5.2) the loadbearing UHPC elements, the bridge deck and the top flanges of the bridge girder are glued together without the help of any further mechanical connectors. The structural analysis revealed shear stresses of max. 2 N/mm^2 under permanent loading. Flexural tensile tests, axial tensile tests and shear tests were carried out on various specimens (see Table 6.1). A customary epoxy resin mortar was used as

Table 6.1 Results of tests on UHPC specimens (scatter of mean values, $n=5$) [128].

	Flexural tensile strength	Axial tensile strength	Shear strength
	N/mm ²	N/mm ²	N/mm ²
Method of testing			
Specimen dimensions	Prisms 160 × 40 × 40 mm Beams 700 × 150 × 80 mm	Prisms 160 × 40 × 40 mm	Middle part 150 × 150 mm Outer parts 150 × 150 × 75 mm
Prism series 1 ^{a)} Influence of – curing – surface roughness – gluing temperature – adhesive thickness – test temperature	10.0–11.7	5.9–7.1	13.5
After 14 frost-thaw cycles in salt solution	13.1		
Prism series 2 ^{b)} 20 °C	22.0		
Beams: Static loading 10 °C; 20 °C; 30 °C	11.3; 11.0; 12.1		

a) Glue applied to concreted surface

b) Glue applied to sawn surface

the adhesive. The bending tests were carried out for both static and dynamic loads. Several test specimens were also subjected to freezing and de-icing salts, which involved storing them in 3% NaCl solution and subjecting them to 14 freeze-thaw cycles before testing them. The bridge elements were subjected to static and dynamic loads at three different temperatures 10 days after completing the glued joints. The dynamic loading had a frequency of 5 Hz and upper and lower flexural tensile stresses of 5 and 1.6 N/mm² respectively. Detailed information on the tests, their results and the experience gained during construction can be found in [127].

Failure in the flexural tensile tests occurred in the concrete directly adjacent to the joint. The flexural tensile strength was about 40% lower than that of a monolithic beam with the same dimensions, an effect that is attributed to the orientation of the fibres next to the surfaces in contact (wall effect). In a dynamic loading test, no damage to either specimen or adhesive joint was observed after 1 million cycles.

A detailed research project investigating glued joints between UHPC components was carried out at the applied science and technology university in Munich within the scope of the German programme of research into sustainable building with UHPC (priority programme SPP 1182) [129, 130]. A conventional cold-curing epoxy resin (EP) adhesive was chosen for the laboratory tests; this adhesive is used in the building industry for structural adhesive joints. As the range of applications for cold-curing EP adhesive is regarded as limited when it comes to unfavourable hygrothermal ambient conditions, an ultra-high-strength mineral adhesive (reactive powder concrete, RPC) was also developed. This latter adhesive was investigated as an alternative to the cold-curing EP adhesive. To establish the suitability of the adhesives for joining UHPC components, fundamental experimental testing was carried out on shear-compression specimens in a standard climate (Figure 6.1).

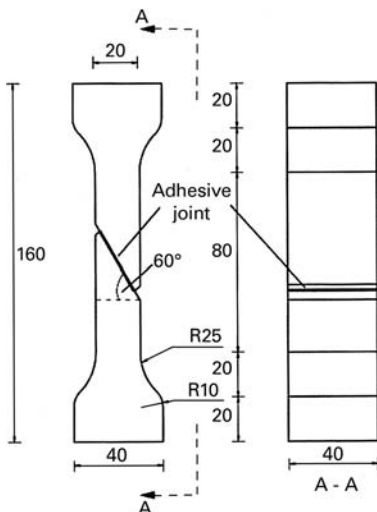


Fig. 6.1 Shear-compression specimen (dims. in mm) as used in [128, 129]

It was found that blast-cleaning the surfaces to be glued with a hard material was the optimum pretreatment for both types of adhesive. It was also found that the EP adhesive cures much faster than the RPC adhesive. However, the shear-compression load applied resulted in the joint with the RPC adhesive achieving a much higher (final) strength than the one with the EP adhesive. A cohesion failure in the adhesive was observed in all joints with the EP adhesive under the given shear-compression load, whereas the joints with the RPC adhesive always resulted in an adhesion failure between the concrete surface and the adhesive. The type of UHPC had no influence on the bond strength of the adhesives under shear-compression loading.

The long-term strength of glued joints between UHPC components under service conditions was also investigated with the help of the shear-compression test specimens for both types of adhesive. To do this, extensive testing was carried out to discover the long-term admissible loading level of the glued joint at various service temperatures and the influence of a long-term load on the strength of the joint. Reduction factors for loads plus temperature and moisture stresses were determined for each adhesive based on the results of the tests. Therefore, the long-term strength of the adhesive joint under service conditions can be calculated by multiplying the individual reduction factors together. It turned out that joints with the RPC adhesive exhibit a much higher long-term strength, compared with their short-term strength, than is the case with the EP adhesive.

Glued connections are an accepted jointing method for structures made up of prefabricated segments. An EP adhesive is applied to the interlocking contact surfaces produced by the match-casting method and the segments are joined together by prestressing. When employing UHPC, this approach is complicated by the autogenous shrinkage of the UHPC, which at 400–900 $\mu\text{m}/\text{m}$ is much greater than the shrinkage strain of conventional concrete. In match-casting, each subsequent segment is cast against the mating surface of the previous segment, which thus serves as formwork for the mating surface of the next segment. Autogenous shrinkage starts within the first few days after concreting (sometimes even after just a few hours). This means that part of the autogenous shrinkage has already taken place in the element cast first, whose mating surface serves as formwork for the next one, while that of the new segment is just beginning. This would lead to a poor fit between the surfaces. In order to prevent this problem, a new method was developed in Japan [131]. This involves setting up a steel end plate on the segment already cast in order to keep the dimensions of the section constant.

6.4 Wet joints

The GSE Bridge in Tokyo [132] (see also Section 7.1.3.2) consists of a series of box beams with bottom flange and webs of UHPC (Figure 6.2) and a deck of C30/37 concrete which was cast later. So-called perfobond shear connectors were used here for the structural connections between the two parts. This method is advantageous due to its compactness, stiffness, load-carrying capacity and fatigue resistance. Owing to the long cantilevers of the deck, the perfobond shear connectors also had to be designed for tension in the vertical direction. The perfobond shear connectors were arranged in two rows. The design equations derived for this material are valid for embedding the

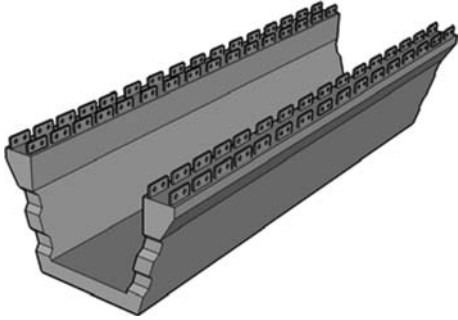


Fig. 6.2 PerfoBond shear connectors between UHPC webs and conventional concrete deck [132]

perfoBond shear connectors in the concrete of the deck (C30/37). Equation 6.1 was used for the shear capacity on the UHPC side:

$$V_d = \left[\left(3.38 \cdot d^2(t/d)^{0.5} \cdot f_{cd} - 121 \right) \right] / 3 \tag{6.1}$$

where

- d hole diameter
- t slab thickness (mm)
- f_{cd} compressive strength of concrete.

The transverse bars passing through the holes were not included in the calculation. Differences in the creep and shrinkage behaviours as well as temperature differences between deck on top and UHPC component below were taken into account.

The advantage of wet joints in construction with prefabricated segments is that the concrete in the joints compensates for any dimensional inaccuracies associated with the match-casting. Figure 6.3 shows the geometry of the wet joints used for the GSE Bridge in Tokyo [132].

For practical reasons, a joint width of 150 mm was maintained for the joints in which the ducts for the prestressing tendons have to be coupled between the segments. The following equation was assumed for determining the shear capacity of the joint:

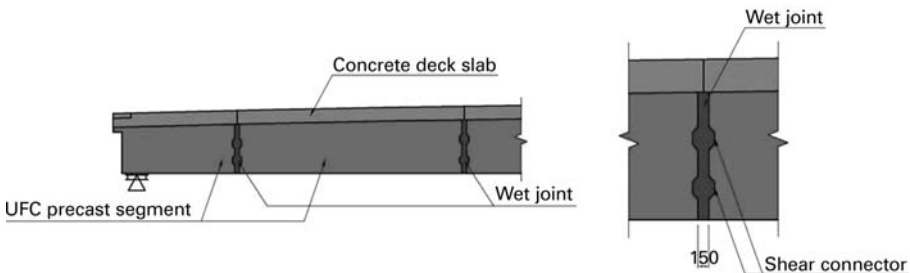


Fig. 6.3 Wet joints between UHPC segments of GSE Bridge in Tokyo [132]

$$V_{Rd} = V_{cwd} + V_{ped} \quad (6.2)$$

where

$$V_{cwd} = (t_c \cdot A_{cc} + V_k) / \gamma_b \quad (6.3)$$

$$t_c = \mu \cdot f_{cd} \cdot f_{nd}^{1-b} \quad (6.4)$$

where

f_{nd} design value of mean concrete compressive stress perpendicular to stress plane

A_{cc} area of shear force transfer on compression side

b a factor (0.4) dependent on the form of the surfaces in contact

μ mean friction coefficient (0.45)

V_k shear capacity of one shear key ($= 0.1 \cdot A_k \cdot f_{cd}$)

A_k cross-sectional area of shear key in compression zone

f_{cd} design value of compressive strength of concrete

V_{ped} vertical component of prestressing force.

As an alternative to the perfobond shear connector, other geometrical forms have been investigated in the meantime, e.g. the puzzle strip shear connector [133, 134], Figure 6.4. The most important advantages of the puzzle strip shear connector are its high initial stiffness and high load-carrying capacity. Furthermore, it is also possible to produce two puzzle strip shear connectors with one cut and without wasting any material. Figure 6.5 shows the results of shear tests, comparing the behaviour of the puzzle strip shear connector for different concrete mixes. All the test specimens in series A were reinforced in the transverse direction with two bars, $d_s = 12$ mm, in each opening and with six bars, $d_s = 10$ mm, above the shear connection. The higher compressive strength of mix A1 (cube strength 180 N/mm^2) compared with mix A2 (90 N/mm^2) leads to a much higher shear capacity and at the same time a much better ductility.

Further tests involving cyclic loading were also carried out. The puzzle strip shear connectors were subjected to a fatigue load with two different stress amplitudes ($R = 0.54$ and 0.42). None of the test specimens had failed by 2 million cycles.

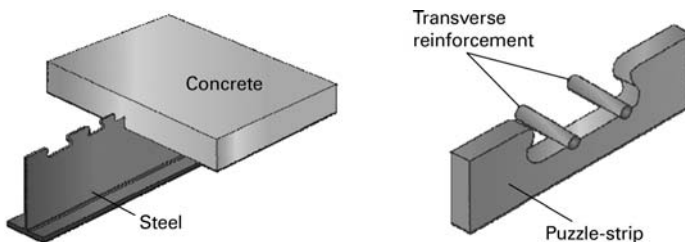


Fig. 6.4 Puzzle strip shear connector [134]

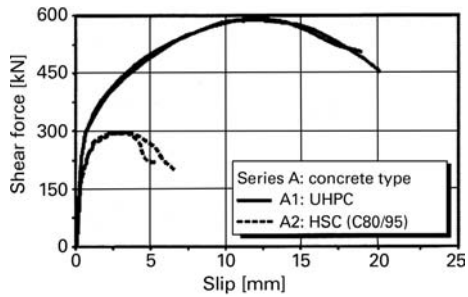


Fig. 6.5 Force–slip relationships for the puzzle strip shear connector in concretes with different strengths [134]

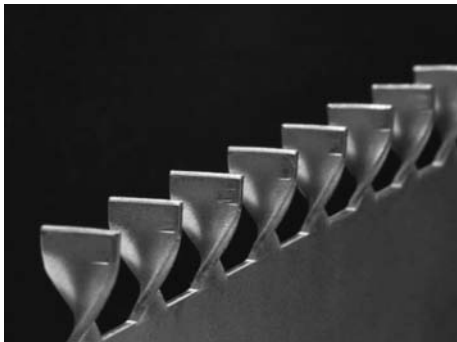


Fig. 6.6 Steel share strip for a shear-resistant connection [135, 136]

Another innovative solution is presented in [135, 136], Figure 6.6. This makes use of rectangular steel teeth that are turned through 90°. Such so-called steel share strips can transfer both shear and tensile forces and can be produced in very small dimensions.

Figure 6.7 shows the load–slip curves, which reveal an excellent load-carrying capacity in conjunction with ductile behaviour. The shares of the strip measured 15 mm long \times 20 mm high and their spacing was 15 mm for curves B-1-1 and B-1-2, 5 mm for B-2 and 10 mm for B-3. Curves B5 and B7 represent steel share strips with a different geometry and curve B-8 represents a different steel strength.

6.5 Grouted joints

Grouted joints have been used in the offshore industry for many years. In this type of joint, steel tubes with different diameters are connected using a grout material. To transfer shear forces, shear keys are provided on the inside faces of the tubes (Figure 6.8) [137]. This arrangement results in a system of struts in the concrete, which in combination with the confining effect of the outer tube and the support provided by the inner tube enable substantial shear forces to be transferred. One important advantage of this type of connection is that the shear capacity is the same in

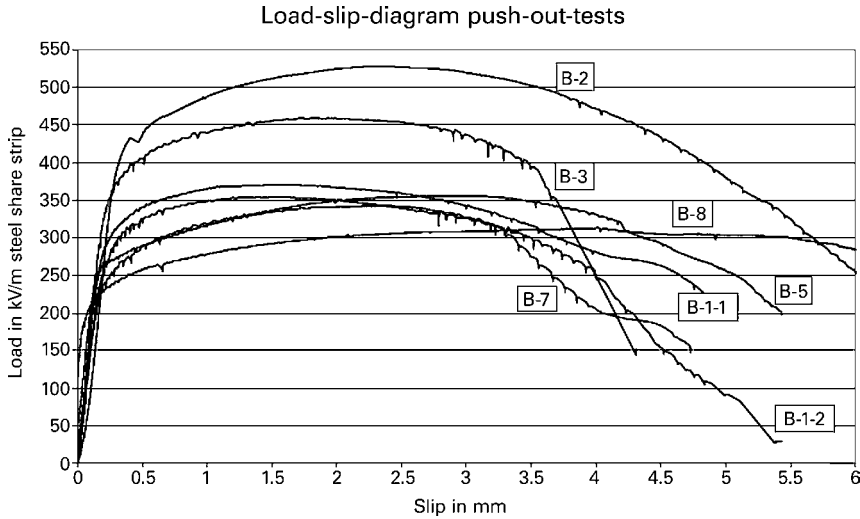


Fig. 6.7 Load–slip relationships for the steel share strip of Figure 6.6 with different geometries [137]

tension and compression. The transfer length can be shortened by using UHPC for the grout [176]. However, this increases the force acting on the shear keys and the force in the confining, outer steel tube.

In a grouted joint with shear keys, we can distinguish between three structural responses: adhesion and friction at the interface between concrete and steel, and the development of struts in the concrete. The main reason for the failure of such a joint is

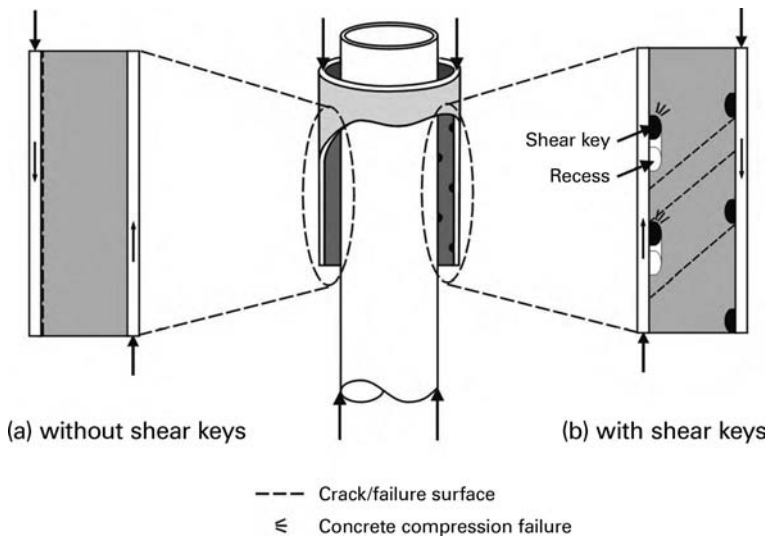


Fig. 6.8 The principle of the forces acting in a grouted joint [137]

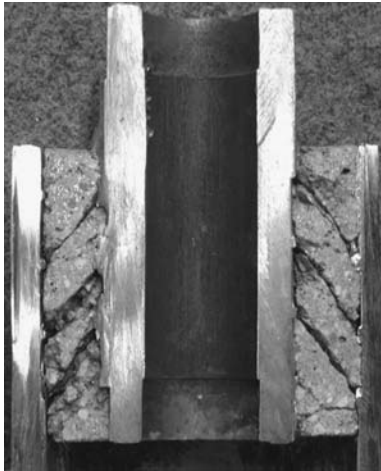


Fig. 6.9 A test to prove the formation of struts in the concrete [137]

either shearing-off along the shear keys when the spacing of the keys is too small, or a compression failure in the concrete above the supporting keys when the key spacing is sufficiently large. In this latter case, diagonal cracks appear in the grout (Figure 6.9). It is assumed that the maximum stress in the concrete at the junction between a strut and a shear key corresponds to 2.5 times the uniaxial concrete compressive strength.

The high strength of UHPC enables the length of the lap between the inner and outer tubes to be shortened if necessary.

6.6 Adding UHPC layers to existing components to upgrade structures

The basic idea of upgrading conventional reinforced concrete components involves adding a 25–80 mm thick UHPC layer to the surface of the existing reinforced concrete. The surface to which the UHPC is to be applied is roughened using high-pressure water jets, sandblasting, etc. in order to achieve a high-quality bond. When reinforcing bars in the primary loadbearing direction are included in the UHPC, we speak of a compact reinforced composite (CRC) or a steel-UHPC composite [138], Figure 6.10.

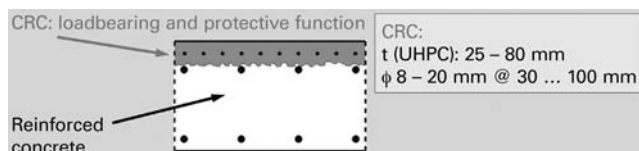


Fig. 6.10 Basic configuration of composite components made from reinforced concrete with a layer of CRC [138]

The addition of a heavily reinforced UHPC layer results in components with a much higher ultimate resistance. At the serviceability limit state, the UHPC layer can accommodate significant tensile forces and thus improve the stiffness without cracks forming, which are detrimental to the durability as well as the appearance. Therefore, layers of UHPC with loadbearing and waterproofing qualities can be applied to those areas of reinforced concrete components that suffer severe exposure to environmental influences (e.g. bridge decks). If the UHPC layer has to fulfil a protective function only, embedded reinforcing bars are unnecessary and the thickness of the layer can be reduced to as little as 25 mm.

Whereas roughening the surface of conventional concrete as preparation to receive a layer of UHPC is relatively straightforward, adding a layer of UHPC to a steel plate is quite a different matter. This issue is particularly interesting for upgrading steel bridges. The effect of cracking due to autogenous shrinkage and temperature gradients



Fig. 6.11 Applying the layer of epoxy resin to the steel plate

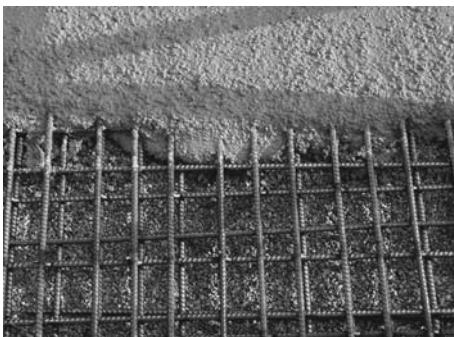


Fig. 6.12 UHPC deck during casting, with the layer of epoxy resin plus aggregate worked into the surface, the steel meshes and the UHPC mix all clearly visible

must also be given special attention. A UHPC with a lower autogenous shrinkage strain and relatively high tensile strength has been developed in the Netherlands for such applications. These improvements allow the tensile stresses to remain below the tensile strength of the concrete. The following procedure was adopted in a pilot project (Calland Bridge):

- Remove old layer of asphalt
- Attach shear studs, $d_s = 16$ mm, 150 mm spacing, to the steel plate along the edges of the area in contact with the concrete to prevent uplift of the new deck (dishing)
- Apply a layer of epoxy resin (Figure 6.11) and work an angular aggregate into the surface (Figure 6.12)
- Provide 8 mm dia. spacer bars for supporting three steel meshes ($d_s = 8$ mm, 50 mm spacing)
- Apply the UHPC
- Float the surface of the concrete
- Cover with a damp material for 24 h
- Blast-clean the new surface to improve the resistance to braking forces.

The entire procedure takes only 120 h. Tests to determine the near-surface tensile strength of the surfaces in contact supplied values of 4–5 N/mm².

7 Projects completed

7.1 Bridges

7.1.1 Canada

7.1.1.1 Bridge for pedestrians/cyclists, Sherbrooke (1997)

The world's first UHPC bridge was built at Sherbrooke in Canada in 1997 (Figure 7.1) [4, 139]. It is 60 m long overall and consists of six precast segments each 10 m long. The precast segments are in the form of trusses and a ribbed concrete deck forms the top chord. UHPC-filled stainless steel tubes serve as diagonals and the bottom chord is made up of two continuous prestressed beams (each with two internal prestressing tendons). The precast segments are connected together by means of external prestressing (3×2 prestressing tendons). The concrete compressive strength for the top and bottom chords is 200 N/mm^2 .

7.1.1.2 Glenmore/Legsby footbridge, Calgary (2007)

Figure 7.2 shows Glenmore/Legsby footbridge, which stands in Calgary [23, 140]. A 33.6 m long prestressed T-beam was used as a drop-in element for this 53 m span. The bridge crosses an eight-lane motorway without any intervening piers. The T-beam was erected with two cranes (one at each end) in just eight hours (from Saturday late to Sunday 7 a.m.). Traffic disruption was therefore minimal, which was rated as a major benefit of this form of construction, especially as this motorway is a main traffic artery in Calgary. Robustness is enhanced through the omission of a central pier (no risk of impact), which is another big advantage. At mid-span the precast beam is 1.10 m deep and 3.60 m wide. It weighs about 100 t. Reinforcement in the UHPC beam is in the form of 2% by vol. steel fibres (13 mm long) and 42 prestressing strands (15 mm dia.). Some 40 m^3 of UHPC was required for the construction of the beam, which was cast in one pour. Formwork elements that might have hindered expansion in the early phase of hardening were removed once the concrete had reached a compressive strength of 35 N/mm^2 . This measure enabled autogenous shrinkage to take place without restraint and thus prevented cracking during the curing phase. Detailed investigations were undertaken in advance to understand the shrinkage behaviour of the beam. After reaching the minimum compressive strength of 100 N/mm^2 necessary to transfer the prestressing forces to the concrete, the rest of the formwork was struck and the beam prestressed. Heat treatment at 90°C over 48 h ensured that the necessary compressive strength and durability was actually achieved.

The client (Calgary City Authority) called for a number of tests to be carried out before erecting the beam. First of all, tests were carried out on 3.3 m long elements. These elements were representative of the large beam and were subjected to a point load in the middle. Firstly, the elements were loaded until the appearance of the first crack. Afterwards, the elements were subjected to 1 million load cycles between 20 and 80% of the maximum service load, then a further 1 million load cycles between 20 and 80% of the load causing the first crack. As the elements did not fail under these loads, and, indeed, there was no decrease in stiffness, another 1 million load cycles between 20 and 80% of the calculated failure load were applied. At the start of this final cycle, a



Fig. 7.1 Footbridge in Sherbrooke – the first ever bridge made from UHPC (1997)



Fig. 7.2 Glenmore/Legsby footbridge, Calgary (2007)

minor reduction in stiffness was detected, although the stiffness stabilised at around two-thirds the stiffness of the uncracked state. Following this fatigue loading, the elements were loaded to failure, and the ultimate load reached was higher than expected. A loading test was carried out on the beam itself prior to erection. First of all, the beam was subjected to a uniformly distributed load over its whole length equal to 1.5 times the maximum service load. After that, the load was positioned asymmetrically on one half of the beam. Measurements revealed no deflections greater than those expected. After relieving the load, the deflections returned to zero, which indicated that no plastic behaviour had taken place. No irreversible damage had been discovered and so the beam was able to be erected.

7.1.2 France

7.1.2.1 Road bridge, Bourg-lès-Valence

The first French UHPC bridge was built at Bourg-lès-Valence [141] (Figure 7.3). This bridge has two spans: 20.5 and 22 m. It is assembled from double-T beams with a depth



Fig. 7.3 Road bridge at Bourg-lès-Valence (left) assembled from prestressed double-T beams (right)

of 900 mm, a top chord width of 2200 mm and a thickness of 150 mm. The use of 3% by vol. steel fibres and prestressing tendons rendered conventional reinforcement virtually unnecessary. Reinforcing bars are only used in the joints between the precast segments and at the junction with each footway. Compared with a design using normal-strength concrete, which would have required 39 t of reinforcement, the UHPC solution needed only 4 t of reinforcing bars and meshes together with 28 t of fibres; and it was possible to reduce the weight of prestressing tendons from 17.4 to 6 t. The weight of the superstructure is only 328 t, instead of the 975 t for a bridge made from normal-strength concrete [141].

7.1.2.2 Pont du Diable footbridge (2005)

The Pont du Diable footbridge over the l'Herault Canyon near Montpellier was built in 2005 [142, 177]. It was the design by the French architect *Rudy Ricciotti* which best met the requirements of the authorities in the l'Herault Valley nature conservation area, who were looking for a 70 m long footbridge without intervening piers whose visual impact on the landscape would be minimal, i.e. arches or stay cables were out of the question. The bridge cross-section is made up of two bone-shaped beams that are 1.8 m deep and have a 120 mm thick web (Figure 7.4). The beams serve as loadbearing members and at the same time function as parapets. There are 15 identical, 4.6 m long precast segments making up the total length of 69 m. Each segment consists of two vertical beams, three transverse ribs and a 30 mm deep deck. The transverse ribs help to provide the necessary lateral stiffening (wind). Eight Freyssinet prestressing tendons are used in this design. There are three type 13C15 and 19C15 tendons in the bottom 'bulb' of each beam and a type 4C14 in the top one. The bridge is designed in such a way that its natural frequency lies outside the critical range caused by pedestrians. In addition, tuned mass dampers were installed at mid-span. Steel formwork with a dimensional accuracy of ± 0.5 mm was used for producing the UHPC segments made from Ductal[®] (compressive strength 180–200 N/mm²). After concreting, each segment was left in the mould for 24 h as part of the curing measures. After removal from the mould, each segment underwent heat treatment at 90 °C for 24 h. According to the French BFUP directive, suitability tests

(a)



(b)

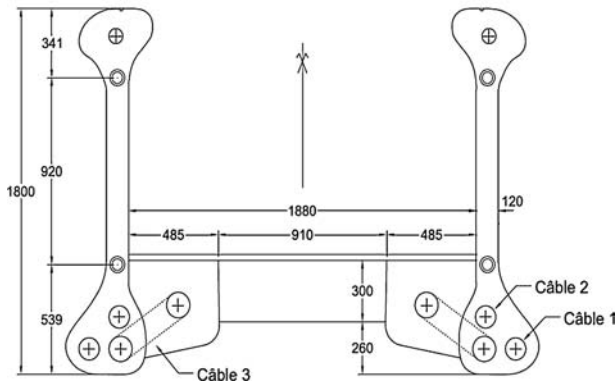


Fig. 7.4 Pont de Diable footbridge, l'Herault Canyon near Montpellier

must be carried out prior to erection. Prisms were cut from a specimen segment and used to establish the fibre orientation factor K for checking the assumptions of the calculations. Once all the individual segments had been cast, they were assembled in the precasting works and braced for transport. On site, a small crane lifted the segments onto a steel erection gantry for installation in their final positions with the help of three rollers plus adjusting bolts. The prestressing tendons were then fed through and tensioned and the tuned mass dampers installed.

7.1.2.3 Pont de la Chabotte road bridge

It was in 2004 that work began on an innovative concept for the new Pont de la Chabotte [143]. The bridge was to have a span of 47.40 m and no intermediate piers. Furthermore, a very long design life had to be guaranteed in the wintry conditions of this region. BCV (Béton Composite Vicat) with a 28-day compressive strength of 130 N/mm^2 without heat treatment and 150 N/mm^2 with heat treatment were the concretes

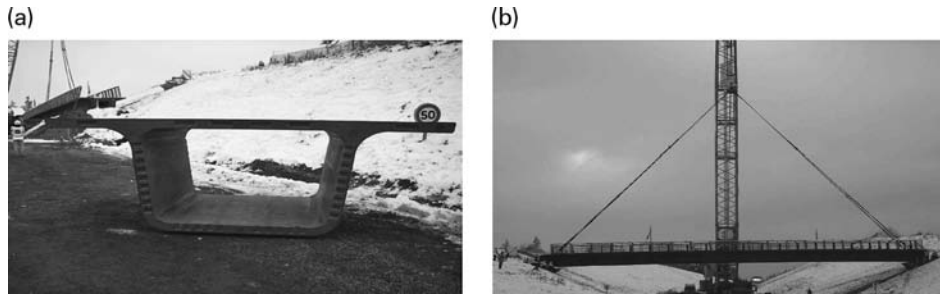


Fig. 7.5 Pont de la Chabotte, 47.40 m span, made up of 22 UHPC segments

chosen. The beam is made up of 22 precast segments (Figure 7.5) which are held together with adhesive and external prestressing.

The 22 segments comprise:

- 18 standard segments each 2.44 m long
- 2 segments 0.59 m long, equipped with saddles in order to render external prestressing possible
- segments 2.04 m long with a special geometry for anchoring the external prestressing tendons.

The UHPC segments are 1.60 m deep and have a web thickness of 120 mm (Figure 7.5). Match-casting was employed to guarantee a good fit between the segments, with the segments being cast in order against each other. Concreting of all 22 segments took a total of eight weeks. When joining the segments together on site, an epoxy resin was spread over the mating surfaces prior to provisional tensioning. Only at the end the 22 segments were post-tensioned with the six permanent tendons. The final erection phase took only 20 min with a jack and two stay cables. The most significant advantages of this form of construction are:

- No intermediate supports are necessary, which leads to a robust design that also blends in very well with the rural landscape.
- The structure is much lighter than the conventional concrete alternative: compared with a bridge in traditional C35/45 concrete, this bridge needs only 40% of the volume of concrete.
- The low weight of the bridge enabled erection work to be completed in a very short time, which overcame the disadvantages of traditional systems.
- Time on site was cut by one-third.

7.1.2.4 Pont Pinel road bridge (2007)

It was necessary to widen the existing Pont Pinel near Rouen from two to five lanes. The concept devised for the new 27 m long and 14 m wide Pont Pinel involved combining a



Fig. 7.6 Pont Pinel under construction

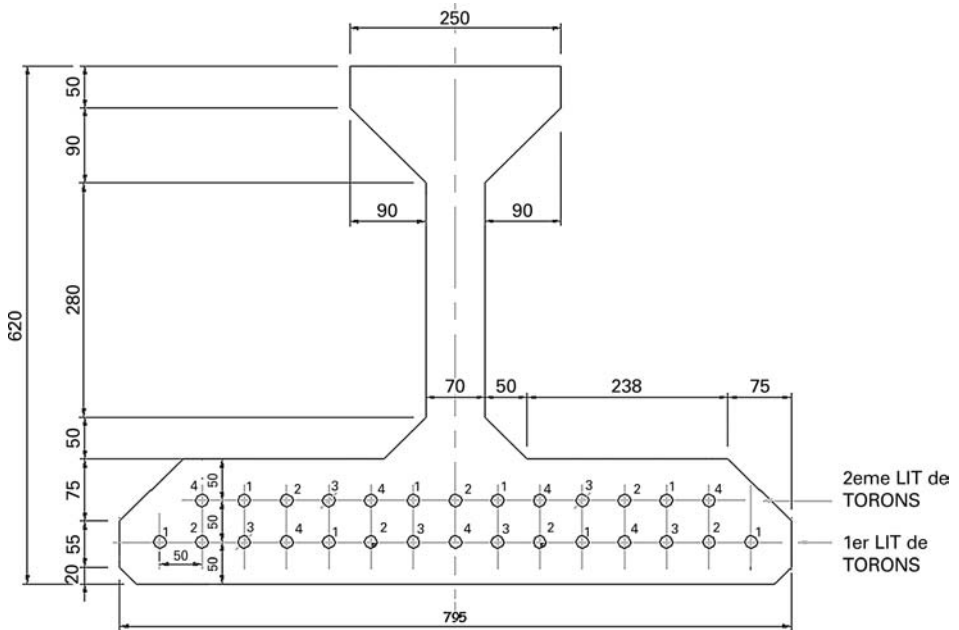


Fig. 7.7 Section through Pont Pinel main beam

C35/45 concrete deck with 17 prestressed UHPC beams (Figures 7.6 and 7.7). The characteristic features of the beams are as follows [144]:

Depth of cross-section:	620 mm
Bottom chord:	795 × 150 mm
Web thickness:	varies from 70 mm in span to 120 mm at end of beam
Top chord:	250 × 50 mm
Prestressing:	28 No. T15.7/1.860 N/mm ² strands, all in the bottom chord, with staggered anchorages in order to avoid excessive stresses in the anchorage zone (adhesive tape was wrapped around the ends of some strands in order to shift the effective anchorage length)
Beam/deck connection:	links projecting from top chord

At the ends of the beams, two transverse beams were cast monolithically with the deck to join the longitudinal beams together. Eight projecting strands from each beam were anchored in the transverse beam to create a good connection (Fig. 7.8). The road deck, the depth of which varies between 210 and 320 mm, was constructed using precast slab segments and *in situ* concrete (strength class C35/45). This design was preferred to the alternatives for economic reasons. The compressive strength of the UHPC was 165 N/mm², achieved with the following mix:

- 2360 kg CERACEM BFM-Millau Premix (dry mix of cement plus aggregate)
- 45 kg high-performance superplasticizer
- 195 kg water
- 195 kg steel fibres.

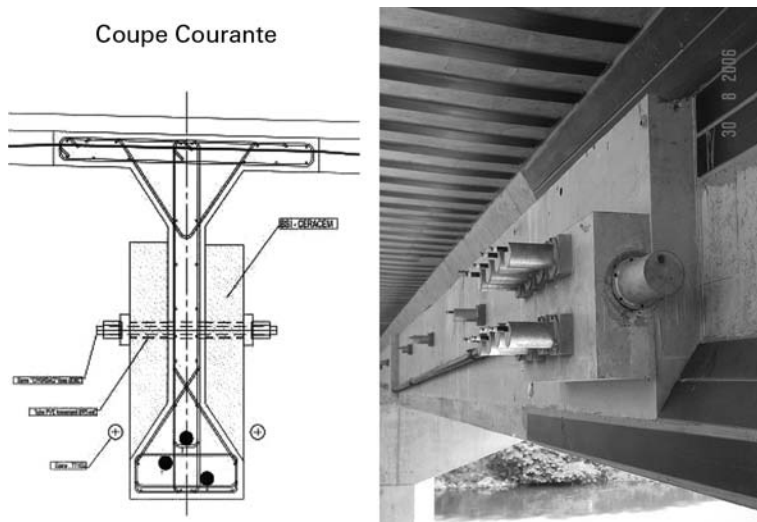


Fig. 7.8 Web thickening with UHPC on the Pont sur l'Huisne [145]

The different shrinkage behaviours of the two types of concrete were given special attention during the design work.

Here again, a suitability test was carried out prior to erecting the beams, as is prescribed in the French directive for UHPC. The test was carried out on a 5 m long beam segment that was concreted in exactly the same way as the real beams. Eighteen prisms were cut from this segment: six vertical, six horizontal and six at an angle. A sawcut was made in the underside of each prism, which was then tested in bending. This approach enabled the fibre orientation factor to be determined in order to check the assumptions in the calculations. The advantages of this form of construction are its durability and the chance to design relatively lightweight bridge superstructures. During construction, the immediate stability and the fast erection of the beams are further benefits. Once in place, the beams form a safe working platform for further operations and traffic can pass underneath without being disrupted.

7.1.2.5 Strengthening the Pont sur l'Huisne, Mans

UHPC was used on the Pont sur l'Huisne in Mans in order to increase the load-carrying capacity with the help of external prestressing [145]. The strengthening was necessary to carry a new tram line over the bridge. The 65 m long bridge was made up of two parallel decks, 15 m wide, supported on precast I-section prestressed concrete beams 31.6 m long. However, the intended solution using external prestressing could not be implemented because the existing bridge cross-section was already utilised to such an extent that it could not carry any additional axial compression. Therefore, the beam webs were thickened with UHPC (BSI/CERACEM, compressive strength 150 N/mm^2). Another key advantage of using UHPC was that the concrete mix developed by Eiffage had a modulus of elasticity of $64\,000 \text{ N/mm}^2$ – twice that of the existing concrete. The higher stiffness of the UHPC cross-section therefore attracts normal forces and spares the existing cross-section. Concreting and compacting below an existing bridge deck is difficult with a conventional concrete and so a self-compacting UHPC mix was developed. Furthermore, the addition of steel fibres to the mix (2.5% by vol., or 200 kg/m^3) rendered traditional reinforcing bars unnecessary. So in this case the UHPC was primarily chosen not because of its high strength, but because of its high modulus of elasticity, its self-compacting properties and the fact that no conventional reinforcement was required.

The mean strength of the concrete was 182 N/mm^2 . The BSI/CERACEM premix was delivered to site and mixed there. The concrete was placed through six openings in the deck on each side of each beam (Figure 7.9). The high strength of the concrete was achieved without heat treatment and despite the low ambient temperatures at the time of the work.

7.1.3 Japan

7.1.3.1 Sakata-Mirai footbridge (2003)

The Sakata-Mirai footbridge was designed to blend in with its tranquil surroundings [146]. The design exploits the advantages of UHPC: it needs no conventional steel reinforcing bars to supplement the steel fibres and its load-carrying capacity is achieved



Fig. 7.9 Placing the UHPC through an opening in the road deck

through external prestressing. The bridge is extremely light, weighing just 56 t, which corresponds to about 20% of the self-weight of a conventional reinforced concrete structure. Another advantage of this was cost-savings of about 10% [146].

Figure 7.10 shows the finished bridge, a single span of 50.2 m, and a section through the bridge at mid-span; the two external prestressing tendons, consisting of 31 strands (15.2 mm dia.), can be seen.

The depth of the cross-section varies from 550 mm at the abutments to 1650 mm at mid-span in order to ensure that the maximum deflection does not exceed $\text{span}/600$. Detailed analyses were carried out with the help of non-linear 3D calculations taking into account the circular openings in the two webs. Six precast segments were needed for this bridge, which were initially supported on temporary trestles (Figure 7.11). Appropriately designed joints enabled the segments to be connected prior to post-tensioning.

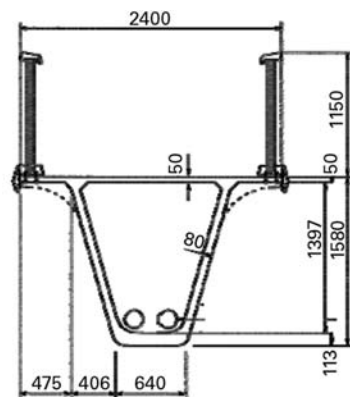


Fig. 7.10 View of bridge and section [Ductal[®]], [147]



Fig. 7.11 The segments being erected on temporary supports [Ductal®]

7.1.3.2 GSE Bridge, Tokyo Airport (2010)

This bridge (Fig. 7.12) enables airport operations traffic to cross a road between the northern and southern airfields of Tokyo Airport (GSE stands for ‘ground support equipment’) [148]. The designers had to comply with a demanding specification: approach ramps with minimum volume and weight plus achieving the necessary clearance between the bridge beams and the road below. This resulted in the need to lower the bridge superstructure as far as possible and keep the depth of the bridge beams as shallow as possible. Fibre-reinforced UHPC was therefore chosen for the superstructure.

The UHPC used in this project has the following properties: a very high characteristic compressive strength of 180 N/mm^2 , good durability, a densely packed microstructure with a w/c ratio lowered to near the hydration limit (≤ 0.24) and a very low proportion of voids. The water permeability and the diffusion coefficient for chloride ions are between about 1/100 and 1/300 of the values for normal-strength concrete. Steel fibres (2% by vol., 0.2 mm dia., 15 mm long) were added to the UHPC mix. Conventional steel reinforcing bars were unnecessary. The UHPC used had good flowing properties and was self-compacting.

The bridge structure consists of three box sections (Figure 7.13). Each box has a top flange of conventional reinforced concrete and webs and bottom flange of steel fibre-reinforced UHPC. The span is 47.6 m (Fig. 7.14) and the prestressing tendons are positioned inside the box sections.

The precast fibre-reinforced UHPC beams were cast in segments to comply with a weight limit of 10 t.

Two rows of perfobond shear connectors are used between each web of the fibre-reinforced UHPC beam and the road deck of normal-strength concrete; these connectors are also subjected to tension due to the long cantilevers of the deck.

(a)



(b)

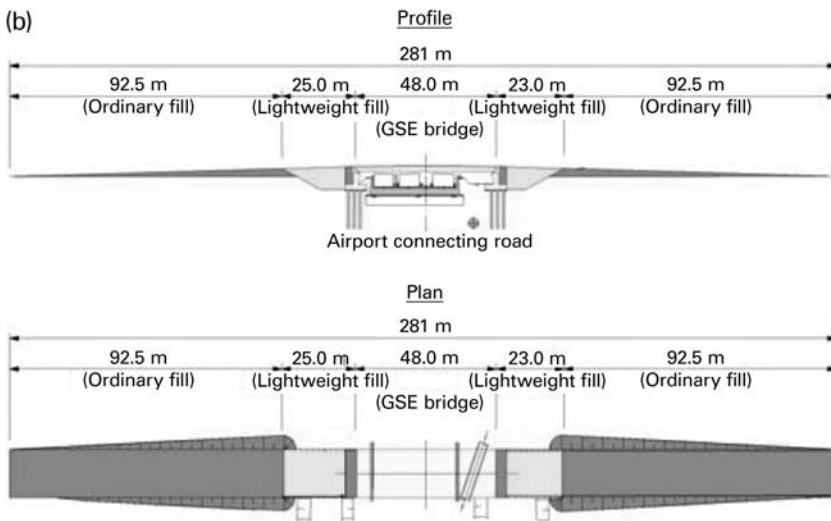


Fig. 7.12 Overall view, elevation and plan of GSE Bridge [JSCE award home page], [148]

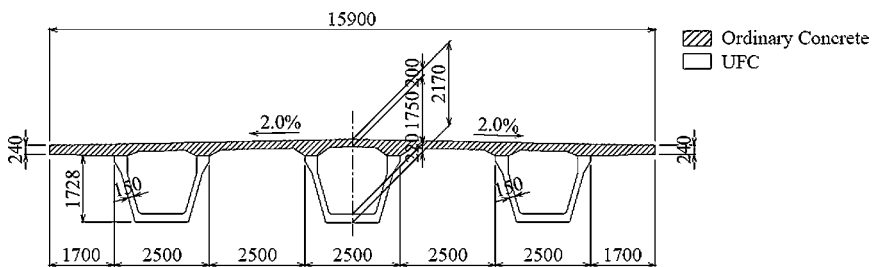


Fig. 7.13 Section through bridge superstructure [148]

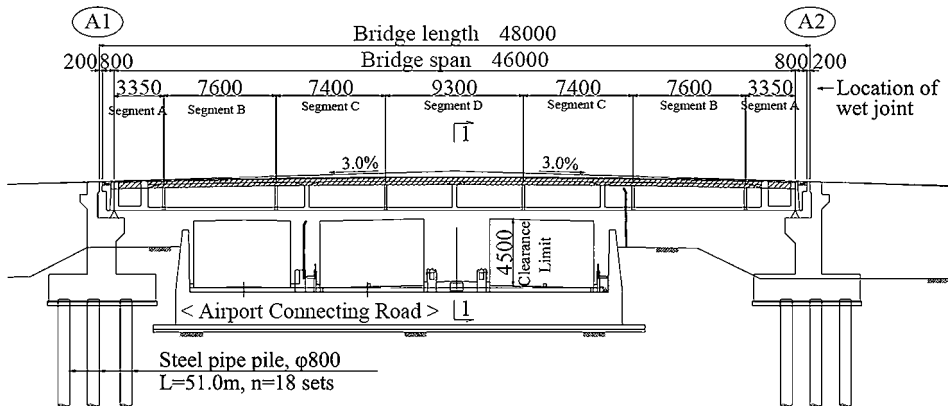


Fig. 7.14 Longitudinal section through GSE Bridge showing the individual segments of the beams [148]

7.1.3.3 Tokyo Monorail, Haneda Airport line

Construction of Tokyo's monorail line began in the 1960s [149]. Normally, the beams are made of prestressed normal-strength concrete, the self-weight of which limits spans to 20 m. Employing fibre-reinforced UHPC reduces the self-weight and thus enables spans to be increased to 40 m. Steel fibres (2% by vol., 0.2 mm dia., 15 mm long, tensile strength 2800 N/mm²) were added to the UHPC mix, which enables the fibre-reinforced UHPC to reach a mean tensile strength $f_{ct} = 11.3 \text{ N/mm}^2$ and a characteristic tensile strength $f_{ctk} = 8.8 \text{ N/mm}^2$.

Transport restrictions forced the 40 m long beams to be divided into three U-shaped segments plus slab segments (Figure 7.16) which were joined together on site with wet and dry joints and then post-tensioned. The horizontal joints between the top flange and the webs were provided with perfbond shear connectors (Fig. 7.15). The vertical joints were provided with epoxy and were prestressed subsequently (Figs. 7.16 and 7.17). This was the first use of fibre-reinforced UHPC for a rail project.

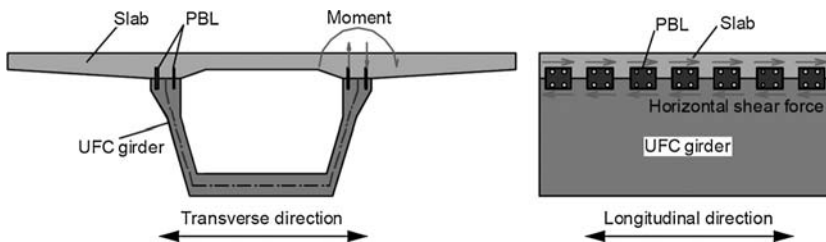


Fig. 7.15 Arrangement of and actions on the perfbond shear connectors [148]

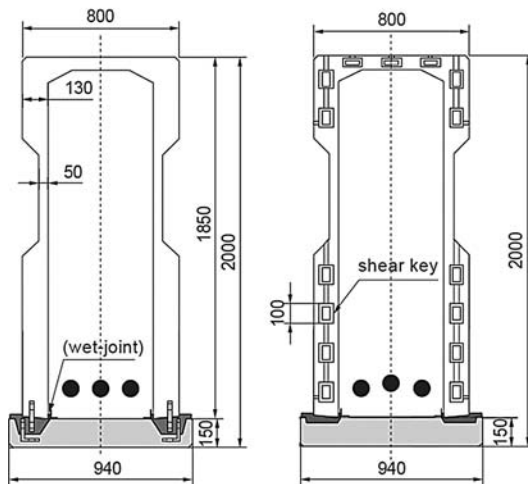


Fig. 7.16 Monorail beams during construction and sections through upturned U-beam [149]

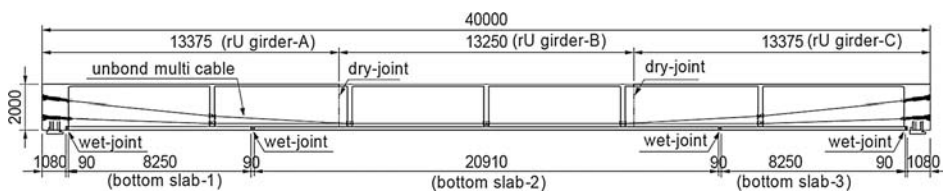


Fig. 7.17 Longitudinal section through monorail beam [149]

7.1.4 South Korea

7.1.4.1 Seonyu 'Bridge of Peace', Seoul

This is an arch bridge that spans 120 m. It consists of six precast, prestressed segments with a double-T cross-section and a deck with transverse ribs (Figure 7.18). The bridge deck is 4.3 m wide, the webs 1.3 m deep (Fig. 7.18). The 30 mm deep slab is supported

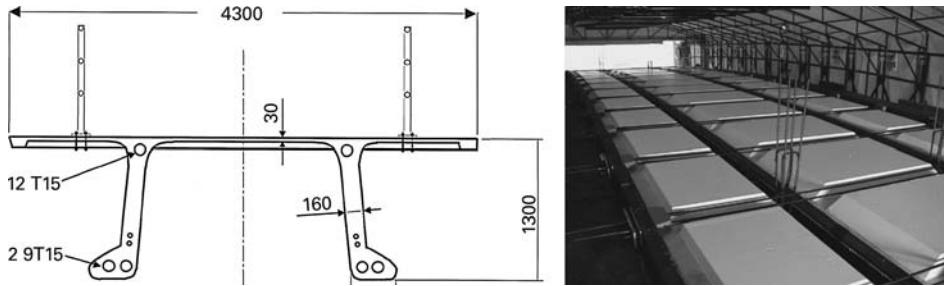


Fig. 7.18 Double-T cross-section and formwork [150]



Fig. 7.19 Erecting the arch and view of segment [150]

by transverse ribs every 1.225 m and one longitudinal rib along each outer edge (Fig. 7.19). The webs below the deck are 160 mm thick [150].

Single, 12.7 mm dia. strands and small, specially fabricated anchors are used for prestressing the transverse ribs. In the longitudinal direction there are three prestressing tendons in each web. To resist the horizontal forces, the arch is supported on two 9 m deep reinforced concrete foundations (Fig. 7.20).



Fig. 7.20 Seonyu 'Bridge of Peace' in Seoul [147]

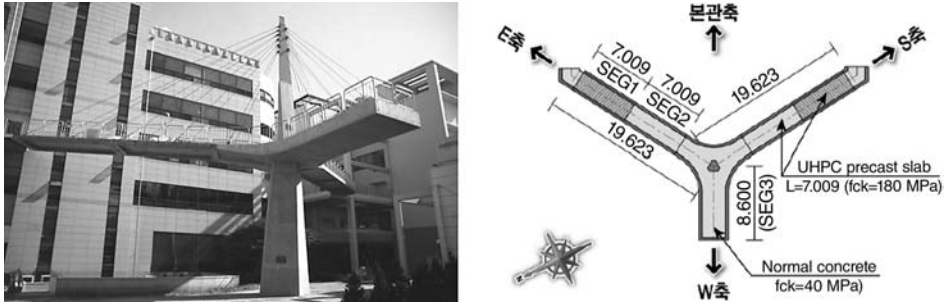


Fig. 7.21 View of cable-stayed footbridge between two office buildings and plan on bridge [151]

7.1.4.2 KICT cable-stayed footbridge (2009) [151]

A cable-stayed footbridge was built in 2009 within the scope of the Super Bridge 200 project of the Korean Institute of Construction Technology (KICT) (Fig. 7.21); the bridge links two office buildings belonging to the institute [151]. Two segments of each bridge deck are constructed from prestressed, precast, steel fibre-reinforced UHPC. The compact dimensions of the edge beams demonstrate the high compressive strength of UHPC.

This bridge represents a full-scale test in preparation for an application on a larger scale based on the results of a KICT research project that looked at the potential use of steel fibre-reinforced UHPC in the decks of long-span cable-stayed bridges.

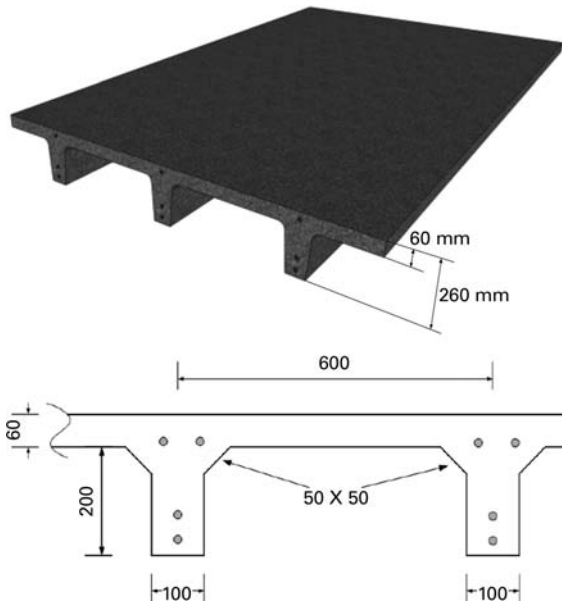


Fig. 7.22 New bridge deck design [151, 152]

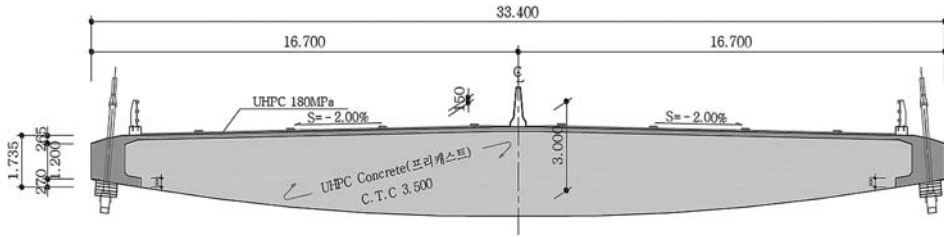


Fig. 7.23 Section through bridge deck showing parabolic cross-beams [151]

7.1.4.3 Design for Jobal Bridge (KICT)

To reduce the self-weight of the decks of long-span cable-stayed bridges, a 60 mm deep slab with prestressed ribs of fibre-reinforced UHPC has been developed at the Korean Institute of Construction Technology (KICT). The centre-to-centre spacing of the ribs is 600 mm (Fig. 7.22). This bridge deck cross-section is 50% lighter than a deck made from conventional concrete [151, 152].

To transfer this method to a full-scale project, a cable-stayed bridge with three 90 m high pylons and a main span of 200 m was designed in 2011 to link the town of Jobal with Dunbyung Island on Korea’s south coast (Fig. 7.24). It is planned to use steel fibre-reinforced UHPC for the bridge deck with transverse ribs and edge beams (Fig. 7.23).

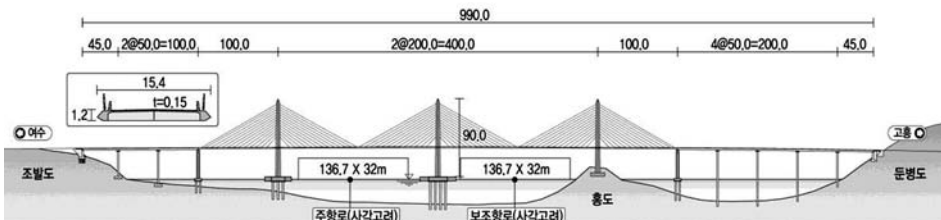


Fig. 7.24 The design for Jobal Bridge [151]

7.1.5 Germany

7.1.5.1 Bridges over River Nieste near Kassel

The first practical use of UHPC in construction in Germany was for a project in 2004 to build a footbridge spanning 12 m over the River Nieste near Kassel [20]. It is a precast, post-tensioned design with two prestressing tendons. Figure 7.25a shows a section through the bridge.

The deck is 10 cm deep, spans 3 m between the edge beams and is reinforced exclusively with fibres. Steel reinforcing bars are only used in the transfer zones for the prestressing forces. The edge beam depth varies to match the internal forces. Owing to its low weight of just 12 t, the superstructure could be transported on a low-loader from the precasting works to the site, where it was lifted into position with a mobile crane and fixed within about two hours. It was opened to the public immediately afterwards (Figure 7.25b).

Owing to the good economics and very short construction time, two more precast UHPC bridges were erected not far from this first one. These span 7 and 9 m and both are 2.9 m wide (Figure 7.26). They are in the form of double-T beams with an 8 cm deep deck and

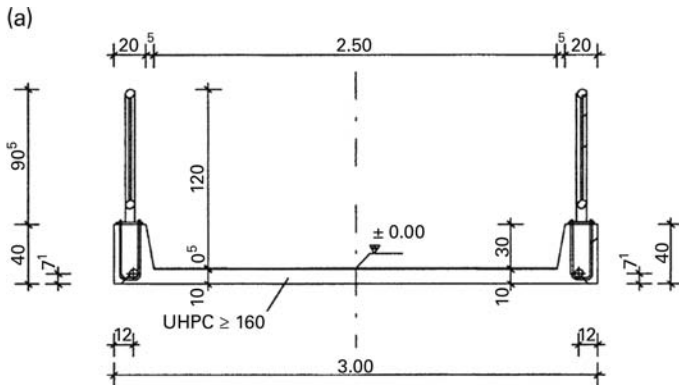
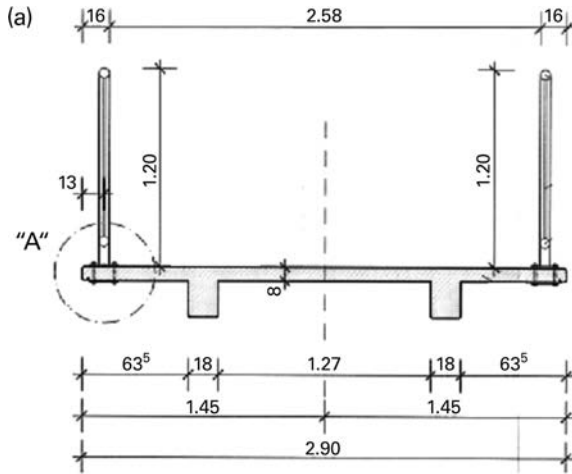


Fig. 7.25 First UHPC bridge in Germany: a) section, b) view of bridge after completion



(b)



Fig. 7.26 Two further UHPC precast bridges over the River Nieste: a) section, b) view of one of the bridges

18 cm wide webs that are 30 cm deep at mid-span. The underside of each web traces a circular arc whereas the top surface remains straight. In the longitudinal direction the webs are pretensioned. No steel reinforcing bars were necessary. In the transverse direction, all the loads are carried exclusively by the fibre-reinforced concrete.

Similar precast concrete bridges, but with spans of about 18 m, have been erected over the River Weschnitz in Weinheim and over the River Usa in Friedberg (Hesse).

7.1.5.2 Gärtnerplatz Bridge over River Fulda, Kassel (2007)

After some practical experience with this new building material had been gained in the foregoing projects, the City of Kassel decided to build a bridge over the River Fulda for pedestrians and cyclists. A hybrid steel-UHPC structure was chosen. Figure 7.27 shows

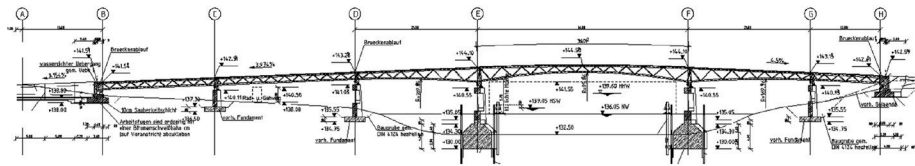


Fig. 7.27 Longitudinal section through Gärtnerplatz Bridge

a longitudinal section through the Gärtnerplatz Bridge designed by Kassel-based consulting engineers IBB Fehling + Jungmann GmbH [20].

The new bridge was intended to replace an existing multi-span timber bridge that was in a poor state. A new structure with six spans and a total length of 134 m was designed, with the longest span being 36 m. The longitudinal beam is a three-chord truss with varying depth (Figure 7.28a). The top chords of the truss are made from UHPC, and the bottom chord and the diagonals are steel tubes connected to the top chords via high-strength friction-grip bolts. Precast UHPC slabs, 5 m wide and pretensioned in the transverse direction, make up the bridge deck. To ensure proper drainage, the slabs are 11 cm deep at the edges, 8 cm deep in the middle. After the truss had been erected, adhesive was used to connect the deck segments together and to the top chords. No mechanical connectors were used.

The glued joints were extensively tested in the laboratory beforehand. Information on the results of the tests and the practical experience gained can be found in [127]

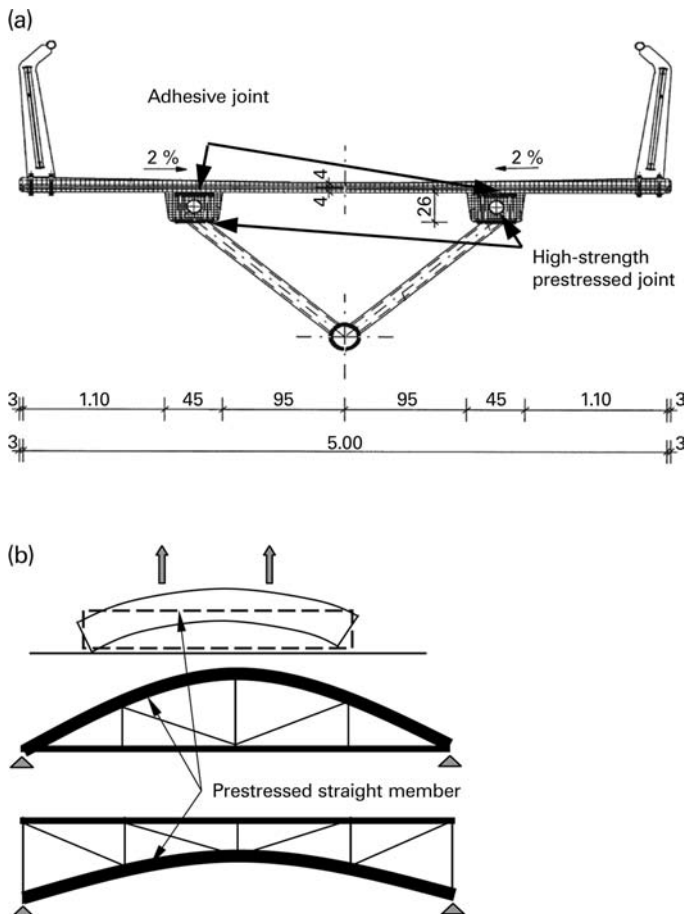


Fig. 7.28 a) Section through Gärtnerplatz Bridge and b) bending the UHPC segments, which were originally cast straight (sketch of principle)



Fig. 7.29 Gärtnerplatz Bridge after completion

and [153] as well as Section 6.3. In order to ensure an adequate level of structural safety for the connections, under both long-term actions and temperature loads, sandblasting the surfaces to be glued beforehand proved to be especially effective.

Exploiting the high deformation capacity of UHPC, the top chords of the truss were first cast straight and afterwards bent to match the gradient as the structural steelwork was attached. The self-weight of the top chord, raised at each end, was sufficient for this. The principle is explained in Figure 7.28b.

The single-span trusses prefabricated in this way were erected span by span and connected via end plates to form a continuous system (Fig. 7.29). In order to avoid permanent tensile stresses in the bridge deck in the longitudinal direction in the final condition, the entire superstructure was post-tensioned with two additional, unbonded, external tendons routed in ducts through the two UHPC top chords.

A monitoring system was installed to track the long-term behaviour of the bridge. This system comprises various sensors, e.g. for temperature, moisture content, deflection, rotations and the relative displacements between the glued components. Accelerometers register any changes to the stiffness of the structure [154].

7.1.5.3 HSLV pilot project

A pilot project carried out by the Hesse State Authority for Roads & Transportation (HSLV) based in Wiesbaden involved applying a layer of UHPC *in situ* to a bridge deck of normal-strength concrete [155]. The layer of UHPC was intended to replace the normal waterproofing to the superstructure and at the same time contribute to the structural strength of the bridge.

An approximately right-angled (i.e. non-skew) two-span bridge with spans of 21.50 and 22.50 m was chosen for this pilot project. The cross-section selected was a multi-web T-beam made from prestressed precast segments with *in situ* concrete joints (Figure 7.30). The layer of UHPC was to be 3 cm deep and reinforced exclusively with fibres (6% by vol.)

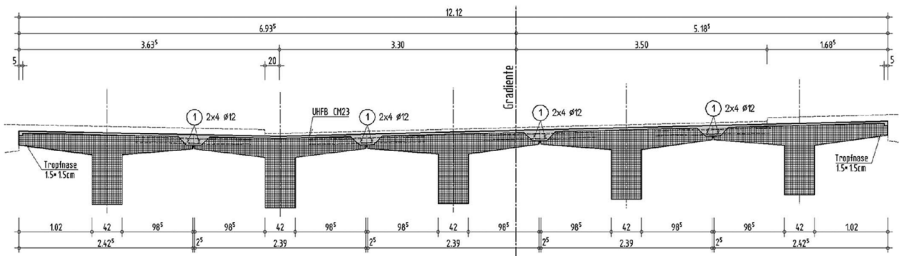


Fig. 7.30 HLSV pilot project: section through bridge superstructure (multi-web T-beam)

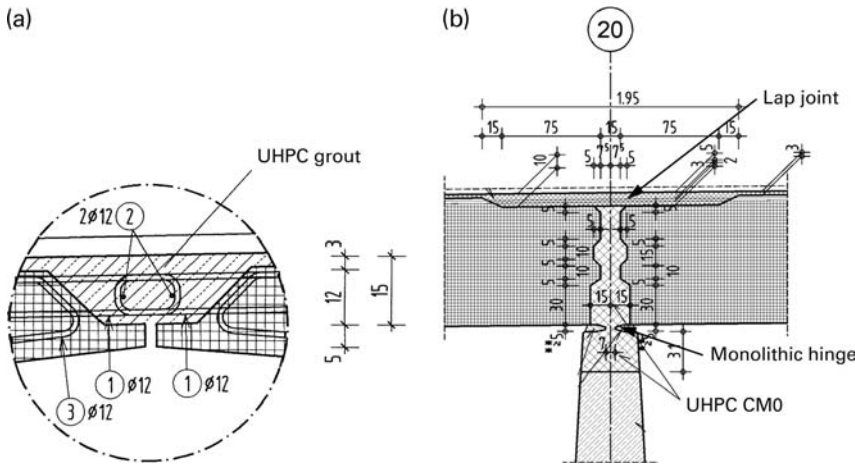


Fig. 7.31 HLSV pilot project: a) longitudinal joint between two precast segments, b) lap joint and monolithic hinge at central support

The joints between each pair of precast segments were designed in such a way that the grout could be placed at the same time as placing the layer of UHPC on the deck. Figure 7.31a shows a detail of the joint with overlapping U-bars.

In order to achieve continuity in the longitudinal direction, the top reinforcement in the precast segments is lapped over the intermediate support. The layer of UHPC at this point would therefore be 8 cm deep. A monolithic hinge was designed for the central support.

The lap in the longitudinal joint was investigated with the help of three-point bending tests carried out on approximately full-size test beams with UHPC grout in the joints. The load was increased monotonically and, with a view to checking fatigue, also applied in cycles. In the static tests, failure always occurred due to yielding of the reinforcement in the joint between the normal-strength concrete and the UHPC (Figure 7.32). Failure in the joint or due to fatigue was not observed.

Similar experiments were also carried out on the lap joint over the central support. With a lap length of 15ϕ , failure occurred at the end of the lap due to yielding of the steel reinforcement.

Precast UHPC bridge footways/parapets were planned, to be connected to the bridge deck with an epoxy resin adhesive.

Unfortunately, the work was not carried out because there were too few bidders.

More recent studies in this field have been looking at a UHPC addition with a combination of low fibre content and steel reinforcement, which would be more economical and is likely to satisfy at least equivalent serviceability and durability specifications.

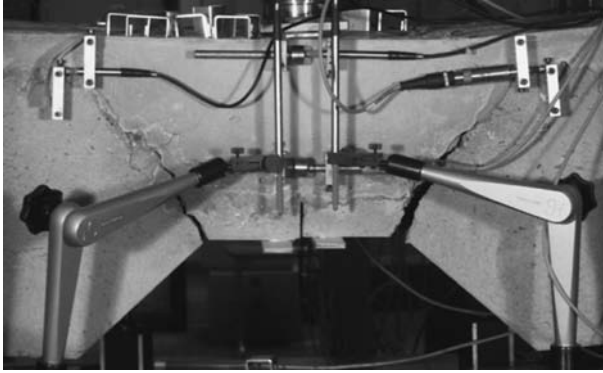


Fig. 7.32 HLSV pilot project: failure of longitudinal joint due to yielding of steel

7.1.5.4 Bridge for pedestrians/cyclists over River Pleiße, Markkleeberg (2012)

A timber bridge in a poor condition carrying a cycle track over the River Pleiße in Markkleeberg near Leipzig is to be replaced by a new structure (Figure 7.33). The client is the Government of Saxony, represented by Leipzig Roadbuilding Authority.



Fig. 7.33 Bridge for pedestrians/cyclists over River Pleiße, Markkleeberg (computer images)

Leipzig-based consulting engineers KHP-Zerna have been appointed to carry out the preliminary and detailed design work.

The new bridge is designed as a single-span arch spanning 31.70 m between the abutments. The clear width between the parapets is 3.50 m.

The two arches are 324 mm dia. hollow steel sections, the bridge deck uses precast fibre-reinforced UHPC segments joined together by post-tensioning in the longitudinal direction. Dry joints will be used between the segments. In the deck there will be conventional reinforcement in the transverse direction.

The UHPC slabs are 8 cm deep in the span. Below the hangers, which are in the form of inclined, non-crossing cables, there is a stiffening beam with a total depth of 30 cm. Ducts are included in these longitudinal beams for routing the post-tensioning cables after erecting the precast segments. The prestressing tendons also function as a tie to resist the horizontal thrust of the arch.

7.1.6 Austria

7.1.6.1 Wild Bridge near Völkermarkt

This bridge carries an access road to the Wild company works over a romantic valley and is the world's first precast UHPC arch bridge [156]. In this case, UHPC enabled the construction of an especially delicate and lightweight structure, as Figure 7.34 shows. The hollow segments of the arch have a wall thickness of just 6 cm and are externally prestressed.

Lowering the arch into position was therefore particularly suited to the erection of this arch because the expensive hinge details then only had to be designed for the forces from the relatively low weight of this innovative structure [156]. The construction principle shown in Figure 7.35 was therefore possible.

Rational connections between the precast segments were achieved by milling the end surfaces to a high accuracy and then using dry joints [157]. The CNC milling technology of the Max Bögl company from Neumarkt in der Oberpfalz, Germany, already proved on the slab tracks for new high-speed railway lines, was used here after the precast segments had been heat-treated. Afterwards, the segments hardly deform or distort any



Fig. 7.34 View of Wild Bridge near Völkermarkt [156]

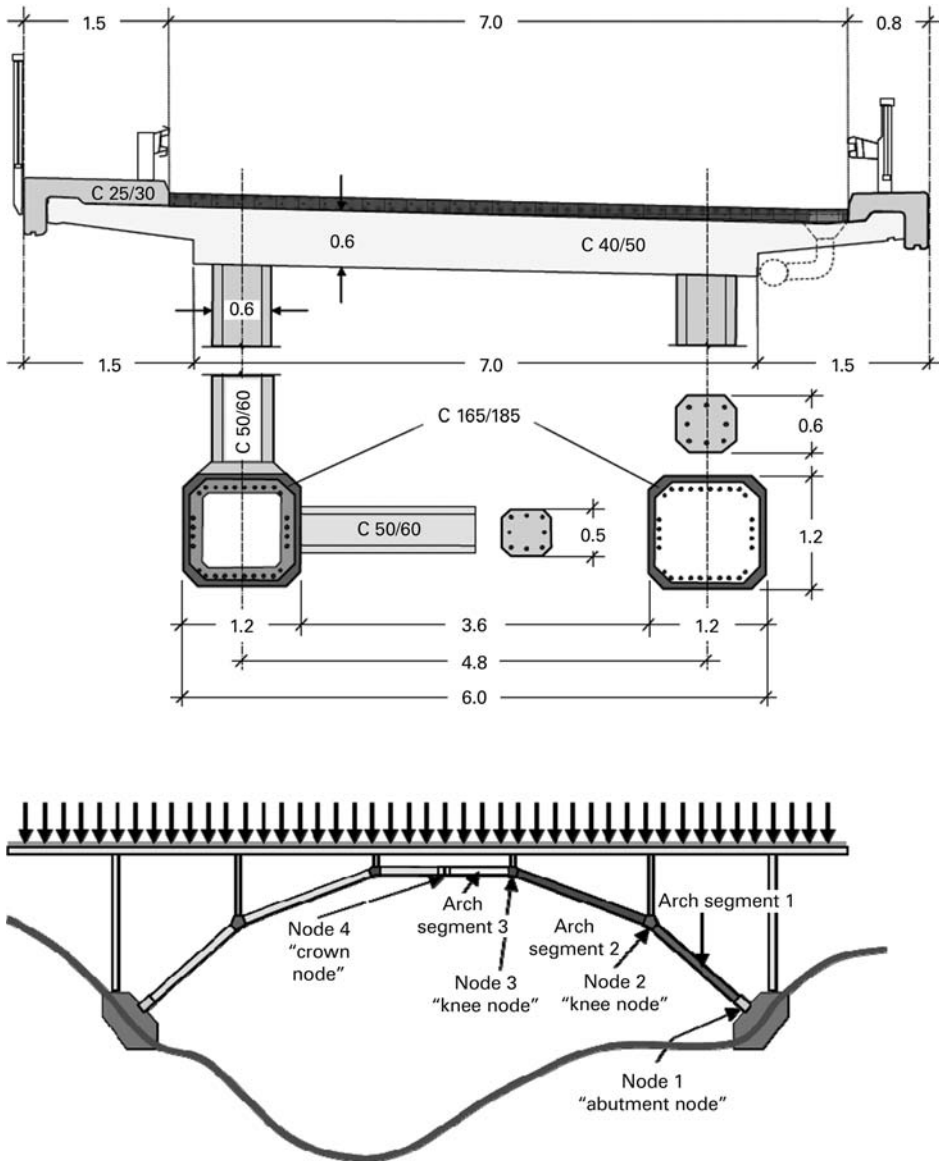


Fig. 7.35 Wild Bridge: section and design principle (modified after [156])

more as a result of shrinkage, which means contact over practically the whole area between the parts to be joined can be guaranteed.

The individual segments of the arch and the columns supporting the deck were connected together with external tendons (Figure 7.36), which lends the knee node elements a special significance (see Figure 7.37).

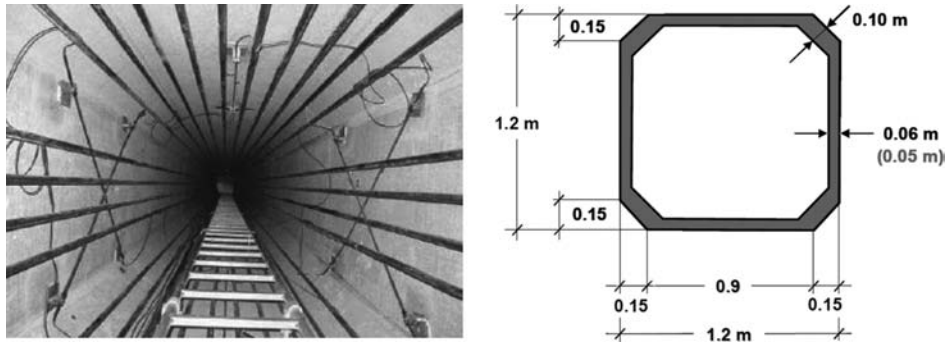


Fig. 7.36 Typical hollow precast segment for the polygon-style arch [156]

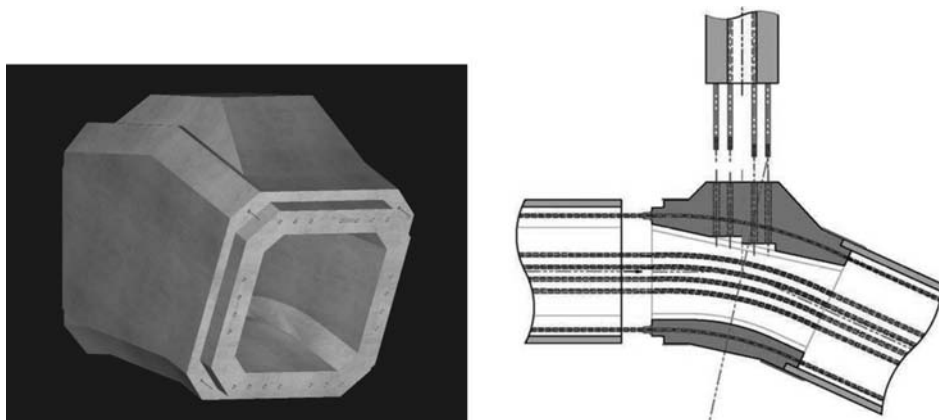


Fig. 7.37 Knee node element [156]

Mixing and concreting of the fibre-reinforced concrete for the precast concrete segments, likewise the structural analysis, had to be accompanied by a comprehensive scientific study in order to demonstrate adequate safety and the feasibility, and also to obtain the necessary acceptance from the client and the authorities responsible. The study included testing full-size arch segments to establish their load-carrying capacity. Erecting the arch by means of lowering it into position is illustrated in Figure 7.38.

7.1.6.2 Bridge for pedestrians/cyclists, Lienz

A new bridge was necessary to improve the network of cycle tracks around the town of Lienz. However, at the site of the new bridge, the depth available for the superstructure was limited and the design brief called for minimum disruption to traffic beneath the bridge during construction [158]. The solution was a three-span bridge made from two precast segments joined together by high-strength bolts. Existing formwork had to be reused, thus defining the geometry of the precast components. The final structure

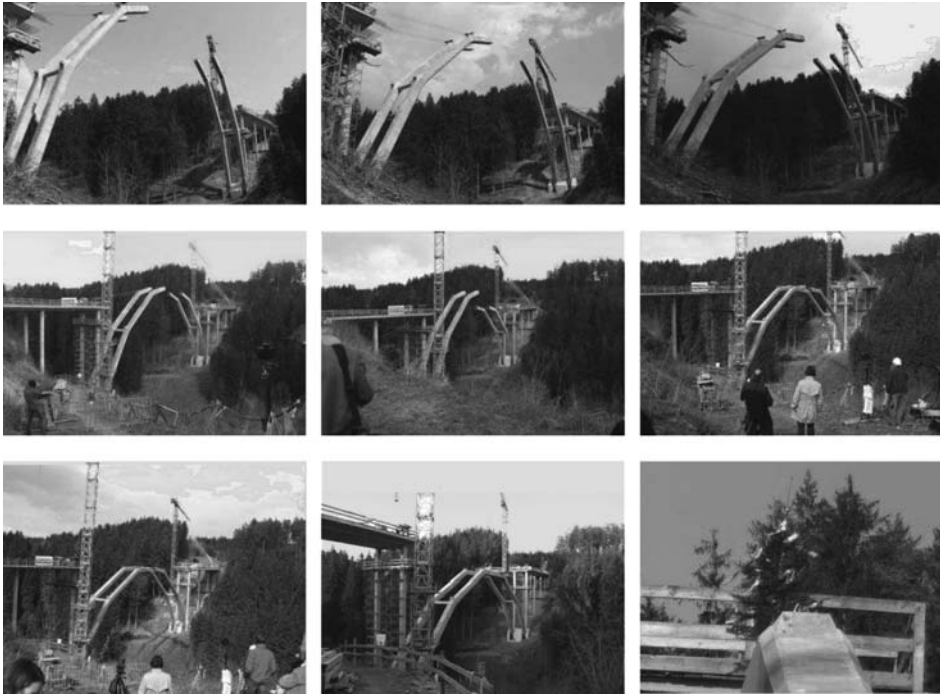


Fig. 7.38 Lowering the arch of the Wild Bridge into position



Fig. 7.39 Bridge for pedestrians/cyclists, Lienz

weighed 22 t and was able to be erected in just three hours (Figure 7.39). The precast segments are prestressed in the longitudinal direction and do not have any steel reinforcing bars to carry the load in the transverse direction. Instead, the structural response in this direction is achieved through the effect of the fibre-reinforced concrete.

7.1.6.3 Modular temporary bridge for high-speed rail lines

Temporary bridges are frequently required within the scope of railway construction work so that rail services are not interrupted. Building such bridges from UHPC

complies with the high demands that high-speed trains place on such bridges regarding stiffness and vibration behaviour. It is also possible to include a continuous bed of ballast. A design in the form of a U-shaped section has proved to be advantageous for complying with overhead clearance requirements and also for reducing noise pollution. Figure 7.40 shows sections through the segments, a longitudinal section and the concept behind these temporary bridges [158].

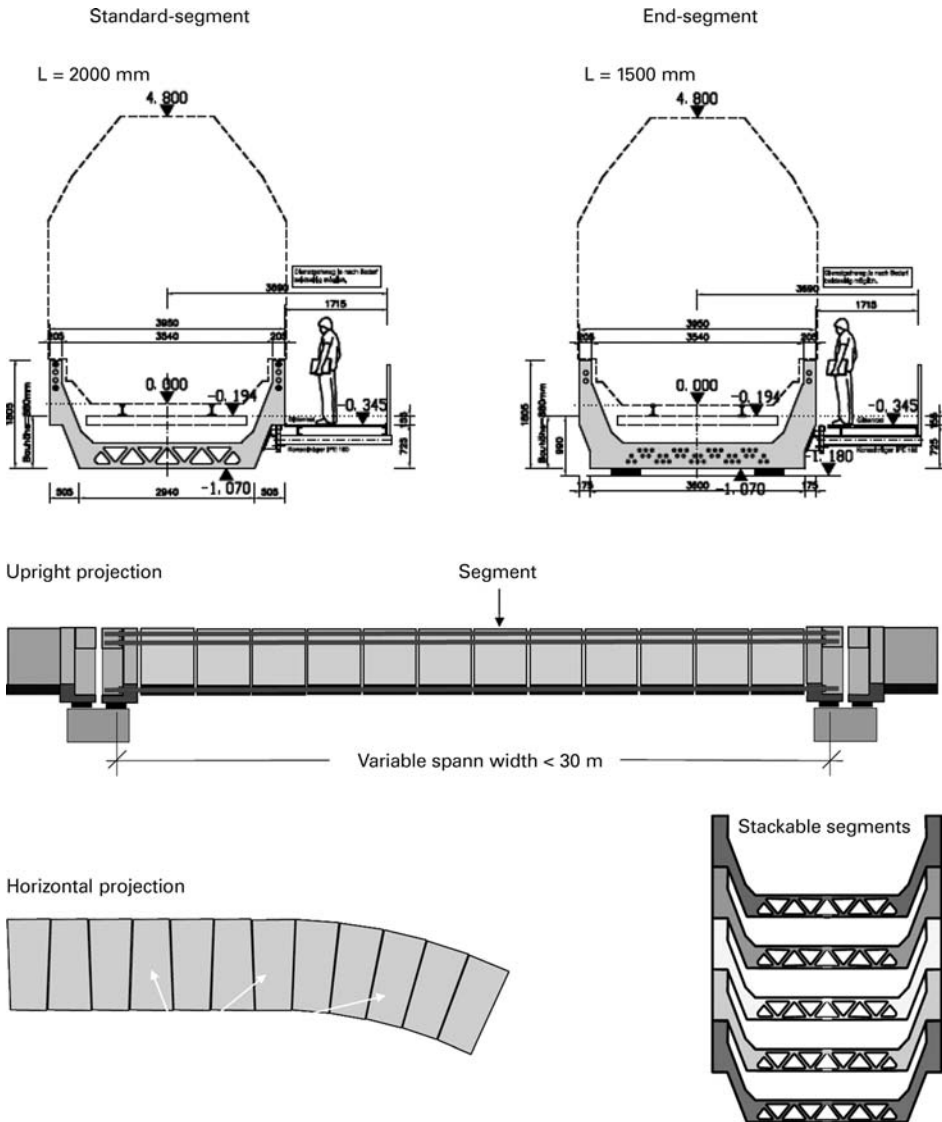


Fig. 7.40 Sections, longitudinal section and concept for a modular temporary bridge made from UHPC for high-speed railway lines



Fig. 7.41 Precast UHPC segments

A length of 2 m was selected for the bridge segments. They are made from fibre-reinforced UHPC. The bottom part of the section has been resolved into a truss, which saves weight and also provides openings for routing most of the unbonded prestressing tendons needed to connect the segments together. CNC-milled dry joints are used between the segments. Each end segment is different because it has to anchor the prestressing forces and accommodate the supports (see Figure 7.41).

7.1.7 Switzerland

One important area of application for UHPC lies in the upgrading of bridge superstructures [138]. In the upgrading projects carried out to date, the concrete surface of the component to be repaired was treated first with high-pressure water jets (and sand-blasting in one case) in order to achieve an adequate bond (without mechanical fixings) and thus be able to assume a monolithic loadbearing behaviour for the UHPC-reinforced concrete composite component [178]. All the applications were preceded by tests so that the UHPC mixing and concreting operations could be carried out properly with the personnel and equipment available and to suit the circumstances of the respective project. Prior testing was important in all situations because it allowed minor corrections to be carried out which then guaranteed that the work could be executed as planned at a later date and with the necessary quality. In all applications, the UHPC was mixed in conventional concrete mixers on the site or at the precasting works without any appreciable difficulties (at extreme temperatures of 4 and 33 °C).

In several cases the surfaces of bridge decks and bridge edge details were waterproofed according to the concept shown in Figure 7.42. UHPC was applied – according to the fundamental idea behind UHPC – in those areas of the structures which are permanently subjected to the severe conditions of exposure classes XD2, XD3. Gradients of up to 10.6% were produced with self-compacting UHPC (Figure 7.43). This required a modified mix that lent the fresh UHPC a thixotropic behaviour, i.e. slow-moving during concreting but firm once in place. Surfaces in fair-face UHPC were cast against rough-sawn formwork or, in one case, a profiled plastic sheet in order to reduce the formation

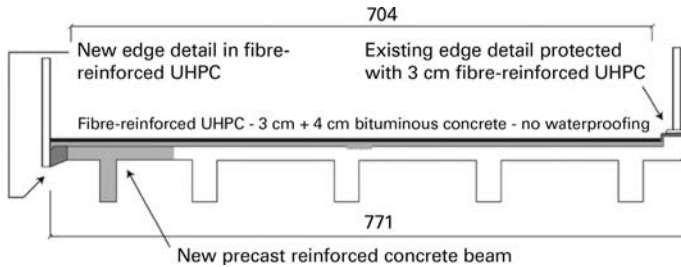


Fig. 7.42 Section through a bridge repaired and widened with UHPC (dims. in cm) [159]



Fig. 7.43 Adding a layer of UHPC to a bridge deck (2004)

of rust spots on the surface of the UHPC in contact with chlorinated water and to prevent protruding fibres.

In Switzerland the optimum combination of different concretes in one structure (hybrid construction) is seen as one interesting potential application for using UHPC wisely. This means using UHPC for the severely exposed areas of a structure only, i.e. as the top surface of a bridge deck and in the bridge footways/parapets. Conventional reinforced concrete is used for all the other parts of the bridge structure because they are only subjected to moderate exposure. In this context, the reader is referred to a corresponding pilot project of the Hesse State Authority for Roads & Transportation, which is described in Section 7.1.5.3 [155].

7.1.8 The Netherlands

So far, UHPC has been used by the Dutch for a few new bridge projects only. Figure 7.44 shows, however, that UHPC represents a reasonable alternative for small bridges as well because the reduced slenderness results in elegant designs. This bridge is 14 m long and only 300 mm deep at mid-span ($l/d = 48$).



Fig. 7.44 Bridge made from UHPC for cyclists/pedestrians, Purmerend, The Netherlands (2008)

Whereas UHPC has only been used for a few new structures up to now, it has been used for upgrading several bridges. The first use of UHPC in The Netherlands was in 2002 and involved replacing a bridge deck made from a tropical timber (115 mm deep beams) with a UHPC deck only 45 mm thick in total [160]. UHPC panels measuring 2.95 m wide \times 7.25 m long now make up the new deck. These 45 mm thick elements have a 9 mm concrete cover on top, three layers of reinforcing bars (8 mm dia., 40 mm spacing) and a concrete cover of 10 mm underneath; the reinforcement ratio is therefore 5.6%. Deeper edges were necessary in order to accommodate the moments at the edge. The thickness here is 65 mm, with five 12 mm dia. bars on top and five 16 mm dia. bars below (Figure 7.45). The concrete was very fluid and reached a compressive strength exceeding 180 N/mm^2 . The panels are designed for a maximum wheel load of 200 kN applied to an area measuring $350 \times 600 \text{ mm}$. Two panels underwent fatigue testing with more than 10 million load cycles at Delft University of Technology. The tests confirmed the expectations. The panels were laid on the longitudinal steel bridge beams (Fig. 7.46) and levelled with four adjusting bolts. It was not necessary to add a wearing coating to the UHPC deck. The loadbearing behaviour has been monitored since 2002 and so far no problems have been detected.

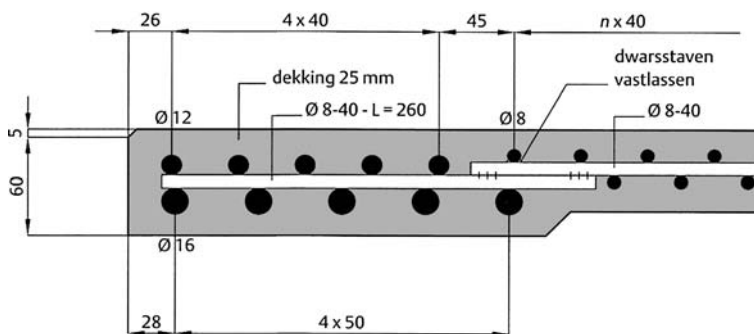


Fig. 7.45 Reinforcement in UHPC bridge deck panel (reinforcement ratio 5.6% in panel, 10% in stiffened edge)



Fig. 7.46 Erecting a UHPC panel (45 mm thick) for the Kaag Bridge in The Netherlands (2003)

Three more bridges with orthotropic steel decks have since been given new high-performance concrete decks (Caland Bridge, Moerdijk Bridge and Hagenstein Bridge). As fatigue cracks had appeared in the structural steelwork, UHPC was not used for the very thin deck because that would not have solved the fatigue problems. Instead, it was decided to opt for an optimum combination of concrete strength on the one hand and weight on the other. The associated concrete mix consisted of 475 kg binder (Portland cement, silica fume, additives), 750 kg sand 0–2 mm, 1170 kg granite 2–5 mm, 75 kg steel fibres ($l = 12$ mm, $d = 0.4$ mm) and 150 l water. The mean 28-day cube compressive strength was about 120 N/mm^2 . The deck is 60 mm thick and reinforced with 12 mm dia. steel bars at 75 mm centres.

7.2 Applications in buildings

7.2.1 Columns

Many architects are keen to reduce the dimensions of columns in buildings. In the lower storeys in particular (e.g. entrance foyers), columns often seem very massive, which mars the aesthetics and the flexibility of the interior spaces. Initial experience with the *in situ* concreting of a heavily reinforced column measuring 1.2×1.3 m was gained during the construction of the 59-storey Park City Musashi-Kosugi skyscraper in Japan [161]. The demands placed on the mix concerned its flowing properties (in conjunction with the considerable amount of reinforcement), its fire resistance and its response to seismic loads. The mix that was developed consisted of 155 kg water, 103 kg cement, 436 kg ultra-fine sand, 840 kg gravel, 2 kg polypropylene fibres and 40 kg steel fibres per m^3 concrete. The compressive strength exceeded 170 N/mm^2 . Figure 7.47 shows a sawcut through a test column that was cast in advance to gain experience with this form of construction. A visual inspection revealed a homogeneous concrete surface with ideal compaction. Experience gained during the construction of a number of high-strength columns on the ground floor was positive.

Korea, too, has experience of UHPC columns in high-rise buildings [162]. A UHPC mix with low-heat Portland cement was developed for these columns. The 28-day compressive strength was 180 N/mm^2 for a w/b ratio of 0.15. A total of 9 m^3 UHPC was pumped



Fig. 7.47 Sawcut through UHPC test column for Park City Musashi-Kosugi high-rise building, Tokyo [161]

into the column formwork in the basement of the 66-storey Metapolis building in Dongtan.

However, the potential of UHPC as a construction material for buildings lies primarily in the development of innovative architectural forms and new configurations. An example of this can be seen in the tree-like columns to the Musée des Civilisations de l'Europe et de la Méditerranée (MuCEM) in Marseille, recently opened [179]. The loadbearing structure of this building consists to a large extent of UHPC components such as the tree-like columns (Figure 7.48), the edge beams to the suspended floors, the façade elements and the footbridge to the neighbouring Fort Saint Jean. The tree-like columns are a characteristic feature of this new building. All the columns are different and carry the vertical loads. Positioned in front of the edge beams to the floors, they had to be designed to carry an eccentric loading.

Prestressed elements are used to fix the columns to the floor edge beams at the top and the foundation at the bottom, which at the same time increases the bending capacity of the whole column. Finite element calculations, with non-linear constitutive equations, were carried out for the static design of the columns. Tests were performed beforehand



Fig. 7.48 Tree-like UHPC columns in the MuCEM, Marseille (2012)

on three straight and three Y-shaped columns. An eccentricity of loading from the edge beams amounting to 225 mm was assumed in the tests, and the results confirmed the assumptions made in the calculations. A seismic analysis was also carried out assuming an elastic response of the columns.

7.2.2 Façades

The MuCEM building described in the preceding section is also distinguished by its special façade. Figure 4.49 shows the façade in context and close-up.

The 6×3 m façade elements with their open texture are used on the south-east and south-west elevations of the museum. These self-supporting elements are joined together with polyurethane connections. The idea behind that is to compensate for inaccuracies in the surfaces and to prevent undesirable stress concentrations.

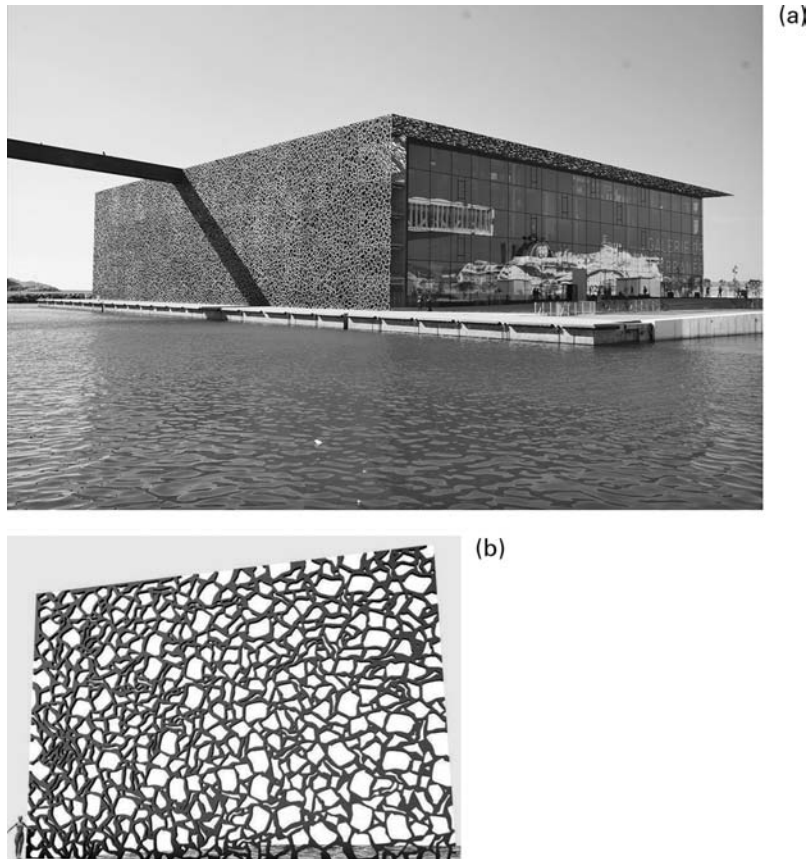


Fig. 7.49 Façade to MuCEM building, Marseille: a) Building shortly after opening (photo: Nicolas Janberg), b) close-up of façade element (photo: Ricciotti)

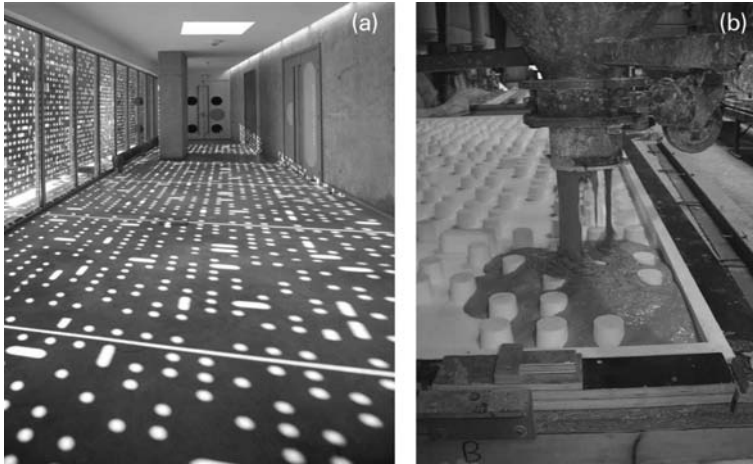


Fig. 7.50 Façade to a building in Sedan, France: a) daylight passing through the perforated UHPC façade panels, b) concreting the panels

Such ‘transparent’ façade elements are also used on a building in Sedan, France (Figure 7.50a). In order to give the building an individual character, it is clad with 330 m² of UHPC façade panels with circular perforations. The panels measure 2 m long × 4 m high and are 45 mm thick. They are positioned 60 cm in front of a glass façade and therefore function as sunshading.

The circular openings have different diameters and the proportion of openings in the area of the façade is 30%. Silicone moulds were used for precasting the panels (Figure 7.50b). The use of silicone as a mould material prevented stress concentrations and cracking around the openings as a result of restricting autogenous shrinkage; silicone also eased the removal of the panels from the moulds. The pale blue colour of the concrete was achieved by using a white premix product to which blue and red pigments were added. Panels were removed from their moulds 16–20 h after concreting.

The police headquarters in Nantes, France, completed in 2010, is another building with an interesting façade [163]. The seven-storey, 140 m long building is divided into four blocks. Sunshades in the form of UHPC strips (Ductal[®]) have been provided to achieve coherence and uniformity (Fig. 7.51). These strips are 7.20 m long, 40 cm wide, 40–50 mm thick and are supported on posts made from white, polished concrete. Two stainless steel cables passing through all the strips and anchored at the top of the structure support the strips at mid-span. The strips were designed for wind and snow loads and have minimal profiling to improve their response to wind. Using cables to support the strips enabled the slenderness ratio to be increased to 144, which resulted in a very attractive appearance.

7.2.3 Stairs and balconies

Stairs and balconies are building components that practically cry out for a lightweight design. UHPC presents especially useful options when fibres are combined with



Fig. 7.51 Police headquarters in Nantes: sunshades after erection [163]

traditional reinforcement. The flow of the forces in stairs and balconies is well understood, which means that one layer of reinforcing steel can carry the loads efficiently. In addition, the effect of the steel fibres results in very thin components. At bar anchorages and laps, the effect of the steel fibres enables very thin concrete covers without this leading to a reduction in the anchoring capacity. Combining fibres and reinforcing steel can lead to very slender, elegant designs as Figures 7.52 and 7.53 prove [164].

In order to keep such components as thin as possible, the concrete often includes a relatively high volume of fibres ($150\text{--}300\text{ kg/m}^3$) combined with high (conventional) reinforcement ratios of 5–20%. A w/b ratio of about 0.16 results in a strength of $140\text{--}150\text{ N/mm}^2$. This form of construction is mainly popular in Denmark. These days, the

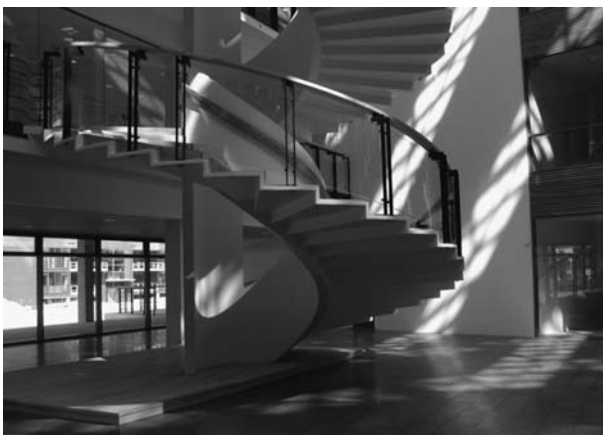


Fig. 7.52 Spiral stair made from fibre-reinforced UHPC (Hi-Con, Denmark [164])



Fig. 7.53 White balconies made from fibre-reinforced UHPC (Hi-Con, Denmark [164])

precast concrete balcony elements are often designed in such a way that they can be bolted to the suspended floor of the building via a projecting ‘flap’. Thermal insulation is provided above and below this ‘flap’ to avoid thermal bridges. The system is very simple: the balcony slab can be attached quickly and easily [164].

Figure 7.54 shows Hi-Con balcony slabs for a high-rise building project in Delft (Poptahof) in 2011. The slabs are 65 mm thick and are connected to the floor of the building via four projecting blocks. A loading test (Figure 7.55) revealed that the balcony slab can carry five times the maximum service load.



Fig. 7.54 Balcony slab for a high-rise building project, Poptahof, Delft, The Netherlands [165]



Fig. 7.55 Loading test on UHPC balcony (timber beams are for safety only)

7.2.4 Roofs

UHPC is ideal for designing roofs with appealing architectural forms. One of the first applications of UHPC was the shell roofs to Shawnessy Light Rail Transit Station in Calgary, Canada, in 2004 (Figure 7.56) [166].

The intention behind the design was to create a protective roof that would require little maintenance and at the same time result in a lightweight, attractive structure. The UHPC used had a compressive strength of 150 N/mm^2 and a flexural tensile strength of 25 N/mm^2 . The 18 mm thick shells are 6 m wide, 5.15 m deep and 5.64 m high. There are no steel reinforcing bars in these double-curvature elements. They were concreted in formwork using an injection method, which essentially excluded any pockets of air and resulted in a high-quality finish. The roofs were concreted lying on their sides, the columns vertically. High dimensional accuracy was necessary for this complex geometry. Tests were carried out on specimens. Stainless steel connectors join the roofs to the columns below.

Figure 7.57 shows a small canopy made from UHPC which was built on the occasion of refurbishing the ‘De Zonnestraal’ Hospital in Hilversum, The Netherlands [167]. The canopy consists of four segments with a maximum span of 8 m. The canopy covering itself is just 25 mm thick. The type BSI UHPC of the canopy was cast in special timber formwork and no steel reinforcing bars were used. Bolts join the four canopy segments together. A single stainless steel column transfers the loads from the four very thin UHPC canopy elements to the foundation.

A special shell of UHPC with a helicoidal form was built in 2004 to roof over the toll station for the Millau viaduct in France [168]. The 2800 m^2 shell consists of 53 unreinforced segments (Figure 7.58).

The method of construction used was similar to that familiar from balanced cantilever erection for bridges, with the precast segments being built out in two directions as a balance beam. Each segment consists of two 100 mm thick UHPC ‘skins’ enclosing



Fig. 7.56 Shell roofs to Shawnessy Light Rail Transit Station, Calgary, Canada (2004)



Fig. 7.57 UHPC canopy at entrance to 'De Zonnestraal' Hospital, Hilversum, The Netherlands (2005) [167]



Fig. 7.58 UHPC roof shell at Millau viaduct, France [168]

polystyrene void formers. The skins are coupled together by vertical fibre-reinforced UHPC ‘partitions’ every 2 m. The only ‘normal’ reinforcement in the structure consists of concentric prestressing tendons that connect the 53 segments together over the 100 m length of the canopy. This prestressing also accommodates the bending moments between the supports. The shell behaves similarly to a slab supported at four points. The flow of forces is complex, with bending and membrane action occurring simultaneously. Despite the exceptional dimensions (area of formwork = 225 m²), it only took one day to produce each segment because the effect of the fibres obviated the need for any further reinforcement. In any case, reinforcement cages would have been impossible because of the thinness of the membrane skins and the twist of the structure.

A UHPC roof to Villa Navarra, a building for art exhibitions, was built in Le Muy, France, in 2007 [169]. This 9.2 × 40 m roof consists of precast UHPC segments (Ductal®) and is made up of 17 identical, ribbed elements that are 2.35 m wide and 9.25 m long (Figure 7.59a). The cantilevering part is 7.8 m long (Figure 7.59b). The ribs are max. 500 mm deep at the supports, 30 mm at the ends. A 30 mm thick slab spans between the ribs.

7.3 Other applications

7.3.1 Runway, Haneda Airport, Tokyo, Japan

Planning work for extending Tokyo’s Haneda Airport began in 2007. However, advanced experimental testing began two years before that. This project is an excellent example of how demands regarding durability and saving weight favour an economic solution employing fibre-reinforced UHPC [147].

Figure 7.60a,b shows the new runway, which was built on reclaimed land in Tokyo Bay because of the lack of space onshore. It was not possible to build up the land for this runway everywhere because part of the runway is located in the mouth of the River Tamagawa, which would otherwise have been blocked. Near the mouth, the runway is founded on a steel substructure (Fig. 7.61) that was driven 70 m below the sea water level. The combination of seawater and the local climatic conditions presented a major challenge for the corrosion protection of the steel piles. This situation was dealt with by adding a stainless steel jacket to each pile over a length of about 15 m.



Fig. 7.59 Roof of precast UHPC segments at Villa Navarra, Le Muy, France [169]. a) several of the 17 identical, ribbed elements; b) cantilevering part

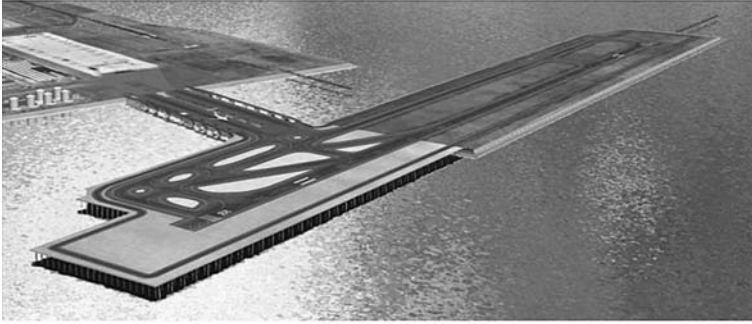
The platform itself is made from UHPC elements supported on a steel frame (Figures 7.62 and 7.63). There were two reasons for choosing UHPC: the platform had to be as light as possible in order to minimise the cost of the substructure and the specification called for a concrete slab with a design life of at least 100 years. A UHPC mix was therefore developed for the slab.

The total area of the UHPC platform is $200\,000\text{ m}^2$. It was built by three Japanese contractors, each one responsible for a certain part of the platform slab. The slab was constructed from precast elements measuring $7.82 \times 3.61\text{ m}$. These elements are ribbed in the direction of the shorter span and are prestressed with wires in both directions. Different concreting procedures were tried out in order to achieve an optimum fibre orientation with respect to the anticipated loading (aircraft wheel load) [171]. The elements concreted in different ways were tested in the laboratory and the element with the most favourable behaviour was then used as the prototype for production. *In situ* UHPC was used to fill the joints between the elements.

The fibre-reinforced, ribbed UHPC slabs are prestressed with high-strength strands and have a structural depth of just 135 mm. They are designed for wheel loads of max. 320 kN. The slab prototypes tested achieved an ultimate loadbearing capacity of 600 kN.

Using UHPC enabled the weight of the slab to be reduced by about 50% compared with a solution employing traditional concrete. So the UHPC design was the most attractive from the economic point of view, too.

(a)



(b)



Fig. 7.60 New runway, Haneda Airport: a) computer image of design [170] for runway D, b) runway during construction. (Ductal®)



Fig. 7.61 Steel substructure with stainless steel jackets [Nippon Steel Corp.]

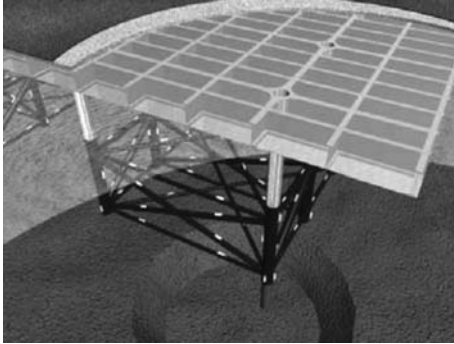


Fig. 7.62 Steel substructure and platform support framework [147]

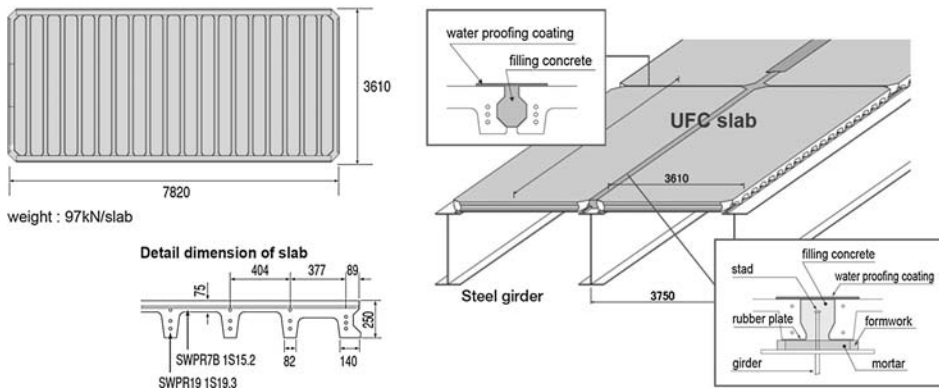


Fig. 7.63 Details of UHPC elements [Taisai Corporation]

7.3.2 Jean Bouin Stadium, Paris

The modernisation project for the Jean Bouin rugby stadium in Paris included a structural, curved shell made up of 20 000 m² of precast UHPC elements [172]. This approach enabled a waterproof roof and façade to be created. The precast triangular elements are 8.2 m long, max. 2.4 m wide and 25 mm thick. There are ribs on the side



Fig. 7.64 Triangular UHPC element for cladding to Jean Bouin Stadium, Paris [172]



Fig. 7.65 Enclosing shell of precast UHPC elements for Jean Bouin Stadium, Paris [172]

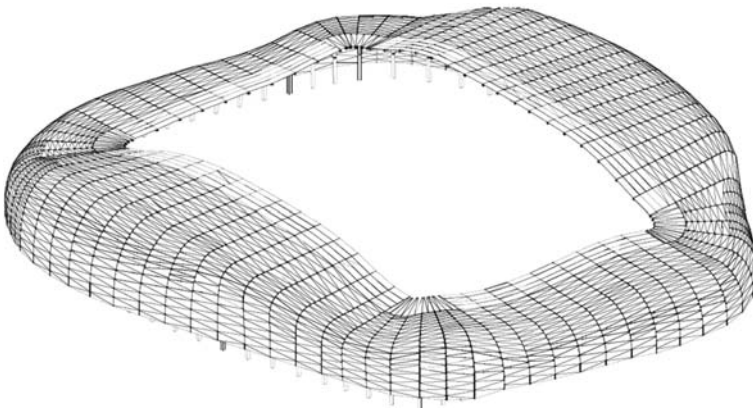


Fig. 7.66 Finite element model of cladding to Jean Bouin Stadium, Paris [172]

where the elements are joined together. Some 1900 elements are required for the roof, 1600 for the façade. They are supported by a steel structure. There are also glass segments within the UHPC elements. Finite element methods were used to analyse the combination of glass and UHPC for different loads, e.g. temperature shock and fatigue. The shape of the ribs, which are designed as overlapping channels, renders the joints between the elements waterproof (Figure 7.64). Figure 7.65 shows the shell and Figure 7.66 the assembly of the triangular UHPC elements.

8 Acknowledgements

The authors would like to thank the German Research Foundation (DFG) for the support it provided for the 'UHPC' research project through its assistance for the German research programme (priority programme SPP 1182 'Sustainable building with ultra high performance concrete'). A sincere vote of thanks goes to Dipl.-Ing. *Jenny Thiemicke* for her help with Chapters 5 and 7, likewise Ms. *Ute Müller* and Dr.-Ing. *Friedrich-Karl Röder* for their critical appraisal of the original German manuscript.

References

1. Naaman, A.E. (23 June 1991) SIFCON: tailored properties for structural performance in high performance fiber reinforced composites. In: Proc. of intl. workshop held by RILEM, ACI and others, Mainz.
2. Kristulovic-Opara, N., Dogan, E., Uang, C.M., and Haghayeghi, A.R. (1997) Flexural behavior of composite R.C. -slurry infiltrated mat concrete (SIMCON) members. *ACI Structural Journal*, **94** (5), 502–512.
3. Bache, H.H. (Jun 1981) Densified Cement Ultra/Fine Particle-Based Materials. In: 2nd Intl. Conf. on Superplasticizers in Concrete, Ottawa, Ontario, Canada.
4. Aitcin, P.C. and Richard, P. (1996) The Pedestrian/Bikeway Bridge of Sherbrooke. In: Proc. of 4th Intl. Symp. on Utilization of High-Strength/High-Performance Concrete, Paris, pp. 1399–1406.
5. Fehling, E., Bunje, K., Schmidt, M., and Schreiber, W. (2008) The Gärtnerplatzbrücke, Design of the first hybrid UHPC-steel bridge across the River Fulda in Kassel, Germany, in *Ultra High Performance Concrete (UHPC), 2nd Intl. Symp. on Ultra High Performance Concrete*, Structural Materials & Engineering Series No. 10 (eds E. Fehling, M. Schmidt, and S. Stürwald), Kassel University Press GmbH, Kassel, pp. 581–588.
6. fédération internationale du béton (*fib*), Task Group 8.6: Draft of Bulletin on Ultra High Performance Fiber Reinforced Concrete, Nov 2011 (unpublished).
7. Tanaka, Y., Maekawa, K., Kameyama, Y. *et al.* (2010) The innovation and application of UHPFRC Bridges in Japan, in *Designing and Building with UHPFRC: State of the Art and Development, Part III, New Frontiers for Bridges* (eds F. Toutlemonde and J. Resplendino), John Wiley & Sons.
8. CEB-FIP Model Code 2010 (2012) Final draft, fédération internationale du béton (*fib*), Bulletins 65 & 66, Lausanne.
9. Schmidt, M. and Jerebic, D. (2008) Basis for Sustainable Structures – the Gaertnerplatz Bridge in Kassel, in *Ultra High Performance Concrete (UHPC), 2nd Intl. Symp. on Ultra High Performance Concrete*, Structural Materials & Engineering Series No. 10 (eds E. Fehling, M. Schmidt, and S. Stürwald), Kassel University Press GmbH, Kassel, pp. 619–625.
10. Schmidt, M. and Jerebic, D. (2010) Nachhaltigkeit von Bauwerken aus UHPC [sustainability of UHPC structures]. *BWI – BetonWerk International*, (3), 50–57.
11. Fehling, E., Schmidt, M., Teichmann, T., Bunje, K., Bornemann, R., and Middendorf, B. (2005) Entwicklung, Dauerhaftigkeit und Berechnung Ultra-Hochfester Betone (UHPC) [development, durability and design of UHPC]. DFG research report FE 497/1-1, Structural Materials & Engineering Series, No. 1, Kassel University Press GmbH, Kassel.

12. Šajna, A., Denarić, E., and Bras, V. (2012) Assessment of a UHPFRC based bridge rehabilitation in Slovenia, two years after application, in *Ultra High Performance Concrete and Nanotechnology in Construction, 3rd Intl. Symp. on Ultra High Performance Concrete and Nanotechnology for High Performance Construction Materials*, Structural Materials & Engineering Series No. 19 (eds M. Schmidt, E. Fehling, C. Glotzbach, S. Fröhlich, and S. Piotrowski), Kassel University Press GmbH, Kassel, pp. 937–944.
13. Schmidt, C. (2012) Whitetopping of asphalt and concrete pavements with thin layers of ultra high performance concrete – construction and economic efficiency. Dissertation, University of Kassel, Structural Materials & Engineering Series, No. 20, Kassel University Press GmbH, Kassel (in German).
14. Piotrowski, S. and Schmidt, M. (2012) Life-cycle cost analysis of a UHPC-Bridge on example of two Bridge Refurbishment Designs, in *Ultra High Performance Concrete and Nanotechnology in Construction, 3rd Intl. Symp. on Ultra High Performance Concrete and Nanotechnology for High Performance Construction Materials*, Structural Materials & Engineering Series No. 19 (eds M. Schmidt, E. Fehling, C. Glotzbach, S. Fröhlich, and S. Piotrowski), Kassel University Press GmbH, Kassel, pp. 957–964.
15. Buitelaar, P. (2004) Heavy reinforced ultra high performance concrete, in *Ultra High Performance Concrete (UHPC), Intl. Symp. on Ultra High Performance Concrete*, Structural Materials & Engineering Series (eds M. Schmidt, E. Fehling, and C. Geisenhanslüke), Kassel University Press GmbH, Kassel, No. 3, pp. 25–35.
16. Scheffler, B. and Schmidt, M. (2012) Application of ultra-high performance concrete for multifunctional road pavements, in *Ultra High Performance Concrete and Nanotechnology in Construction, 3rd Intl. Symp. on Ultra High Performance Concrete and Nanotechnology for High Performance Construction Materials*, Structural Materials & Engineering Series No. 19 (eds M. Schmidt, E. Fehling, C. Glotzbach, S. Fröhlich, and S. Piotrowski), Kassel University Press GmbH, Kassel, pp. 913–920.
17. Schmidt, M. and Braun, T. (2012) Grouted connections with HPC and UHPC for offshore wind power plants – material properties and quality assurance, in *Ultra High Performance Concrete and Nanotechnology in Construction, 3rd Intl. Symp. on Ultra High Performance Concrete and Nanotechnology for High Performance Construction Materials*, Structural Materials & Engineering Series No. 19 (eds M. Schmidt, E. Fehling, C. Glotzbach, S. Fröhlich, and S. Piotrowski), Kassel University Press GmbH, Kassel, pp. 1019–1026.
18. BMBF project – FKZ: 03X0067C: Kalt härtende Keramik durch nanotechnologische Gefügeoptimierung [cold-curing ceramics through nanotechnology microstructure optimisation]. Sponsored by Federal Ministry of Education & Research, project duration: 2009–2012.
19. Tänzer, R., Stephan, D., and Schmidt, M. (2012) Alkali-activated ground granulated blast furnace slag binders for high performance concretes with improved acid

- resistance, in *Ultra High Performance Concrete and Nanotechnology in Construction, 3rd Intl. Symp. on Ultra High Performance Concrete and Nanotechnology for High Performance Construction Materials*, Structural Materials & Engineering Series No. 19 (eds M. Schmidt, E. Fehling, C. Glotzbach, S. Fröhlich, and S. Piotrowski), Kassel University Press GmbH, Kassel, pp. 385–392.
20. Schmidt, M., Fehling, E., Bunje, K., and Teichmann, T. (2006) Brückenfamilie aus ultrahochfestem Beton in Niestetal und Kassel [series of UHPC bridges in Niestetal Valley and Kassel], in *Beton- und Stahlbetonbau*, vol. **101**, No. 3, Ernst & Sohn Verlag, Berlin, pp. 198–204.
 21. DFG research project SPP 1182: Nachhaltiges Bauen mit Ultra-Hochfestem Beton (UHPC) [sustainable building with UHPC]. Sponsored by German Research Foundation (DFG), project duration: 2005–2012.
 22. Schmidt, M., Bunje, K., Dehn, F. *et al.* (2008) Sachstandsbericht Ultrahochfester Beton [UHPC – state of the art report], in *German Committee for Structural Concrete (DAfStb)*, No. 561, Beuth Verlag GmbH, Berlin.
 23. Perry, V.H. and Seibert, P.J. (2008) The use of UHPFRC (Ductal[®]) for bridges in North America – The technology, applications and challenges facing commercialization, in *Ultra High Performance Concrete (UHPC), 2nd Intl. Symp. on Ultra High Performance Concrete*, Structural Materials & Engineering Series No. 10 (eds E. Fehling, M. Schmidt, and S. Stürwald), Kassel University Press GmbH, Kassel, pp. 815–822.
 24. Schmidt, M. and Geisenhanslüke, C. (2005) Optimierung der Zusammensetzung des Feinstkorns von Ultra-Hochleistungs- und von selbstverdichtendem Beton [optimising the grading of ultrafine particles for UHPC and SCC]. *Beton*, **55** (5), 224–235.
 25. Schmidt, M., Fehling, E., Teichmann, T. *et al.* (2003) Ultra-high performance concrete: Perspective for the precast concrete industry, in *Beton + Fertigteil-Jahrbuch*, Bauverlag, Gütersloh, pp. 10–23.
 26. Teichmann, T. (2009) Influence of the granulometry and the water content on the strength and density of cement stone. Dissertation, University of Kassel, Structural Materials & Engineering Series, No. 12, Kassel University Press GmbH, Kassel (in German).
 27. Fennis-Huijben, S.A.A.M. (2008) Design of Ecological Concrete by Particle Packing Optimization. Dissertation, Delft University of Technology.
 28. Puntke, W. (2002) Wasseranspruch von feinen Kornhaufwerken [water requirement of fine granular media]. *Beton*, **52** (5), 242–248.
 29. Geisenhanslüke, C. (2008) Influence of the granulometry of fine particles on the rheology of pastes. Dissertation, University of Kassel, Structural Materials & Engineering Series, No. 13, Kassel University Press GmbH, Kassel (in German).
 30. de Larrard, F. and Sedran, T. (2002) Mixture-proportioning of high-performance concrete. *Cement and Concrete Research*, **32** (11), 1699–1704.

31. Stovall, T. and de Larrard, F. (1986) Linear packing density model of grain mixtures. *Powder Technology*, **48** (1), 1–12.
32. de Larrard, F. (1999) *Concrete Mixture Proportioning: A Scientific Approach. Modern Concrete Technology 9*, E & FN Spon, London.
33. Geisenhanslüke, C. (2002) Herleitung eines dreidimensionalen Partikelverteilungsmodells zur Entwicklung verbesserter UHPC-Mischungen [derivation of a 3D particle distribution model for developing improved UHPC mixes]. Diploma thesis, University of Kassel.
34. Schwanda, F. (1966) Das rechnerische Verfahren zur Bestimmung des Hohlraumes und Zementleimanspruches von Zuschlägen und seine Bedeutung für den Spannbetonbau [numerical method for determining volume of pores and cement paste requirement of aggregates and its significance for prestressed concrete], in *Zement und Beton*, vol. **37**, Vienna, pp. 8–17.
35. Reschke, T. (2001) *Der Einfluss der Granulometrie der Feinstoffe auf die Gefügeentwicklung und die Festigkeit von Beton [influence of granulometry of fine materials on microstructure development and strength of concrete]*, Schriftenreihe der Zementindustrie No. 62, Verein Deutscher Zementwerke e.V., Düsseldorf.
36. Schießl, P., Mazanec, O., Lowke, D. *et al.* (2010) Investigations on the workability and microstructure development of UHPC; Part 1: Effect of superplasticisers and silica fume on mixing and workability of UHPC. *Cement International*, **8** (4), 60–71.
37. DIN EN 13263-1:2009-07: (2009) Silica fume for concrete – Part 1: Definitions, requirements and conformity criteria; German version EN 13263-1:2005+A1.
38. Heinz, D., Urbonas, L., and Gerlicher, T. (2012) Effect of heat treatment method on the properties of UHPC, in *Ultra High Performance Concrete and Nanotechnology in Construction, 3rd Intl. Symp. on Ultra High Performance Concrete and Nanotechnology for High Performance Construction Materials*, Structural Materials & Engineering Series No. 19 (eds M. Schmidt, E. Fehling, C. Glotzbach, S. Fröhlich, and S. Piotrowski), Kassel University Press GmbH, Kassel, pp. 283–290.
39. Glotzbach, C., Stephan, D., Amrhein, K. *et al.* (2009) Charakterisierung der interpartikulären Wechselwirkungen von Feinstoffleimen [characterising the inter-particle interactions of fine material pastes]. In: 17th Int. Baustofftagung (ibasil) – Proc. vol. 1 (ed. J. Stark), Weimar, pp. 0319–0324.
40. Gerlicher, T., Heinz, D., and Urbonas, L. (2008) Effect of Finely Ground Blast Furnace Slag on the Properties of Fresh and Hardened UHPC, in *Ultra High Performance Concrete (UHPC), 2nd Intl. Symp. on Ultra High Performance Concrete*, Structural Materials & Engineering Series No. 10 (eds E. Fehling, M. Schmidt, and S. Stürwald), Kassel University Press GmbH, Kassel, pp. 367–374.
41. Plank, J., Schroefl, C., Gruber, M. *et al.* (2009) Effectiveness of polycarboxylate superplasticizers in ultra-high strength concrete: The importance of PCE compatibility with silica fume. *Journal of Advanced Concrete Technology*, **7** (1), 5–12.

42. DIN EN 14889-1:2006-11: Fibres for concrete – Part 1: Steel fibres – Definitions, specifications and conformity; German version EN 14889-1:2006.
43. Bornemann, R. and Faber, S. (2004) UHPC with steel- and non-corroding high-strength polymer fibres under static and cyclic loading, in *Ultra High Performance Concrete (UHPC), Intl. Symp. on Ultra High Performance Concrete*, Structural Materials & Engineering Series No. 3 (eds M. Schmidt, E. Fehling, and C. Geisenhanslüke), Kassel University Press GmbH, Kassel, pp. 673–682.
44. Scheydt, J. and Müller, H. (2012) Microstructure of ultra high performance concrete (UHPC) and its impact on durability, in *Ultra High Performance Concrete and Nanotechnology in Construction, 3rd Intl. Symp. on Ultra High Performance Concrete and Nanotechnology for High Performance Construction Materials*, Structural Materials & Engineering Series No. 19 (eds M. Schmidt, E. Fehling, C. Glotzbach, S. Fröhlich, and S. Piotrowski), Kassel University Press GmbH, Kassel, pp. 349–356.
45. Bornemann, R., Schmidt, M., Fehling, E., and Middendorf, B. (2001) Ultra-Hochleistungsbeton UHPC – Herstellung, Eigenschaften und Anwendungsmöglichkeiten [UHPC – production, properties and application options], in *Beton- und Stahlbetonbau*, vol. **96**, No. 7, Ernst & Sohn Verlag, Berlin, pp. 458–467.
46. Fröhlich, S. and Schmidt, M. (2012) Influences on Repeatability and Reproducibility of Testing Methods for Fresh UHPC, in *Ultra High Performance Concrete and Nanotechnology in Construction, 3rd Intl. Symp. on Ultra High Performance Concrete and Nanotechnology for High Performance Construction Materials*, Structural Materials & Engineering Series No. 19 (eds M. Schmidt, E. Fehling, C. Glotzbach, S. Fröhlich, and S. Piotrowski), Kassel University Press GmbH, Kassel, pp. 225–232.
47. Schmidt, M. and Fröhlich, S. (2010) Testing of UHPC. In: 2010 *fib* Congress and PCI Convention Bridge Conf. Proc., Washington, D.C. (pub.: Precast/Prestressed Concrete Institute, Chicago).
48. Mazanec, O., Lowke, D., and Schießl, P. (2010) Mixing of high performance concrete: effect of concrete composition and mixing intensity on mixing time. *Materials and Structures*, **43**, 357–365.
49. Projekt: Prüfung von UHPC [testing UHPC]. Sponsored by German Research Foundation (DFG), SPP 1182 project Schm 1589/10, project duration: 2008–2012.
50. DIN EN 206-9:2010-09: Concrete – Part 9: Additional rules for self-compacting concrete (SCC); German version EN 206-9:2010.
51. DAfStb directive: (Mar 2010) Stahlfaserbeton – Ergänzungen und Änderungen zu DIN 1045, Teile 1 bis 3 und DIN EN 206-1 [steel fibre-reinforced concrete – addenda & amendments to DIN 1045, parts 1–3, & DIN EN 206-1].
52. DIN EN 14651:2007-12: Test method for metallic fibre concrete – Measuring the flexural tensile strength (limit of proportionality (LOP), residual); German version EN 14651:2005 +A1:2007.

53. RILEM TC 162-TDF (2002) Test and design methods for steel fibre reinforced concrete: Bending test – Final recommendation. *Materials and Structures*, **35**, 579–582.
54. Lange, J., Rauscher, S., Benning, W., and Hegger, J. (2008) Ellipsen- und Kreisdetektion zur Bestimmung der Orientierung von Stahl- und Glasfasern in Beton [detection of ellipses and circles to determine orientation of steel and glass fibres in concrete]. *tm – Technischen Messen*, **75** (10), 529–536.
55. Tue, N.V., Henze, S., Küchler, M., Schenck, G., and Wille, K. (2007) An optoanalytic method for the determination of the distribution and orientation of fibres in steel fibre reinforced UHPC, in *Beton- und Stahlbetonbau*, vol. **102**, No. 10, Ernst & Sohn Verlag, Berlin, pp. 674–680 (in German).
56. Schnell, J., Schladitz, K., and Schuler, F. (2010) Direction analysis of fibres in concrete on basis of computed tomography, in *Beton- und Stahlbetonbau*, vol. **105**, No. 2, Ernst & Sohn Verlag, Berlin, pp. 72–77 (in German).
57. Bunje, K. and Fehling, E. (2002) About the Fatigue Limit (Mechanical Durability) of Ultra High Performance Concrete. in Proc. of 4th Intl. PhD Symp. in Civil Engineering, Munich, Sept.
58. Ma, J., Orgass, M., Dehn, F. *et al.* (2004) Comparative Investigations on Ultra-High Performance Concrete with and without Coarse Aggregates, in *Ultra High Performance Concrete (UHPC)*, Intl. Symp. on Ultra High Performance Concrete, Structural Materials & Engineering Series No. 3 (eds M. Schmidt, E. Fehling, and C. Geisenhanslüke), Kassel University Press GmbH, Kassel, pp. 205–212.
59. CEB-FIP Model Code 1990: (1993) Design Code, Comité Euro-International du Béton. Thomas Telford Services Ltd, London.
60. Tue, N., Dehn, F. *et al.* (2004) Composite elements made of steel tubes and ultrahigh strength concrete as motor of innovation. Leipzig University, final report to Bilfinger Berger AG (unpublished, in German).
61. EN 1992-1-1:2004-12 Eurocode 2: Design of concrete structures – Part 1-1: General rules and rules for buildings. European Committee for Standardization (CEN), Brussels.
62. DIN EN 1992-1-1/NA:2011-01: National Annex – Nationally determined parameters – Eurocode 2: Design of concrete structures – Part 1-1: General rules and rules for buildings. DIN Construction Standards Committee (NABau), Beuth Verlag GmbH, Berlin.
63. Reineck, K.-H., Greiner, S., and Lichtenfels, A. (2003) Wasserspeicher aus UHFB – Bemessung [water reservoirs made from UHPC – design], in *Innovationen im Bauwesen: Ultrahochfester Beton* (eds G. König, K. Holschemacher, and F. Dehn), Bauwerk Verlag GmbH, Berlin, pp. 257–268.
64. Association Française de Génie Civil (AFGC) (Jan 2002) Documents scientifiques et techniques: Bétons fibrés à ultra-hautes performances (Recommandations provisoires).

65. Richard, P. and Cheyrezy, M. (1995) Composition of reactive powder concretes. *Cement and Concrete Research*, **25** (7), 1501–1511.
66. Ma, J., Schneider, H., and Wu, Z. (2003) Bruchmechanische Kenngrößen von UHFB [fracture-mechanics parameters of UHPC], in *Innovationen im Bauwesen: Ultrahochfester Beton [innovations in construction: UHPC]* (eds G. König, K. Holschemacher, and F. Dehn), Bauwerk Verlag GmbH, Berlin, pp. 121–130.
67. Stürwald, S. (2011) Versuche zum Biegetragverhalten von UHPC mit kombinierter Bewehrung [tests for the bending behaviour of UHPC with combined reinforcement]. Research report, Concrete Construction Dept, Faculty of Civil Engineering, University of Kassel.
68. Leutbecher, T. (2008) Rissbildung und Zugtragverhalten von mit Stabstahl und Fasern bewehrtem Ultrahochfesten Beton (UHPC) [crack formation and tensile loadbearing behaviour of UHPC reinforced with steel bars and fibres]. Dissertation, University of Kassel, Structural Materials & Engineering Series, No. 9, Kassel University Press GmbH, Kassel.
69. Pfyl, T. (2003) Tragverhalten von Stahlfaserbeton [structural behaviour of steel fibre-reinforced concrete]. Dissertation, ETH No. 15005, ETH Zurich.
70. Holmberg, Å. (1986) *An Effect from Reinforcement in Concrete Cracks*, Nordic Betong, Stockholm.
71. Holmberg, Å. (1989) Tensile strength of concrete as a test result. *Byggningsstatiska Meddelelser, Danish Society for Structural Science & Engineering*, **60** (3/4), 121–134.
72. Li, V.C. and Leung, C.K.Y. (1992) Steady-state and multiple cracking of short random fiber composites. *Journal of Engineering Mechanics*, **188** (11), 2246–2264.
73. Behloul, M. (1996) Analyse et modélisation du comportement d'un matériau à matrice cimentaire fibrée à ultra hautes performances. Dissertation, E.N.S. Cachan, France.
74. Behloul, M. (1996) Les micro-bétons renforcés de fibres: de l'éprouvette aux structures, Rencontres universitaires de génie civil No. 14 (Clermont-Ferrand, 9–10 May 1996; 1, COS'96: comportement des ouvrages en service; 2, Prix des jeunes chercheurs).
75. Jungwirth, J. (2006) Zum Zugtragverhalten von zugbeanspruchten Bauteilen aus Ultra-Hochleistungs-Faserbeton [on the tensile loadbearing behaviour of fibre-reinforced UHPC components in tension]. Dissertation thesis No. 3429, Faculty of Architecture, Civil & Environmental Engineering (ENAC), École Polytechnique Fédérale de Lausanne (EPFL).
76. Markovic, I. (2006) High-Performance Hybrid-Fibre Concrete – Development and Utilisation. Dissertation, Delft University of Technology, DPU Science, Delft University Press.

77. Fehling, E. and Stürwald, S. (2011) Flexural Behaviour of UHPC with Fibres and Rebars. In: Concrete engineering for excellence and efficiency (ed. V. Šruma), vol. 1, *fib Symp.*, Prague pp. 535–538.
78. Bornemann, R., Faber, S., and Schmidt, M. (2004) UHPC mit Stahl- und hochfesten Kunststofffasern [UHPC with steel and high-strength polymer fibres]. Test report, Construction Materials Dept, Faculty of Civil Engineering, University of Kassel (unpublished).
79. Reineck, K.-H. and Greiner, S. (2004) Tests on ultra-high performance fibre reinforced concrete for designing hot-water tanks and UHPFRC-shells, in *Ultra High Performance Concrete (UHPC), Intl. Symp. on Ultra High Performance Concrete*, Structural Materials & Engineering Series No. 3 (eds M. Schmidt, E. Fehling, and C. Geisenhanslüke), Kassel University Press GmbH, Kassel, pp. 361–374.
80. Schlaich, J. and Schäfer, K. (1998) Konstruieren im Stahlbetonbau [reinforced concrete design], in *Beton-Kalender 1998, Part 2* (ed. J. Eibl), Ernst & Sohn Verlag, Berlin, pp. 721–895.
81. Orgass, M. and Klug, Y. (2004) Fibre reinforced ultra-high strength concretes, in *Ultra High Performance Concrete (UHPC), Intl. Symp. on Ultra High Performance Concrete*, Structural Materials & Engineering Series No. 3 (eds M. Schmidt, E. Fehling, and C. Geisenhanslüke), Kassel University Press GmbH, Kassel, pp. 637–647.
82. Teutsch, M. and Grunert, J.P. (2004) Design for bending and bending with axial force of ultra high performance concrete, in *Beton- und Stahlbetonbau*, vol. **99**, No. 8, Ernst & Sohn Verlag, Berlin, pp. 1–5 (in German).
83. Bernier, G. and Behloul, M. (4–5 Jul 1996) Effet de l'orientation des fibres sur le comportement mécanique des BPR, in *2e colloque international francophone sur les bétons renforcés de fibres métalliques*, Toulouse, pp. 233–240.
84. Müller, H.S., Burkart, I., Budelmann, H. *et al.* (2010) Time-dependent Behaviour of Ultra High Performance Concrete (UHPC). In: 2010 *fib* Congress and PCI Convention Bridge Conf. Proc., Washington, D.C. (pub.: Precast/Prestressed Concrete Institute, Chicago).
85. Burkart, I. and Müller, H.S. (2008) Creep and shrinkage characteristics of ultra high strength concrete (UHPC), in *Creep, Shrinkage and Durability Mechanics of Concrete and Concrete Structures, Proc. of CONCREEP 8 conf., Ise-Shima, Japan, 30 Sept – 2 Oct 2008* (eds R. Sato, K. Maekawa, T. Tanabe, K. Sakata, H. Nakamura, and H. Mihashi), Taylor & Francis, chap. 91, pp. 689–694.
86. Tue, N.V., Ma, J., and Orgass, M. (2006) Kriechen von ultrahochfestem Beton (UHFB) [creep of UHPC], in *Bautechnik*, vol. **83**, No. 2, Ernst & Sohn Verlag, Berlin, pp. 119–124.

87. Speck, K. (2008) Concrete under multiaxial loading conditions – A constitutive model for short-time loading of high performance concretes. Dissertation, TU Dresden (in German).
88. Klausen, D. and Weigler, H. (1979) Betonfestigkeit bei konstanter und veränderlicher Dauerschwellbeanspruchung [concrete strength under constant and variable persistent fluctuating loads]. *Betonwerk + Fertigteiltechnik*, **45** (3), 158–163.
89. Wefer, M. (2010) Materialverhalten und Bemessungswerte von ultrahochfestem Beton unter einaxialer Ermüdungsbeanspruchung [material behaviour and design values for UHPC under uniaxial fatigue loading]. Dissertation, Leibniz University Hannover, Berichte aus dem Institut für Baustoffe, No. 7.
90. Grünberg, J., Ertel, C., Lohaus, L. *et al.* (2010) Failure Models for Ultra High Performance Concrete (UHPC). In: 2010 *fib* Congress and PCI Convention Bridge Conf. Proc., Washington, D.C. (pub.: Precast/Prestressed Concrete Institute, Chicago).
91. Grünberg, J., Lohaus, L., Ertel, C., and Wefer, M. (2007) Mehraxiales mechanisches Ermüdungsverhalten von Ultra-hochfestem Beton – Experimentelle und analytische Untersuchungen [multi-axial mechanical fatigue behaviour of UHPC – experimental and analytical studies], in *Beton- und Stahlbetonbau*, vol. **102**, No. 6, Ernst & Sohn Verlag, Berlin, pp. 388–398.
92. Grünberg, J. and Ertel, C. (2012) A Triaxial Fatigue Failure Model for ultra high performance concrete (UHPC), in *Ultra High Performance Concrete and Nanotechnology in Construction, 3rd Intl. Symp. on Ultra High Performance Concrete and Nanotechnology for High Performance Construction Materials*, Structural Materials & Engineering Series No. 19 (eds M. Schmidt, E. Fehling, C. Glotzbach, S. Fröhlich, and S. Piotrowski), Kassel University Press GmbH, Kassel, pp. 603–610.
93. Lappa, E.S. (2007) High Strength Fibre Reinforced Concrete. Static and Fatigue Behaviour in Bending. Dissertation, Delft University of Technology.
94. Grünewald, S. (2004) Performance based design of self-compacting fiber reinforced concrete. Dissertation, Delft University of Technology.
95. Millon, O., Nöldgen, M., Thoma, K. *et al.* (2009) Fiber-reinforced ultra-high performance concrete under tensile loads, in *DYMAT 2009 – 9th Intl. Conf. on the Mechanical and Physical Behaviour of Materials under Dynamic Loading*, vol. **1**, EDP Sciences, pp. 671–677.
96. Nöldgen, M. (2010) Modellierung von ultrahochfestem Beton (UHPC) unter Impaktbelastung – Auslegung eines Hochhauskerns gegen Flugzeuganprall [modelling of UHPC under impact loading – designing a high-rise service core to resist aircraft impact]. Dissertation, University of Kassel, Structural Materials & Engineering Series, No. 14, Kassel University Press GmbH, Kassel.
97. Bornemann, R., Schmidt, M., and Vellmer, C. (2002) Brandverhalten ultrahochfester Betone [behaviour of UHPC in fire]. *Beton*, (9), 418–422.

98. Hosser, D., Kampmeier, B., and Hollmann, D. (2012) Behavior of Ultra High Performance Concrete (UHPC) in Case of Fire, in *Ultra High Performance Concrete and Nanotechnology in Construction, 3rd Intl. Symp. on Ultra High Performance Concrete and Nanotechnology for High Performance Construction Materials*, Structural Materials & Engineering Series No. 19 (eds M. Schmidt, E. Fehling, C. Glotzbach, S. Fröhlich, and S. Piotrowski), Kassel University Press GmbH, Kassel, pp. 573–582.
99. Luping, T. and Nilsson, L.-O. (1992) Rapid determination of the chloride diffusivity in concrete by applying an electrical field. *ACI Materials Journal*, **89** (1), 49–53.
100. Schmidt, M. and Rafiee, A. (2013) Impact of cracks on the durability and on the service-life of fiber reinforced ultra high performance concrete – evaluation, modeling and structural measures, in *Life-Cycle and Sustainability of Civil Infrastructure Systems: Proc. of 3rd Intl. Symp. on Life-Cycle Civil Engineering (IALCCE 2012)* (eds A. Strauss, D.M. Frangopol, and K. Bergmeister), Taylor & Francis Group, London, pp. 289.
101. Rafiee, A. (2012) Computer Modeling and Investigation on the steel corrosion in Cracked Ultra High Performance Concrete. Dissertation, University of Kassel, Structural Materials & Engineering Series, No. 21, Kassel University Press GmbH, Kassel.
102. Franke, L., Deckelmann, G., and Schmidt, H. (2009) Behaviour of ultra high performance concrete with respect to chemical attack. In: 17th Int. Baustofftagung (ibautil) – Proc., vol. 1 (ed. J. Stark), Weimar, pp. 1099–1104.
103. Setzer, M.J. and Palecki, S. (20 Apr 2007) Untersuchungen zum Frost/Frost-Taumittelwiderstand, dem autogenen Schwinden und der Gefügestruktur von UHPC [studies of freezing/freezing–de-icing salt resistance, autogenous shrinkage and microstructure of UHPC]. DFG research project Se 336/61-1 (SPP 1182), report, University of Essen.
104. Tue, N.V., Schenck, G., and Schwarz, J. (Jan. 2005) Absicherung der statistisch erhobenen Festbetonkennwerte für die neue Normengeneration [support for the hardened concrete parameters ascertained statistically for the new generation of standards]. Research report, Leipzig University, Institute of Concrete Construction & Construction Materials Technology.
105. Fehling, E. and Leutbecher, T. (2011) Bemessung von Bauteilen aus UHPC [design of UHPC members], in *9th Münchener Baustoffseminar [Munich construction materials seminar] “Ultra-Hochfester Beton (UHPC), Stoffliche Grundlagen, Bemessung und Praxiseinsatz” [UHPC: materials, design, practice]*, Förderverein Baustoff-Forschung e.V., Munich, pp. 24–25.
106. Stürwald, S. and Fehling, E. (2012) Design of Reinforced UHPFRC in Flexure, in *Ultra High Performance Concrete and Nanotechnology in Construction, 3rd Intl. Symp. on Ultra High Performance Concrete and Nanotechnology for High Performance Construction Materials*, Structural Materials & Engineering Series No. 19

- (eds M. Schmidt, E. Fehling, C. Glotzbach, S. Fröhlich, and S. Piotrowski), Kassel University Press GmbH, Kassel, pp. 443–450.
107. Fehling, E., Bunje, K., and Leutbecher, T. (2003) Bemessung für Biegung und Querkraft bei Bauteilen aus UHFB [design for bending and shear for UHPC members], in *Ultrahochfester Beton, Schriftenreihe Innovationen im Bauwesen* (eds G. König, K. Holschemacher, and F. Dehn), Bauwerk Verlag GmbH, Berlin, pp. 183–198.
 108. Zink, M. (1999) Zum Biegeschubversagen schlanker Bauteile aus Hochleistungsbe- ton mit und ohne Vorspannung [on the flexural-shear behaviour of slender UHPC members with and without prestressing]. Dissertation, Leipzig University.
 109. Bunje, K. and Fehling, E. (2004) About shear force and punching shear resistance of structural elements of Ultra High Performance Concrete, in *Ultra High Performance Concrete (UHPC), Intl. Symp. on Ultra High Performance Concrete*, Structural Materials & Engineering Series No. 3 (eds M. Schmidt, E. Fehling, and C. Geisenhanslüke), Kassel University Press GmbH, Kassel, pp. 401–411.
 110. Hillerborg, A., Modéer, M., and Petersson, P.-E. (1976) Analysis of crack formation and crack growth in concrete by means of fracture mechanics and finite elements. *Cement and Concrete Research*, **6** (6), 773–782.
 111. Rimmel, G. (1994) Zum Zug- und Schubtragverhalten von Bauteilen aus hochfestem Beton [on the tensile and shear behaviour of components made from high-strength concrete], in *German Committee for Structural Concrete (DAfStb)*, No. 444, Beuth Verlag GmbH, Berlin.
 112. Grimm, R. (1997) Einfluss bruchmechanischer Kenngrößen auf das Biege- und Schubtragverhalten hochfester Betone [influence of fracture-mechanics parameters on bending and shear behaviour of high-strength concrete], in *German Committee for Structural Concrete (DAfStb)*, No. 477, Beuth Verlag GmbH, Berlin.
 113. Fehling, E. and Thiemicke, J. (2012) Experimental Investigations on I-Shaped UHPC-Beams with Combined Reinforcement under Shear Load, in *Ultra High Performance Concrete and Nanotechnology in Construction, 3rd Intl. Symp. on Ultra High Performance Concrete and Nanotechnology for High Performance Construction Materials*, Structural Materials & Engineering Series No. 19 (eds M. Schmidt, E. Fehling, C. Glotzbach *et al.*), Kassel University Press GmbH, Kassel, pp. 477–484.
 114. Bertram, G. and Hegger, J. (2012) Shear behavior of pretensioned UHPC beams – tests and design, in *Ultra High Performance Concrete and Nanotechnology in Construction, 3rd Intl. Symp. on Ultra High Performance Concrete and Nano- technology for High Performance Construction Materials*, Structural Materials & Engineering Series No. 19 (eds M. Schmidt, E. Fehling, C. Glotzbach, S. Fröhlich, and S. Piotrowski), Kassel University Press GmbH, Kassel, pp. 493–500.

115. Hegger, J. and Bertram, G. (5–6 Jun 2008) Vorgespannter Ultrahochfester Beton (Querkraft- und Verankerungsverhalten) [prestressed UHPC (shear force and anchorage behaviour)]. In: 49th DAfStb Research Colloquium, Aachen, pp. 169–178.
116. Bertram, G. and Hegger, J. (2012) Bond Behavior of Strands in UHPC – Tests and Design, in *Ultra High Performance Concrete and Nanotechnology in Construction, 3rd Intl. Symp. on Ultra High Performance Concrete and Nanotechnology for High Performance Construction Materials*, Structural Materials & Engineering Series No. 19 (eds M. Schmidt, E. Fehling, C. Glotzbach, S. Fröhlich, and S. Piotrowski), Kassel University Press GmbH, Kassel, pp. 525–532.
117. Sato, Y., Pansuk, W., den Uijl, J., and Walraven, J. (2008) Shear capacity of high performance fiber reinforced concrete I-beams. In: Proc. of 8th Intl. Symp. on Utilization of High-Strength and High-Performance Concrete, Japan Concrete Institute, Tokyo, pp. 369–376.
118. Moreillon, L., Nseir, J., and Suter, R. (2012) Shear and flexural strength of thin UHPC slabs, in *Ultra High Performance Concrete and Nanotechnology in Construction, 3rd Intl. Symp. on Ultra High Performance Concrete and Nanotechnology for High Performance Construction Materials*, Structural Materials & Engineering Series No. 19 (eds M. Schmidt, E. Fehling, C. Glotzbach, S. Fröhlich, and S. Piotrowski), Kassel University Press GmbH, Kassel, pp. 749–756.
119. Muttoni, A. (2008) Punching Shear Strength of reinforced Concrete Slabs without Transverse Reinforcement. *ACI Structural Journal*, **105** (4), 440–450.
120. Fehling, E., Leutbecher, T., Röder, F.-K., and Stürwald, S. (2008) Structural behavior of UHPC under biaxial loading, in *Ultra High Performance Concrete (UHPC), 2nd Intl. Symp. on Ultra High Performance Concrete*, Structural Materials & Engineering Series No. 10 (eds E. Fehling, M. Schmidt, and S. Stürwald), Kassel University Press GmbH, Kassel, pp. 569–576.
121. Curbach, M. and Speck, K. (2007) *Biaxial compressive strength of ultra high performance concrete. Beton- und Stahlbetonbau*, vol. **102**, No. 10, Ernst & Sohn Verlag, Berlin, pp. 664–673 (in German).
122. Klotz, S. and Holschemacher, K. (2003) Teilflächenpressung bei UHFB [patch-load bearing pressure for UHPC], in *Ultrahochfester Beton, Schriftenreihe Innovationen im Bauwesen* (eds G. König, K. Holschemacher, and F. Dehn), Bauwerk Verlag GmbH, Berlin, pp. 215–226.
123. Leutbecher, T. and Fehling, E. (2012) Compressive Strength of UHPC in Bottle-Shaped Compression Fields, in *Ultra High Performance Concrete and Nanotechnology in Construction, 3rd Intl. Symp. on Ultra High Performance Concrete and Nanotechnology for High Performance Construction Materials*, Structural Materials & Engineering Series No. 19 (eds M. Schmidt, E. Fehling, C. Glotzbach, S. Fröhlich, and S. Piotrowski), Kassel University Press GmbH, Kassel, pp. 1027–1034.

124. Lohaus, L. and Oneschkow, N. (2012) New fatigue design model for all concrete strengths, in *Ultra High Performance Concrete and Nanotechnology in Construction, 3rd Intl. Symp. on Ultra High Performance Concrete and Nanotechnology for High Performance Construction Materials*, Structural Materials & Engineering Series No. 19 (eds M. Schmidt, E. Fehling, C. Glotzbach, S. Fröhlich, and S. Piotrowski), Kassel University Press GmbH, Kassel, pp. 611–618.
125. Leutbecher, T. and Fehling, E. (2011) Design for serviceability of ultra high performance concrete structures, in *High Performance Fiber Reinforced Cement Composites 6*, Proc. of 6th Intl. Workshop on High Performance Fiber Reinforced Cement Composites (HPFRCC6) (eds G.J. Parra-Montesinos, H.W. Reinhardt, and A.E. Naaman), Springer, Dordrecht, Ann Arbor, MI, USA, pp. 445–452.
126. Tue, N.V., Hegger, J., Winkler, M., and Schoening, J. (9–11 Aug 2011) Connections of Precast Ultra-High Performance Concrete Elements. In: 9th Intl. Symp. on High Performance Concrete: Design, Verification & Utilization, Rotorua, New Zealand, paper B6-3.
127. Schmidt, M., Krelaus, R., Teichmann, T., Leutbecher, T., and Fehling, E. (2007) *Adhesive assembling of structural UHPC elements – Preliminary investigations and applications at the Gärtnerplatzbrücke in Kassel*. *Beton- und Stahlbetonbau*, vol. **102**, No. 10, Ernst & Sohn Verlag, Berlin, pp. 681–690 (in German).
128. Schmidt, M. and Teichmann, T. (Jun 2006) New Developments in Ultra High Performance Concrete – non-corrosive PVA-fibres and gluing of structural elements. Presentation, 2nd *fib* Congress, Naples.
129. Mühlbauer, C. and Zilch, K. (2010) Glued joints of ultra high performance concrete structures. In: 2010 *fib* Congress and PCI Convention Bridge Conf. Proc., Washington, D.C. (pub.: Precast/Prestressed Concrete Institute, Chicago).
130. Mühlbauer, C. (2012) Fügen von Bauteilen aus ultrahochfestem Beton (UHPC) durch Verkleben [joining UHPC components with adhesives]. Dissertation, TU Munich.
131. Tanaka, Y., Ishido, M., Kobayashi, T. *et al.* (2008) Development and structural performance of a 40 m long monorail girder applying ultra high strength fiber reinforced concrete. In: Proc. of 8th Intl. Symp. on Utilization of High-Strength and High-Performance Concrete, Japan Concrete Institute, Tokyo, pp. 1153–1158.
132. Watanabe, N., Matsukawa, F., Takeda, Y., and Fuuhara, T. (2008) Design of GSE Bridge using ultra high strength fiber reinforced concrete. In: Proc. of 8th Intl. Symp. on Utilization of High-Strength and High-Performance Concrete, paper S3-6-5, Japan Concrete Institute, Tokyo.
133. Hegger, J., Rauscher, S., and Gallwoszus, J. (2010) Modern hybrid structures made of UHPC and high strength steel. In: 2010 *fib* Congress and PCI Convention Bridge Conf. Proc., Washington, D.C. (pub.: Precast/Prestressed Concrete Institute, Chicago).

134. Hegger, J., Gallwoszus, J., and Rauscher, S. (9–11 Aug 2011) Shear connectors in UHPC under cyclic loading. In: 9th Intl. Symp. on High Performance Concrete: Design, Verification & Utilization, Rotorua, New Zealand, paper B6-4.
135. Wiese, S., Kurz, W., and Schnell, J. (9–11 Aug 2011) Research on innovative shear connectors for lightweight composite structures. Presentation 9th Intl. Symp. on High Performance Concrete: Design, Verification & Utilization, Rotorua, New Zealand.
136. Wiese, S., Schnell, J., and Kurz, W. (2011) *Innovative shear connectors in ultra high performance concrete*. *Beton- und Stahlbetonbau*, vol. **106**, No. 10, Ernst & Sohn Verlag, Berlin, pp. 694–699 (in German).
137. Anders, S. (2007) *Betontechnologische Einflüsse auf das Tragverhalten von Grouted Joints [concrete technology influences on structural behaviour of grouted joints]*. Dissertation, University of Hannover.
138. Brühwiler, E. (2011) Entwurf, Bemessung und Ausführung von Stahl-UHFB – Stahlbeton Verbundbauteilen [design and construction of steel fibre-reinforced UHPC/RC composite members], *Ultra-Hochleistungs-Faserbeton, entwerfen, bemessen, bauen [design and construction of fibre-reinforced UHPC]*, conf., 27 Oct 2011 (eds E. Brühwiler, L. Moreillon, and R. Suter), School of Engineering & Architecture, Fribourg, Switzerland, pp. 121–136.
139. Blais, P.Y. and Couture, M. (1999) Precast, prestressed pedestrian bridge – world’s first reactive powder concrete structure. *PCI-Journal*, **44** (5), 60–71.
140. Parsekian, G.A., Shrive, N.G., Brown, T.G. *et al.* (2008) Innovative ultra-high performance concrete structures, in *fib Conf. “Tailor Made Concrete Structures – New Solutions for our Society”* (eds J.C. Walraven and D. Stoelhorst), Elsevier Amsterdam, pp. 325–330.
141. Thibaux, T. and Tanner, J.A. (Oct. 2002) Construction of the first French road bridges in ultra high performance concrete. In: Proc. of 1st *fib* Congress “Concrete Structures in the 21st Century”, Osaka, Japan.
142. Behloul, M., Ricciotti, R., Ricciotti, R.F. *et al.* (2008) Ductal® Pont du Diable footbridge, France, in *fib Conf. “Tailor Made Concrete Structures – New Solutions for our Society”* (eds J.C. Walraven and D. Stoelhorst), Elsevier Amsterdam, pp. 335–340.
143. Delauzun, O., Rogat, D., Boutillon, L. *et al.* (2010) Construction of the PS34 UHPFRC bridge, in *Designing and Building with UHPFRC, Proc. of intl. workshop “Designing and Building with Ultra-High Performance Fibre-Reinforced Concrete (UHPFRC): State of the Art and Development”* (eds J. Resplendino and F. Toulemonde), John Wiley & Sons, pp. 137–148.
144. Thibaux, T. (2008) UHPFRC prestressed beams as an alternative to composite steel-concrete decks, in *fib Conf. “Tailor Made Concrete Structures – New Solutions for our Society”* (eds J.C. Walraven and D. Stoelhorst), Elsevier Amsterdam, pp. 1077–1083.

145. Thibaux, T. (2008) Cha p. 57. Strengthening of Huisne bridge using Ultra-High-Performance Fibre-Reinforced Concrete, in *fib Conf. "Tailor Made Concrete Structures – New Solutions for our Society"* (eds J.C. Walraven and D. Stoelhorst), Elsevier Amsterdam, pp. 331–334.
146. Tanaka, Y., Musya, H., Ootake, A. *et al.* (Oct 2002) Design and Construction of Sakata-Mirai Footbridge Using Reactive Powder Concrete. In: Proc. of 1st *fib* Congress "Concrete Structures in the 21st Century", Osaka, Japan, vol. 1, pp. 103–104.
147. Rebentrost, M. and Wight, G. (2008) Experience and applications of ultra-high performance concrete in Asia, in *Ultra High Performance Concrete (UHPC), 2nd Intl. Symp. on Ultra High Performance Concrete*, Structural Materials & Engineering Series, No. 10 (eds E. Fehling, M. Schmidt, and S. Stürwald), Kassel University Press GmbH, Kassel, pp. 19–30.
148. Watanabe, N., Musha, H., and Yoshinaga, K. (Nov. 2007) Design and Performance tests for Bridge using Ultra High Strength Fiber Reinforced Concrete. In: 23rd US-Japan Bridge Engineering Workshop.
149. Tanaka, Y., Ishido, M., Kobayashi, T., and Ohkawa, M. (2008) Technical development of a long span monorail girder applying ultra high strength fiber reinforced concrete, in *Ultra High Performance Concrete (UHPC), 2nd Intl. Symp. on Ultra High Performance Concrete*, Structural Materials & Engineering Series No. 10 (eds E. Fehling, M. Schmidt, and S. Stürwald), Kassel University Press GmbH, Kassel, pp. 803–810.
150. Behloul, M. and Lee, K.C. (2003) *Ductal® Seonyu Footbridge. Structural Concrete 4*, No. 4, Thomas Telford, London, pp. 195–201.
151. Kim, B.-S., Kim, S., Kim, Q.-J. *et al.* (2012) R & D activities and application of ultra high performance concrete to cable stayed bridges, in: *Ultra High Performance Concrete and Nanotechnology in Construction, 3rd Intl. Symp. on Ultra High Performance Concrete and Nanotechnology for High Performance Construction Materials*, Structural Materials & Engineering Series No. 19 (eds M. Schmidt, E. Fehling, C. Glotzbach, S. Fröhlich, and S. Piotrowski), Kassel University Press GmbH, Kassel, pp. 865–872.
152. Park, S.Y., Cho, K., Cho, J.R. *et al.* (2012) Structural Performance of Prestressed UHPC Ribbed Deck for Cable-Stayed Bridge, in *Ultra High Performance Concrete and Nanotechnology in Construction, 3rd Intl. Symp. on Ultra High Performance Concrete and Nanotechnology for High Performance Construction Materials*, Structural Materials & Engineering Series No. 19 (eds M. Schmidt, E. Fehling, C. Glotzbach, S. Fröhlich, and S. Piotrowski), Kassel University Press GmbH, Kassel, pp. 873–880.
153. Krelaus, R., Freisinger, S., and Schmidt, M. (2008) Adhesive bonding of UHPC structural members at the gaertnerplatz bridge in Kassel, in *Ultra High Performance Concrete (UHPC), 2nd Intl. Symp. on Ultra High Performance Concrete*, Structural

- Materials & Engineering Series No. 10 (eds E. Fehling, M. Schmidt, and S. Stürwald), Kassel University Press GmbH, Kassel, pp. 597–604.
154. Fröhlich, S., Link, M., Fehling, E. *et al.* (2009) Identifikation von Steifigkeitsveränderungen im Zuge der Dauerüberwachung der Gärtnerplatzbrücke in Kassel unter Verwendung gemessener Einflusslinien [identification of stiffness changes during permanent monitoring of Gärtnerplatz Bridge, Kassel], in *3rd VDI Conf., Baudynamik 2009, VDI Report 2063*, VDI-Verlag, Düsseldorf, pp. 93–108.
 155. Brühwiler, E., Fehling, E., Bunje, K., and Pelke, E. (2007) Design of an innovative composite road bridge combining reinforced concrete with Ultra-High Performance Fibre Reinforced Concrete. In: Proc. of IABSE Symp. “Improving Infrastructure Worldwide”, Weimar, IABSE report 93, pp. 80–81.
 156. Freytag, B., Heinzle, G., Reichel, M., and Sparowitz, L. (2012) WILD-bridge scientific preparation for smooth realisation, In *Ultra High Performance Concrete and Nanotechnology in Construction, 3rd Intl. Symp. on Ultra High Performance Concrete and Nanotechnology for High Performance Construction Materials*, Structural Materials & Engineering Series No. 19 (eds M. Schmidt, E. Fehling, C. Glotzbach, S. Fröhlich, and S. Piotrowski), Kassel University Press GmbH, Kassel, pp. 881–888.
 157. Hecht, M. (2012) Practical use of fibre-reinforced UHPC in construction – production of precast elements for Wild-Brücke in Völkermarkt, in *Ultra High Performance Concrete and Nanotechnology in Construction, 3rd Intl. Symp. on Ultra High Performance Concrete and Nanotechnology for High Performance Construction Materials*, Structural Materials & Engineering Series No. 19 (eds M. Schmidt, E. Fehling, C. Glotzbach, S. Fröhlich, and S. Piotrowski), Kassel University Press GmbH, Kassel, pp. 889–896.
 158. Sparowitz, L., Freytag, B., and Reichel, M. (28–29 Jul 2012) UHPFRC bridges built in Austria. in: Proc. of 5th Intl. Conf. on New Dimensions in Bridges, Flyovers, Overpasses & Elevated Structures, Wuyishan, China, pp. 45–63.
 159. Brühwiler, E., Denarié, E., and Putallaz, J.C. (2005) Instandsetzung einer Betonbrücke mit Ultrahochleistungsfähigem Fasereinkornbeton (UHLFB) [repairing a concrete bridge with fibre-reinforced, single-sized aggregate UHPC], in *Beton- und Stahlbetonbau*, vol. **100**, No. 9, Ernst & Sohn Verlag, Berlin, pp. 822–827.
 160. Kaptijn, N. and Blom, J. (2004) A new bridge deck for the Kaag Bridges, in *Ultra High Performance Concrete (UHPC), Intl. Symp. on Ultra High Performance Concrete*, Structural Materials & Engineering Series No. 3 (eds M. Schmidt, E. Fehling, and C. Geisenhanslüke), Kassel University Press GmbH, Kassel, pp. 49–57.
 161. Kojima, M., Mitsui, K., Wachi, M., and Sato, T. (2008) Application of 150 N advanced performance composites to high-rise R/C building, in *Proc., of 8th Intl. Symp., on Utilization of High-Strength and High-Performance Concrete*, Japan Concrete Institute, Tokyo, pp. 1199–1206.

162. Park, C., Kim, D., Lee, J. *et al.* (2008) Development of 200 N/mm² ultra high strength concrete and test application for super high rise building, in *Proc. of 8th Intl. Symp. on Utilization of High-Strength and High-Performance Concrete*, Japan Concrete Institute, Tokyo, pp. 1276–1281.
163. Jacques, L., Fournier, Y., Jousseing, J.Y., and Batoz, J.F. (2010) UHPFRC sunshades: An elegant solution for regulating heat input in buildings, in *Designing and Building with UHPFRC, Proc. of intl. workshop “Designing and Building with Ultra-High Performance Fibre-Reinforced Concrete (UHPFRC): State of the Art and Development”* (eds J. Resplendino and F. Toulemonde), John Wiley & Sons, pp. 349–362.
164. Aarup, B. (2010) Precast applications of UHPFRC, in *Designing and Building with UHPFRC, Proc. of intl. workshop “Designing and Building with Ultra-High Performance Fibre-Reinforced Concrete (UHPFRC): State of the Art and Development”* (eds J. Resplendino and F. Toulemonde), John Wiley & Sons, pp. 319–330.
165. Van Nalta, R. and Baek Hansen, T. (2012) Ultra thin Hi-Con Balconies – First Application in Holland, in *Ultra High Performance Concrete and Nanotechnology in Construction, 3rd Intl. Symp. on Ultra High Performance Concrete and Nanotechnology for High Performance Construction Materials*, Structural Materials & Engineering Series No. 19 (eds M. Schmidt, E. Fehling, C. Glotzbach, S. Fröhlich, and S. Piotrowski), Kassel University Press GmbH, Kassel, pp. 1005–1010.
166. Vicenzino, E., Culham, G., Perry, V.H. *et al.* (2005) First use of UHPFRC in thin precast concrete roof shell for Canadian LRT station. *PCI Journal*, **50** (5), 50–67.
167. Van Herwijnen, F. and Fiel, R.W.S. (2005) Zonnestraal folly in very-high-strength concrete. *Cement*, vol. 57(3), pp. 39–43 (in Dutch).
168. Thibaux, T. (2010) UHPFRC development: The experience of BSI applications. in *Designing and Building with UHPFRC, Proc. of intl. workshop “Designing and Building with Ultra-High Performance Fibre-Reinforced Concrete (UHPFRC): State of the Art and Development”* (eds J. Resplendino and F. Toulemonde), John Wiley & Sons, pp. 63–76.
169. Ricciotti, R., Ricciotti, R., and Behloul, M. Villa Navarra (2011) The Enrico Navarra Gallery, from Designing and Building with UHPC, State of the Art and Development, Chapter 6, Wiley, pp. 79–86.
170. Walraven, J. (2011) Finalizing of the *fib*-Model Code 2010. In: Concrete engineering for excellence and efficiency (ed. V. Šruma), *fib Symp.*, Prague, vol. 1, pp. 71–86.
171. Kono, T., Ichinomiya, T., Ohno, T. *et al.* (2008) Influence of placing methods on structural performance of slab with ultra high strength fiber reinforced concrete – Tokyo International Airport Runway D, in *Proc. of 8th Intl. Symp. on Utilization of High-Strength and High-Performance Concrete*, Japan Concrete Institute, Tokyo, paper S3-3-4.
172. Ricciotti, R., Lamoureux, G., and Ricciotti, R. (2010) The Jean Bouin Stadium, in *Designing and Building with UHPFRC, Proc. of intl. workshop “Designing and Building with Ultra-High Performance Fibre-Reinforced Concrete (UHPFRC): State*

- of the Art and Development*” (eds J. Resplendino and F. Toulemonde), John Wiley & Sons, pp. 101–108.
173. Leutbecher, T. and Fehling, E. (2009) Crack formation and tensile behaviour of concrete members reinforced with rebars and fibres exemplified by ultra-high-performance concrete – Part 1: Crack mechanical relationships, in *Beton- und Stahlbetonbau*, vol. **104**, No. 6, Ernst & Sohn Verlag, Berlin, pp. 357–367 (in German).
 174. Leutbecher, T. and Fehling, E. (2009) Crack formation and tensile behaviour of concrete members reinforced with rebars and fibres exemplified by ultra-high-performance concrete – Part 2: Experimental investigations and examples of application, in *Beton- und Stahlbetonbau*, vol. **104**, No. 7, Ernst & Sohn Verlag, Berlin, pp. 406–415 (in German).
 175. Fitik, B., Niedermeier, R., and Zilch, K. (2010) Fatigue Behaviour of Ultra-High Performance Concrete under cyclic stress Reversals. In: 2010 *fib* Congress and PCI Convention Bridge Conf. Proc., Washington, D.C. (pub.: Precast/Prestressed Concrete Institute, Chicago).
 176. Anders, S. and Lohaus, L. (2008) Optimized High-Performance Concrete in Grouted Connections, in *fib Conf. “Tailor Made Concrete Structures – New Solutions for our Society”* (eds J.C. Walraven and D. Stoelhorst), Elsevier Amsterdam.
 177. Maccazane, P., Ricciotti, R., and Teply, F. (2010) The passerelle des anges foot-bridge, in *Designing and Building with UHPFRC, Proc. of intl. workshop “Designing and Building with Ultra-High Performance Fibre-Reinforced Concrete (UHPFRC): State of the Art and Development”* (eds J. Resplendino and F. Toulemonde), John Wiley & Sons, pp. 111–124.
 178. Dénarié, E. (Nov 2009) Recommendations for the use of UHLFB in composite structural members. Deliverable D14, European Research Project ARCHES – Assessment and Rehabilitation of Central European Highway Structures.
 179. Ricciotti, R., Portelatine, J., and Nicolas, F. (2010) Museum of European and Mediterranean Civilizations (MuCEM): High UHPFRC Content Structure Design, in *Designing and Building with UHPFRC, Proc. of intl. workshop “Designing and Building with Ultra-High Performance Fibre-Reinforced Concrete (UHPFRC): State of the Art and Development”* (eds J. Resplendino and F. Toulemonde), John Wiley & Sons, pp. 487–500.

Index

A

- Austria
 - bridge for pedestrians/cyclists, Lienz 143, 144
 - modular temporary bridge for high-speed rail lines 144–146
 - Wild bridge near Völkermarkt 141–143
- average bond stress 92
- axial force 70, 74, 77, 94
- axial strain 48
- axial tensile strength 33–36
- axial tensile test 29, 83, 105

B

- balcony 152–155
- bar-type shear reinforcement 79
- bauxite 23
- behaviour in compression 23, 24
- behaviour in tension 27
- bending/shear failure 78
- bending test 107
- Blastfurnace slag cement CEM III/A 12
- bond 24
- bond stress 14, 30, 31, 81, 92, 93, 97
- bridge 117–149
- brittle behaviour 6, 23, 27, 32, 44, 66, 69, 88, 97

C

- Canada 117
 - bridge for pedestrians/cyclists, Sherbrooke 117
 - Glenmore/Legsby footbridge, Calgary 117, 118
- capillary pore 61
- CDF test 62
- CEB-FIP Model Code 90 88, 89
- cement mortar 1
- centroid axis 98
- chloride ion diffusion depths 60
- coarse-grained 21, 23, 36
- CO₂ emission 3
- cohesion failure 107

- column 149–151
- compact reinforced composite 113
- compact reinforced concrete 2
- compression failure 88, 113
- compression test 23, 24, 32
- compression testing machine 32
- compressive strain 68, 69
- compressive strength 7, 27, 48, 50, 74, 79, 105
 - cylinder 23, 68
- compressive stress 25, 72
- concrete compressive strength 81
- connection 105
 - steel share strip for a shear-resistant connection 111
- connector
 - perfobond shear connector 108, 109
 - puzzle strip shear connector 110
- construction time 1
- corrosion rate, mortar 61
- corrosion-resistant
 - high-strength synthetic fibres 14
 - sulphuric acid 61
- cracking 95, 101
 - due to autogenous shrinkage 114
 - force 31, 99
 - formation 32, 51
 - patterns, of UHPC beams 83
 - spacing 90, 101
 - stresses 89, 99
 - temperature gradients 114
- cracking stress 100
- crack spacing 40, 92
- crack width 30, 31, 71, 73, 86, 89, 92, 93, 94
- creep 43, 44, 92, 109
- curing 17–18

D

- DAfStb guideline 22, 34
- deformation 36
 - behaviour 6
 - calculation 99, 102

- de-icing salt 62
- design, for bending and normal force 72
- design for shear tests 75
- Delft University of Technology 81–84
 - RWTH Aachen University 79–81
 - the University of Kassel 75–79
- design principles 65
- fibre distribution and fibre orientation, influence of 65
- design rules, for UHPC 3
- design value, of fibre efficiency 71
- DIF. *See* dynamic increase factor (DIF)
- dimensional tolerance 105
- dry joint 105
- Ductal® 2, 26
- ductile failure 81
- durability 1, 59–64
- aggressive media 59–63
 - ammonium nitrate solution 62
 - chloride ion diffusion depths 60
 - exposure classes, classification 63, 64
 - freeze-thaw and freezing/de-icing salt resistance 63
 - microstructure 59
 - pore radius 60
 - water absorption 62
- dynamic action 51–53
- dynamic increase factor (DIF) 51, 52
- dynamic tension load 52
- E**
- effective reinforcement ratio 97, 101
- elastic limit, for steel reinforcement 74
- embedment length 30
- energy consumption, of UHPC mixes 17
- EP adhesive 105, 108
- equilibrium condition 74, 96
- exposure class 64
- F**
- façade application
- to a building in Sedan 152
 - circular openings 152
 - to MuCEM building 151
 - police headquarters in Nantes, France 152, 153
- use of silicone 152
 - using white premix product 152
- fatigue 44–51, 88, 89, 110
- approximation of test results 46
 - behaviour of various concretes 45
 - fracture values
 - in Rendulic plane and stress–strain behaviour on 45
 - influence of hydrostatic pressure 45
 - S-N curve 46
 - test 48, 50, 51
 - triaxial testing machine 45
 - typical example of development of strains 47
- fibre bond strength 71
- fibre content 24, 81
- fibre efficiency 30, 31, 32, 65, 71, 90, 92, 94, 103
- fibre geometry 24
- influence behaviour of UHPC in tension 36
- fibre orientation 22, 24, 26, 65
- influence behaviour of UHPC in tension 36
 - influences flexural tensile strength and ductility 37
- fibre-reinforced concrete 31, 37, 39, 42, 53, 72, 90, 94
- fibre-reinforced UHPC
- beam without shear links, failure of 79
 - flexural tensile strength of 21
 - mixes 19
- fibres 26, 31, 51, 72, 79, 81
- activation phase 70, 73
 - and bar reinforcement, interaction 41, 42
 - cocktails 34, 53
 - distribution 65
 - high-strength steel 23, 24
 - pull-out phase 71
- fine-grained 23
- fire resistance 53
- fire tests, overview of results 54
- flexural tensile strength 32, 33, 34, 37, 55, 57, 79, 107
- flexural tensile stress 50, 51

flexural tensile test 32, 36, 105
flow table test 18, 19
fracture energy 28, 34, 37, 69
France
– Pont de la Chabotte, road bridge 120, 121
– Pont du Diable footbridge 119, 120
– Pont Pinel, road bridge 121–124
– road bridge, Bourg-lès-Valence 118, 119
– strengthening the Pont sur l’Huisne, Mans 124
freeze-thaw cycle 63
freezing/de-icing salt resistance 62
friction coefficient 105

G

gap grading 9
geometric reinforcement ratio 97, 100
German Committee for Reinforced Concrete (DAfStB) 6
German research programme 14, 20, 22, 61, 62, 79
Germany
– Bridge for pedestrians/cyclists over River Pleiße, Markkleeberg 140, 141
– Bridges over River Nieste near Kassel 133, 134
– Gärtnerplatz Bridge over River Fulda, Kassel 134–137
– HSLV pilot project 137–140
glued joints 105
Goodman diagram 48
grading optimization 8–11
– admixtures, use of 6–7
– ultrafine particles and residual pores 8
grain size 2, 23, 48
granulometric coefficient 7

H

hardened concrete
– fibre orientation 22
– mechanical properties 23
heat-treated UHPC 63
heat treatment 17–18, 27
high-strength concrete 88

J

Japan
– GSE Bridge, Tokyo Airport 126–128
– Runway, Haneda Airport, Tokyo 157–160
– Sakata-Mirai footbridge 124, 125
– Tokyo Monorail, Haneda Airport line 128, 129
Jean Bouin Stadium, Paris 160, 161
joints
– dry 105
– glued 105, 107, 108
– grouted 111–113
– wet 108–111

L

linear elastic–ideal plastic curve 69
load-carrying behaviour 30
load-carrying capacity 3, 81, 86, 87
load-carrying effect 29
load-deflection curves
– for beams with different types of reinforcement 79
load-deformation behaviour 41, 81, 103
load-slip relationship, for steel share strip 112
load transfer length 90, 92
localized deformation 29
longitudinal reinforcement 76, 77, 83

M

macrocrack 53
mass-based composition, of UHPC mixes 16
mechanics-based model, for determining contribution of fibres 85
microcracks 23
microstructure 6–8, 12, 17
mix composition 7, 15–17
model for design, for bending and axial force 74
modular ratio 92
modulus of elasticity 23, 68, 79
moment–curvature relationship 103
multi-axial loading 48

multi-axial strength 87
 multi-axial stress 44

N

the Netherlands 147
 – Bridge made from UHPC for cyclists/
 pedestrians, Purmerend 148
 – erecting a UHPC panel for the Kaag
 Bridge 149
 – new bridge projects, the Dutch 147
 – reinforcement in UHPC bridge deck
 panel 148
 normal-strength concrete 24, 34, 35, 60,
 87, 88

P

packing density 2, 9, 10, 11, 59
 partially loaded area 88
 particle size 23, 36
 perfbond shear connector 108, 109
 pilot project 115
 ‘plastic’ behaviour 41
 Poisson’s ratio 24, 25
 polycarboxylate ether 11
 polypropylene (PP) 53
 polyvinyl alcohol (PVA) 14
 pore radius 60
 Portland cement 61
 post-cracking behaviour 28, 37
 post-cracking flexural tensile strength
 36
 post-cracking shrinkage strain 92
 post-cracking strength 31
 post-cracking tensile strength 83
 precast 134
 prestrain 103
 prestress, contribution to shear
 capacity 80
 prestressing force 82, 110
 prestressing steel 96, 97
 – effective reinforcement ratio 97
 – geometric reinforcement ratio 97
 pulverized fly ash (PFA) 13
 punching shear 84, 85
Puntke method 8, 11, 15
 puzzle strip shear connector 110, 111

Q

quartz powder 14

R

rapid chloride migration (RCM) test 59
 raw material
 – cement 12
 – ground granulated blast furnace slag 13
 – inert admixtures 14
 – reactive admixtures 12–13
 – silica fume 12–13
 – steel fibres 14–15
 – superplasticizer 14
 reactive powder concrete 2
 reinforcement
 – basic 78
 – minimum 97
 – ratio 101
 reinforcing bars 68, 114
 relaxation factor 92
 resistance 1
 restraint 105
 rheological properties 18
 rhombohedral packing 9
 RILEM method 55
 RILEM TC 162-TDF 21
 roofs designing 155
 – applications of UHPC 155
 – roof of precast UHPC segments at Villa
 Navarra, Le Muy, France 158
 – Shell roofs to Shawnessy Light Rail
 Transit Station, Calgary, Canada 155,
 156
 – UHPC canopy at entrance to ‘De
 Zonnestraal’ Hospital, Hilversum, The
 Netherlands 155, 156
 – UHPC roof shell at Millau viaduct,
 France 155, 156
 – UHPC roof to Villa Navarra 155, 157
 round robin test 20
 RPC adhesive 108

S

safety factor 68, 89
 scale effect 33
 scale factor 77

- secant modulus 39
- self-compacting concrete (SCC) 6, 18
- serviceability limit state 89
 - calculating deformations 99–103
 - limiting crack widths 89–97
 - minimum reinforcement 97–99
- shape coefficient for strain distribution 91
- shear behaviour 79, 82
- shear capacity 76, 77, 82, 83, 84, 105, 109, 110
- shear-compression test specimens 107, 108
- shear cracks 65, 79
- shear displacement 105
- shear force 65, 83, 105
 - model 76
- shear links 79, 82
- shear reinforcement 76, 79
- shear stress 105
- shear test 105, 110
- shrinkage 1, 42, 43, 92, 100
 - autogenous 42
 - drying 59
 - internal restraint caused by 100
- silica fume 1, 12, 13
- single-shaft compulsory mixer 15
- slab impact test 51
- slump-flow class 19
- slump-flow test 18
- slurry infiltrated fibre CONcrete (SIFCON) 1
- slurry infiltrated mat CONcrete (SIMCON) 1
- S-N curves 46, 49
- softening behaviour 69
- solidity 94
- solidity coefficient of stress distribution 39
- South Korea
 - Design for Jobal Bridge 132
 - KICT cable-stayed footbridge 131
 - Seonyu ‘Bridge of Peace,’ Seoul 129, 130
- spalling behaviour 55
- splitting tensile strength 36
- stair 152
- steel beams 2
- steel fibres 1, 2, 5, 14–15, 18, 19, 28
 - combination 56
- steel reinforcement 42, 100
- steel reinforcing bar 90
- steel strain 92
- steel stress 101
- stiffness 23
- strain hardening 28, 29, 74
- strength reduction 23, 53
- stress block 73, 92, 94
- stress–crack width behaviour 29
- stress–crack width diagram 42, 73
- stress–crack width relationship 29, 31, 33, 70, 71, 72, 85, 89, 92, 95
- stress–deflection diagram 36
- stress distribution 72, 73, 94
- stress–strain curve 24, 26, 69, 95, 101
 - for design 67, 68
 - for (fibre-reinforced) UHPC 100
- stress–strain diagram 24
 - for axial tension 28
 - compression 26, 69, 70
 - converting stress-crack width relationship into 39
- stress–strain line
 - for axial tension 39
- stress–strain relationship 26, 72
- structural length 40
- strut-and-tie models 85, 86
 - load-carrying capacity
 - of nodes 87
 - of struts 86, 87
 - of ties 87
- strut inclination 82
- struts in concrete
 - test to prove the formation 113
- sufficiently ductile 86
- sulphate resistance 12
- superplasticizer 5, 13, 14
- superposition
 - of matrix softening and fibre activation 30
- surface properties 24

- Switzerland 146, 147
 - adding a layer of UHPC to a bridge deck 147
 - bridge repaired and widened with UHPC 147
 - conventional reinforced concrete, usage 147
 - waterproofed surfaces of bridge decks and bridge edge 146
- T**
- temperature-dependent compressive strength, of UHPC 56
- tensile/compressive strength ratio 88
- tensile forces 111, 114
- tensile strength 5, 17, 20–22, 28, 31, 32, 33, 35, 37, 70, 74, 76
- tensile stress 72, 91, 94, 115
 - transferred by fibres at crack 98
- tensile test 21
- tension stiffening 101
- testing
 - compressive/flexural tensile strengths 20–22
 - fresh concrete 18–20
 - machines 20
- thermal insulation 18, 154
- transfer length 40
- transverse tension 48
- U**
- UHPC layer 113, 114
- ultimate limit state 66, 67
 - partial safety factors 67
 - safety concept 66
- uniaxial compression test 24
- uniaxial compressive stress 88
- V**
- volumetric water/solids ratio 8
- W**
- waterproofing qualities 114
- web 1, 75, 77, 79–82, 108, 123, 134
- X**
- X-ray computed tomography
 - magnetic methods 22
 - photo-optical 22
- Y**
- yield point
 - of reinforcement at a crack 73
- yield stress 82

WILEY END USER LICENSE AGREEMENT

Go to www.wiley.com/go/eula to access Wiley's ebook
EULA.